THE APPLICATION OF ELECTROANALYTICAL METHODS TO THE MEASUREMENT OF METAL COMPLEX-NUCLEIC ACID INTERACTIONS

By

MEHMET ASLANOGLU B.Sc. G.R.S.C.

A THESIS SUBMITTED FOR THE DEGREE OF DOCTOR OF PHILOSOPHY OF THE UNIVERSITY OF NEWCASTLE UPON TYNE

DEPARTMENT OF CHEMISTRY

BEDSON BUILDING

UNIVERSITY OF NEWCASTLE UPON TYNE

NEWCASTLE UPON TYNE

ENGLAND

APRIL 1997

ABSTRACT

This thesis reports voltammetric and quartz crystal microgravimetric studies of the binding of metal complexes to nucleic acids in solution and immobilised on metal surfaces.

Cyclic voltammetry and steady-state microelectrode voltammetry were applied to the solution phase interactions between metal complexes and nucleic acids. The binding constants were obtained by the analysis of bound and free metal complex concentrations. The binding of N,N,N-1-propylthyminedimethylaminomethylferrocene (Fc-Th), N,N,N-trimethylaminomethylferrocene (Fc-NMe_3), bis(hexamethybenzene)iron(II), hexammine-ruthenium(III), tris(1,10-phenanthroline)iron(II) and tris-(bipyridyl)iron(II) to DNA and RNA was observed. The application of microelectrode voltammetry for metal complex-nucleic acid binding studies has not been reported before and this thesis demonstrates the advantages of the method due to increased signal-to noise ratio and better discrimination between free and nucleic acid-bound metal complex. These voltammetric results showed the binding of Fc-Th to DNA is stronger than the binding of Fc-NMe_3 to DNA, indicating that even a single nucleobase can influence the binding. The binding of singly charged ferrocenyl derivatives to DNA or RNA is mainly electrostatic plus some non-electrostatic contribution from interaction of the thymine with DNA. $Fe(bz)_2^{2+}$ binds to DNA electrostatically and the binding is senstive to ionic strength. $Ru(NH_3)_6^{3+}$ binds more strongly to DNA due to its higher charge. The binding of $Fe(phen)_3^{2+}$, a known intercalator, is stronger than the binding of $Fe(bipy)_3^{2+}$ to DNA and the measured binding constants were in agreement with previous reports, however more precise data could be obtained using the microelectrode technique devised in this thesis.

This thesis also describes a novel modification of gold and platinum surfaces by the adsorption of 4-mercaptopyridine and subsequent methylation with methyliodide to produce a positively charged suface at which DNA adsorbs strongly. Cyclic voltammetry was applied to quantify the binding of Fc-Th, Fc-NMe_3 , hexammineruthenium(III), and tris(1,10-phenanthroline) iron(II) to DNA or RNA immobilised on a gold electrode. A detectable binding of Fc-Th, $Ru(NH_3)_6^{3+}$ to DNA was observed, while no bound $FcNMe_3$ and $Fe(phen)_3^{2+}$ were detected using cyclic voltammetry. The difference in binding to immobilised DNA compared to dissolved DNA could be rationalised by the effect of the electrostatic interactions of the metal complexes with the charged pyridinium monolayer. Quartz crystal microgravimetry was used to estimate the surface coverage of DNA, Fc-Th, $Ru(NH_3)_6^{3+}$ and $Fe(phen)_3^{2+}$on gold and platinum crystals modified as above. Crystal admittance measurements showed no significant change on DNA adsorption indicating approximate rigid-layer behaviour. In agreement with the CV studies no binding of Fc-NMe_3 was detected. Some binding of $Fe(phen)_3^{2+}$ was observed and the negative result of the CV experiment may be due to instability of the monolayer at the high potentials required to oxidise $Fe(phen)_3^{2+}$. In general, the QCM results showed higher surface coverages than detected by CV. Two factors may be important, the absence of solution phase metal complex in the CV experiment leads to some desorption and the QCM measurements are complicated by the unknown extent of solvation of the metal complexes.

ACNOWLEGMENTS

I am very grateful to my supervisor Dr. Benjamin R. Horrocks, for his great help and advice. Dr. Horrocks always generously gave his time to frequent discussion and offered numerous suggestions, which were very much appreciated.

I also would like to thank Dr. Andrew Houlton and Clayton Price for their collaboration in this project and synthesis of metal complexes.

My sincere thanks are extended to Professor A. K. Covington for his supervision in my first year, and the practice viva and David Early for providing me gold surfaces.

I would like to give special thanks to my parents and family for their encouragement and support.

I am also thankful to the University of Newcastle upon Tyne for the equipment fund, and Harran University and The Higher Educational Council of Turkey for a postgraduate studentship and fully support.

I also wish to thank following friends, colleagues, and other staffs for the enjoyable time in the Department of Chemistry: Jim, Rob. Chris, Christine, Ibrahim, Angela, Gareth, Simon Tonks, Brian, Natalie, Rossy, Linda, Lindsey, Dr. A. Russel, Dr. A. Doherty, Alan, and others.

TABLE OF CONTENTS

CHAPTER TWO

THEORETICAL FUNDAMENTALS OF ELECTROCHEMICAL AND ANALYTICAL TECHNIQUES USED IN THIS THESIS 36

CHAPTER THREE

EXPERIMENTAL 62

CHAPTER FIVE

CHAPTER SIX

MEASUREMENTS OF DNA-METAL COMPLEX BINDING BY THE APPLICATION OF THE QUARTZ CRYSTAL MICROBALANCE

LIST OF FIGURES

CHAPTER ONE

CHAPTER TWO

CHAPTER THREE

CHAPTER FOUR

CHAPTER FIVE

CHAPTER SIX

LIST OF TABLES

CHAPTER ONE

GENERAL INTRODUCTION

1.1. INTRODUCTION

DNA is the molecular target of a number of clinically important anticancer antibiotics, including adriamycin, actinomycin, bleomycin, and mitomycin C [1]. One of the most important lines of drug development and current chemotherapy against cancer involves drugs which interact with DNA. The applications of transition metal complexes to probe DNA have grown after the discovery of the anticancer activity of a number of platinum and ruthenium complexes [2-4]. The recognition that DNA-binding of cisplatin is important, has directed many studies to focus upon the area of metal-nucleobase interactions [5-10]. Transition metal complexes have a long history of use as chemotherapeutic agents. In addition to potential chemotherapeutic applications, due to their electrochemical behavior, many small molecules capable of recognising DNA and RNA are anticipated to be useful in electrochemical and analytical applications. Nucleic acids interact reversibly with a broad range of chemical species that include metal ions and their complexes. Metal complex-DNA interactions may also be used for conformational recognition to find new structures of DNA and sequence-specific differences along the helix of a DNA molecule [11-16].

The aim of this research is to determine the structural and chemical factors which control the binding of metal complexes to nucleic acids. This thesis reports studies of the interaction of several transition metal complexes with nucleic acids using voltammetric (cyclic voltammetry and steady-state voltammetry), and gravimetric (quartz crystal microbalance) methods.

It describes the applications of electroanalytical chemistry to characterize these interactions as well as to quantify the modification of surfaces for DNA immobilisation.

Voltammetric measurements have been developed to probe and quantify the binding of small electroactive molecules to DNA and RNA. This method is generally applicable for the study of the interactions between small electroactive species and biopolymers.

1.2. STRUCTURES OF DNA AND RNA

Nucleic acids are polymers of ribonucleotides or deoxyribonucleotides in RNA and DNA respectively. The deoxyribonucleic acid (DNA) molecule contains all the genetic information for cellular function. Ribonucleic acid (RNA) molecules ensure the transcription of this information. Nucleotides are the building blocks of all nucleic acids. The pentose sugars found in nucleic acids give them their names. Ribonucleic acids (RNAs) contain ribose while deoxyribonucleic acids (DNAs) comprise deoxyribose. Nucleosides comprise a sugar and a base as in figure 1.1, whereas nucleotides contain an additional phosphate group as shown in figure 1.2. The base is attached at C-1$'$ of the sugar and the phosphate group may be attached at the C-5$'$ or C-3$'$ or both places. Figures 1.3 and 1.4 show the structures of the five nucleoside bases, their numbering schemes, and Watson-Crick base-pairing.

The structural units of nucleotides consist of three essential components;

a) heterocyclic nitrogen base

i) purines: adenine and guanine

ii) pyrimidines: cytosine, thymine and uracil

b) pentose sugar: ribose in RNA and deoxyribose in DNA

c) phosphate group: anionic $^{-}OPO_3^{2--}$ group

Both DNA and RNA contain adenine, cytosine and guanine, only DNA contains thymine, whereas only RNA contains uracil [17]. Watson and Crick showed that a DNA molecule exists in the form of a double helix. Figure 1.5. The DNA double helix is generated by two strands aligning antiparallel with each other and being held together by specific hydrogen bonding interactions between pairs of bases. The bases are on the inside of the helix, the phosphate and sugars are on the outside. The double helix is highly charged anionic polymer due to the negatively charged phosphate groups. The existence of internal hydrophobic forces and external ionic forces provides great stability to the DNA helix. The dominant base-pairing patterns are the Watson-Crick pairings. In these adenine is paired with thymine (or uracil in RNA) through 2 hydrogen bonds and guanine with cytosine through 3 hydrogen bonds. The structure of RNA is similar to DNA, but with several major exceptions; ribose replaces deoxyribose and uracil replaces thymine, and also RNA is usually a single strand. Several forms of DNA have been described (A to E and Z), but most of them are only observed under extreme conditions. These forms vary in: (1) the distance between base pairs, (2) the number of bases per turn, (3) the diameter of the molecule, (4) the handedness (right or left) of the helix and (5) the sugar ring confomation. The most common DNA conformation is the right handed B-form. The Watson-Crick DNA model has several important features (2,3); two helical chains are coiled around the central axis, the chains are antiparallel, one chain is in the $5^{'}$-$3^{'}$ while the second is in the $3^{'}$-$5^{'}$ orientation. The distance between the base pairs is about 0.34 nm. The double helix contains 10 base pairs in each turn and each turn is about 3.4 nm. The double helix is about 2.0 nm in diameter.

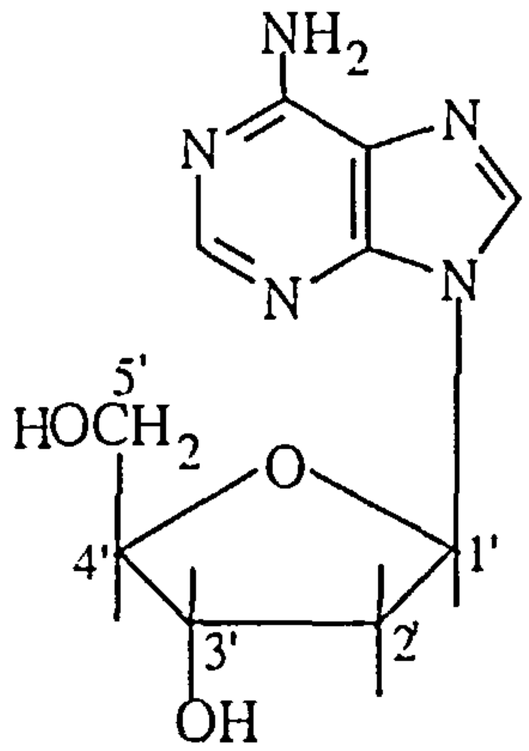

Nucleoside

Figure 1.1.

A nucleoside unit

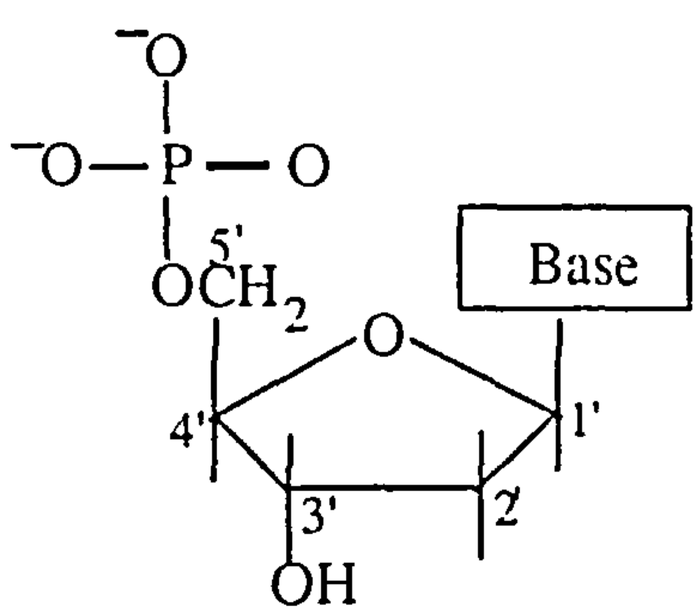

Nucleotide 5-phosphate

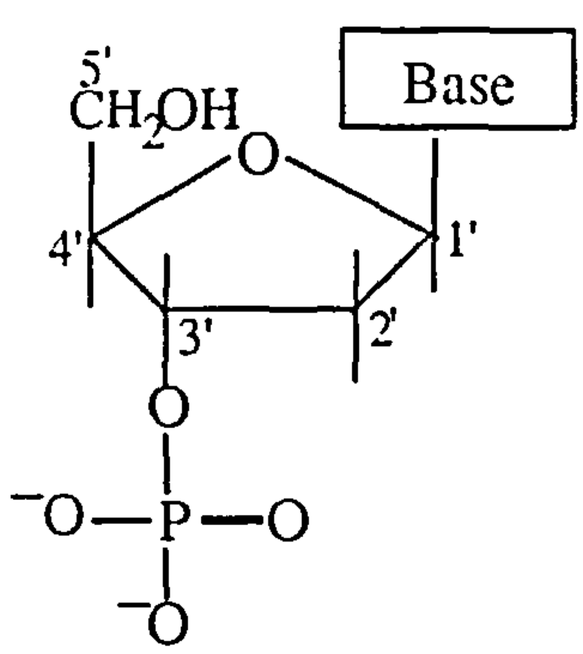

Nucleotide 3-phosphate

Figure 1.2.

Structures of nucleotide units.

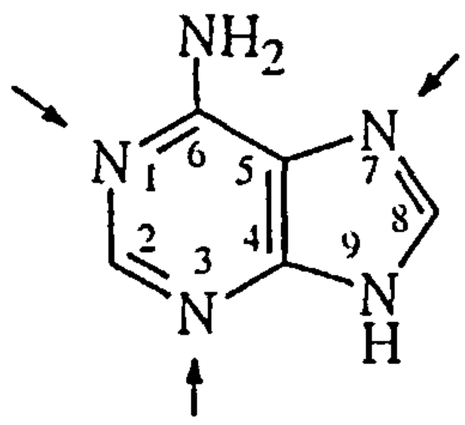

Adenine

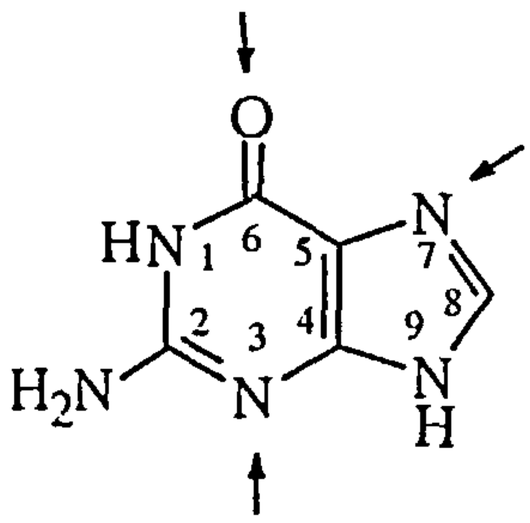

Guanine

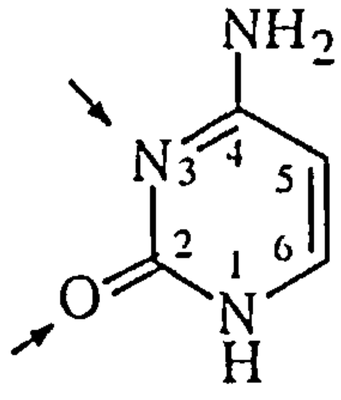

Cytosine

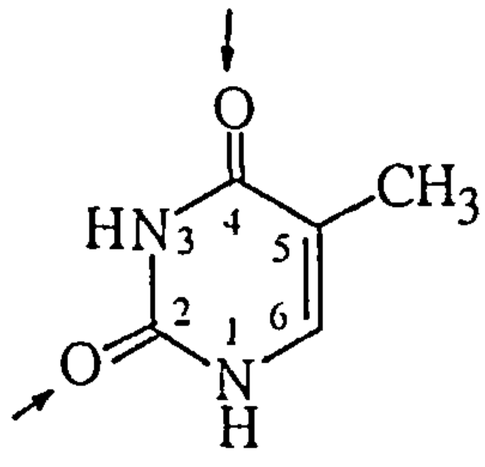

Thymine

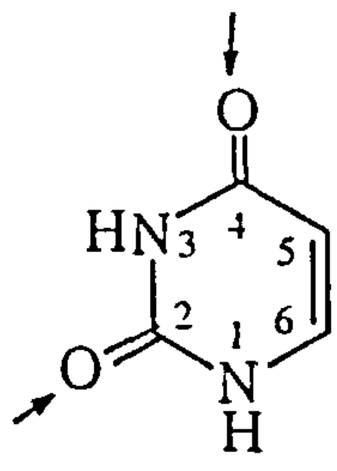

Uracil

Figure 1.3.

Structures and numbering schemes ofbases found in DNA and RNA. Arrows show the most common metal-binding sites on nucleobases [54].

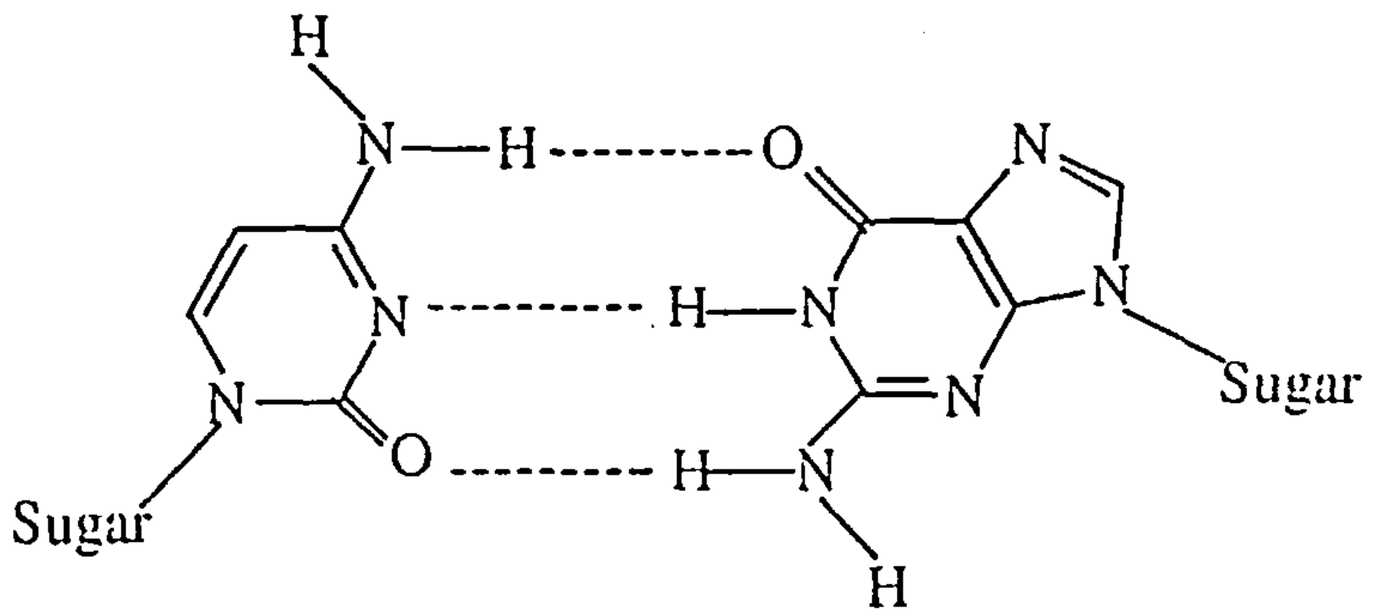

C-G

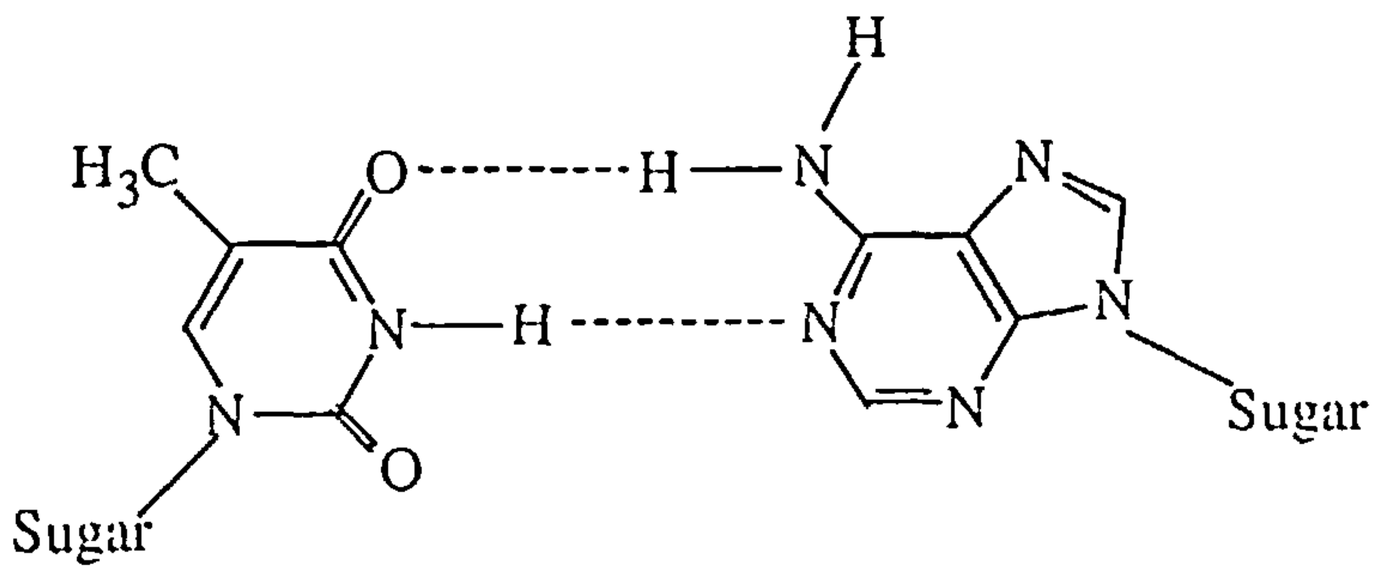

T-A

Figure 1.4.

Watson-Crick base pairing.

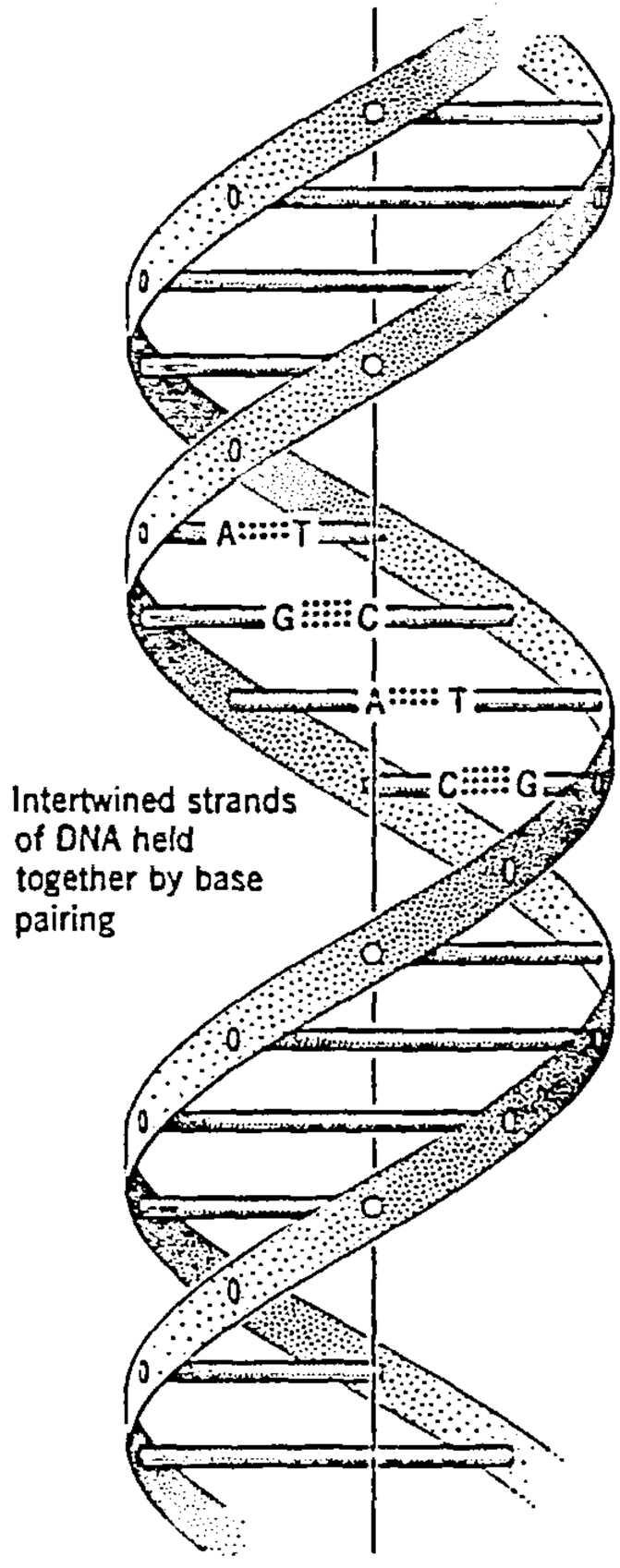

Figure 1.5.

Structure of DNA.

1.3. INTERACTIONS OF METAL COMPLEXES WITH DNA

Many small molecules interact with DNA. These interactions are important because they can effect DNA replication and play a role in obtaining the base sequence in DNA and understanding DNA structure. Some interactions are rather nonspecific, for instance, the stabilization of nucleic acid structures by Na^+ and Mg^{2+} ions through electrostatic interactions that shield the charged phophate groups from one another. There are several modes of interaction. Figure 1.6 shows the sites of metal ion-DNA interaction and possible modes of binding to DNA. The interactions between metal complexes and DNA may be summarised as:

1) Inner sphere binding

2) Outer sphere binding

3) Intercalation

4) Strand breakage

1.3.1. INNER SPHERE BINDING

This mode of interaction involves covalent bond formation between metal complexes and the bases of nucleic acids. A number of complexes containing heavy metals bind to the bases of DNA covalently. The preferred binding sites are N1 of adenine, N3 of cytosine, N7 of adenine and guanine [21]. An important example is the antitumor drug cis-dichlorodiammineplatinum (II) (cis-DDP) which binds covalently to the N7 nitrogen atoms of adjacent guanine residues [16]. The clinical success of cis-DDP and increasing

understanding of its chemistry in the cell is stimulating research into metal-containing antitumor drugs.

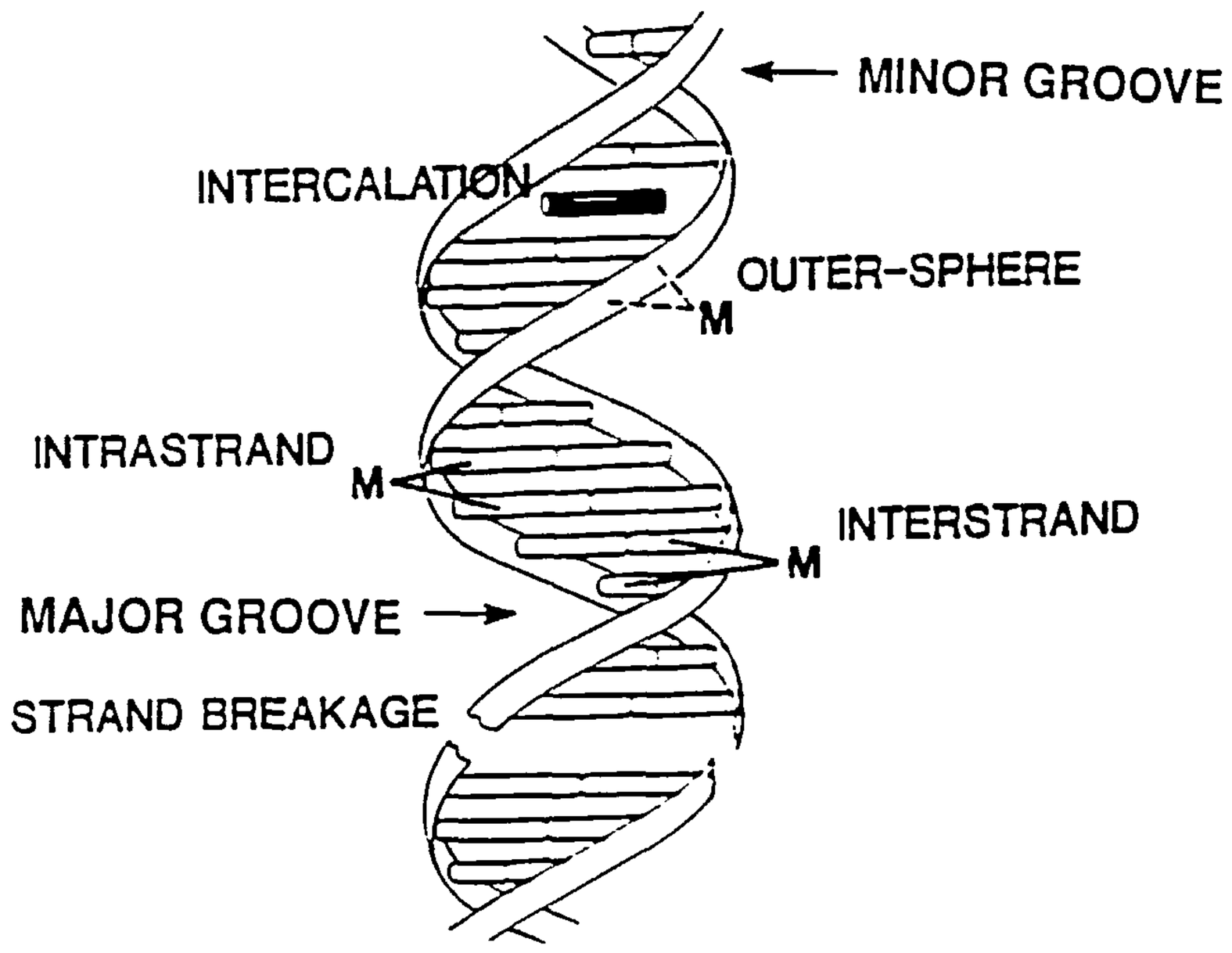

Figure 1.6.

Schematic presentation of the modes of interaction of metal complexes with DNA.

It has also been reported that some octahedral metal complexes with labile ligands such as $Ru(phen)_2Cl_2$ bind to the bases of DNA [22].Another example of similar binding is osmium tetraoxide [17]. In the presence of single stranded DNA osmium tetraoxide binds to thymine. Interaction modes of Pb(II) ions with nucleic acids are much more complicated. At low concentrations Pb(II) binds to phosphate groups, but at high concentrations Pb(II) binds to bases of DNA [23]. It has been shown that there are two different alternatives for Pb(II) base interactions, in the G-C rich regions and A-T [24-28].

A number of aqua metal ions such as mercury and silver also bind to the bases of DNA covalently. In this interaction Hg does not destabilize the helix. This effect is explained by the fact that hydrogen bonds are substituted by Hg which forms very strong cross links with the thymine base (T-Hg-T) [29-31]. Cu(II) and Ag(I) ions have similar behavior. Cu(II) forms metal cross links with thymine and the Ag(I) binds to G-C rich regions stabilizing the helix [29,31], It has also been suggested that Cu(II) binds directly to nuclear bases even at low ion concentration [32]

1.3.2. OUTER SPHERE BINDING

1.3.2.1.Electrostatic interactions

The negatively charged backbone of the DNA helix is able to interact with positively charged molecules, through coulombic interactions or coordination to phosphate via oxygen atoms. The overall charge of the helix is reduced with effects on stability and

conformation. The binding of metals to phosphate groups generally stabilizes the double helix.

In the series Cu(II) < Cd(II) < Zn(II) < Mn(II) < Ni(II) < Co(II) < Mg(II) the affinity for phosphate binding relatively to base complexation increases from the left to the right with Mg(II) being the most stabilizing [33,34]. The inert metal-amine complexes such as $[Co(NH_3)_6]^{3+}$, interact with nucleic acids by an outer-sphere mechanism and the main reaction is considered to be Coulombic attraction. The helix structure can be also stabilized by hydrogen bonding, either directly to phosphate or via water molecules. Such interactions are very effective in stabilizing nucleic acids (35-37]. Hard metal ions such as Mg(II) associate with anionic phosphates and stabilize the double helix [38]. Pb(II) binds to phosphate groups only at a very low ion concentrations [17]. Tris(2,2-bipyridyl) metal complexes associate with phosphate groups [39-41]. $Os(bipy)_3^{2+}$, $Fe(bipy)_3^{2+}$ and $Co(bipy)_3^{3+}$ show electrostatic binding to DNA [42,43].

1.3.2.2.Groove binding

This mode of binding involves direct hydrogen bonding between the groove-binding molecule and the edges of the base-pairs of the DNA helix. Groove-binding can occur in two ways: minor and major groove-binding. Generally, large molecules bind to DNA through major groove, while small molecules usually exhibit binding via minor groove.

Minor groove-binding molecules typically have series of simple aromatic rings such as furan, pyrrole or benzene linked by single bonds to allow rotational freedom. This makes compounds which, with appropriate twist, can fit into the helical curve of the minor groove interacting via hydrogen bonds, electrostatic interaction and Van der Walls forces [18]. In addition to this some groove-binding molecules also have cationic charges to enhance binding through electrostatic binding. Netropsin and distamycin A which belong to the group of pyrrole-amidine antibiotics are minor groove-binders [19]. It has also been reported that the natural antibiotic distamycin containing three N-methylpyrrole carboxamides that binds in the minor groove of double helical DNA with a strong preference for A + T rich regions [44].

On the other hand, a number of DNA binding proteins and oligonucleotides interact primarily with the major groove.

Groove binding molecules typically are crescent shaped molecules with hydrogen-bonding N-H groups on the interior of the crescent. These NH groups form hydrogen bonds with A:T base-pairs in the minor groove rather than similar interactions with G:C base-pairs[20].

1.3.3. INTERCALATION

This interaction involves the insertion of a planar aromatic molecule between neighbouring base pairs of DNA to which it is held by Van der Waals forces. The base

pairs of DNA must separate and the duplex partially unwind to accommodate the planar, aromatic intercalator.

Platinum complexes with aromatic ligands, such as terpyridine and o-phenanthroline, bind to DNA by intercalation. Chelating ligands, such as 1.10 phenanthroline and their metal complexes are also intercalating agents. Zinc complexes, $[ZnCl_2(phen)]$, $[Zn(phen)_2]^{2+}$ and $[Zn(phen)_3]^{2+}$ bind to DNA by intercalation [45]. Tris(1,10 phentroline) ruthenium(II), iron(II) and cobalt(III) complexes have been extensively demonstrated to be intercalators [43,46]. In general, cationic metal complexes possessing planar aromatic ligands bind to DNA by intercalation [47]. Aromatic dyes such as proflavine , acridine and ethidium bromide bind to DNA in an intercalative manner [48,49]. The binding mechanism for simple, classical intercalators such as proflavine is thought to involve two steps. First, the cationic intercalator interacts with the double helix through an external electrostatic complex with the negatively charged backbone of the DNA helix. The intercalator will then diffuse along the surface of the helix until it encounters gaps between pairs of bases which have separated to create a cavity for intercalation. The molecule can then bind in an intercalation complex. Molecules with large side chains require wider openings with significant distortions or breaking of base pair hydrogen bonds before intercalating. It has been reported that the classical intercalators such as acridines and ethidium bromide, stabilize the DNA helix against thermal denaturation [50]. A large number of drugs having planar chromophores binds to DNA. Most of them form a strong, but reversible, non-covalent complex with DNA by intercalating between adjacent pairs of bases. These drugs are powerful probes of nucleic acid structure as well as being clinically useful chemotherapeutic agents. Generation of an intercalation site causes an extention of the DNA helix, local unwinding of the helix and

other possible distortions in the DNA backbone, such as bends, which are charateristics of intercalators. These changes are as a result of the untwisting of the base pairs and helical backbone needed to accommodate the intercalator. Intercalation also results in an ordered stacking of the bound species between base pairs at 0.34 nm separation.

1.3.4. STRAND BREAKAGE

Some natural and synthetic reagents have been found which have the ability to bind to DNA and cause strand cleavage. A metal ion associated with the bound molecule frequently initiates the cleavage reaction and O_2 is involved in some activated form. Strand beakage involves covalent bond cleavage of the helix. DNA binding drugs commonly show their activity by altering the DNA structure, either by inner sphere binding or by introduction of lesions that damage the DNA. Strand breakage, either single or double strand, may be effected by metal complexes which are capable of undergoing redox reactions. Reduction of the metal complex, subsequent reaction of the reduced species with oxygen to produce active $OH^{\bullet}$ produces strand breaks. Most of the DNA cleaving agents consist of metal complexes such as EDTA-Fe(II), bis(phenantroline)Cu(II) and porphyrin-M[M=Fe(III), Mn(III), Co(III) [51,52]. These complexes in presence of molecular oxygen or hydrogen peroxide promote DNA strand breakage. It has been reported that tris(phenantroline)Co(III) at low concentration cleaves DNA [53]. The Distamycin-EDTA-Fe(II) has been found to be a sequence-specific cleaving agent. In the presence of O_2 DE-Fe(II) cleaves the DNA backbone adjacent to a four base pair A + T recognition site [13].

1.4. METHODS TO STUDY BINDING OF METAL COMPLEXES TO DNA

Several methods have been used to examine the interaction of metal complexes with DNA. Binding of metal complexes to DNA, as mentioned previously, can affect the stability of the double helix. A number of techniques investigate these interactions. NMR spectroscopy can be applied to probe binding modes and structural properties of paramagnetic complexes with oligonucleotides [55]. The UV/VIS spectroscopy gives information on overall stability [56]. Circular dichroism is used to study chiral compounds for qualitative information on conformational changes [46]. The quartz crystal microbalance can be used to obtain quantative information by monitoring frequency changes as metal ions interact with immobilised DNA. Electrochemical methods are especially employed for both qualitative and quantitative information via changes in the diffusion current of the metal complex with addition of DNA.

In this thesis, we report the application of electroanalytical methods (cyclic voltammetry, steady-state voltammetry and quartz crystal microgravimetry) to the study of the interaction of metal complexes with nucleic acids.

1.5. REFERENCES

1. L. H. Hurley and D. R. Needham-Vandevanter, *Acc. Chem. Res.*, **1986**, 19, 230.

2. B. Rosenberg, L Van Camp, J. E. Trosko and V. H. Mansour, *Nature*, **1969**, 222, 385.

3. M. J. Clarke, *Met. Ions, Biol. Syst.*, **1980**, 11, 231.

4. M. J. Clarke, in A. E. Martell (ed.) *Inorg. Chem. in Biology and Medicine*, ACS Symposium Series, Vol. 190, Am. Chem. Soc. Washington DC, **1980**, 157.

5. J. J. Roberts and A. J. Thomson, *Progr. Nucl. Acid. Res. Mol. Biol.*, **1979**, 22. 71.

6. M. P. Hacker, E. B. Douple and I. H. Krakoff, eds, *Platinum Coordination Compounds in Cancer Chemotherapy*, Martinus Nijhoff, Boston **1984**.

7. H. Sigel, ed., Nucleotides and Derivatives; their ligating ambivalency, *Metal ions in biological systems*, vol. 8, M. Dekker, New York, **1979**.

8. L. G. Marzilli and G. L. Eichhorn, eds., *Metal ions in Genetic Information Transfer*, New York, Elsevier **1984**.

9. R. B. Martin, *Acc. Chem. Res.*, **1985**, 18, 32.

10. D. J. Hogson, *Prog. Inorg. Chem.*, **1977**, 23, 211.

11. J. H. Griffin and P. B. Dervan, *J. Am. Chem. Soc.*, **1987**, 109, 6840.

12. M. W. Van Dyke and P. B. Dervan, *Biochemistry*, **1983**, 22, 2373.

13. P. G. Shultz and P. B. Dervan, *J. Am. Chem. Soc.*, **1983**, 105, 7748.

14. R. S. Youngquist and P. B. Dervan, *J. Am. Chem. Soc.*, **1985**, 107, 5528.

15. J. K. Barton, *Science*, **1986**, 233, 727.

16. J. K. Barton, *Comm. Inorg. Chem.* **1985**, 3, 321.

17. J. Swiatek, *J. Coord. Chem.*, **1994**, 33, 191.

18. G. M. Blackburn and M. J. Gait, *in Nucleic Acids in Chemistry and Biology*, IRL Press, New York, **1990**.

19. C. Zimmer and U. Wahnert, *Prog. Biophys. Mol. Biol.*, **1986**, 47, 31.

20. M. L. Kopka, C. Yoon, D. Goodsell, P. Pjura and R. E. Dickerson, *Proc. Nat. Acad. Sci.*, **1985**, 82, 1376.

21. J. K. Barton and S. J. Lippard, *Metal ions in biology*, **1980**, 1, 31.

22. J. K. Barton and E. Lolis, *J. Am. Chem.*, **1985**, 107, 708.

23. J. K. Barton, *Inorg. Chim. Acta*, **1985**, 106, L1.

24. A. C. Lepre and S. J. Lippard, *Nucl. Acid Mol. Biology* (F. Eckstein and D. M. Lilley, eds., Springer Verlag, Berlin **1990**) Vol 4, p 9.

25. J. Swiatek and B. Gulanowski, *Acta Biochim.*, **1990**, 37, 7.

26. H. A. Tajmir-Riahi, M. Longlais and R Savoic, *Nucl. Acid Res.*, **1988** 16, 751.

27. J. Swiatek, E. Koglin and J-M. Sequaris, *Proc.II Symp. Inorg. Biochem. and Mol. Biphys.* Karpacz, **1989**, 335.

28. J. Widom and R. L. Boldwin *Biopolymers*, **1983**, 32, 1621.

29. W. Seanger, *Principles of Nucl. Acid Strc.*, New York, **1994**.

30. I. Jissoeff, J. Grisward and E. Guille *Prog. Biophys. Mol. Biol.*, **1976**, 31, 165.

31. M. W. Lieberman, D. J. Harvan, D. E. Amacher and J. B. Patterson, *Biochem. Biophys. Acta*, **1976**, 425, 265.

32. T. Pawlowski, J. Swiatek, K. Gasiorowski and H. Kozlowski, *Inorg. Chim. Acta.*, **1987**, 136, 185.

33. G. L. Eichhorn, *Nature.*, **1962**, 194, 474.

34. G. L. Eichhorn and Y. A. Shin, *J. Am. Chem. Soc.*, **1968**, 90, 7323.

35. F. Ascoli, M. Branca, C. Mancini and B. Pispisa *J. Chem. Soc. Faraday Tras.*, **1972**, 1213.

36. R. L. Karpel, N. S. Miller, A. M. Lesk and J. R. Fresco, *J. Mol. Biol.*, **1975**, 144, 519.

37. J. Widom and R. L. Boldwin, *J. Mol. Biol.*, **1980**, 144, 431.

38. J. K. Barton, *Prog. Inorg. Chem.*, **1990**, 38, 413.

39. J. M. Kelly, A. G. Tossi and D. J. Mc Connel, *Nuc. Acid. Res.*, **1995**, 13, 6017.

40. C. V. Kumar, J. K. Barton and N. J. Turro, *J. Am. Chem. Soc.*, **1985**, 107, 5518.

41. T. Hard and B. Norden, *Biopolymers*, **1986**, 25, 1209.

42. M. Rodriquez and A. J. Bard, *Anal. Chem.*, **1990**, 62, 2658.

43. M. T. Carter, M. Rodriquez and A. J. Bard, *J. Am. Chem. Soc.*, **1989**, 111, 8901.

44. P. G. Schultz and P. B. Dervan, *J. Am. Chem. Soc.*, **1982**, 104, 6861.

45. J. K. Barton, J. J. Donnenberg and A. L. Raphael, *J. Am. Chem. Soc.*, **1982**, 104, 4967.

46. J. K. Barton, A. T. Denishefsky and J. M. Goldberg, *J. Am. Chem. Soc.*, **1984**, 106, 2172.

47. S. J. Lippard, *Acc. Chem. Res.*, **1978**, 11, 211.

48. L. S. Lerman, *J. Mol. Biol.*, **1961**, 3, 18.

49. W. Fuller and M. J. Waring, *Ber. Bunsenges, Phys. Chem.*, **1964**, 68, 805.

50. M. J. Waring, *Symp. Soc. Gen. Microbiol.*, **1966**, 16, 235.

51. P. D. Dervan, *Science*, **1986**, 232, 464.

52. D. S. Sigman, D. R. Graham and V. D. Aurara, *J. Biol. Chem.*, **1979**, 254, 12269.

53. J. K. Barton and A. L. Raphael, *J. Am. Chem. Soc.*, **1984**, 106, 2466-2468.

54. S. J. Lippard and J. M. Berg, *Principles of Bioinorganic Chemistry*, University Science Books, **1994**, USA.

55. J. P. Rehmann and J. K. Barton, *Biochemistry*, **1990**, 29, 1701.

56. Nicolas Farrel, *Transition Metal Complexes as Drugs and Chemotherapeutic Agents*, Kluver Academic Publishers, USA, **1989**.

CHAPTER TWO

THEORETICAL FUNDAMENTALS OF ELECTROCHEMICAL AND ANALYTICAL TECHNIQUES USED IN THIS THESIS

Several techniques were applied to the study of the interaction of metal complexes with nucleic acids both in solution and on the surface. A brief description of these techniques is given in this section. More details may be found elsewhere [1-4].

2.1. GENERAL FEATURES OF VOLTAMMETRY

Voltammetry consists of a group of electroanalytical techniques which is based upon the measurement of current as a function of potential. Voltammetry is widely used for the fundamental studies of oxidation and reduction processes in various media, adsorption processes on surfaces and electron-transfer mechanisms at chemically modified electrode surfaces. In this technique, a potential is applied across the working electrode-solution interface to oxidize or reduce species present in solution, and the current which results from the oxidation and reduction of the species is plotted as a function of potential. The voltammogram obtained is related to the chemical identity of the redox species and its concentration [5-7]. Thus, voltammetry provides both a qualitative and quantitative determination of electroactive species. Three electrodes are generally used; the working electrode at which the redox reaction takes place, the reference electrode through which no current flows, and the counter electrode which completes the circuit. The three electrodes are connected through a potentiostat which provides the desired potential between the working electrode and reference electrode and that the counter electrode is

kept at a sufficient potential to drive the appropriate oxidation or reduction to balance the current produced at working electrode [8]. In the case of microelectrodes (electrodes of μm dimension) the currents area of the order of nA and the reference electrode potential is not perturbed by the current. The circuit can then be simplified to a two electrode system where the reference also functions as a counter electrode [9].

2.1.1 CYCLIC VOLTAMMETRY (CV)

Cyclic voltammetry (CV) is one of the most convenient electroanalytical techniques for the study of electroactive species in solution and on surfaces. This technique is used principally to characterize the redox properties of compounds and to study the mechanisms of redox reactions.

Cyclic voltammetry consists of cycling the potential of the working electrode and the resulting current is recorded as a function of potential to give a cyclic voltammogram. This gives information about electrochemical reactions occuring at the electrode surface. The potential of the working electrode is controlled versus a reference electrode via a potentiostat. The controlling potential applied across these two electrodes can be considered as an excitation signal. The excitation signal for CV is a linear potential scan with a triangular waveform as illustrated in figure 2.1. The voltage applied to the working electrode is scanned linearly from an initial value, E_1, to a predetermined limit, E_2, where the direction of the scan is reversed.. The current response is plotted as a function of the applied potential.

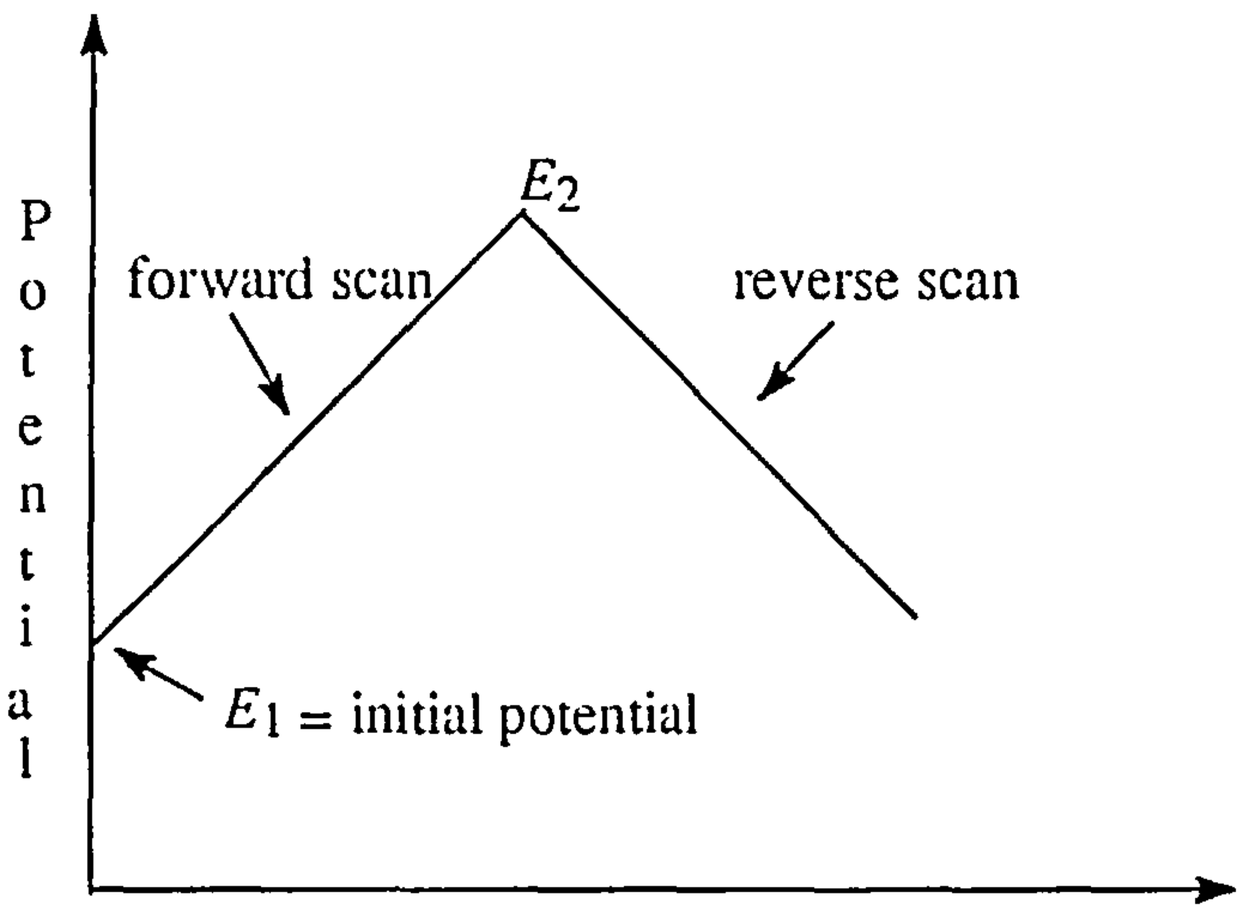

Figure 2.1.

Typical excitation signal for cyclic voltammetry-a triangular potential waveform.

2.1.1.1. Solution Processes

A typical cyclic voltammogram is shown in figure 2.2 for a platinum working electrode in a solution containing 0.5 mM $Ru(NH_3)_6^{+3}$ in 10 mM Tris buffer pH 7. As the potential is scanned in the negative direction, on the forward scan, the current rises to a peak. When the potential is sufficiently negative to reduce $Ru(NH_3)_6^{+3}$, cathodic current is produced due to the electrode process . The cathodic current rises rapidly until the concentration of $Ru(NH_3)_6^{+3}$ at the working electrode surface is diminished and a cathodic peak appears. The current then decays with time. The scan direction is switched to positive at -0.5 V for the reverse scan. When the electrode becomes a sufficiently strong oxidant, $Ru(NH_3)_6^{+2}$ can be oxidized at the electrode. The anodic current rapidly increases until the surface concentration of $Ru(NH_3)_6^{+2}$ is diminished. causing the anodic peak. The current

then starts decaying, because the solution which is surrounding the working electrode is depleted of $Ru(NH_3)_6^{+2}$. The first cycle is completed when the potential reaches 0.1 V. Simply stated, in the forward scan $Ru(NH_3)_6^{+2}$ is electrochemically generated from $Ru(NH_3)_6^{+3}$ as indicated by the cathodic current. In the reverse scan this $Ru(NH_3)_6^{+2}$ is oxidized back to $Ru(NH_3)_6^{+3}$ as indicated by the anodic current. The magnitudes of the anodic peak current, i_{pa}, and cathodic peak current, i_{pc}, and the anodic peak potential, E_{pa}, and cathodic peak potential, E_{pc}, are the important parameters of a cyclic voltammogram.

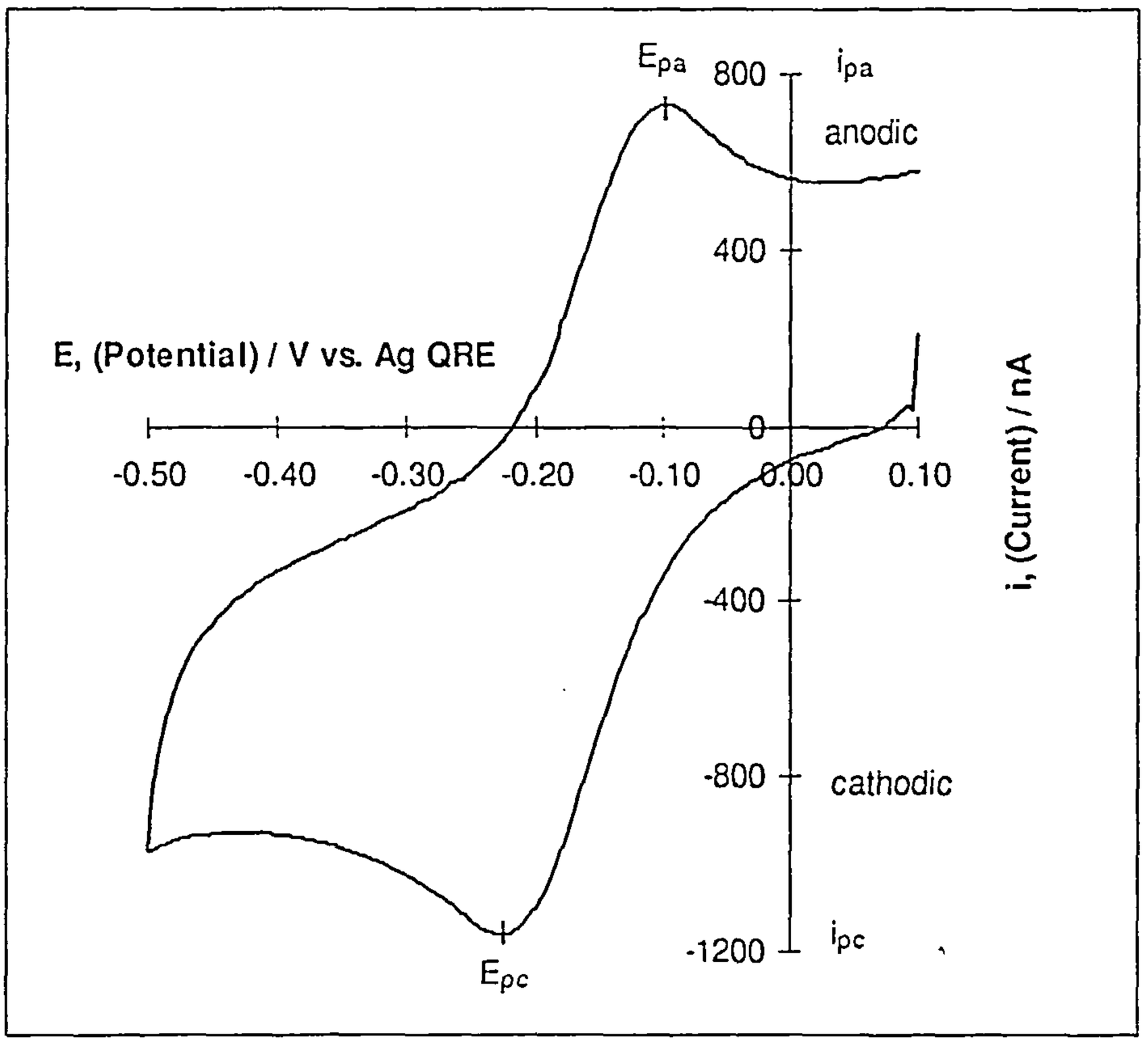

Figure 2.2.

Cyclic voltammogram of 0.5 mM $Ru(NH_3)_6^{+3}$ in 10 mM Tris buffer pH 7. Scan initiated at *ca.* 0.1 V versus Ag QRE (Quasi reference electrode) in negative direction at 50 mVs^{-1}. Platinum electrode, area 0.0785 cm^{-2}.

A reaction in which both species rapidly exchange electrons to maintain the concentrations of the oxidized and the reduced forms in equilibrium with each other at electrode surface is termed a reversible electrode process. The simplest electrode reaction can be described as follows:

$$O + ne^- \rightleftharpoons R.$$

In this reaction, both species O and R are completely stable and soluble in the electrolysis medium containing an excess of an electrolyte which is electroinactive. The equilibrium ratio at a given potential is determined by the Nernst Equation:

$$E = E^{0'} - \frac{RT}{nF} \ln\left(\frac{[R]}{[O]}\right) \qquad (2.1)$$

where O is the oxidized form and R is the reduced form. The formal reduction potential for a reversible system is centered between E_{pa} and E_{pc}

$$E^{0'} = \frac{E_{pa} + E_{pc}}{2} \qquad (2.2)$$

The anodic peak and cathodic peak currents have equal magnitudes in a reversible process

$$\frac{i_{pa}}{i_{pc}} = 1 \qquad (2.3)$$

In a reversible reaction, the separation of the peak potentials, ΔE_p, is

$$\Delta E = E_{pa} - E_{pc} = \frac{59}{n} mV \qquad (2.4)$$

where E_{pa} is the anodic peak potential and E_{pc} is the cathodic peak potential, n is the number of electrons transfered.

The peak current for a reversible process is given by the Randles-Sevcik equation for the forward sweep of the first cycle

$$i_p = (2.69 \times 10^5) n^{3/2} A D^{1/2} C \nu^{1/2} \qquad (2.5)$$

where i_p is peak current (amperes), n is number of electrons transferred in the process, A is electrode area (cm^2), D is diffusion coefficient (cm^2/s), C is concentration (mol/cm^3), and ν is the scan rate (V/s). According to this equation, i_p is proportional to $\nu^{1/2}$ and directly proportional to concentration.

For a reversible system, a plot of i_p as a funtion of $\nu^{1/2}$ is both linear and passes through the origin. A complete list of diagnostic tests for cyclic voltammograms of reversible systems is given below [1].

Consequently, a reversible cyclic voltammogram can only be observed if both O and R are stable and electron transfer is fast and electron transfer process on the surface is in equilibrium, so that surface concentrations satisfy the Nernst Equation.

REVERSIBLE

1. $\Delta E_p = E_{pa} - E_{pc} = 59/n$ mV
2. $\lvert E_p - E_{p/2} \rvert = 59/n$ mV
3. $\lvert i_{pa} / i_{pc} \rvert = 1$
4. $i_p \alpha \nu^{1/2}$
5. E_p is independent of ν
6. At potentials beyond E_p , $i \alpha t^{-1/2}$

In the case of quasi-reversible systems, the separation in the peak potentials is greater than *59/n mV* and E_{pc} shifts negatively with increasing sweep rate. Diagnostics for cyclic voltammograms of quasi-reversible systems are given below [1].

QUASI REVERSIBLE

1. i_p increases with $\nu^{1/2}$ but is not proportional to it
2. $\lvert i_{pa}/i_{pc} \rvert = 1$ if $\alpha_c = \alpha_a = 0.5$
3. $\Delta E_p > 59/n\ mV$ and increases with ν
4. E_{pc} shifts negatively with incresing ν

Irreversibilty is caused by slow electron exchange of the redox species with the working electrode. In this case, there is no reverse peak and i_{pc} is proportional to sweep rate and E_{pc} varies with sweep rate. Irreversible voltammograms can result from decomposition of *R* or *O* during the scan via chemical reactions.

2.1.1.2. Surface processes

So far the discussion of cyclic voltammetry has assumed that all reactants and products are freely soluble in the solution. Cyclic voltammetry has also proved useful for quantitative investigation of reactions involving adsorption processes. In this case, a reaction involving adsorption is that where only the adsorbed species, O and R, are electroactive in the potential range under investigation. In a reversible redox process of adsorbed species compared to a voltammogram for a reaction in which both product and reactant are in solution, the peaks are sharp and symmetrical, the current rising from zero to a peak value and then falling again to zero, and there is no peak separation ($E_{pa} = E_{pc}$). The peak current is proportional to the sweep rate, and not its square root. Also the charges under the anodic and the cathodic peaks are equal. The peak current density is given by equation

$$i_p = \frac{n^2 F^2 \Gamma_0}{4RT\ v} \qquad (2.6)$$

where Γo is the surface excess of O before the start of the sweep. The area under the cathodic peak Q corresponds to the charge associated with the reduction of the adsorbed layer of O and this enables the surface excess of O to be determined by equation

$$\Gamma_0 = \frac{Q}{nF} \qquad (2.7)$$

In case of quasi-reversible reactions there will be a reverse peak but both peaks will be asymmetric and the peak potentials will not be coincident. For an irreversible reaction the forward peak ceases to be symmetric and there is no reverse peak.

2.1.2. VOLTAMMETRY AT MICROELECTRODES

This section deals with the properties of voltammetric electrodes of micrometre dimensions. It has been demonstrated that many changes occur in voltammetric behavior, as the dimensions of electrodes become smaller. The advantageous properties of electrodes with very small dimensions were recognised a long time ago, but research in the area of microvoltammetry did not become very active until the late 1970s [10]. The improvements made in electronics, especially in the measurement of very small currents, and the occurrence of microstructural materials provided the tools that were necessary to make and use microelectrodes [11]. There have been many reports dealing with studies of microelectrodes and exploiting their advantageous properties over conventional size electrodes such as steady state diffusion-limited current, minimized ohmic drop and increased current density [10,12-14]. Previously impossible experiments have become possible with microelectrodes. Microelectrodes also provide some other advantages: redox processes can be examined at very positive and very negative potentials [15] and electrochemical measurements can be made in the absence of added supporting electrolyte [16]. Microdisc electrodes have been shown to provide the potential for considerably greater analytical sensitivity than large electrodes [12], i.e., the ratio of faradaic current to charging current is larger for microelectrodes than for large electrodes [17,18]. The rate of mass transport rises, as the electrode size gets smaller. As a result of reduced charging

current and increased mass transport rate, microelectrodes show good signal-to-noise (S/N) characteristics [18]. Disc-shaped microelectrodes also permit electrode reactions to be investigated at very fast scan rates due to reduced ohmic drop [13,14,19-26]. Since the current is very small, ohmic drop is reduced and polarization of the reference electrode is not important; microelectrode voltammetry is often carried out with a two-electrode system [17].

2.1.3. STEADY-STATE VOLTAMMETRY (SSV)

Steady-state voltammetry [27] is the simplest form of voltammetry and offers a number of advantages over the more familiar transient voltammetric techniques. Voltammetric steady states are naturally attained at small electrodes having convergent diffusion geometries provided that all the linear dimensions of microelectrode are less than about 50 μm. A feature of steady-state voltammetry is that the current vs. potential relationship is totally independent of the experimental method used to achieve the steady state. The most popular method for recording steady state voltammograms uses the same potential waveform used in cyclic voltammetry: a slow, linear sweep to negative potentials (for a reduction), followed by a reverse scan. The resulting voltammogram is, however, very different from a classical cyclic voltammogram. The voltammogram has the sigmoidal shape characteristic of a steady state voltammogram and should retrace itself provided that the sweep rate is slow enough, as in figure 2.3. If the sweep rate is not quite slow enough, there will be gap between the two current branches as in figure 2.4. Since the waves during the forward and backward potential scans are non-coincident, the forward current will be larger, at a given potential, than the backward current. Steady state voltammetry where the

response is time independent actually provides minimal ohmic drop [28,29]. As well as minimal ohmic drop being observed at steady state, the background current due to double layer charging also approaches zero. Thus, steady state measurements can easily be carried out at low concentrations of analyte with only minimal interference from background current. Steady state measurements with reduced ohmic drop and minimal background current are inherently more attractive if high precision is required.

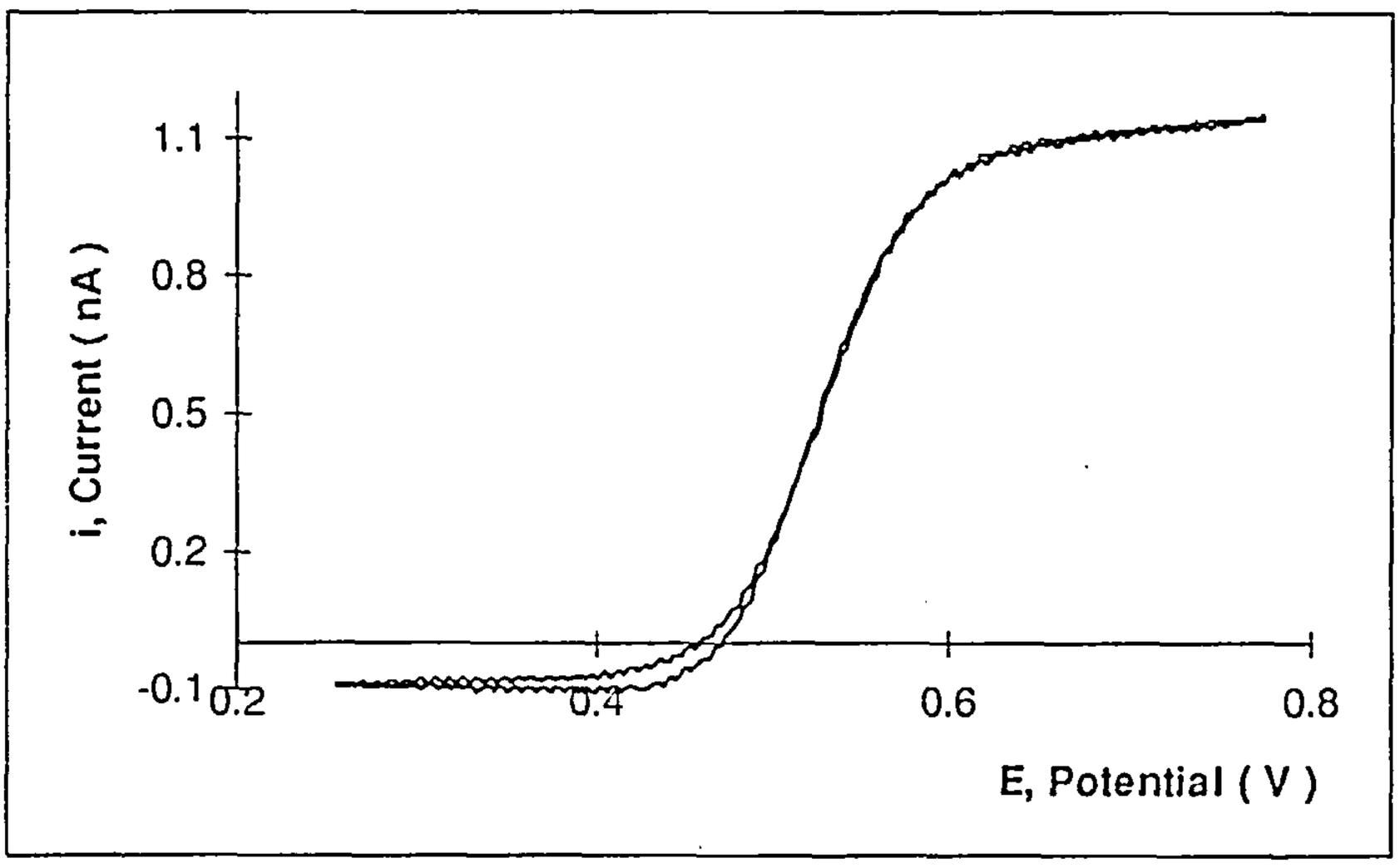

Figure 2.3.

A steady-state voltammogram in which the two branches of current retrace itself.

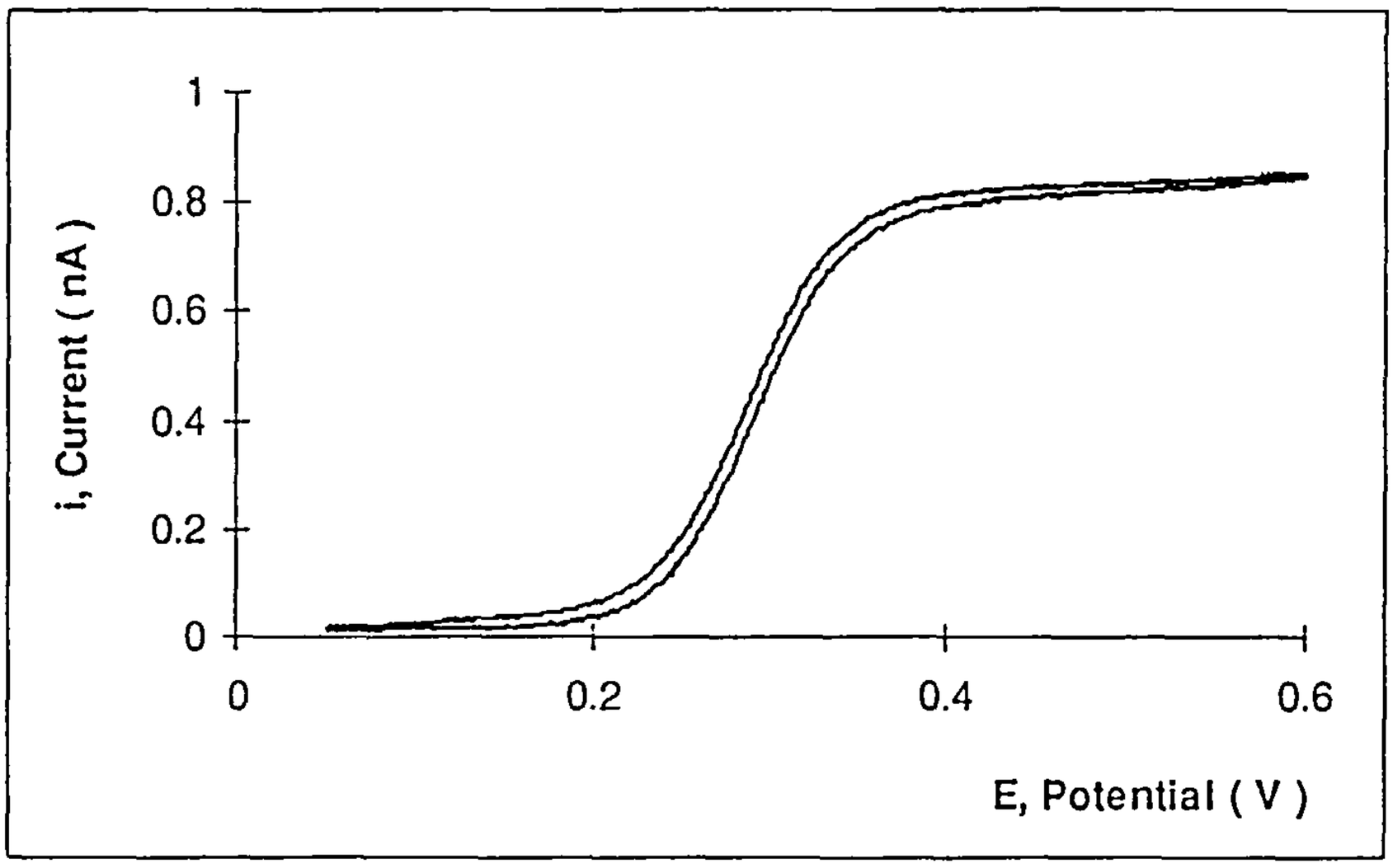

Figure 2.4.

A near steady-state voltammogram showing the gap between two branches of current.

2.1.4. STEADY-STATE MICROELECTRODE EXPERIMENTS

The length of time required to attain steady state is determined by the size of the electrode and the convergent transport field which is essential to sustain the steady state is provided by the shape of the electrode. Geometries of three common microelectrodes that attain steady state are illustrurated in Figure 2.5 as (a) inlaid disc. (b) inlaid ring and (c) hemispherical [30,31].

A hemispherical electrode possessing uniform accessibility is resting on a plane and all parts of the electrode surface behave similarly. The plane which the hemispherical electrode is resting on, forces diffusion to occur radially, even at the junction between the

electrode and its surrounding insulator. It is difficult, but possible to fabricate microhemispherical electrodes from solid metals. Mercury hemispheres electroplated onto inlaid discs of solid metal [19,32-34] or carbon [35-37] have been used in almost all experimental studies of hemispherical microelectrodes.

The phrase *inlaid disc* describes a section of wire or fibre, the electrode material, imbedded in a surrounding insulator. The junction between the electrode marerial and its surrounding insulation is called the *edge* of the electrode. At this edge, diffusion occurs radially and is enhanced with respect to the diffusion to the centre of the electrode. The construction of disc microelectrodes is very simple. Inlaid disc microelectrodes can be prepared by sealing fine wires into glass tubes, followed by polishing. Platinum, gold and carbon are commonly used electrode materials with electrode radii down to 0.5 μm for both platinum and gold and 2 μm for carbon microdisc electrodes [38].

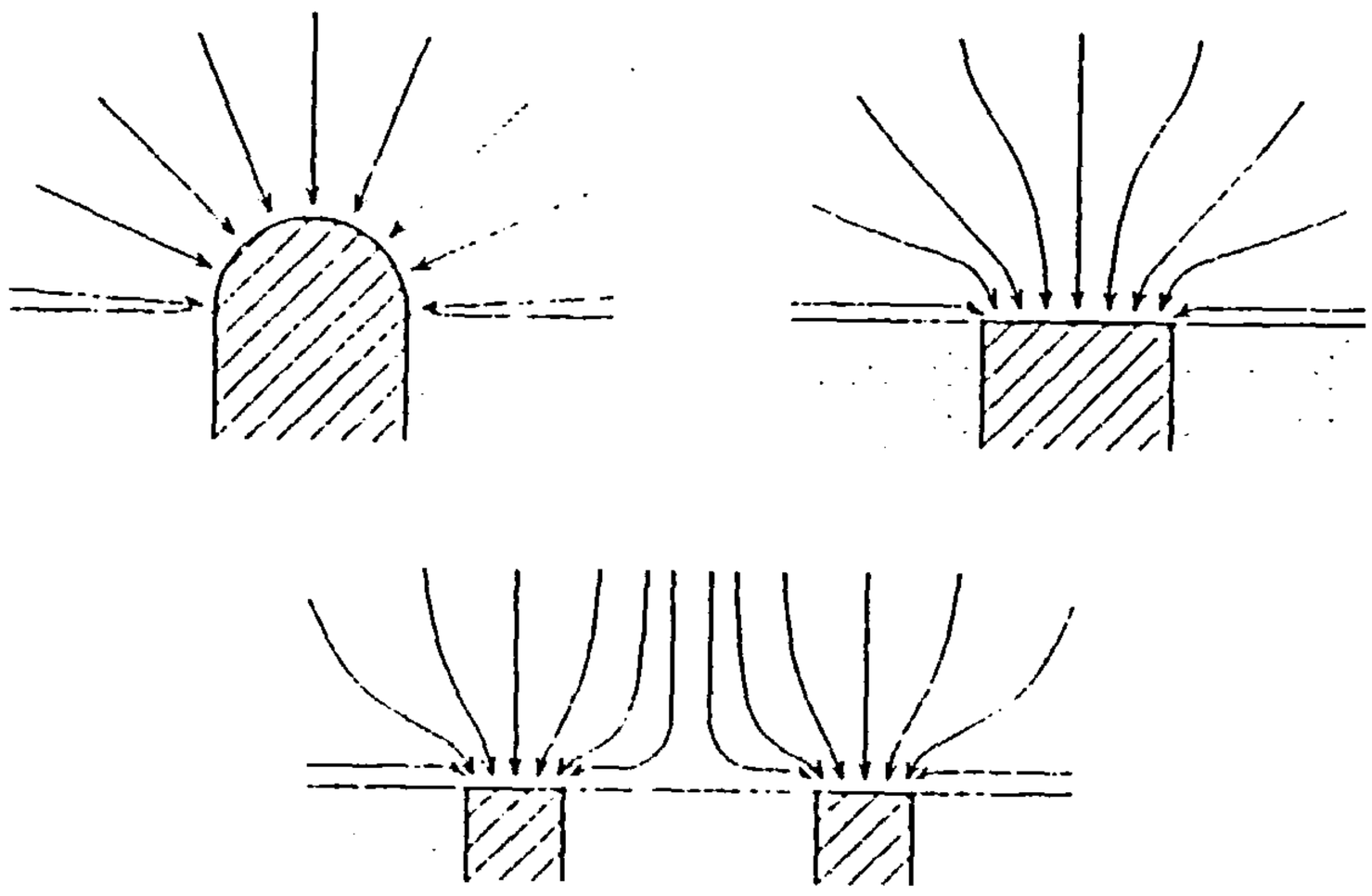

Figure 2.5.

Geometries of most common microelectrodes.

Ring microelectrodes are fabricated by applying a conductor to the walls of an insulating cylindirical support [9,39-42]. Commonly the insulating support is a glass rod [42]. The insulating ring can be painted with organometallic compounds [9,39-42] or coated by vapour deposition or sputtering of metal onto a rotating glass rod [39]. Both platinum and gold rings can be prepared by this method. The coated support is then insulated from solution by sealing into a larger glass tube with epoxy resin or by collapsing the glass around the rod. The structure is then polished to expose the inlaid ring. Carbon ring electrodes with tip diameters as small as 1 μm have been fabricated. The exposed ring is surrounded by an insulator, both interior and exterior to the ring, which forms a geometric continuation of the electrode plane. There are two edges to consider: one formed by an inner radius and the other by an outer radius. Diffusion occurs radially at both of the edges of a thin ring.

Steady state current under diffusion-controlled conditions is supported by both hemispherical and disc microelectrodes, but there is a difference in distribution of current for these two electrodes: the surface of the hemisphere has a uniform current, whereas the current over the disc is nonuniform. Current density is proportional to r^{-1} for both hemisphere and disc microelectrodes.

$$I \alpha \frac{1}{r} \tag{2.8}$$

where I is the current density. The time to reach steady state after a potential step for a disc microelectrode is

$$t_{ss} \equiv \frac{(5r)^2}{2D} \tag{2.9}$$

The steady state diffusion limiting current at a disc microelectrode is

$$i_{lim} = 4nFDCr \tag{2.10}$$

2.1.5. STEADY-STATE DIFFUSION AT MICROELECTRODES

During an electrochemical process, a concentration gradient is generated between the surface of an electrode and solution. Thus, the current which is measured at all voltammetric electrodes depends upon the modes of mass transport that are operating in the electrolysis medium. Diffusion is the predominant mode of mass transport at microelectrodes [10]. Since the dimensions of the diffusion layer can exceed the dimensions of the microelectrode, voltammograms obtained at microelectrodes are different from those obtained at large electrodes depending on the time scale of the experiment. The diffusion layer is the region adjacent to the electrode surface where the concentrations of the species are different from those in the bulk. The main factor which determines the shape of the voltammogram and magnitude of the faradaic current through this region is mass transport. The current reaches steady state at values of $Dt/r_o^2 >> 1$ where r_o is the smallest dimension of the electrode, t is the time, and D is the diffusion coeffient of the species. Since the dimensions of the diffusion layer under these conditions exceed the dimensions of the electrode the volume from which molecules diffuse to support current is large. Voltammograms obtained under condition of small values of

Dt/r_o^2 where the dimensions of electrode are larger than the dimensions of the diffusion layer have the peak-shaped behavior seen at large electrodes and faradaic current is proportional to the electrode area. The electrochemical processes that take place at hemispherical electrodes exemplify several factors which happen at other geometries of microelectrode.

The concentration profiles at large and small electrodes are shown in figure 2.6. The concentration profile keeps extending into solution as a function of time for planar diffusion. Whereas, the growth of the region, the diffusion layer, at small hemispherical electrodes is initially similiar to those observed at a planar electrode, but at longer times the growth slows considerably.

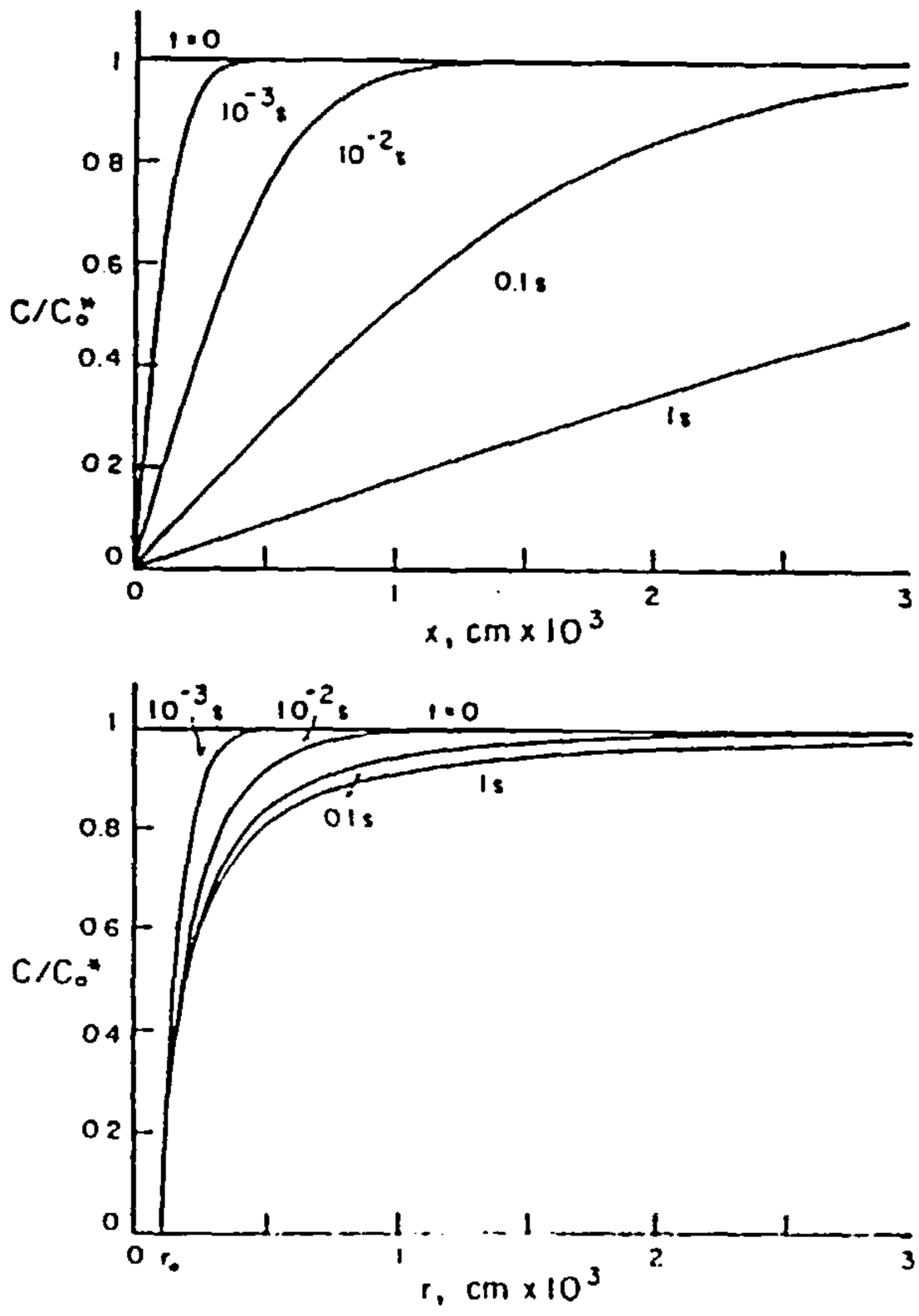

Figure 2.6.

Concentration profiles at large and small electrodes.

At short times the dimensions of the diffusion layer are smaller than the dimensions of the electrode and the electrode appears as a large planar surface to a molecule at the farthest point of the diffusion layer as illustrated in figure 2.7. However, when the dimensions of the diffusion layer becomes larger than the dimensions of the electrode, the population of molecules feeding the electrode comes from a solid angle which contains an ever increasing volume. Thus, the number of electroactive molecules that have access to a spherical electrode exceeds that of a planar electrode.

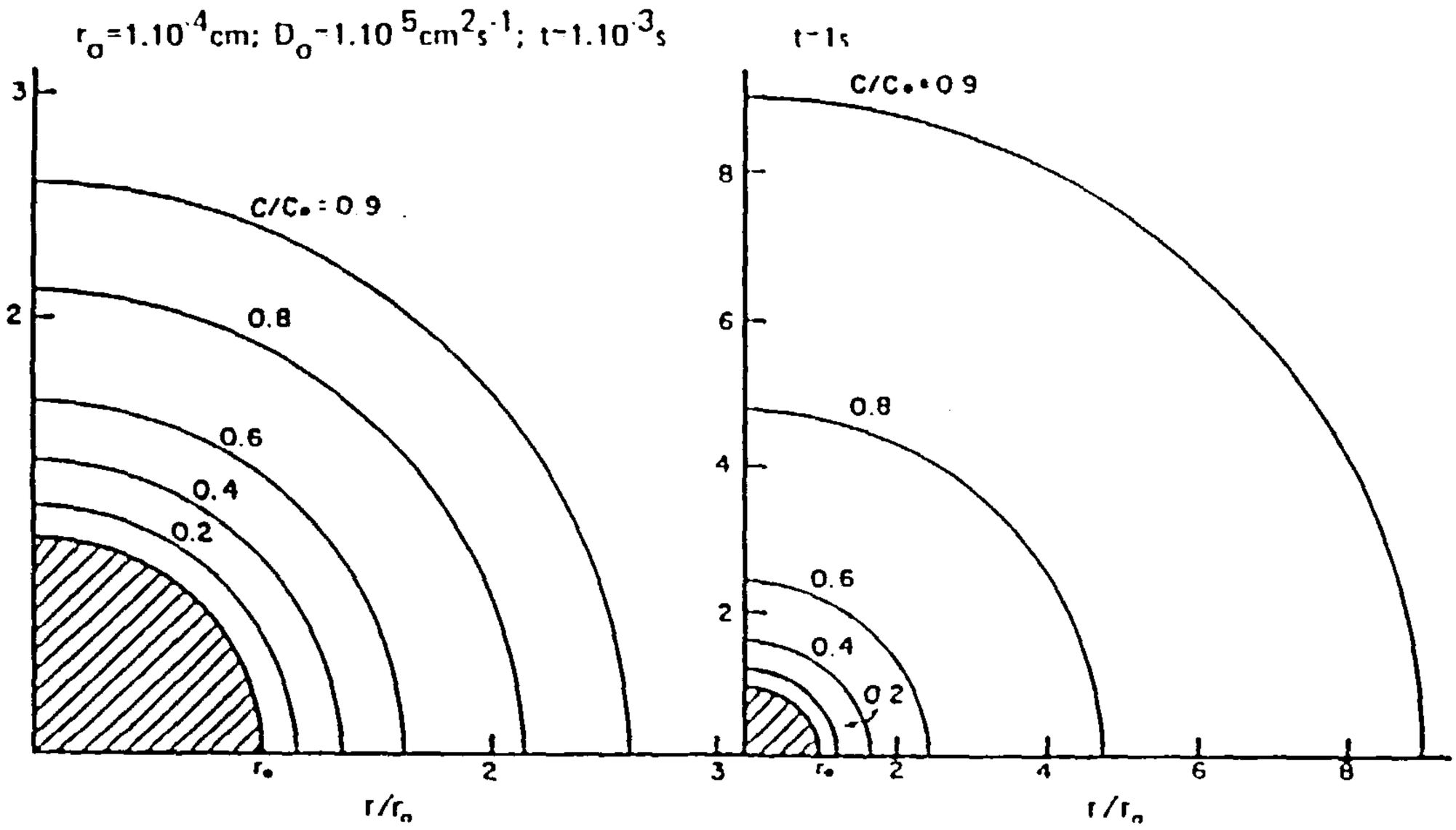

Figure 2.7.

Diffusion layer profiles for a hemispherical electrode.

The following equation gives the current at a hemispherical electrode and describes the relationship between the current and time [43].

$$i\,(t) = i\,(\infty)\,[1 \div r\,/(\pi Dt)^{1/2}] \qquad (2.11)$$

The steady state diffusion limited current for a hemisphere electrode [19] is given by equation (2.12)

$$i_{lim} = 2\pi nFDCr. \qquad (2.12)$$

At a disc microelectrode for a reversible process, the relationship between the current and time is [43-45];

$$i\,(t) = i\,(\infty)\,[1 \div 2r/(\pi Dt)^{1/2}\ ]. \qquad (2.13)$$

The steady state diffusion limited current for a microdisc electrode is expressed by equation [46].

$$i_{lim} = 4nFDCr. \qquad (2.14)$$

As seen from the diffusion-layer profile under steady state conditions in figure 2.8 for a disc electrode the steady state solution is seen to be of a form similar to that for a hemispherical electrode. Table 2.1. shows the dependence of the time required to reach a steady state at hemispherical and disc microelectrodes.

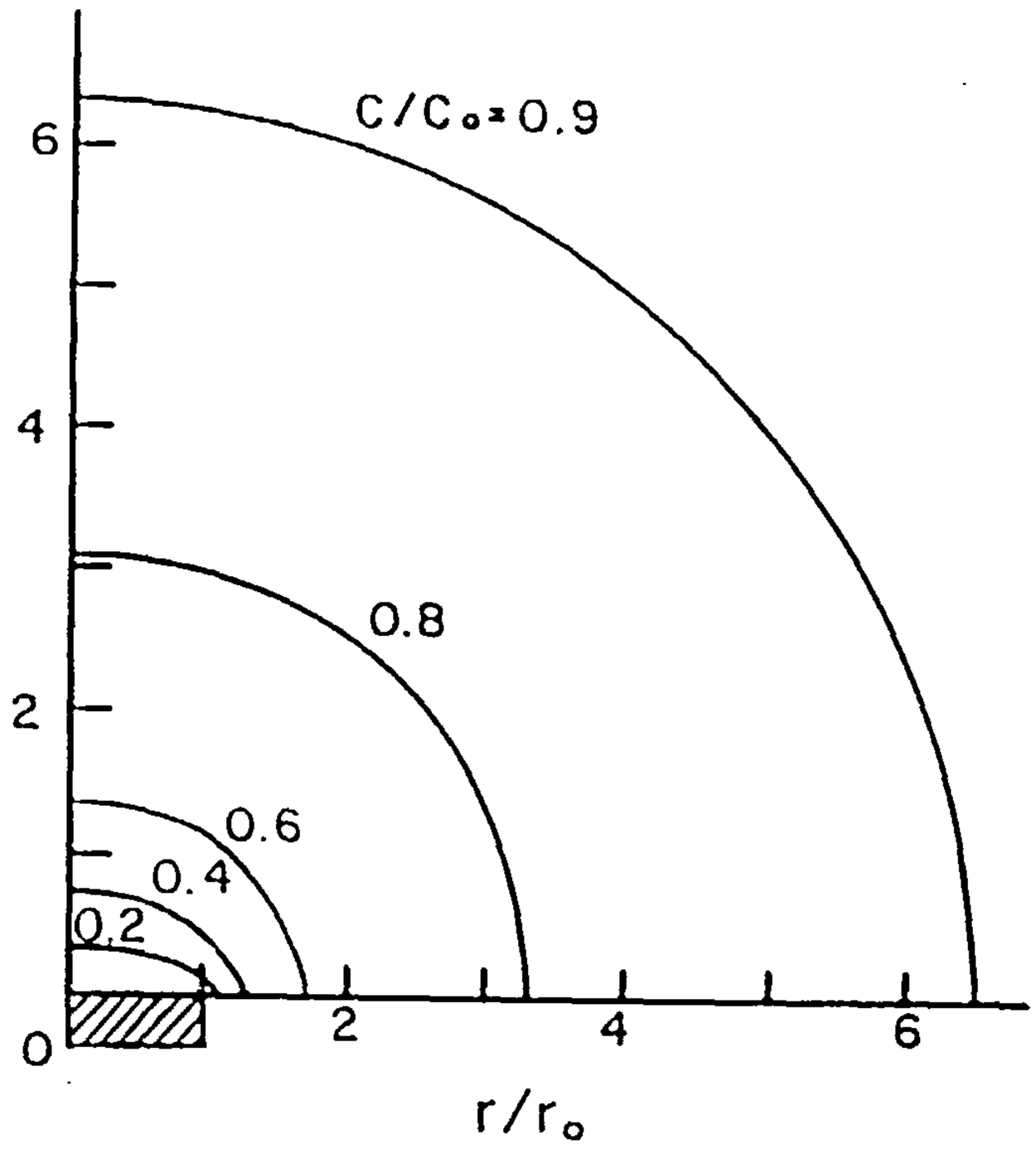

Figure 2.8.

Diffusion profile at a disc electrode

r_0 (μm)/hemis.	0.16	0.32	0.64	1.6	3.2	6.4	16
r_0 (μm)/disc	0.25	0.50	1.0	2.5	5.0	10	25
d (μm)	0.50	1.0	2.0	5.0	10	20	50
t_s (s)	0.0032	0.013	0.052	0.32	1.3	5.2	32

Table 2.1. Times to reach a steady state at hemispherical and disc microelectrodes to within 5% for a diffusion coefficient of 1.00×10^{-9} m^2 s^{-1} and the superficial diameters listed.

2.2. QUARTZ CRYSTAL MICROBALANCE (QCM)

The piezoelectric effect was first discovered by Jacques and Pierre Curie. When a mechanical stress is applied to a surface of a crystal , such as quartz and rochelle salt ($NaKC_4H_4O_6 \cdot 4H_2O$), an electric potential is produced across the crystal. Also, the application of a potential establishes a mechanical strain. This is known as the converse piezoelectric effect. In the 1920s Cady succeeded in developing an oscillating electronic circuits in which an oscillating quartz crystal produces an oscillating voltage with well defined frequency. Generally, thin, disc-shaped transducers are used as the quartz crystals. They oscillate in a pure shear mode when an alternating electric field of the frequency is applied accros the disc.

The quartz crystal microbalance (QCM) is an extremely sensitive sensor that can be used for the measurement of mass changes, in the nanogram range, that occur at a solid/liquid interface. It comprises of a piezoelectric quartz crystal sandwiched between two electrodes on which foreign masses may attach. Sauerbrey discovered that these sensors could be used to measure mass changes at the crystal surface [47]. The oscillation frequency depends on the density and viscosity of the substance in contact with the crystal [48]. In 1957, it was shown by Sauerbrey that mass deposited on the face of a quartz crystal slows down the vibration in a quantitative manner. This effect was used to build a sensitive balance known as the quartz crystal microbalance. An AT-cut crystal is generally used. The AT-cut crystal is about 0.1 mm thick and a few cm in diameter with a thin gold or platinum film electrode on each face. The resonant frequency is related to the thickness of the crystal.

$$f = \frac{const}{t} \tag{2.15}$$

where f is the resonant frequency and t is the thickness of the quartz wafer. As the mass deposited on the surface of the crystal increases, the vibration slows and the frequency decreases according to the Sauerbrey equation.

$$\Delta f = -\frac{const.\, f^2}{A}\Delta m \tag{2.16}$$

where Δm is the mass which is on the surface of the crystal, Δf is the change in the frequency, A is the area of the crystal and f is the fundemantal frequency of the crystal.

The Sauerbrey equation assumes that the deposited mass is rigid. In other words, the effect of the deposit on the crystal can be treated simply as though it were an increase in crystal thickness. However, many films may not be rigid, in this case the frequency change is not simply related to the mass of the film. Non-rigid films dissipate the energy of the oscillation in a similar manner to the damping of the oscillation of a mass on a spring by friction. The amplitude of the vibration is related to the AC current in the crystal. This effect can be detected through changes in the crystal admittance.

Figure 2.9 shows the variation of crystal admittance with frequency for rigid (a) and non-rigid films(b). The frequency at the peak is the resonant frequency and is measured by the EG&G instrument.

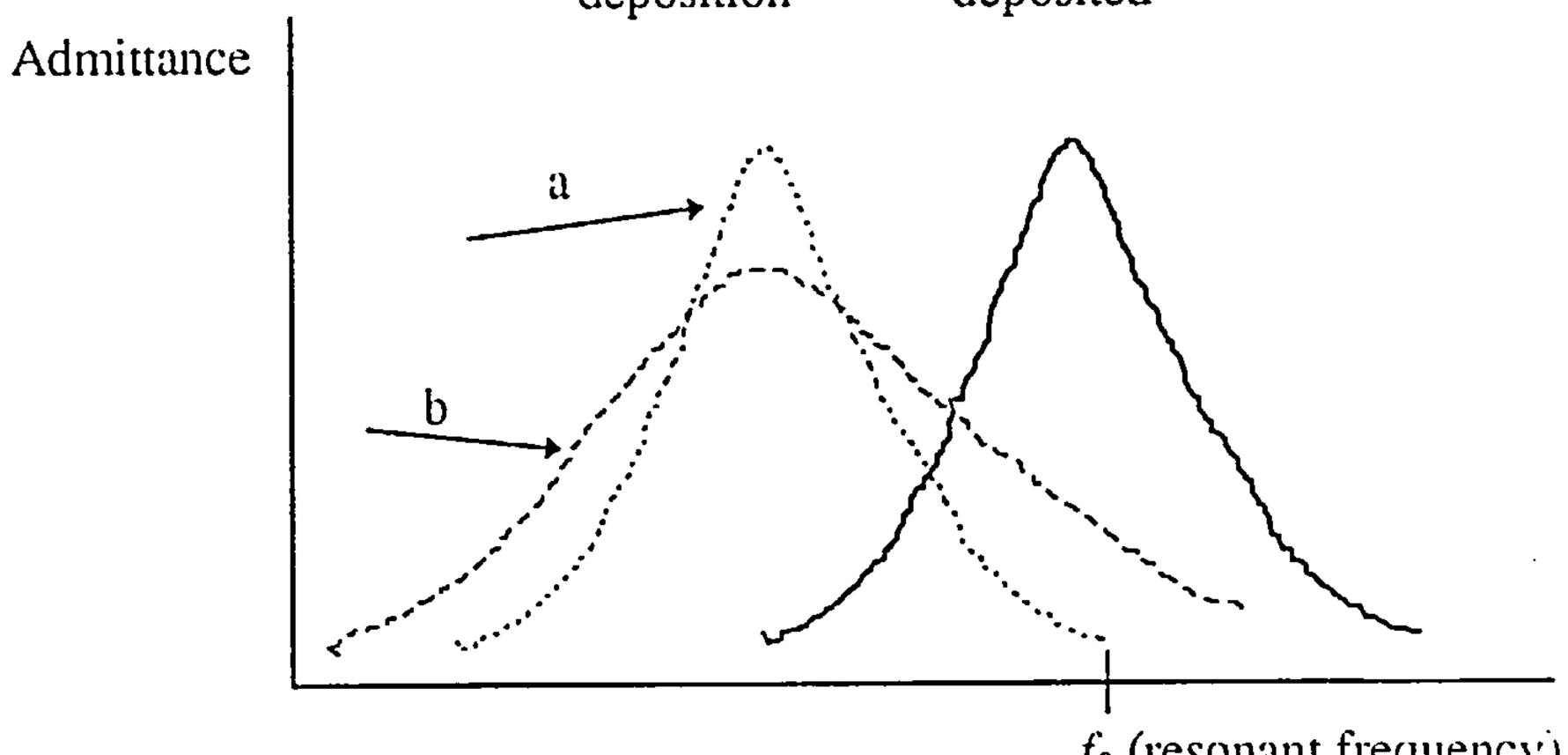

Figure 2.9.

A plot of amittance against the crystal frequency before and after mass deposition.

EG&G instrument also measures admittance at the resonant frequency and if this does not change (fig. 2.9a) when mass is deposited then the Sauerbrey equation can be applied to convert frequency change to mass.

2.3. REFERENCES

1. R. Greef, R. Peat, L. M. Peter, D. Pletcher and J. Robinson, *Instrumental Methods in Electrochemistry*, 1985, J. Wiley & Sons, Inc.

2. A. J. Bard and L. R. Faulkner, *Electrochemical Methods, Fundamentals and Applications*, 1980, J. Wiley & Sons, Inc.

3. P. T. Kissinger and W. R. Heineman, *Laboratory Techniques in Electroanalytical Chemistry*, Marcel Dekker, Inc. 1996, NY.

4. D. A. Buttry, *in Electroanalytical Chemistry*. A. J. Bard Ed., Marcel Dekker, NY, 1991 Vol 17.

5. G. Mabbott, *J. Chem. Ed.*, 1983, Vol 60, No 9, 697

6. P. T. Kissinger and W. R. Heineman, *J. Chem. Ed.*, 1983, Vol 60, No 9, 702

7. D. A. Skoog and J. J. Leary, *Principles of Instrumental Analysis*, Fourth Edition

8. C. A. Widrig, M. D. Porter, M. D. Ryan, T. G. Strein and A. G. Ewing, *Anal. Chem.*, 1990, 62, 1R.

9. D. R. Rolison, in M. Fleischmann, S. Pons, D. R. Rolison and P. P. Schmidt (Eds.), *Ultramicroelectrodes*, Datatech Systems Publishers, Morganton, NC, 1987, Chap. 3.

10. R. Mark Wightman and David O. Wipf, in A.J. Bard (Ed.), *Electroanalytical Chemistry*, Vol. 15, page 268, Marcel Dekker, New York

11. R.M. Wightman, *Science*, 1988, 240, 415.

12. J. Heinze, Ber. Bunsenges. *Phys. Chem.* 1981, 85, 1096.

13. J. O. Howell and R.M. Wightman, *J. Phys. Chem.*, 1984, 88, 3915.

14. J. O. Howell and R.M. Wightman, *Anal. Chem.*, 1984, 56, 524.

15. J. Cassidy, S. B. Khoo, S. Pons and M. Fleischmann, *J. Phys. Chem.*, 1985, 89, 3933.

16. A. M. Bond, M. Fleischmann and J. Robinson, *J. Electroanal. Chem.*, 1984, 168, 299.

17. J. W. Bixler, A. M. Bond, P. A. Lay, W. Thormann, P. Van Den Bosch, M. Fleischmann and B. S. Pons, *Anal. Chim. Acta*, **1986**, 187, 67.

18. S. Pons and M. Fleischman, *Anal. Chem.*, **1987**, 59, 1391A.

19. K. R. Wehmeyer and R. M. Wightman *Anal. Chem.*, **1985**, 57, 1989.

20. J. O. Howell, W. G. Kuhr, R. E. Ensman and R. M. Wightman, *J. Electroanal. Chem. Interfacial Electrochem.*, **1986**, 209, 77.

21. M. I. Montenegro and D. Pletcher, *J. Electroanal. Chem. Interfacial Electrochem.*, **1986**, 200, 371.

22. A. Fitch and D. H. Evans, *J. Electroanal. Chem. Interfacial Electrochem.*, **1987**, 202, 83.

23. C. Amatore, A. Jutland and F. Pfluger. *J. Electroanal. Chem. Interfacial Electrochem.*, **1987**, 218, 361.

24. D. O. Wipf and R. M. Wightman, *Anal. Chem.*, **1988**, 60, 2460.

25. D. O. Wipf, E. W. Kristensen, M. R. Deakin and R. M. Wightman, *Anal. Chem.*, **1988**, 60, 306.

26. C. P. Andrieux, P. Hapiot and J. M. Seveant, *Chem. Rev.*, **1990**, 62, 723 and references cited therein.

27. A. M. Bond, K. B. Oldham and C. G. Zoski, *Anal. Chim. Acta*, **1989**, 216, 177.

28. K. B. Oldham, *J. Electroanal. Chem. Interfacial Electrochem.*, **1987**, 237, 303.

29. S. Bruckenstein, *Anal. Chem.*, **1987**, 59, 2098.

30. C. G. Zoski, *J. Electroanal. Chem.*, **1990**, 296. 317.

31. M. I. Montenegro, M. A. Querios and J. L. Daschbach (Eds.), *Microelectrodes: Theory and Applications*, Kluwer, Dordrecht, **1991**.

32. R.M. Wightman and D.O. Wipf, in A.J. Bard (Ed.), *Electroanalytical Chemistry*, Vol. 16, M. Dekker. New York.

33. C. Guminski, H. Roslenek and Z. Galus, *J. Electroanal. Chem.*, **1983**, 158, 357.

34. J. Golas, Z. Galus and J. Osteryoung, *Anal. Chem.*, **1987**, 59, 389.

35. B. Scharifker and G. Hills, *J. Electroanal. Chem.*, **1981**, 130, 81.

36. P. Bindra, A. P. Brown, M. Fleischmann and D. Pletcher, *J. Electroanal. Chem.*, **1975**, 58, 31.

37. M. Ciszkowska and Z. Stojek, *J. Electroanal. Chem.*, **1985**, 191, 101.

38. JAS Instrument Systems, Salt Lake, UT.

39. D. R. Macfarlane and D. K. Y. Wong, *J. Electroanal. Chem.*, **1985**, 185, 197.

40. A. M. Bond, M. Fleischmann, S. B. Khoo, S. Pons and J. Robinson, *Indian J. Technol.*, **1986**, 24, 492.

41. A. Russel, K. Repka, T. Dibble, J. Ghoroghchian, J. J. Smith, M. Fleischmann, C. H. Pitt and S. Pons, *Anal. Chem.*,**1986**, 58, 2961.

42. Y. T. Kim, D. M. Scarnulis and A. G. Ewing, *Anal. Chem.* **1986**, 58, 1782.

43. C. G. Zoski, A. M. Bond, E. T. Allinson and K. B. Oldham, *Anal. Chem.* **1990**, 62, 37.

44. D. Shoup and A. Szabo, *J. Electroanal. Chem.*, **1982**, 140, 237.

45. D. K. Cope and D. E. Tallman, *J. Electroanal. Chem.*, **1987**, 235, 97.

46. Y. Saito, *Rev. Polarogr.* Jpn. **1968**, 15, 177.

47. G. Sauerbrey, *Z. Phys.*, **1959**, 155, 206.

48. J. A. Roush, D. L. Thacker and M. R. Anderson, *Langmiur*, **1994**, 10, 1642.

CHAPTER THREE

EXPERIMENTAL

3.1. MATERIALS

Unless otherwise stated all chemicals were purchased from Aldrich and used as received. DNA (type III, sodium salt from Salmon Testes and type XIV, sodium salt from Herring Testes) and RNA (type XI from baker's yeast) were purchased from Sigma Chemical Company and used without any further purification. The DNA Na^+ salt was stored at 4 ^{0}C. RNA was stored at 0 ^{0}C. For solutions of DNA in 10 mM NaCl , 10 mM Tris buffer pH 7.0, the ratio of absorbance at 260 nm and 280 nm was A_{260}/A_{280} = 1.8-1.9 indicating that the DNA was substantially free of protein. All stock solutions were prepared in the appropriate buffer using deionised water and stored at 4 ^{0}C and discarded after no more than four days. The concentration of DNA per nucleotide phosphate was determined by UV absorbance at 260 nm with ε_{260} = 6600 M^{-1} cm^{-1}.

3.1.1. STRUCTURES OF METAL COMPLEXES USED IN THIS WORK

Hexammineruthenium(III) chloride was purchased from Strem Chemicals Limited.

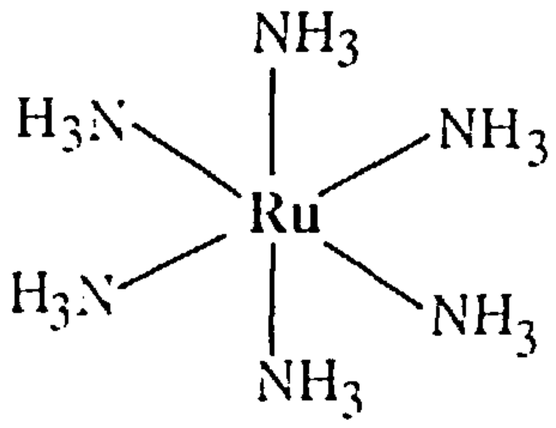

" $Ru(NH_3)_6^{3+}$ "

N,N,N-1-propylthyminedimethylaminomethylferrocene tetrafluoroborate was prepared by reaction of 1-(3-bromopropyl)thymine and N,N-dimethylaminomethyl-ferrocene in methanol (C. Price and A. Houlton, Department of Chemistry, University of Newcastle upon Tyne). The crude product was converted into the tetrafluoroborate salt [1].

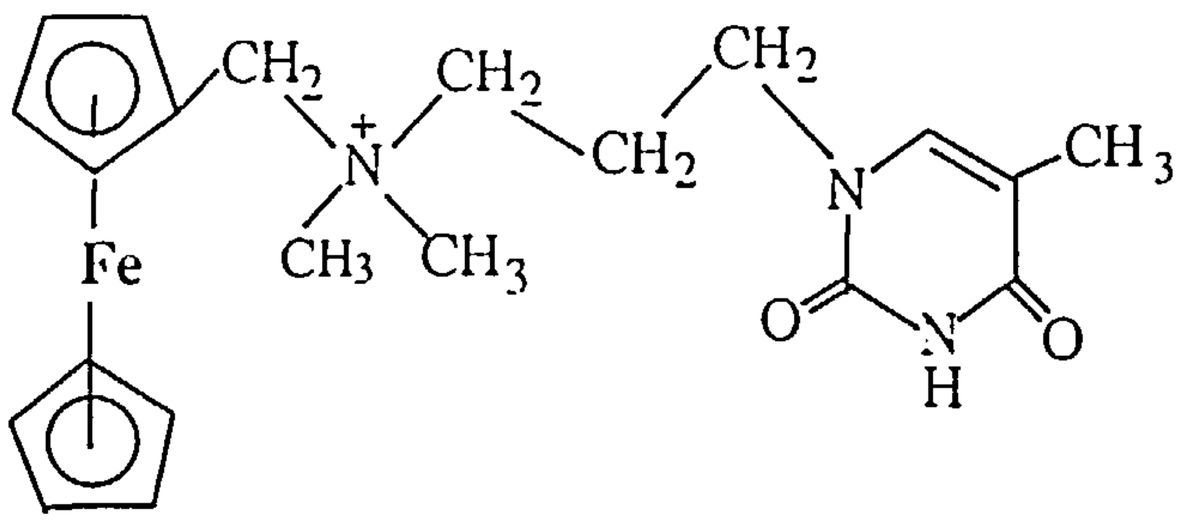

" Fc-Th"

N,N,N-trimethylaminomethylferrocene iodide (or tetrafluoroborate) was prepared by reaction of N,N-dimethylaminomethylferrocene and methyl iodide [1].

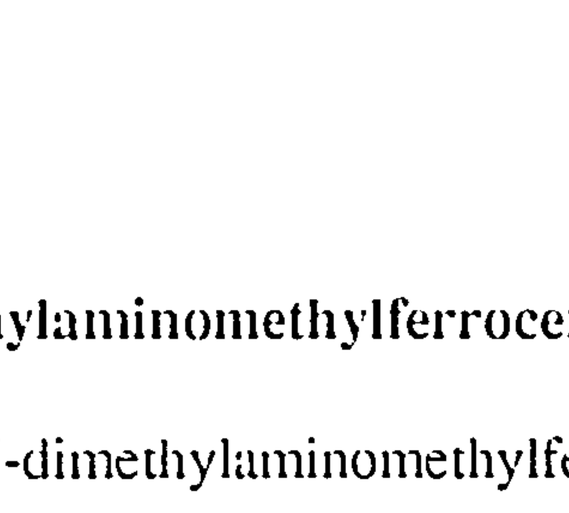

" Fc-NMe$_3$"

Bis(hexamethylbenzene)iron(II) chloride was prepared by the reaction of hexamethylbenzene and iron(III) chloride in refluxing cyclohexane. The product was then extracted with water. The compound was isolated as the PF_6 salt by addition of $NaPF_6$ and then converted to water soluble chloride salt.

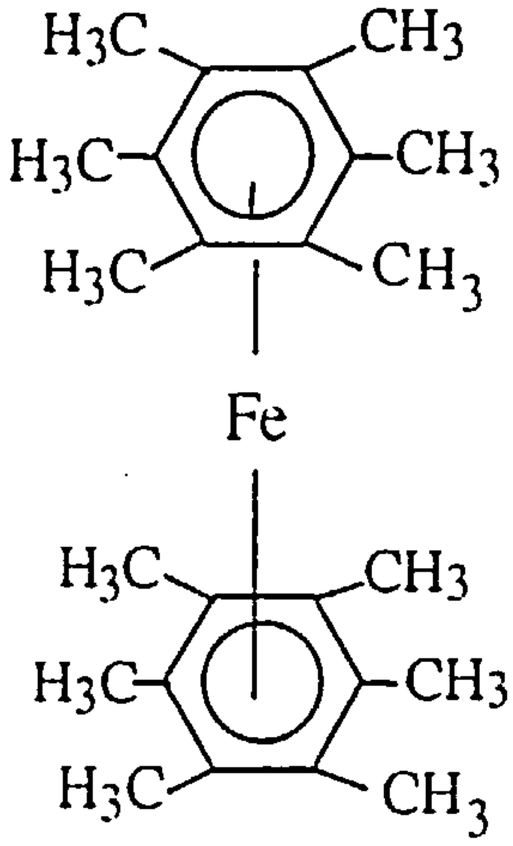

2+

" $Fe(bz)_2^{2+}$ "

Tris(2,2-bipyridine)iron(II) chloride was prepared by the reaction of 2,2-bipyridine and iron(II) chloride.

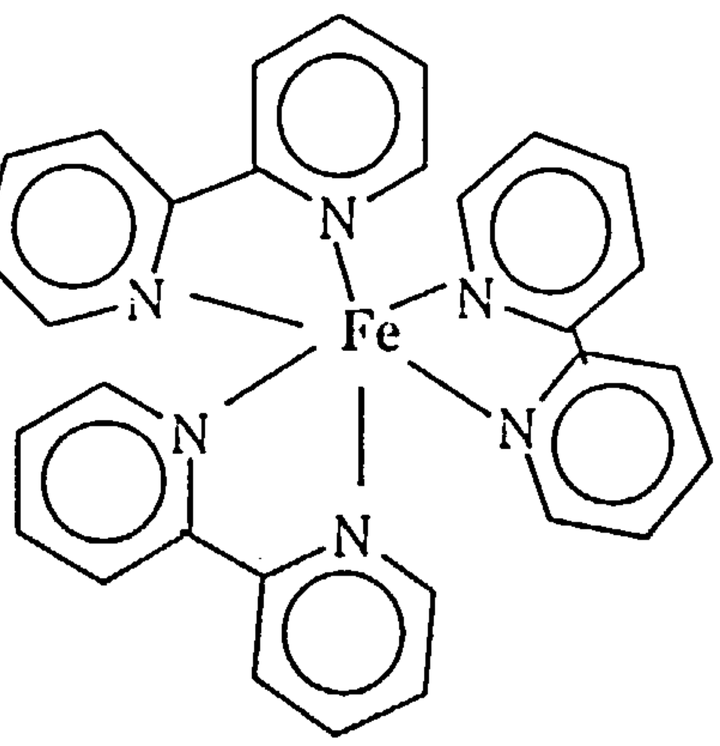

2+

" $Fe(bipy)_3^{2+}$ "

Tris(1,10-phenanthroline)iron(II) perchlorate was prepared by the reaction of 1,10-phenanthroline and iron(II) chloride.

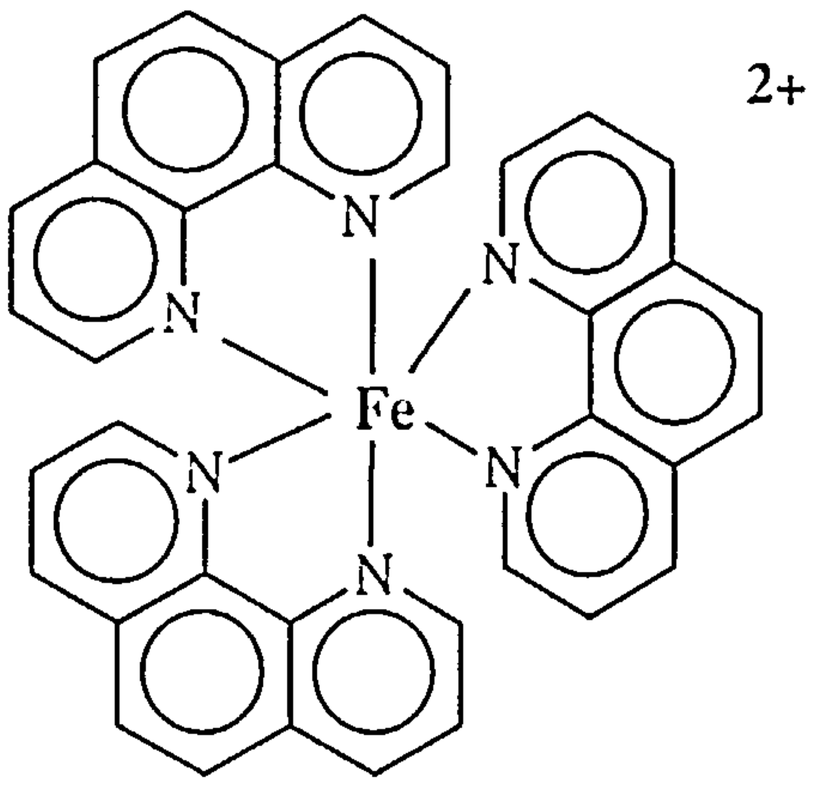

" $Fe(phen)_3^{2+}$ "

3.2. INSTRUMENTATION AND PROCEDURES

Cyclic voltammetric and microelectrode voltammetric studies with a three electrode system were carried out in a standard two compartment electrochemical cell of volume about 15 mL. The working electrodes used in this work were Pt or Au discs. The working electrode surface was polished with 0.25 μm alumina paste on a cloth pad and then washed with doubly distilled water prior to each experiment. Both cyclic voltammetry and microelectrode voltammetry were performed with a computer controlled OxSys Micros (Oxford, U.K.) low current potentiostat. Platinum microdisc electrodes were prepared by heat sealing 50 μm, 25 μm or 10 μm diameter Pt wires (Goodfellow, Cambridge, UK) in 2 mm o.d. glass tubes.. Electrical contact to the Pt was made via In/Ga eutectic and copper wire. Macroscopic Pt and Au electrodes for cyclic voltammetry were

prepared by potting 1 mm diameter wires in epoxy. Approximately 1 cm of platinum or gold wire was soldered to a copper wire to make the electrical contact. The gold and platinum disc electrodes were polished with 0.05 μm alumina. A silver wire or SCE was used as a reference electrode. A Pt wire served as a counter electrode. Cyclic voltamograms were recorded with a computer controlled potentiostat.

Quartz crystals (Pt-coated, area 0.196 cm^2) for quartz crystal microgravimetry were obtained from EG&G PARC for use with a QCA017 Quartz Crystal Microbalance (EG&G PARC, Reading, U.K.).

3.3. EXPERIMENTAL PROCEDURES

3.3.1. CYCLIC VOLTAMMETRY

Cyclic voltammetry has been applied to determine the binding of metal complexes to nucleic acids both in solution and on the gold electrode surface.

3.3.1.1. Titration of nucleic acids with metal complexes

Cyclic voltammetric titration of nucleic acids with transition metal complexes in solution were carried out in a standard two compartment electroctrochemical cell using Pt or Au disc working electrodes. Before starting titration experiments, elecrodes were cleaned using alumina paste to achieve a smooth surface. Solutions were prepared as required. Titration experiments were carried out in two steps. First, 5 mls of the required

concentration of a buffer. pH 7.0, was placed in the electrochemical cell, and the required amount of stock solution of a metal complex was added to this buffer to increase the concentration of a metal complex each time and for each metal complex. In the second step, 5 mls of required amount of DNA or RNA was placed in the electrochemical cell and the procedure was the same as that in the first step. A cyclic voltammogram was run of the buffer solution and the DNA or RNA alone in each experiment, to determine the background current for the following cyclic voltammograms. Cyclic voltammograms were run both in the absence and presence of nucleic acids for each concentration of metal complexes. For each cyclic voltammogram, the background reading was substracted to measure the peak current value. A graph of peak current vs. concentration was plotted for both total metal complex and free metal complex.

3.3.1.2. Preparation of the modified gold electrodes

Adsorptive cyclic voltammetry was performed with a computer controlled OxSys Micros (Oxford, U.K.) low current potentiostat. Gold disc electrodes were polished with 0.05 μm alumina paste and washed with deionised water prior to each experiment. Reference electrodes were SCE or Ag wire. A Pt wire served as the counter electrode. Solutions were prepared fresh before each experiment. Monolayers of 4-thiopyridine were prepared by immersing Au electrodes in 1 mM ethanol solutions of 4-thiopyridine for about 10 minutes. These monolayers were methylated by immersion in 5% iodomethane in methanol for 10 minutes. After producing a methylated surface, gold electrodes were kept in the DNA solution for 1 hour and rinsed with 10 mM Tris buffer. Then electrodes were dipped into solutions of metal complexes for 5 minutes and rinsed again with 10 mM Tris

buffer. After transfer to a fresh 10 mM Tris buffer solution in the electrochemical cell, electrodes were placed in the cell and nitrogen gas was bubbled for approximately 10 minutes. Then cyclic voltammograms were run for each metal complex. The charge passed in the cyclic voltammogram was calculated numerically after transferring the raw data to a spreadsheet.

3.3.2. MICROELECTRODE VOLTAMMETRY

Titration of nucleic acids with metal complexes using the microelectrode voltammetric technique followed a similar procedure to that used in cyclic voltammetry. In this case small platinum microelectrodes were used as the working electrode, instead of macroelectrodes. Platinum microelectrodes were prepared by heat sealing 25 μm or 10 μm diameter Pt wire in 2 mm o.d. tubes. Glass tubes served as the insulator and the body of the electrode. Approximately 1 cm of wire was inserted into the sealed end of the glass tube. The wire was sealed into the glass by melting the glass under vacuum. Electrical contact to the Pt was made via In/Ga eutectic and copper wire. An OxSys Micros low current potentiostat was used for microelectrode voltammetry. Electrodes were gently polished and cleaned by 0.05 μm alumina and doubly distilled water prior to each experiment. Solutions were prepared as required. Titration experiments were carried out in the same manner as for CV in 3.3.1.1.

3.3.3. QUARTZ CRYSTAL MICROGRAVIMETRY (QCM)

Quartz crystals (Au and Pt-coated, area 0.196 cm^2) for quartz crystal microgravimetry were obtained from EG&G PARC for use with a QCA017 QCM (EG&G PARC, Reading).

Au or Pt-coated crystals were cleaned with 50% H_2SO_4 + 50% H_2O_2 and rinsed with water then dried prior to each experiment. Monolayers of 4-thiopyridine were prepared by immersing Pt coated crystal in 1 mM ethanol solutions of 4-thiopyridine for 10 minutes. These monolayers were methylated by immersion in 5% iodomethane in methanol for 10 minutes. Methylated crystals were placed in the appropriate cells and attached to the Quartz Crystal Analyzer which measures the changes in frequency. A small quantity of 10 mM Tris buffer was placed in the cell and frequency was allowed to stabilise, before adding the DNA solution. The frequency was again allowed to stabilise giving the DNA time to bind to the methylated cationic surface. Then the cell was emptied and rinsed with 10 mM Tris buffer. A small quantity of Tris buffer was added to the cell, and once the frequency was stable it was recorded. Next, a small quantity of the metal complex solution was added, upon stabilising, the frequency was recorded.

3.4. THEORY OF METAL COMPLEX-NUCLEIC ACID BINDING IN SOLUTION PHASE

3.4.1. MODELS OF THE EFFECT OF POLYELECTROLYTES ON DIFFUSION OF METALS AND COMPLEXES

Several recent papers have described theoretical treatments for the quantitative description of the effect of polyelectrolytes on the transport of metal cations or complexes in solution [2-5]. Two general kinds of models have been proposed to treat the data. In the first, the metal cations form an ionic atmosphere around the anionic polyelectrolyte and long range electrostatic interaction by the slowly moving macromolecules retards the diffusion of the cations. In the second model, the metal cations are divided into two distinct populations designated bound and free. Bound metal is assumed to move through the solution associated with a particular polyelectrolyte molecule as a single unit. The diffusion current is the the sum of the diffusion current of the free metal and the macromolecule bound metal weighted by the fractional population of bound and free metal. Osteryoung and coworkers have obtained accurate microelectrode data for the diffusion of simple metal cations and protons in the presence of polystyrene sulphuric acid that show good agreement with the first model. In particular the ratio of diffusion coefficients of several monocations (H^+, Tl^+, Ag^+) in the presence and absence of polyelectrolyte could be calculated from standard theories of electrolytes using the Poisson-Boltzman formulation. For this reason they prefer the first model. In this work we do however adopt the second model for the following reason; the complexes we have used can interact with DNA via short range interactions as well as purely electrostatic modes

and further, in all our experiments the salt concentration exceeds that of the polyelectrolyte.

3.4.2. DATA ANALYSIS

The simplest model of metal complex-DNA binding equilibria consits of a fixed number of binding sites of identical affinity on a given length of DNA.

$$M + DNA \Leftrightarrow M\text{-}DNA \qquad (3.1)$$

If the concentration of DNA is expressed in terms of nucleotide phosphate concentration then the binding constant K is given by (3.2):

$$K = \frac{[M\_DNA]}{[M]\frac{[NP]}{2s}} = \frac{C_b}{C_f \frac{[NP]}{2s}} \qquad (3.2)$$

Where C_b and C_f are the concentration of free and bound metal complex and s is the size of the binding site in base pairs. Using the mass balance equations for NP and metal complex C_f can be expressed in terms of the total metal concentration (C_T), total NP concentration ($[NP]_0$), K and s [6]:

$$KC_f^2 - (1 + KC_T + \frac{K[NP]_0}{2s})C_f - C_T = 0 \qquad (3.3)$$

Experimentally the ratio C_f/C_b can be obtained from the diffusion currents in the absence (i) and presence of DNA (i_{dna}):

$$i_{dna} = BD_f^x C_f + BD_b^x C_b \qquad (3.4)$$

$$i = BD_f^x (C_T) \qquad (3.5)$$

Where $x = 0.5$ and $B = (2.69\times10^5)\ A\ n^{3/2}\ v^{1/2}$ (A is the electrode area, n is the number of electrons involved, v is the scan rate) for cyclic voltammetry and $x = 1$ and $B = 4nFr$ (n is the number of electrons involved, F is the Faraday constant, r is the electrode radius) for a steady-state microdisc experiment and D_f and D_b are the diffusion coefficients of the bound and free metal complex. It should be noted that equation assumes that the kinetics of the equilibrium are fast on the experimental timescale of CV. Using $C_T = C_f + C_b$ we obtain:

$$\frac{D_f(i - i_{dna})}{D_f i_{dna} - D_b i} = \frac{C_b}{C_f} \qquad (3.6)$$

If $D_b << D_f$ the left-hand side of (3.6) reduces to:

$$\frac{i - i_{dna}}{i_{dna}} = \frac{C_b}{C_f} \qquad (3.7)$$

Where the left-hand side can be obtained directly from the experimental diffusion currents. The experimental data were therefore expressed as plots of $(i\text{-}i_{dna})/i_{dna}$ against total metal concentration at a fixed concentration of DNA and K and s were obtained by least squares

fitting. This method of data analysis was chosen because it increases the weighting of the data at the beginning of the titration where most of the information on the binding constant is contained.

3.4.3. LEAST-SQUARES

Error estimates on the fitted parameters were obtained by a bootstrap method which avoids the necessity to make any assumptions about the distribution or standard deviation of individual data points [7]. Briefly, the bootstrap method consists of drawing, with replacement, a random sample of n datapoints from the dataset of n points. This process was repeated to generate 250-1000 simulated data sets which were fitted by the Levenberg-Marquardt method for each data set. This bootstrap sample was used to approximate the sampling distribution of K and s and to compute standard deviations. Preliminary least squares fits were carried out on a spreadsheet, MS Excel 4.0™. Bootstrap resampling was performed using software written in-house in MS Fortran 5.1™ incorporating commercial routines for nonlinear least squares fitting by the Levenberg-Marquardt method [8] and executed on a 486DX PC.

3.5. THE EFFECT OF VISCOSITY ON THE BINDING OF METAL COMPLEXES TO DNA IN SOLUTION PHASE

Nucleic acids are large molecules and can increase the viscosity of aqueous solutions. In a medium of high viscosity, diffusion of free metal complex is slower. Also,

the electrode surface can be blocked by adsorbed layer of DNA. It is important to distinguish decreases in the voltammetric current observed due to binding of metal complex to DNA from decreases due to viscosity effects. A cyclic voltammetric experiment was carried out, by previous workers [5], on a mixture of 0.11 mM $Co(phen)_3^{2+}$ and 0.11 mM $Mo(CN)_8^{4-}$ in 50 mM NaCl, 5 mM Tris, pH 7.1, in the absence and presence of DNA. No significant decrease in the peak current of $Mo(CN)_8^{4-}$ was observed because $Mo(CN)_8^{4-}$ is a negatively charged molecule and is expected to experience coulombic repulsion with the highly negatively charged DNA phosphate backbone. $Co(phen)_3^{2+}$ binds via intercalation in DNA and the peak current decreased as expected. This confirmed that the decrease in the voltammetric currents is due to the metal complex binding to DNA and not viscosity effects. The difference in diffusion rates of free and bound species to the electrode will lead to changes in the current response. This effect is used to quantify the binding of the metal complex to DNA. Further, our data show the titration curves running parallel at high metal concentrations indicating that the diffusion of free metal is not effected significantly at the DNA concentrations used. Viscosity of DNA therefore has a very small effect on diffusion at the concentrations employed in this work.

3.6. THE EFFECT OF TEMPERATURE ON THE MEASUREMENT OF FREQUENCY CHANGES WITH THE QUARTZ CRYSTAL MICROBALANCE

The effect of temperature on frequency measurement was also investigated to determine if the change in room temperature has a role in frequency change. For this purpose, 10 mM Tris buffer solution was placed in the cell and we measured time and

frequency change. The change in room temperature and in frequency against time is plotted in figures 6.7 and 6.8 . The change in temperature is not bigger than 1 ^{0}C.

We also prepared 10 mM Tris buffer solutions of varying temperature. Then the buffer solution was placed in the cell including a thermometer. The dependency of the frequency change against temperature is plotted in figure 6.9. As seen here, the change in frequency per 10 ^{0}C is appoximately 100 Hz. This means that 1 ^{0}C change in temperature may effect the frequency decrease by 10 Hz. But the change in temperature of the cell was less than 1 ^{0}C. Frequency changes > 10 Hz can therefore be attributed to mass and/or viscosity effects.

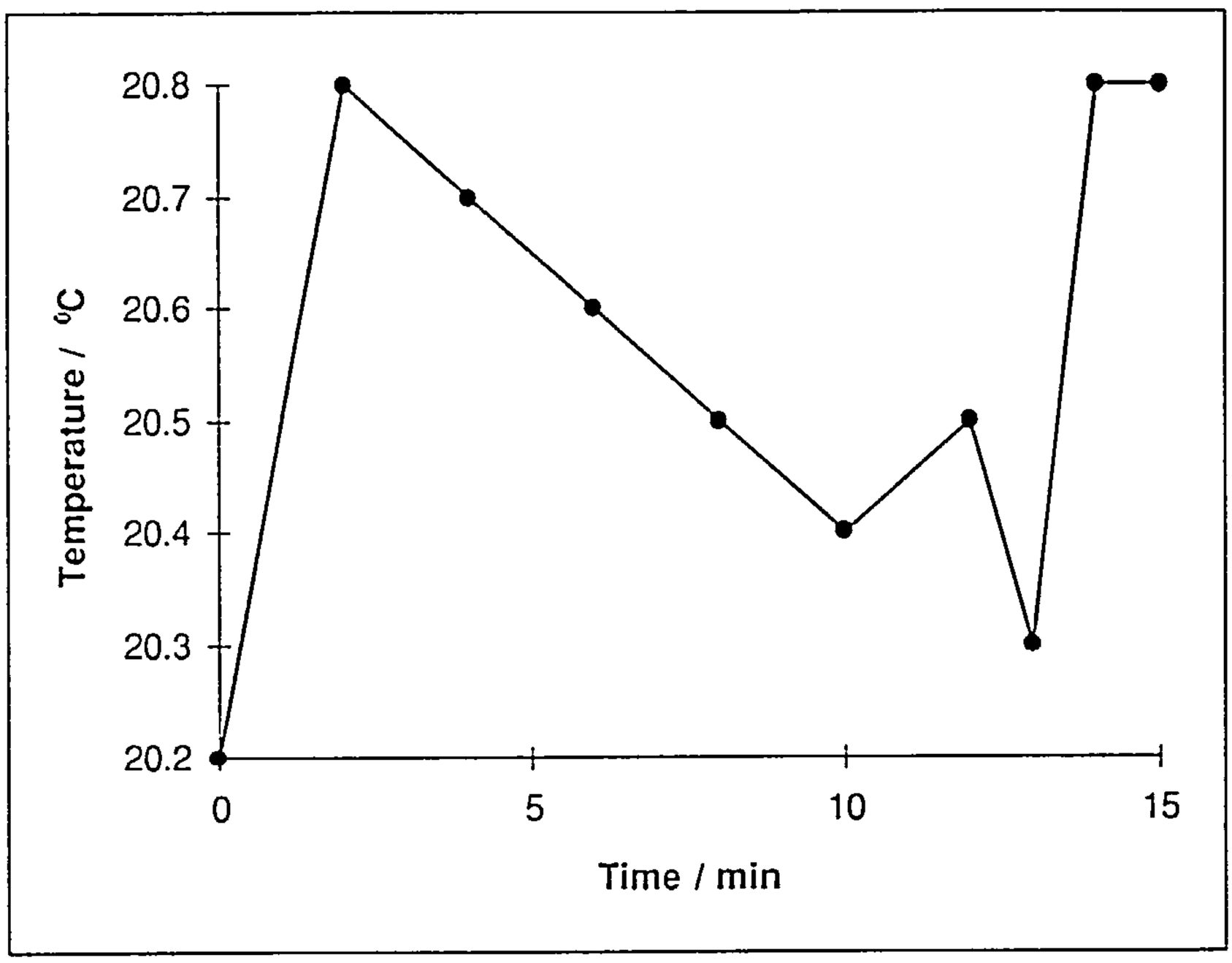

Figure 1.1.

A plot of time against room temperature measured in the cell containing 10 mM Tris buffer solution.

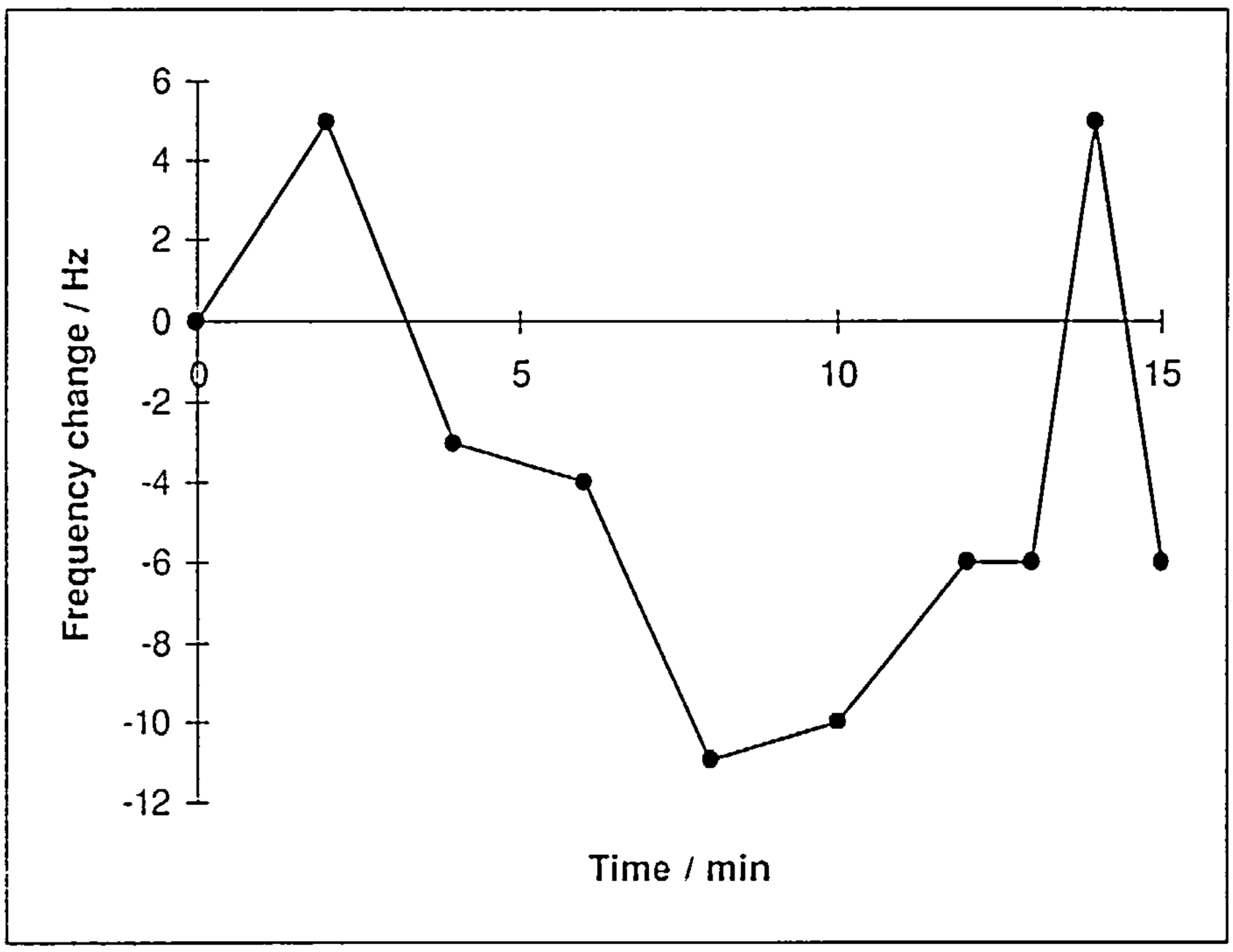

Figure 1.2.

A plot of time against the frequency change measured in the QCM cell containing 10 mM Tris buffer.

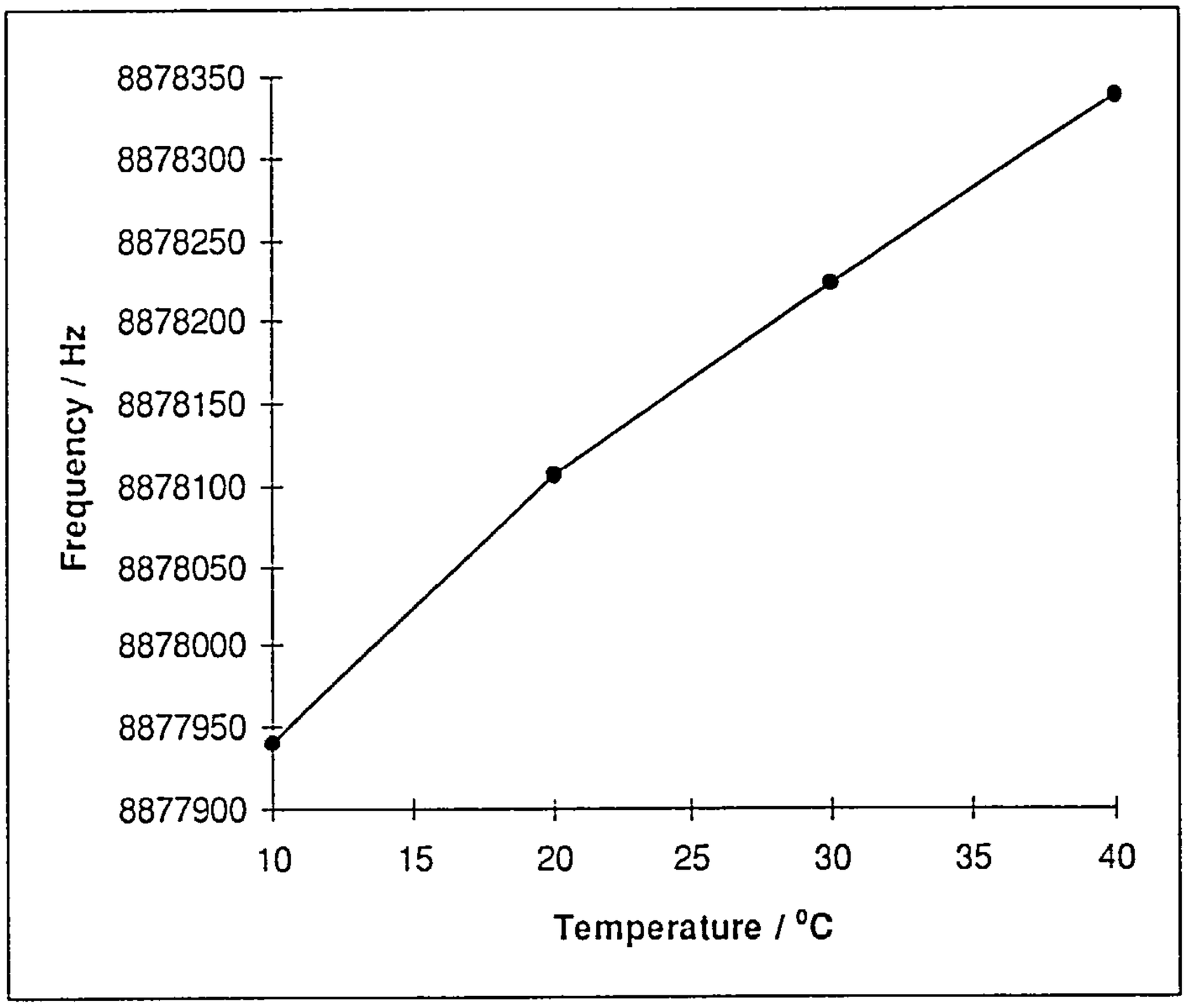

Figure 1.3.

A plot of frequency against temperature of the solution.

3.7. REFERENCES

1. C. Price, M. Aslanoglu, C. J. Isaac, M. R. J. Elsegood, W. Clegg, B. R. Horrocks and A. Houlton, *J. Chem. Soc.*, **1996**, 4115.

2. S. E. Morris, M. Ciszkowska and J. G. Osteryoung, *J. Phys. Chem.*, **1993**, 97, 10453.

3. M. Ciszkowska and J. G. Osteryoung, *J. Phys. Chem.*, **1994**, 98, 11791.

4. M. Ciszkowska and J. G. Osteryoung, *J. Phys. Chem.*, **1994**, 98, 3194.

5. R. Jiang and F. C. Anson, *J. Phys. Chem.*, **1991**, 95, 5701.

6. M. T. Carter, M. Rodriguez and A. J. Bard, *J. Am. Chem. Soc.*,**1989**, 111, 8911.

7. T. L. Lai and L. Zhang, *Biometrics*, **1994**, 50, 782.

8. "*Numerical Recipes in Fortran*" Ch 19, 2nd Edition, W. H. Press, S. A. Teulkolsky, W. T. Vetterling and B. P. Flannery, Cambridge University press, Cambridge, **1992**.

CHAPTER FOUR

ELECTROCHEMICAL STUDIES OF THE INTERACTION OF METAL COMPLEXES WITH NUCLEIC ACIDS IN SOLUTION PHASE

4.1. INTRODUCTION

This chapter describes voltammetric studies of the interaction of several metal complexes with nucleic acids in solution. Studies of the binding of metal complexes to DNA and RNA were carried out by the application of cyclic voltammetry and microelectrode voltammetry to determine the free metal concentration in solution. Cyclic voltammetry and microelectrode voltammetry are discussed and compared as techniques for the study of the metal complex binding.

Metal complex-nucleic acid interactions are important because transition metal complexes have been used in chemotherapy [1-5], as DNA cleveage agents [6-9], as structural probes for nucleic acids [10-14], and as spectroscopic probes for different DNA conformations [15-23].

Binding of iron(II) and cobalt (III) with 1,10-phenantholine and 2,2-bipyridine to DNA has been studied using cyclic voltammetry [24,31]. In this work, we take advantage of voltammetry to study the binding of hexammineruthenium(III) chloride to DNA. We also selected to study the interaction of ferrocene derivatives with nucleic acids. The electrochemical behavior, stability and reversibility of these ferrocene derivatives make them good candidate for our binding studies. The fundamental principles of voltammetric

methods are employed in this work to obtain the binding constant of the metal complex to nucleic acid.

Voltammetric methods have become important to the investigation of nucleic acids. Several reports have appeared concerning the electrochemistry of DNA and RNA and its monomeric components [25-30]. However, application of electrochemistry in the studies of metal-nucleic acid interaction has been limited. In particular, ultramicroelectrodes have not been employed for binding studies of DNA with small molecules.

In this chapter, we describe the application of electrochemistry to obtain both qualitative and quantitative information about the binding of metal complexes to nucleic acids. The parameters of the interaction, such as the binding constant, (K), for the interaction of metal complex with nucleic acid and the number of base pairs, (s), between binding sites were obtained using the voltammetric titrations. The voltammetric behavior also allowed some inference of the binding forces involved in the interaction. The use of cyclic voltammetry and steady-state voltammetry at microelectrodes for the determination of metal-DNA binding is compared and some advantages of microelectrodes in this application are demonstrated.

4.2. RESULTS & DISCUSSION

4.2.1. HEXAMMINERUTHENIUM(III) CHLORIDE

We started our investigation of the binding of metal complexes to nucleic acids with hexammineruthenium(III) chloride using cyclic voltammetry and steady-state voltammetry at microelectrodes. CV experiments are first presented for each metal complex following UME results. General discussion for each metal complex is given after revealing both CV and UME data.

Cyclic voltammetry was applied to the interaction of $Ru(NH_3)_6^{3+}$ with DNA. CV behavior of $Ru(NH_3)_6^{3+}$ with and without DNA is given in figure 4.1.

Cyclic voltammetric titration of DNA with $Ru(NH_3)_6^{3+}$ was carried out to measure the binding constant. Since precipitation occurs at higher concentration of DNA, we used a lower concentration of DNA. The peak current for reduction of $Ru(NH_3)_6^{3+}$ in 10 mM Tris buffer pH 7 with and without 0.4 mM DNA is plotted against total concentration of $Ru(NH_3)_6^{3+}$ in figure 4.2. Since the slopes of the current against the concentration curves in the titration of DNA with $Ru(NH_3)_6^{3+}$ are almost same, the effect of the viscosity on the binding is small. The titration results were used to calculate the amount of the bound $Ru(NH_3)_6^{3+}$. The ratio of [bound]/[free] against the total concentration of $Ru(NH_3)_6^{3+}$ is plotted in figure 4.3. The magnitude of the binding constant of $Ru(NH_3)_6^{3+}$ to DNA determined here is [$K = (1.0 \pm 0.18) \times 10^4$ dm^3 mol^{-1} , $s = (1.84 \pm 0.03)$]. Since CV detects $i \propto D^{-1/2}$, bound metal contributes to the diffusion current. However, at UME the current is directly proportional to the diffusion coefficient ($i \propto D$). Therefore, UME detects almost

no bound metal. As a result of the current decreasing less in CV, the binding constant is apparently small compared to that obtained by microelectrode voltammetry. As ionic strength was increased by the addition of potassium chloride to a solution of $Ru(NH_3)_6^{3+}$ containing DNA the peak current increased. This effect is due to a decrease in the binding constant. This behavior suggests that the electrostatic forces have a major role in the binding of $Ru(NH_3)_6^{3+}$ to DNA. A plot of peak current against the concentration of potassium chloride is given in figure 4.4.

Epa = -0.10 V	Epc = -0.22 V	ΔEp = 120 mV	$E^{o'}$ = 0.16 V

Table 4.1. Parameters of $Ru(NH_3)_6^{3+}$ CV determined in this work.

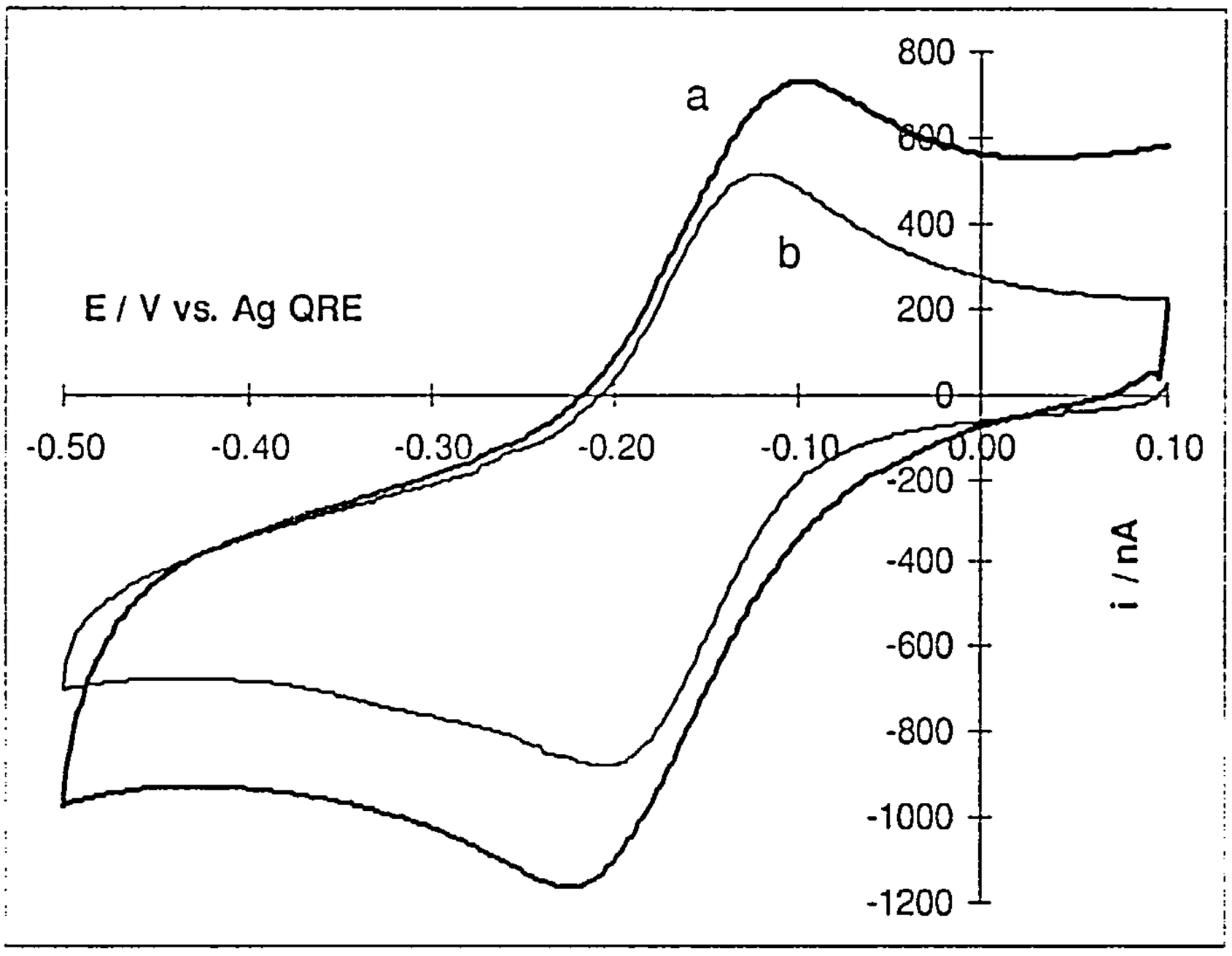

Figure 4.1.

Cyclic voltammograms of 0.5 mM $Ru(NH_3)_6^{3+}$ in the (a) absence and (b) presence of 0.4 mM DNA.

Supporting electrolyte, 10 mM Tris pH 7. Working electrolyte, platinum disc (area, 0.0785 cm^2). Scan rate, 50 mV s^{-1}.

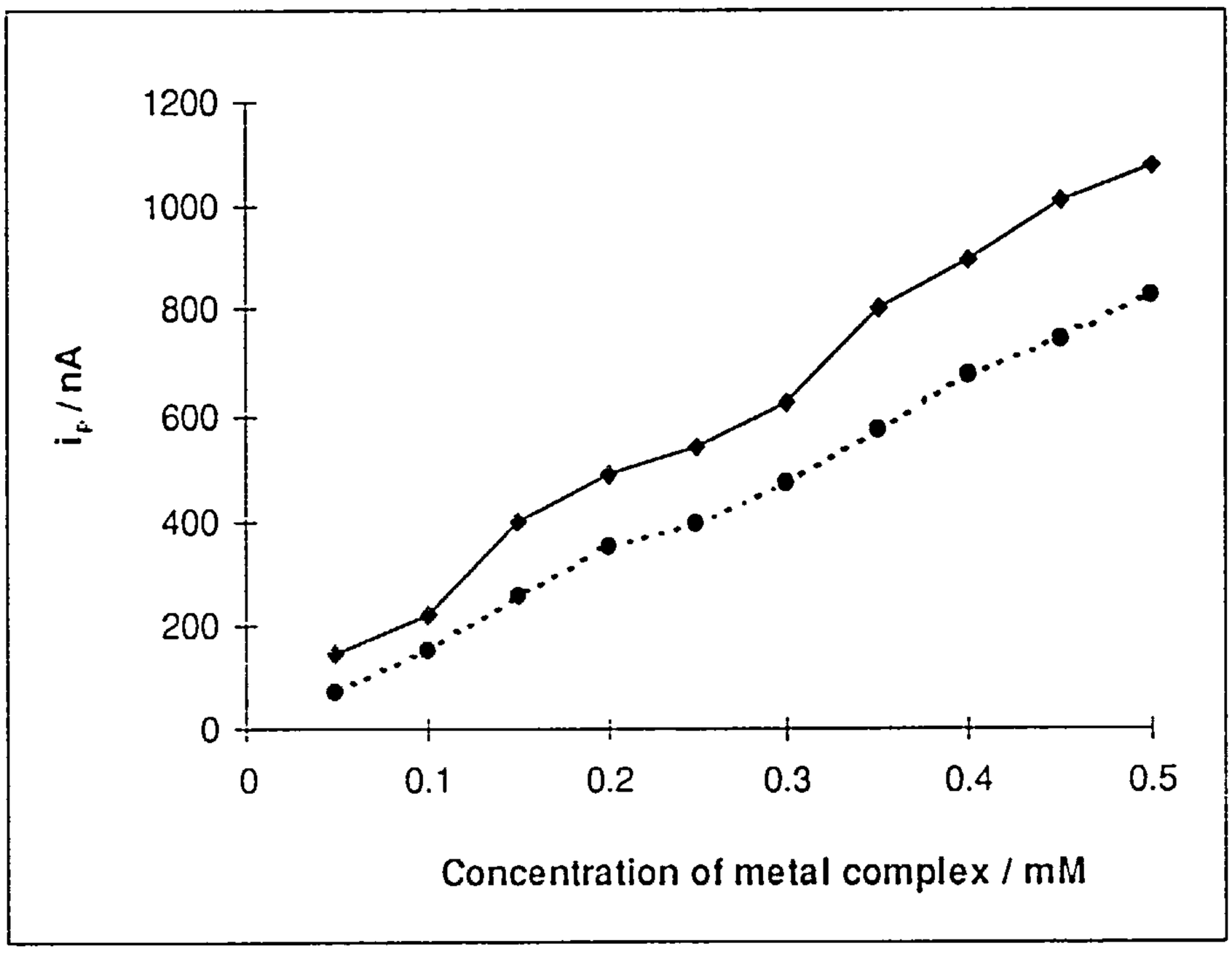

Figure 4.2.

The CV titration of 0.4 mM DNA with $Ru(NH_3)_6^{3+}$ (dashed line).

A plot of current against the total concentration of $Ru(NH_3)_6^{3+}$ (solid line).

Supporting electrolyte, 10 mM Tris pH 7. Working electrode, platinum disc (area, 0.0785 cm^2). Scan rate, 50 mV s^{-1}.

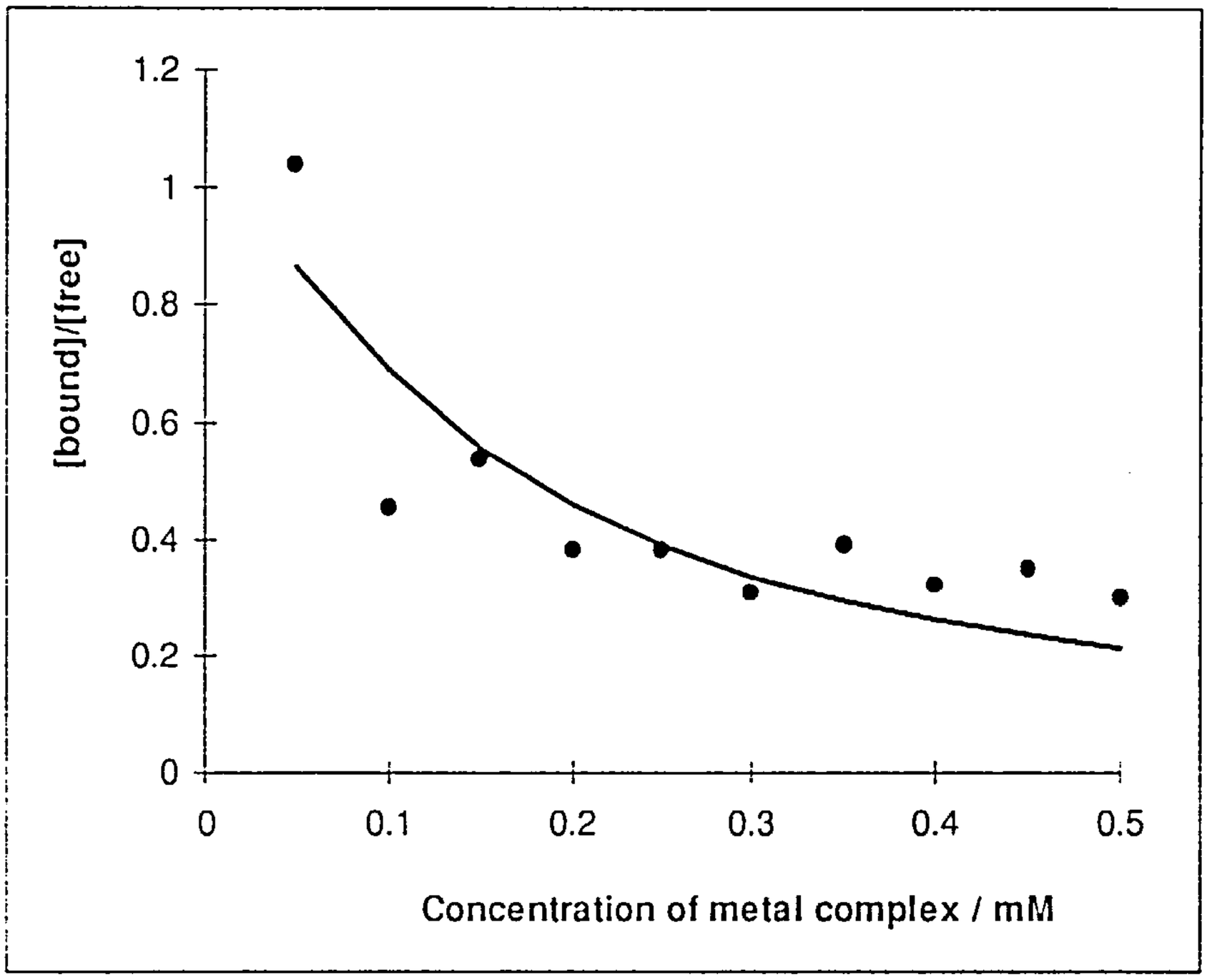

Figure 4.3.

Plot of the ratio of [bound]/[free] against the total concentration of $Ru(NH_3)_6^{3+}$ calculated from the CV titration of 0.4 mM DNA with $Ru(NH_3)_6^{3+}$.

The solid line is a least-squares fit with a binding constant, [$K = (1.0 \pm 0.18) \times 10^4$ dm^3 mol^{-1}, $s = (1.8 \pm 0.03)$].

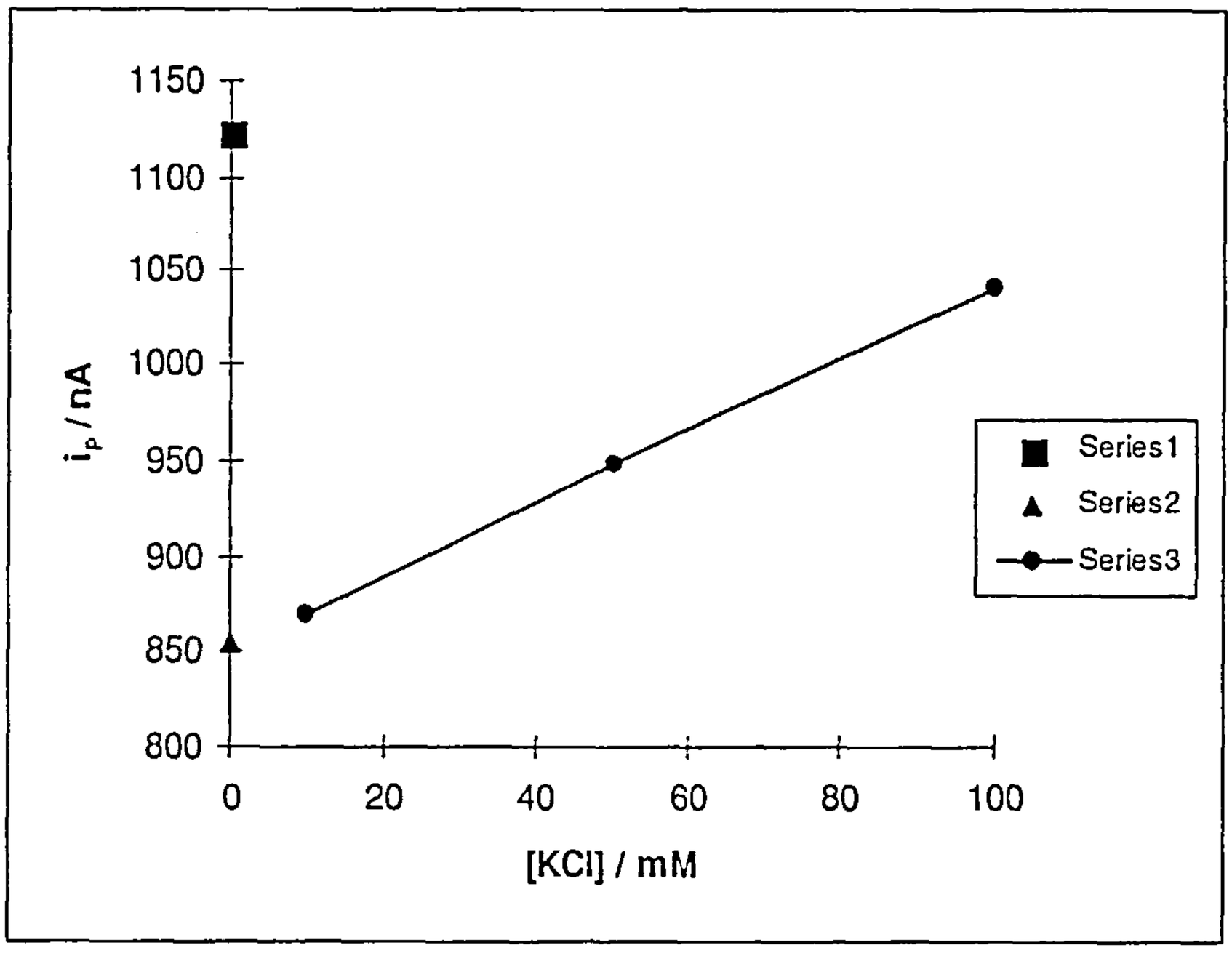

Figure 4.4.

The dependence of ionic strength on the binding. Plot of current against the concentration of potassium chloride in the experiment of the binding of $Ru(NH_3)_6^{3+}$ to DNA.

Series 1. The peak current for a solution containing only $Ru(NH_3)_6^{3+}$ in 10 mM Tris buffer.

Series 2. The peak current for a solution containing $Ru(NH_3)_6^{3+}$and DNA in 10 mM Tris buffer.

Series 3. The peak current for a solution containing $Ru(NH_3)_6^{3+}$, DNA and potassium chloride in 10 mM Tris buffer.

Microelectrode voltammetry was also applied to interaction of the binding of $Ru(NH_3)_6^{3+}$ to DNA. Figure 4.5 shows the microelectrode voltammograms of $Ru(NH_3)_6^{3+}$, in 10 mM Tris buffer pH 7, in the absence and presence of 0.4 mM DNA at a 10 μm diameter platinum microelectrode.

Titration of DNA with $Ru(NH_3)_6^{3+}$ was also carried out to obtain the binding constant and the binding site sizes using microelectrode voltammetry. This interaction was also carried out to see the difference between cyclic voltammetry and steady-state voltammetry as electrochemical methods and also to compare the magnitude of the binding constants determined by each technique. Figure 4.6 shows the titration results of $Ru(NH_3)_6^{3+}$-DNA interaction in 10 mM Tris buffer, pH 7.0 at a 10 μm platinum microdisc electrode. The decrease in the diffusion limiting current for the reduction of $Ru(NH_3)_6^{3+}$ was used to calculate the amount of bound $Ru(NH_3)_6^{3+}$ at each concentration. Figure 4.7 shows the ratio of [bound]/[free] versus the total concentration of $Ru(NH_3)_6^{3+}$. The magnitude of the binding constant of $Ru(NH_3)_6^{3+}$ to DNA determined here is [$K = (1.47 \pm 0.04) \times 10^5$ dm^3 mol^{-1} , $s = (1.62 \pm 0.01)$]. At higher concentration of $Ru(NH_3)_6^{3+}$, the points in the plot of the current against the total concentration of $Ru(NH_3)_6^{3+}$ ran parallel. This means diffusion of free metal in the absence and presence of DNA is equal at higher concentration of metal ($D_f \cong D_f$) and viscosity is not a problem. The magnitude of the binding constant of $Ru(NH_3)_6^{3+}$ to DNA determined by microelectrode voltammetry and cyclic voltammetry should be same. But in case of UME, the binding constant is approximately 10 times larger ($K_{UME} > K_{CV}$). In cyclic voltammetry the current is proportional to $D^{1/2}$ ($i \propto D^{1/2}$). But at UME the current is directly proportional to D ($i \propto D$) and UME detects almost no bound metal. But, in CV bound metal contributes to the

diffusion current and the current decreases less and K is apparently smaller. Therefore, the assumption of $\frac{i_{noDna} - i_{dna}}{i_{dna}} = \frac{bound}{free}$ may not be true for CV. The titration plot determined using a microelectrode shows that at smaller concentration of $Ru(NH_3)_6^{3+}$, the current in the presence of DNA is very small. So, this results confirmed that the contribution of bound $Ru(NH_3)_6^{3+}$ to the current at UME is very small. Because the decrease in the limiting current is a direct measure of the amount of bound metal complex microelectrode voltammetry can be used to calculate the binding constant with a simple treatment of the data.

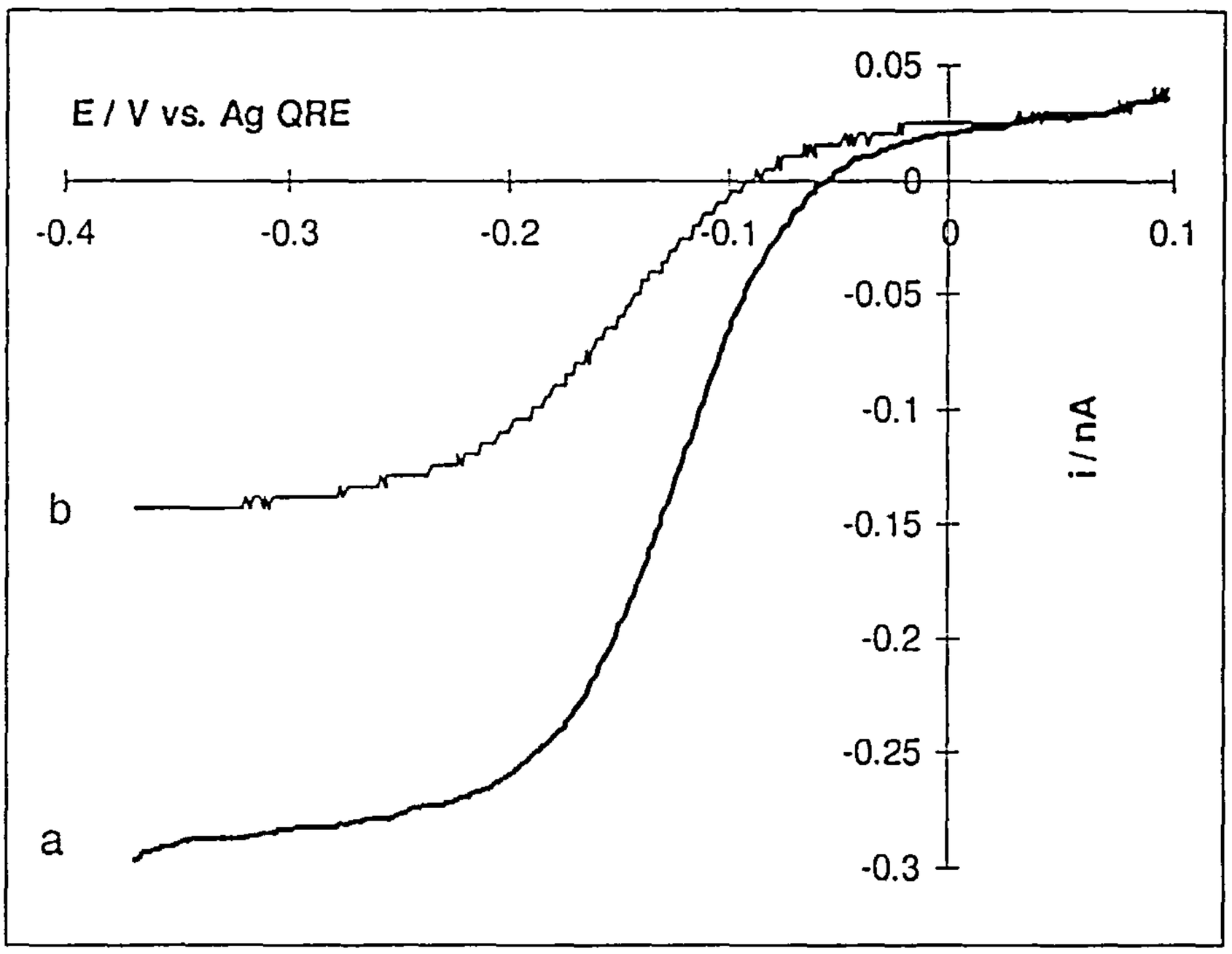

Figure 4.5.

Microelectrode voltammograms of 0.2 mM $Ru(NH_3)_6^{3+}$ in the (a) absence and (b) presence of 0.4 mM DNA.

Supporting electrolyte, 10 mM Tris pH 7. Working electrode, platinum disc (diameter, 10 μm).

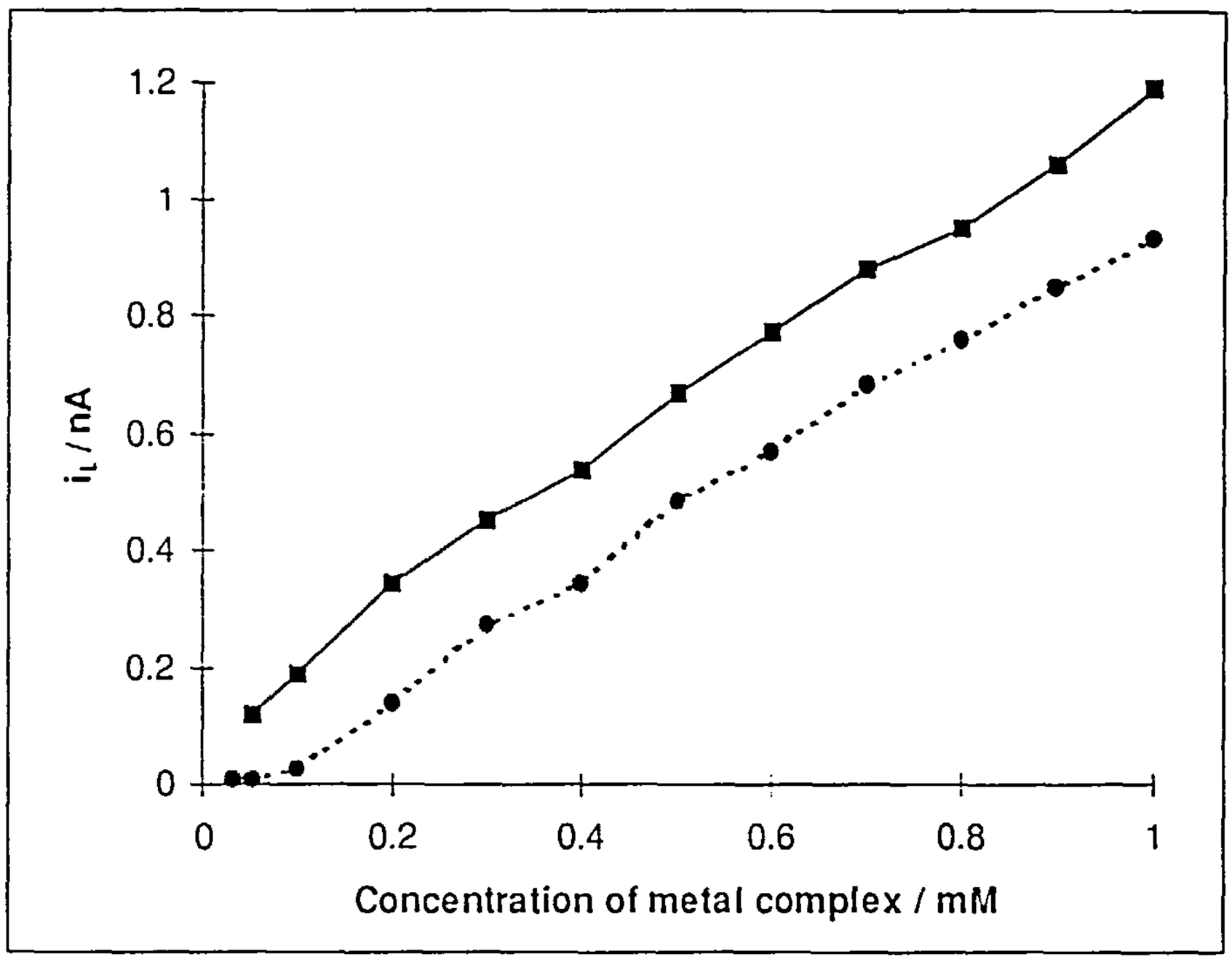

Figure 4.6.

The UME titration of 0.4 mM DNA with $Ru(NH_3)_6^{3+}$ (dashed line).

A plot of current against the total concentration of $Ru(NH_3)_6^{3+}$ (solid line).

Supporting electrolyte, 10 mM Tris pH 7. Working electrode, platinum disc (diameter, 10 μm).

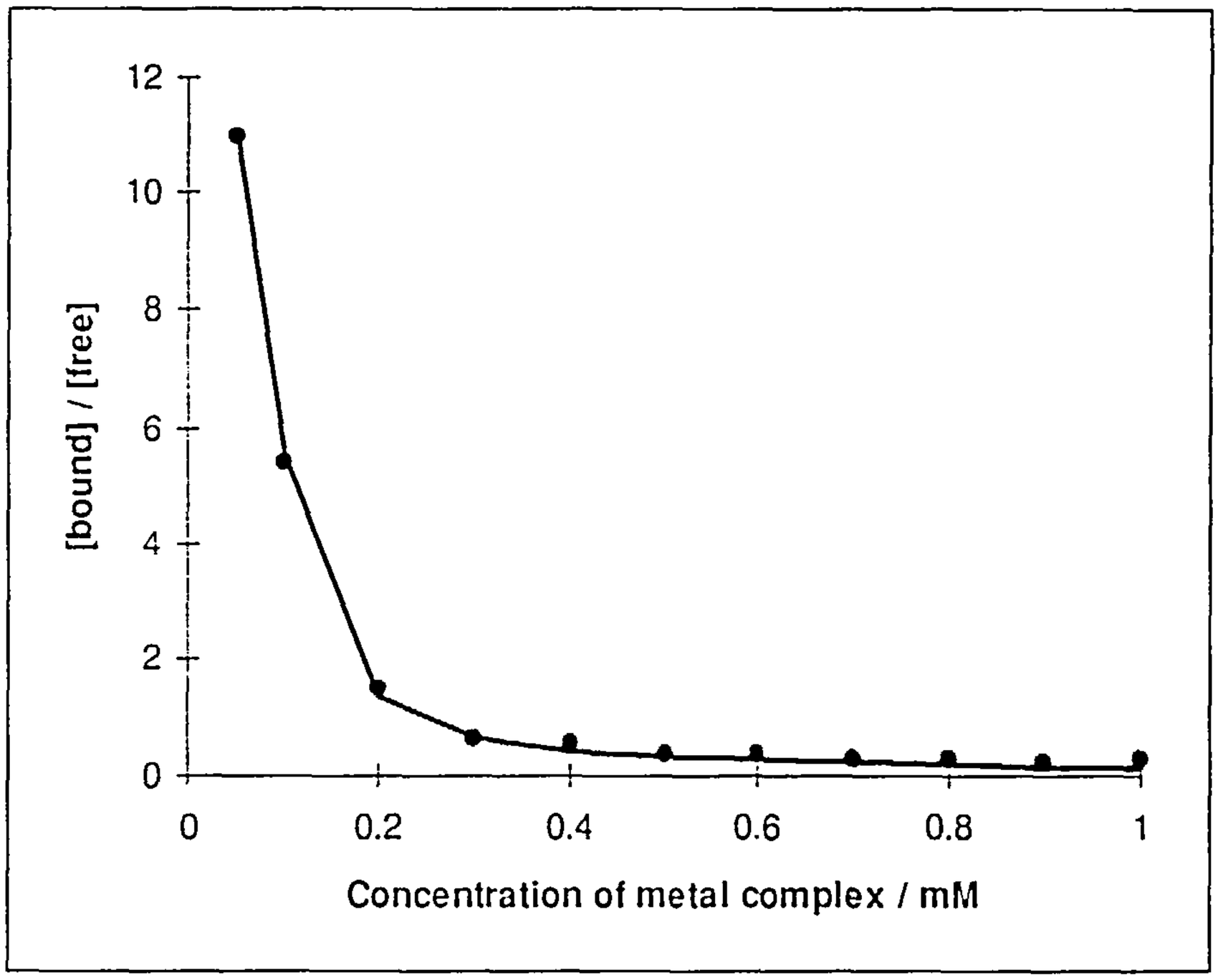

Figure 4.7.

Plot of the ratio of [bound]/[free] against the total concentration of $Ru(NH_3)_6^{3+}$ calculated from the UME titration of 0.4 mM DNA with $Ru(NH_3)_6^{3+}$.

The solid line is a least-squares fit with a binding constant, [$K = (1.47 \pm 0.04) \times 10^5$ dm^3 mol^{-1} , $s = (1.62 \pm 0.01)$].

4.2.2. N,N,N-TRIMETHYAMINOMETHYLFERROCENE IODIDE (Fc-NMe_3)

We also selected Fc-NMe_3 which is a singly positively charged metal complex and an expected weak DNA-electrostatic binder to study the metal complex-DNA interactions.

The cyclic voltammetric behavior of Fc-NMe_3 in 50 mM Tris buffer pH 7.0, in the absence and presence of double stranded DNA is given in figure 4.8. Titration of 2.7 mM DNA with Fc-NMe_3 was carried out in 50 mM Tris buffer, pH 7.0. A plot of titration of DNA with Fc-NMe_3 while measuring the peak current as a function of metal complex added is shown in figure 4.9. The titration curve in which the forward peak current was measured after addition of Fc-NMe_3 to a solution of DNA was used to obtain the binding constant and binding site size. Titration results were analysed by the combination of the equations that describes the binding equilibrium with that of the voltammetric response. In the presence of nucleic acids, the current is mainly due to free metal complex, as the diffusion rate of bound metal complex is small. The decrease in the peak current was used to calculate the amount of bound Fc-NMe_3. A plot of the ratio of [bound]/[free] against the total concentration of Fc-NMe_3 is given in figure 4.10. The binding constant of Fc-NMe_3 to DNA was determined as [$K = (2.1 \pm 1.3) \times 10^3$ dm^3 mol^{-1} , $s = (18.6 \pm 9.2)$]. The plots of the titration curves run parallel at high metal concentrations *i.e.* slopes are same. This shows that diffusion of free metal in the absence and presence of DNA is equal. The solution viscosity therefore has a small effect on the measurement of the binding. The scatter in figure 4.10 is large as could be expected for a weakly bound molecule.

Epa = 0.517V	Epc = 0.420V	ΔEp = 97 mV	$E^{o'}$ = 0.468 V

Table 4.2. Parameters of Fc-NMe_3 CV determined in this work.

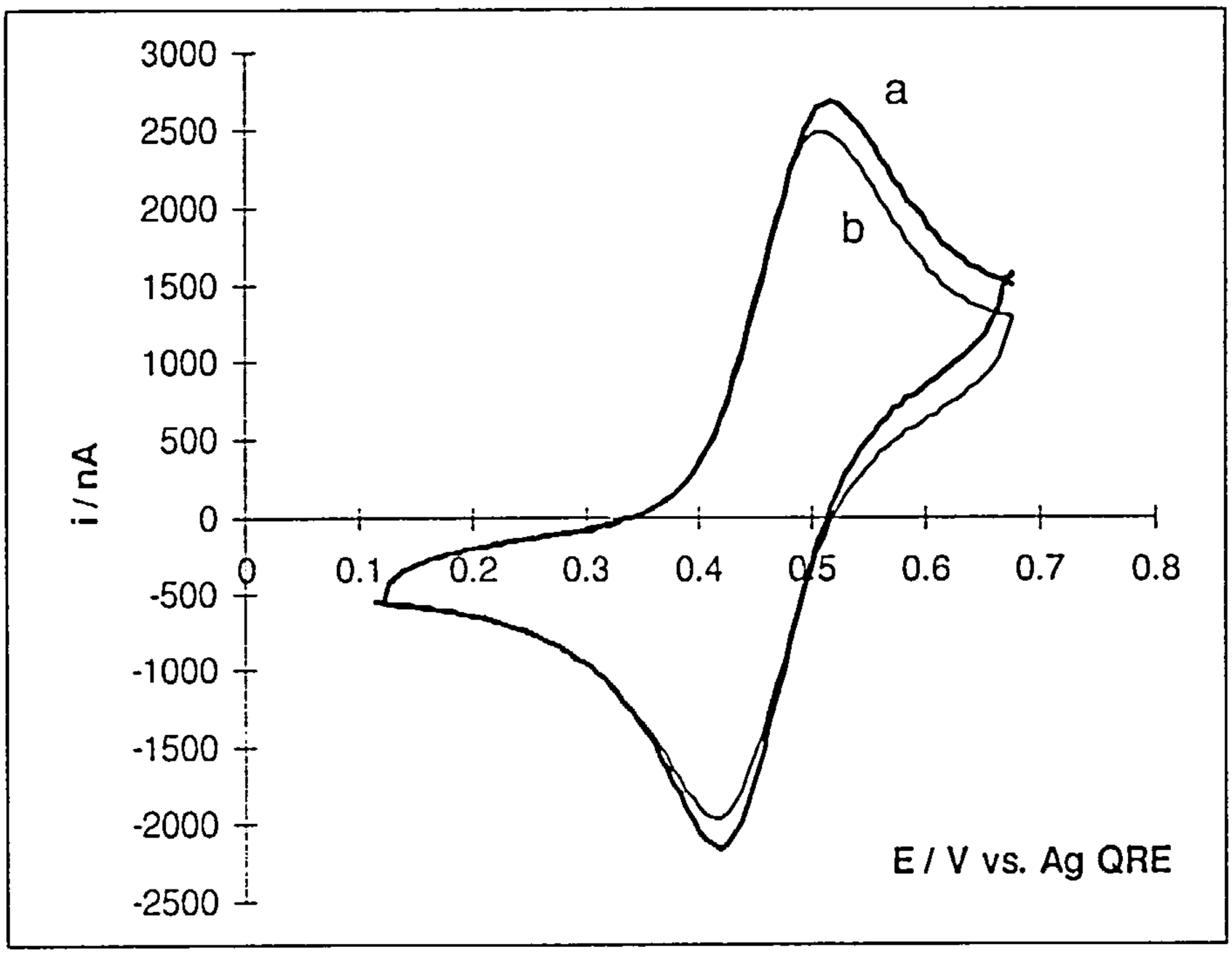

Figure 4.8.

Cyclic voltammograms of 0.45 mM Fc-NMe_3 in the (a) absence and (b) presence of 2.7 mM DNA.

Supporting electrolyte, 50 mM Tris, pH 7. Working electrode, gold disc (area, 0.0785 cm^2). Scan rate, 500 mV s^{-1}.

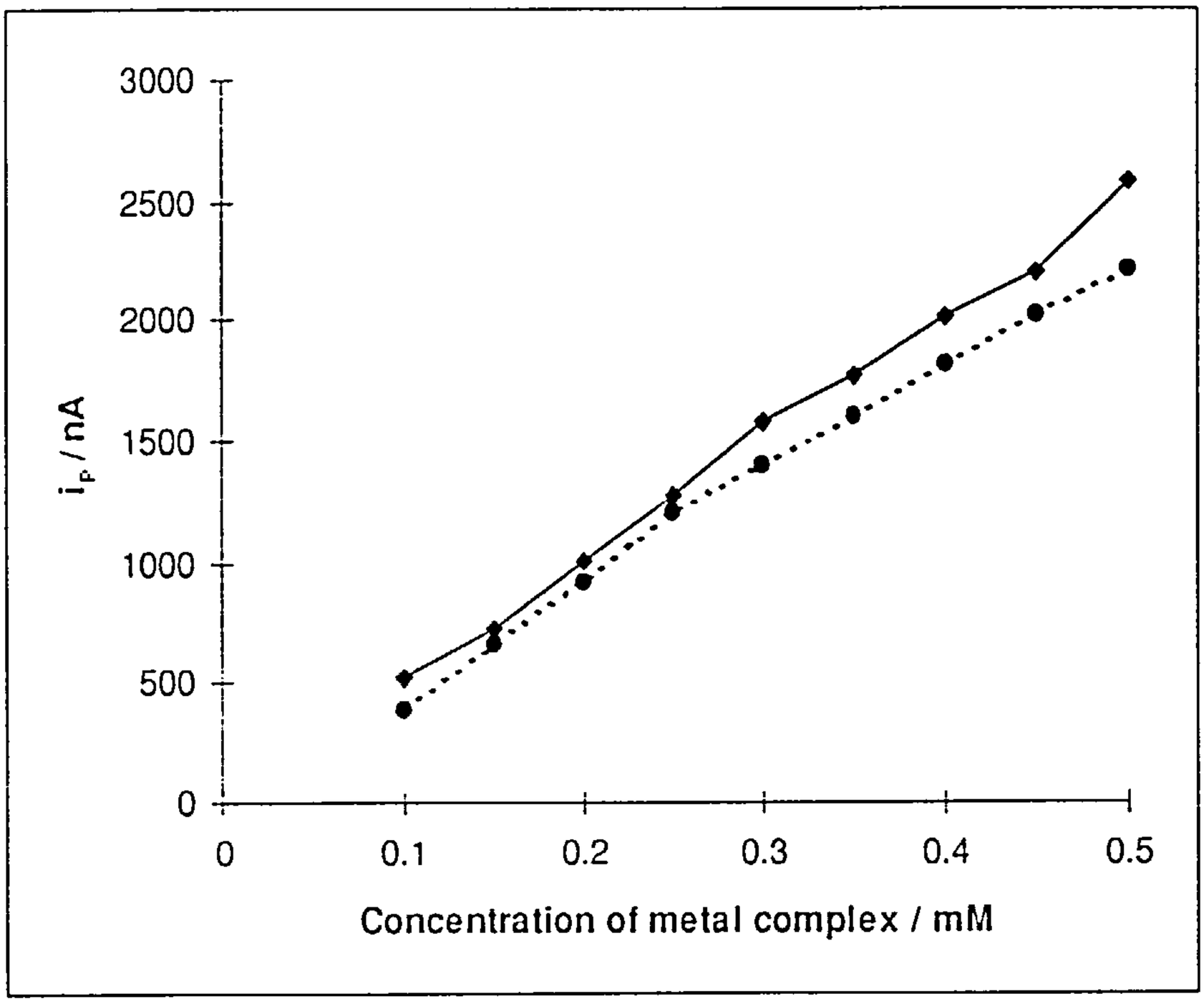

Figure 4.9.

The CV titration of 2.7 mM DNA with Fc-NMe_3(dashed line).

A plot of current against the total concentration of Fc-NMe_3 (solid line).

Supporting electrolyte, 50 mM Tris, pH 7. Working electrode, gold disc (area, 0.0785 cm^2). Scan rate, 150 mVs^{-1}.

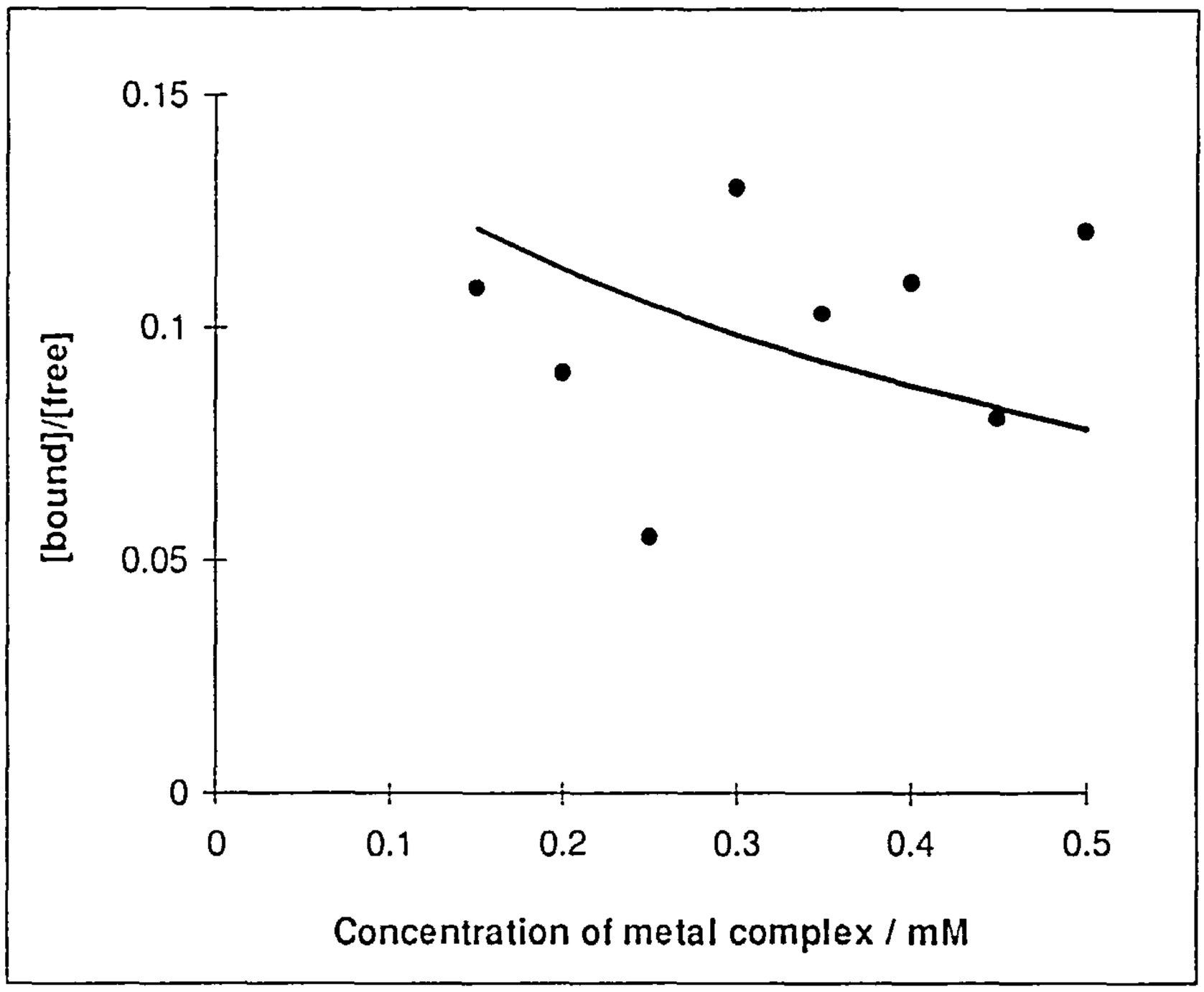

Figure 4.10.

Plot of the ratio of [bound]/[free] against the total concentration of Fc-NMe_3 calculated from the CV titration of 2.7 mM DNA with Fc-NMe_3.

The solid line is a least-squares fit with a binding constant, [$K = (2.1 \pm 1.3)\times10^3$ dm^3mol^{-1}, $s = (18.6 \pm 9.2)$].

Steady-state voltammetry was also applied to the study of metal complex-nucleic acid binding. Voltammetric behavior of Fc-NMe_3 at a 10 μm platinum microelectrode in the absence and presence of DNA is given in figure 4.11. The decrease in the limiting current as seen in figure 4.12, in the presence of DNA is the amount of bound Fc-NMe_3. The shift in the potential is probably due to the reference electrode.

Interaction of DNA with Fc-NMe_3 was carried out using a microelectrode to determine the binding constant of Fc-NMe_3 to DNA. Titration of DNA with Fc-NMe_3 was carried out to determine the binding constant, (*K*), and the binding site sizes, (*s*), of this interaction. Results for the titration of Fc-NMe_3 with DNA in 10 mM Tris buffer, pH 7.0 at a 10 μm platinum microelectrode are given in figure 4.5. The reduction in the limiting current was used to calculate the amount of bound metal complex. A plot of the ratio of [bound]/[free] against the total concentration of Fc-NMe_3 is given in figure 4.13. The binding constant and the binding site sizes of Fc-NMe_3 to DNA was then calculated using the reduction in the limiting current. The magnitude of the binding constant of Fc-NMe_3 to DNA was [$K = (1.4 \pm 0.2) \times 10^3$ dm^3 mol^{-1} , $s = (19.4 \pm 1.2)$]. The plot of [bound]/[free] *vs.* the concentration calculated from UME results has less scatter. Therefore, the binding constant is more precise.The standard deviations of binding constant and binding site sizes determined from the titration studies of the interaction of Fc-NMe_3 with DNA are therefore smaller for the UME results.

As the ionic strength was increased by adding KCl into a solution of Fc-NMe_3-DNA, the limiting current rose as the magnitude of the binding constant decreased. Figure 4.14 shows the dependence of the binding of the Fc-NMe_3 to DNA with increasing salt concentration. The limiting current was increased further at higher ionic concentration.

This behavior shows a typical electrostatic interaction between Fc-NMe_3 and DNA. The large scatter in figures 4.10 and 4.13 are a result of the weak binding of Fc-NMe_3 to DNA. The values of binding constant obtained, *ca.* 10^3 $moldm^{-1}$ represent the weakest binding detectable by this technique.

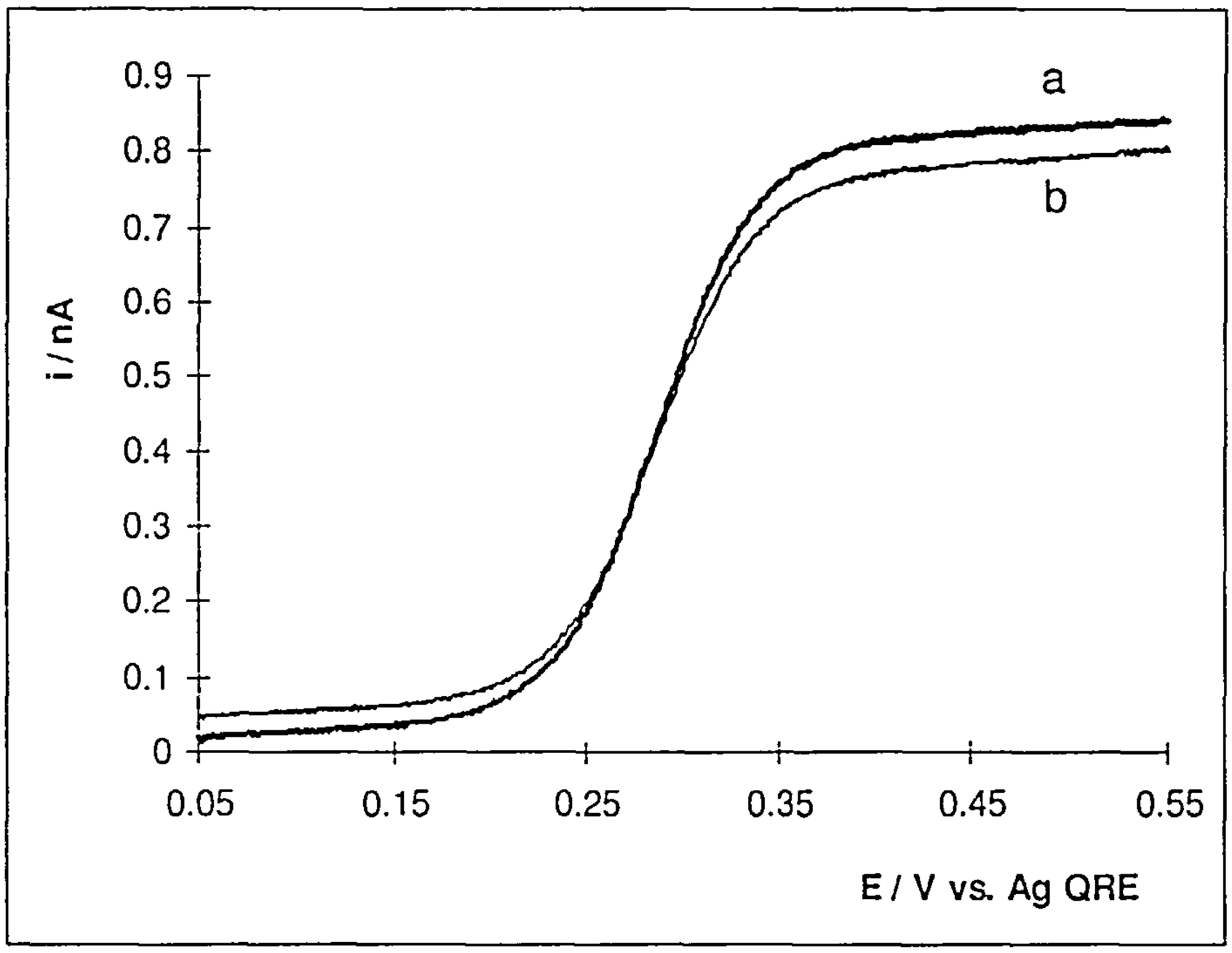

Figure 4.11.

Microelectrode voltammograms of 0.55 mM Fc-NMe_3 (a) in the absence and (b) presence of 4.0 mM DNA.

Supporting electrolyte, 10 mM Tris pH 7. Working electrode, platinum disc (diameter, 10 μm).

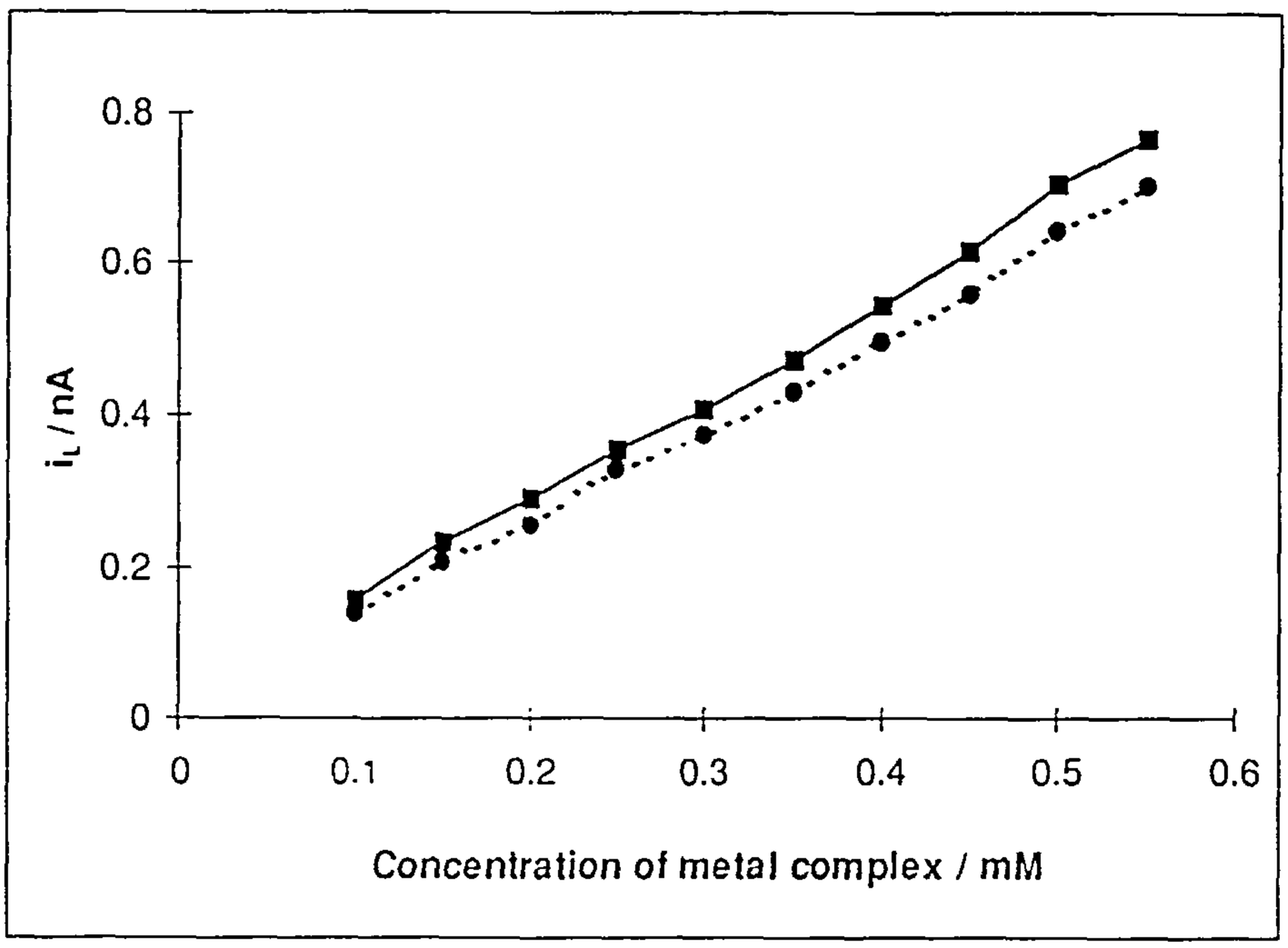

Figure 4.12.

The UME itration of 4.0 mM DNA with Fc-NMe_3 (dashed line).

Plot of current against the total concentration of Fc-NMe_3 (solid line).

Supporting electrolyte, 10 mM Tris pH 7. Working electrode, platinum disc (diameter, 10 μm).

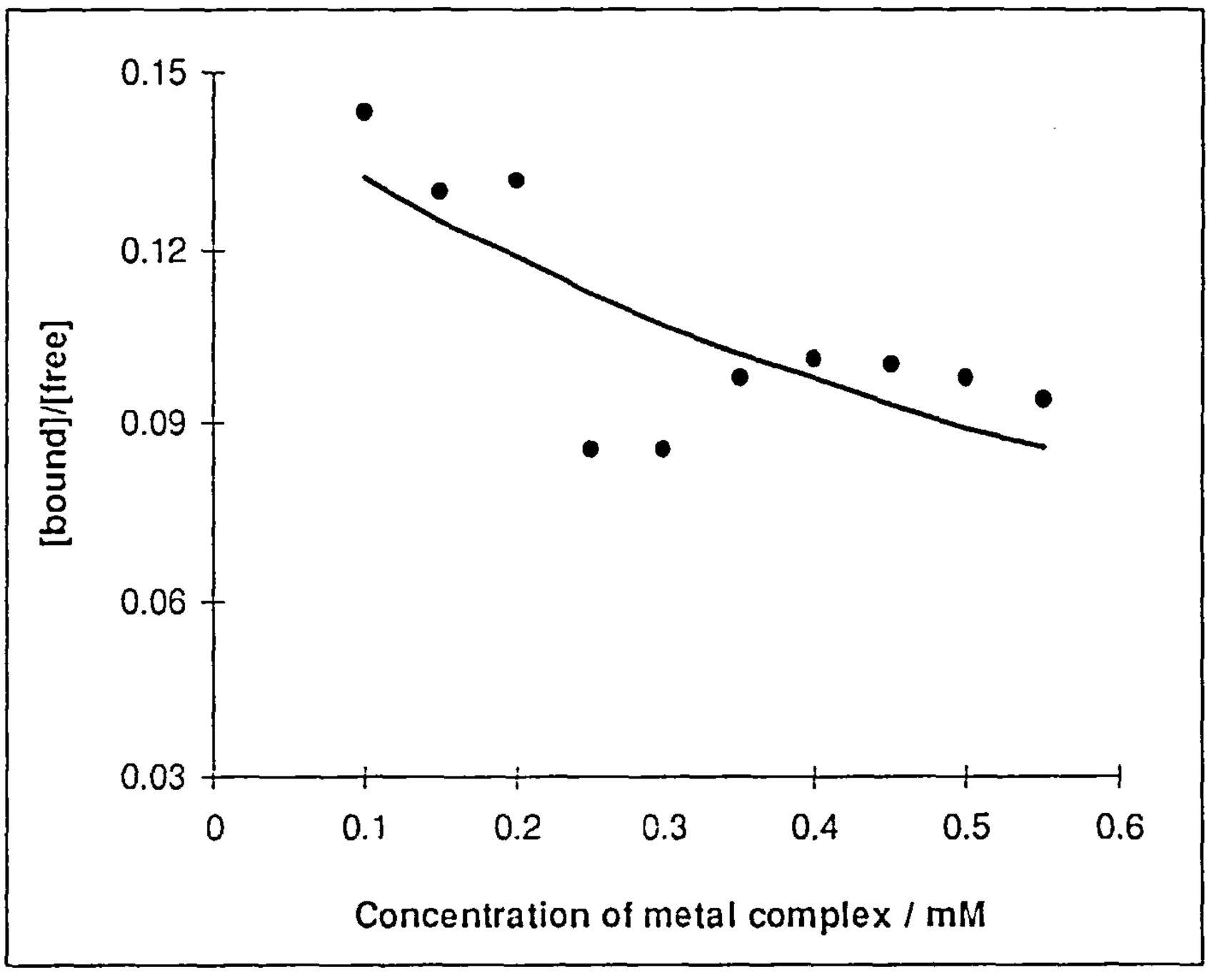

Figure 4.13.

Plot of the ratio of [bound]/[free] against the total concentration of Fc-NMe_3 calculated from the UME titration of 4.0 mM DNA with Fc-NMe_3 using microelectrode voltammetry.

The solid line is a least-squares fit with a binding constant, [$K = (1.4 \pm 0.2) \times 10^3$ dm^3 mol^{-1}, $s = (19 \pm 1.2)$].

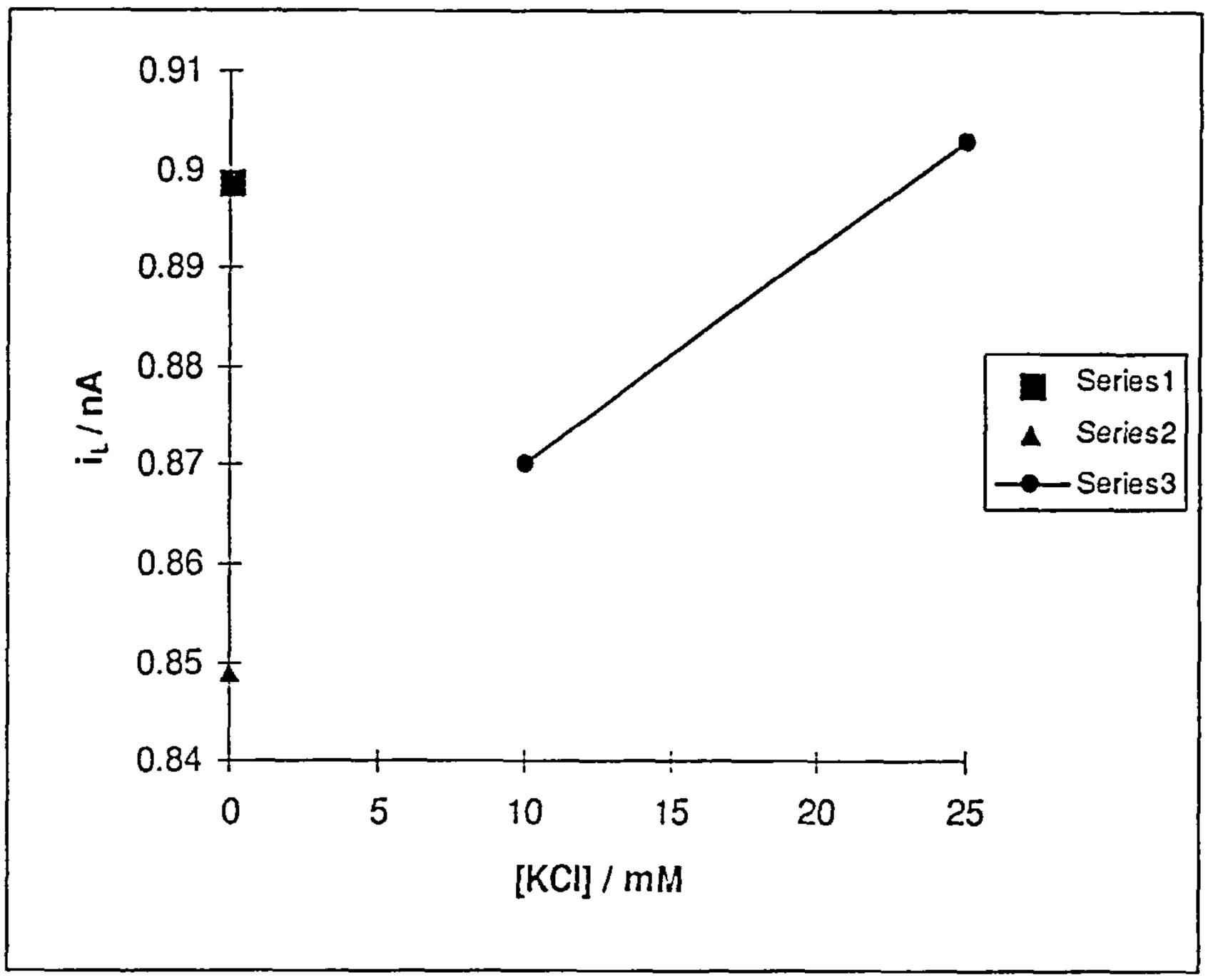

Figure 4.14.

The ionic strength dependence of the binding of Fc-NMe_3 to DNA determined using a 10 μm diameter platinum microdisc electrode.

Series 1. The limiting current of a solution containing only Fc-NMe_3 in 10 mM Tris buffer.

Series 2. The limiting current of a solution containing Fc-NMe_3 and DNA in 10 mM Tris buffer.

Series 3. The limiting current of a solution containing Fc-NMe_3, DNA and potassium chloride in 10 mM Tris buffer.

4.2.3. N,N,N-1-PROPYLTHYMINEAMINOMETHYLFERROCENE TETRAFLUOROBORATE (Fc-Th)

Cyclic voltammetry and steady-state voltammetry were applied to the interaction Fc-Th with both DNA and RNA to determine binding constants and to determine the effect of thymine on the binding.

Fc-Th was interacted with both RNA in 50 mM Tris buffer, pH 7.0 and in 10 mM Tris buffer, pH 7.0 and DNA in 10 mM Tris, pH 7.0. The results for RNA+50 mM Tris buffer are discussed first and then DNA and RNA are compared in 10 mM Tris.

CV behavior of Fc-Th in 50 mM Tris, pH 7.0 in the absence and presence of RNA is given in figure 4.15. Cyclic voltammetry was also applied to see any changes at lower concentration of Tris buffer and CV behavior of Fc-Th in 10 mM Tris, pH 7.0 in the absence and presence of RNA is given in figure 4.17.

Cyclic voltammetric titration results of Fc-Th with RNA in 50 mM Tris buffer, pH 7.0 at a gold disc electrode are shown in figure 4.18. The amount of bound metal complex was calculated from the decrease in the cyclic voltammetric anodic peak current. A plot of the ratio of [bound]/[free] against the total concentration of Fc-Th is given in figure 4.19.

In 50 mM Tris buffer, we found the binding constant of the interaction between Fc-Th and RNA as [$K = (2.3 \pm 2.\ 1) \times 10^3$ dm^3 mol^{-1} , $s = (23.3 \pm 13.5)$]. The standard deviations of K and s are very large and the scatter is large as seen in the plot of [bound]/[free].

Cyclic voltammetry of Fc-Th in 10 mM Tris, pH 7.0 in the absence and presence of DNA is shown in figure 4.16.

Epa = 0.404 V	Epc = 0.320 V	ΔEp = 84 mV	$E^{o'}$ = 0.362 V

Table 4.3. Parameters of Fc-Th CV determined in this work.

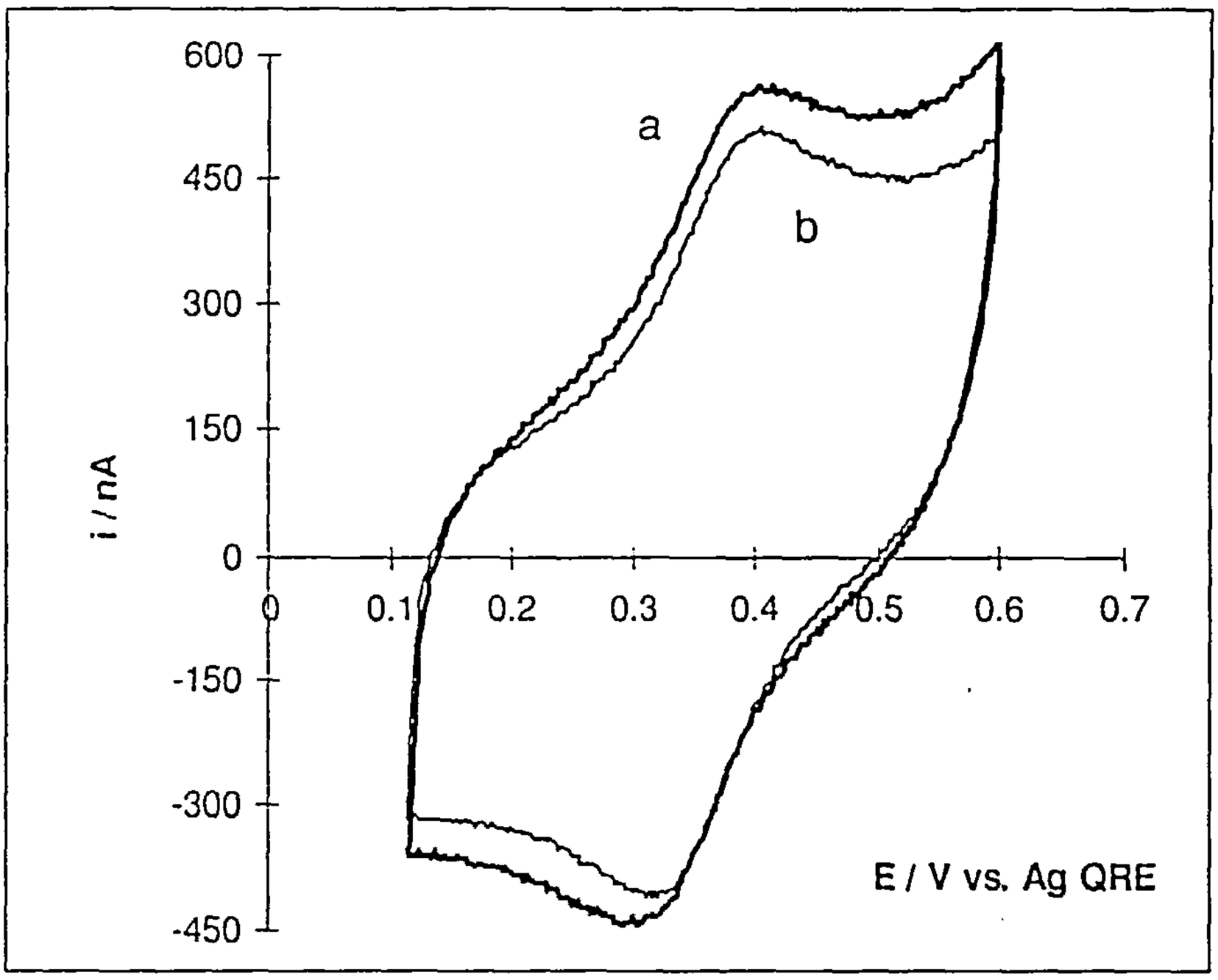

Figure 4.15.

Cyclic voltammograms of 0.4 mM Fc-Th in the (a) absence and (b) presence of 2.7 mM RNA.

Supporting electrolyte, 50 mM Tris, pH 7. Working electrode, gold disc (area, 0.0785 cm^2). Scan rate, 150 mV s^{-1}.

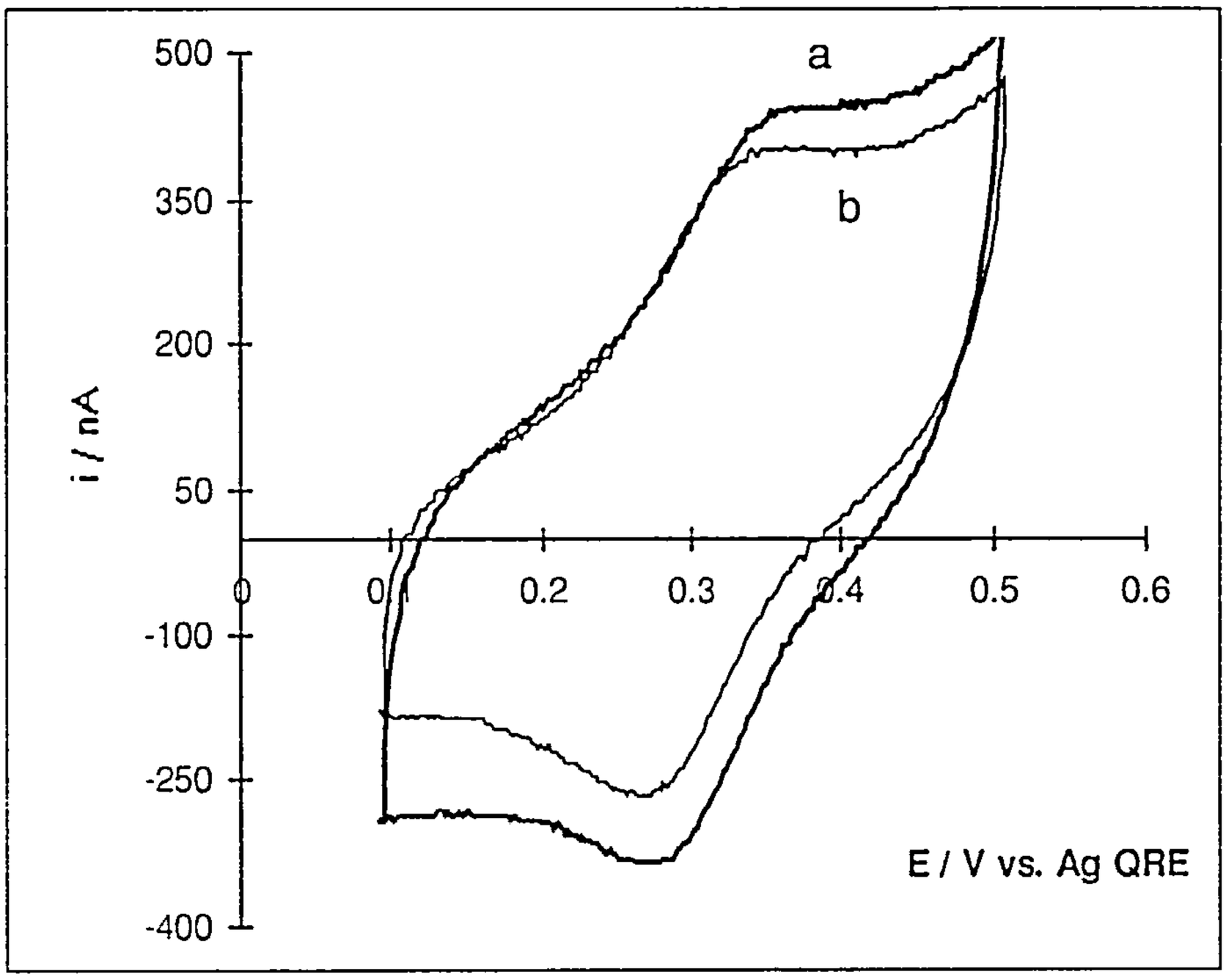

Figure 4.16.

Cyclic voltammograms of 0.3 mM Fc-Th in the (a) absence and (b) presence of 2.7 mM DNA.

Supporting electrolyte, 10 mM Tris, pH 7. Working electrode, gold disc (area, 0.0785 cm^2). Scan rate, 150 mV s^{-1}.

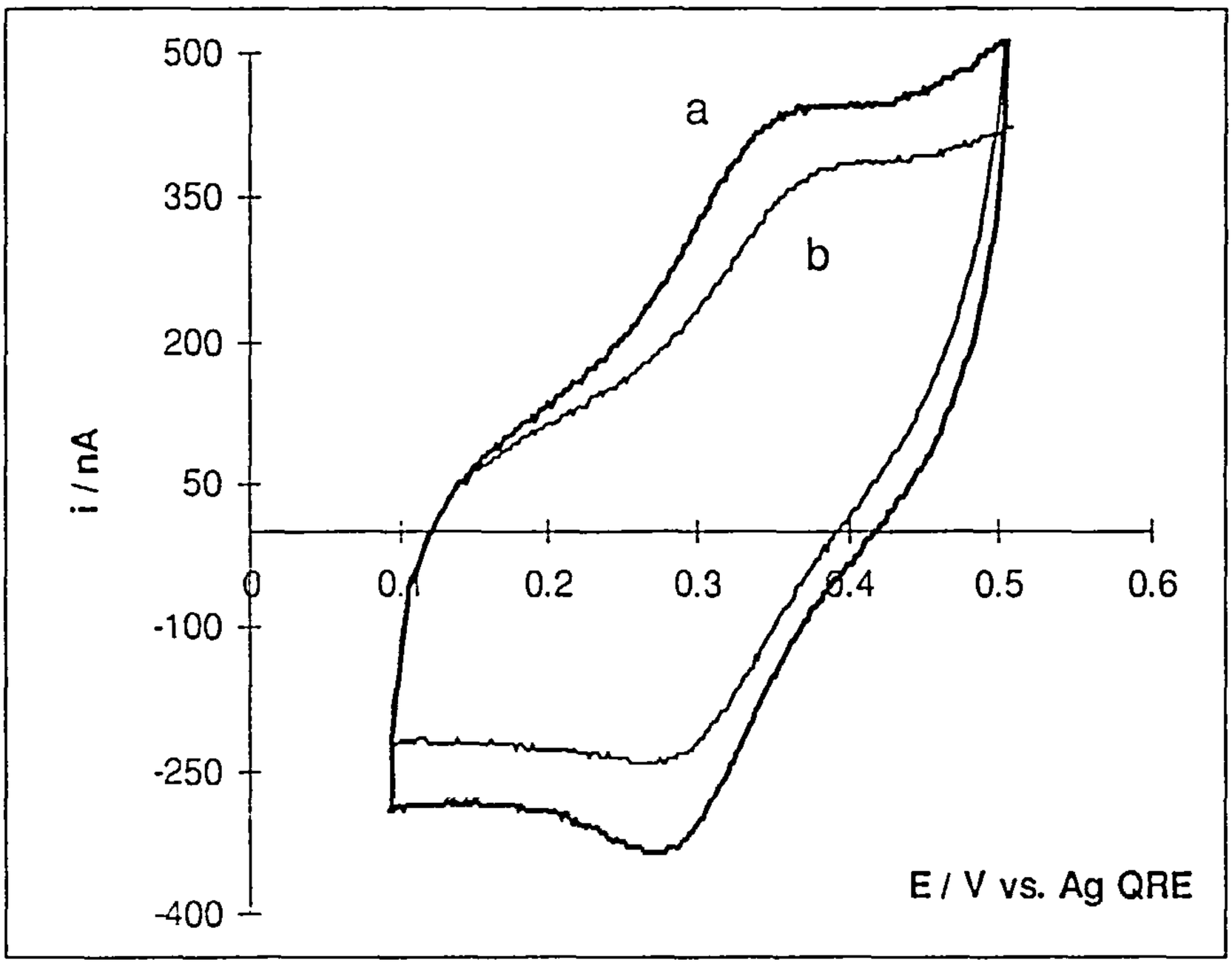

Figure 4.17.

Cyclic voltammograms of 0.3 mM Fc-Th in the (a) absence and (b) presence of 2.7 mM RNA.

Supporting electrolyte, 10 mM Tris, pH 7. Working electrode, gold disc (area, 0.0785 cm^2). Scan rate. 150 mV s^{-1}.

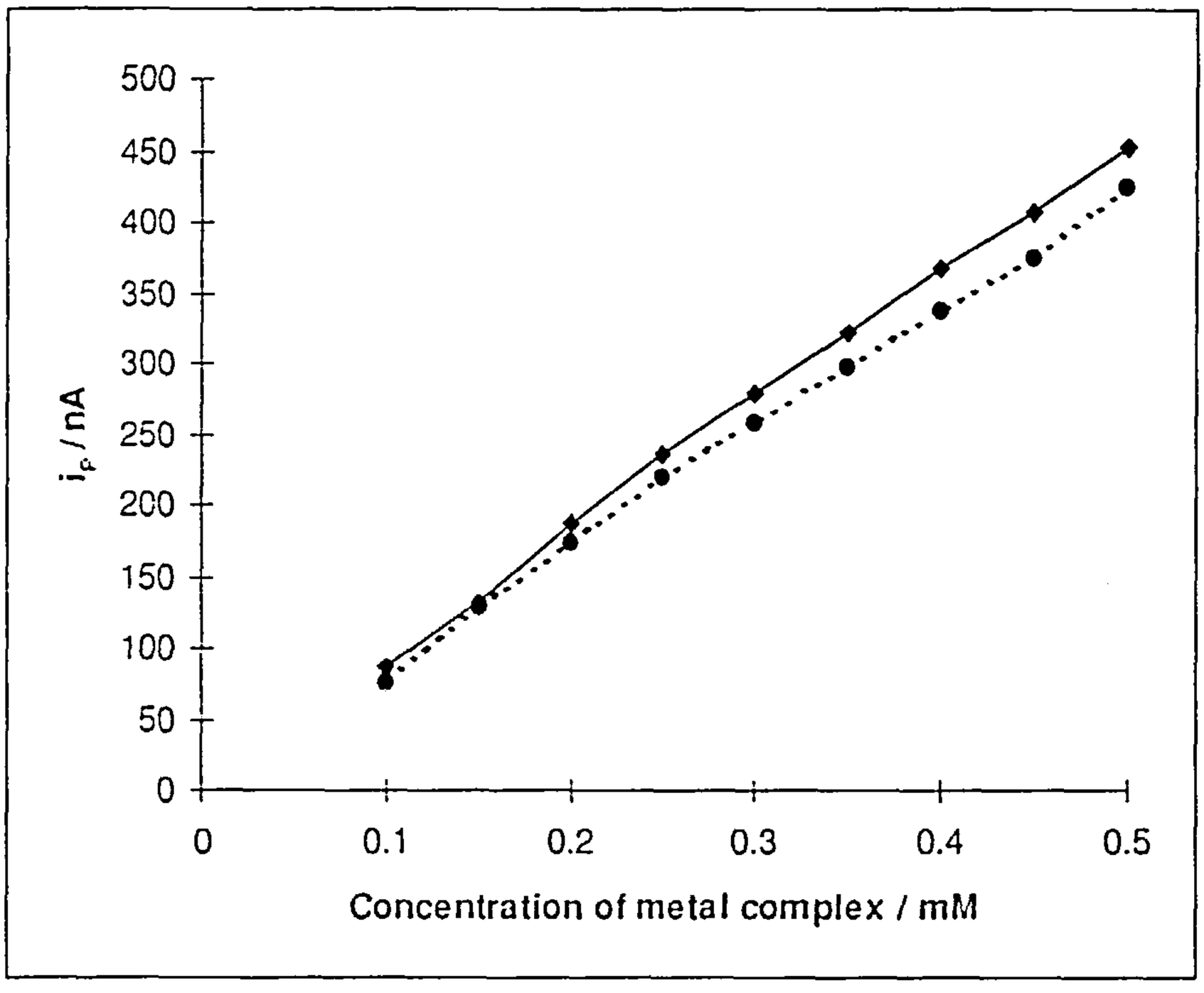

Figure 4.18.

The CV titration of 2.7 mM RNA with Fc-Th (dashed line).

A plot of current against the total concentration of Fc-Th (solid line).

Supporting electrolyte, 50 mM Tris pH 7. Working electrode, gold disc (area, 0.0785 cm^2). Scan rate, 150 mVs^{-1}.

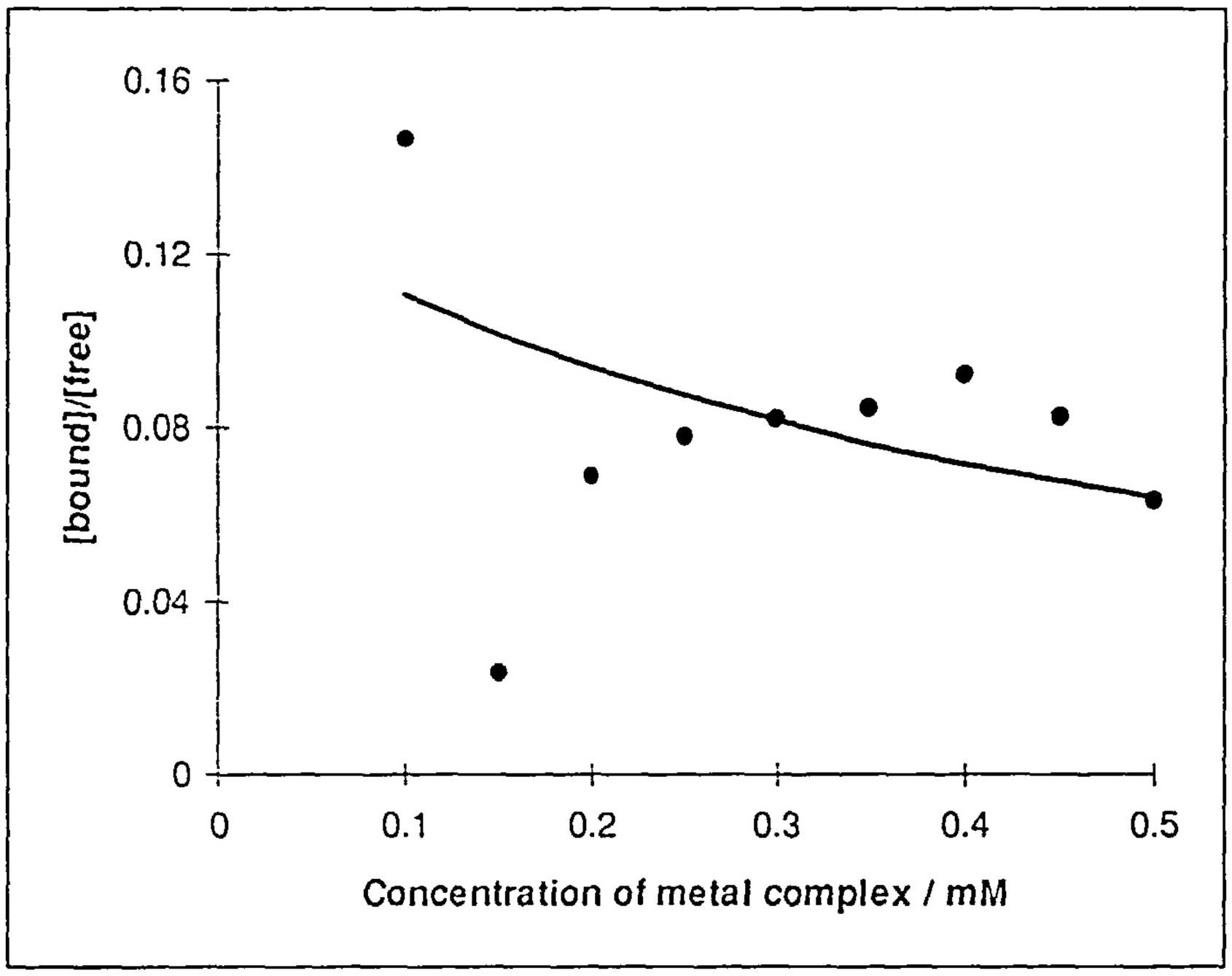

Figure 4.19.

Plot of the ratio of [bound]/[free] against the total concentration of Fc-Th calculated from the CV titration of 2.7 mM RNA with Fc-Th.

The solid line is a least-squares fit with a binding constant, [$K = (2.3 \pm 2.1) \times 10^3$ dm^3 mol^{-1}, $s = (23.3 \pm 13.5)$].

To determine the magnitude of the binding constant of Fc-Th to DNA in a 10 mM Tris buffered electrolytic media, the titration was carried out by the application of cyclic voltammetry. Titration results of Fc-Th with DNA in 10 mM Tris buffer, pH 7.0 are illustrated in figure 4.20. The anodic current response for Fc-Th with and without was used to determine the bound metal complex and the binding constant. A plot of the ratio of [bound]/[free] against the total concentration of Fc-Th is given in figure 4.22.The magnitude of the binding constant of Fc-Th to DNA in 10 mM Tris buffer, was found as [$K = (3.5 \pm 2.4) \times 10^3$ dm^3 mol^{-1} , $s = (26 \pm 12.4)$].

Voltammetric titration of the interaction of Fc-Th with RNA was also carried out in 10 mM Tris buffer. Cyclic voltammetric titration results of Fc-Th with RNA in 10 mM Tris buffer, pH 7.0 are illustrated in figure 4.21. The current response for oxidation of Fc-Th with and without RNA were used to plot the results for the titration. The plot of the ratio of [bound]/[free] against the total concentration of Fc-Th is given in figure 4.23. The magnitude of the binding constant of Fc-Th to RNA in 10 mM Tris buffer, was found as [$K = (7.1 \pm 4.7) \times 10^3$ dm^3 mol^{-1} , $s = (28 \pm 10)$]. The magnitude of the binding constant of Fc-Th to RNA in 10 mM Tris buffer obtained is larger than that of in 50 mM Tris. This is probably due to an ionic strength effect. Also, Fc-Th in 10 mM Tris buffer bound more strongly to RNA than DNA. This is probably because RNA is a single stranded nucleic acid. Therefore, some of the binding energy may be due to a hydrogen bonding interaction between Fc-Th and the bases of RNA.

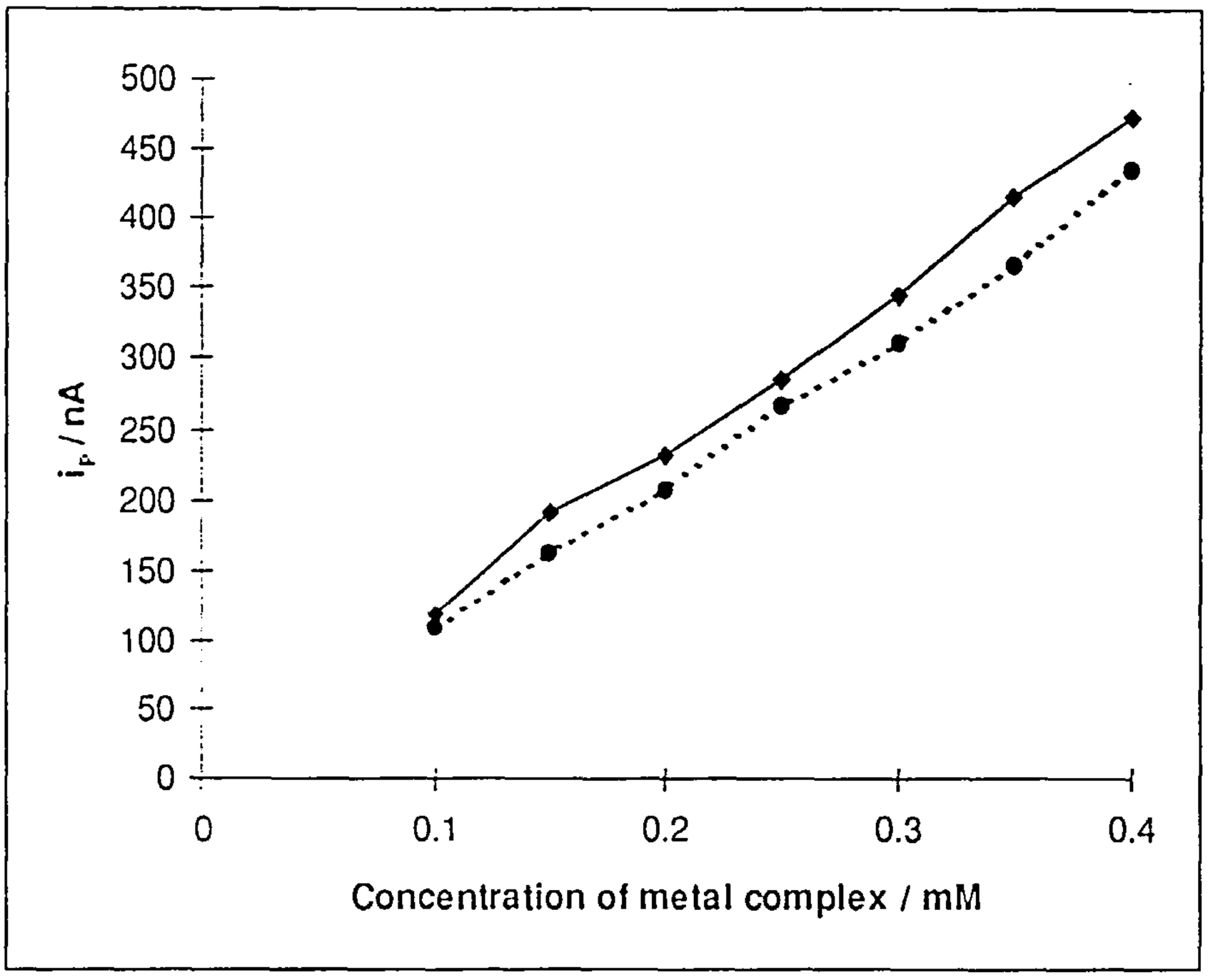

Figure 4.20.

The CV titration of 2.7 mM DNA with Fc-Th (dashed line).

A plot of current against the total concentration of Fc-Th (solid line).

Supporting electrolyte, 10 mM Tris pH 7. Working electrode, gold disc (area, 0.0785 cm^2). Scan rate, 150 mVs^{-1}.

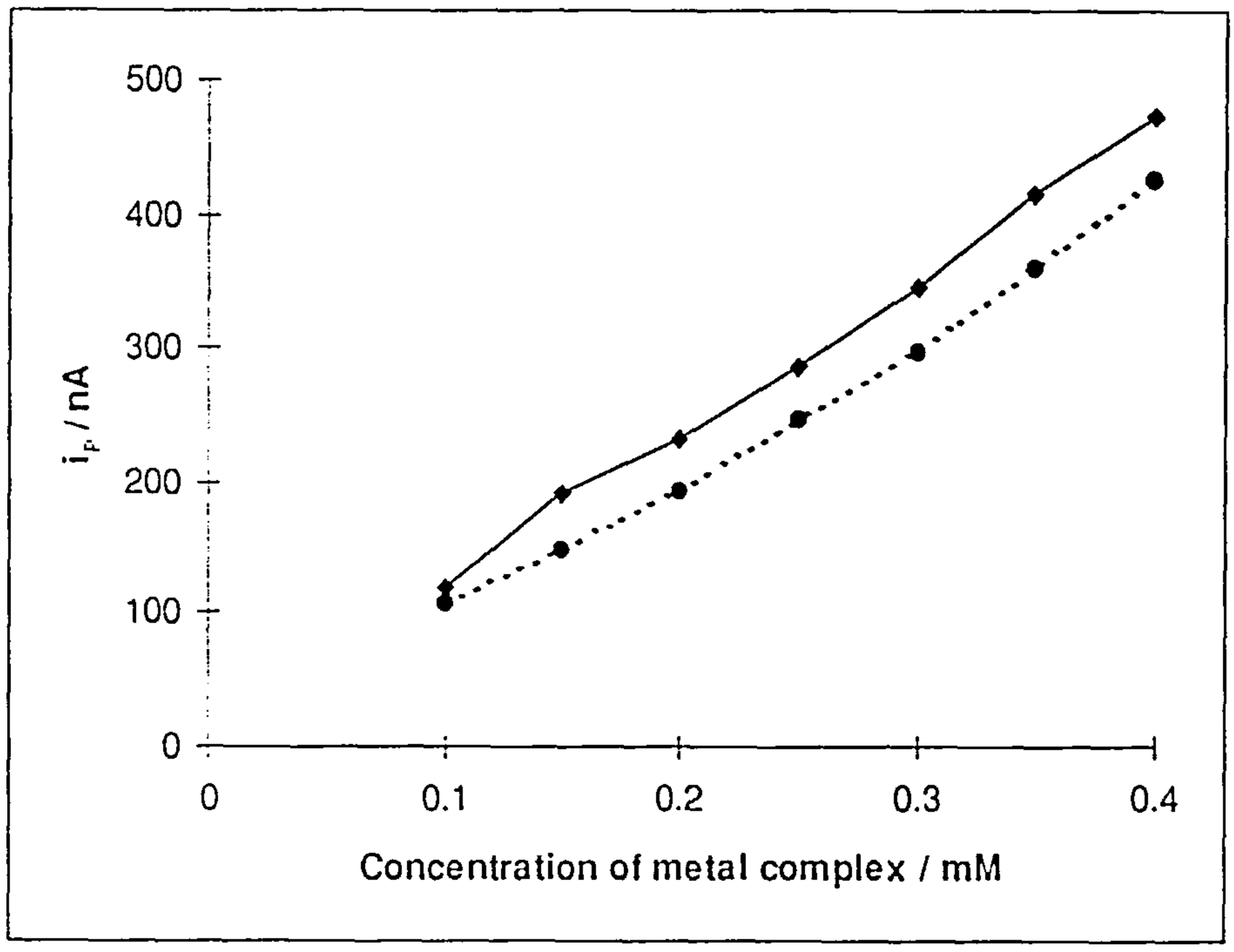

Figure 4.22.

The CV titration of 2.7 mM RNA with Fc-Th (dashed line).

A plot of current against the total concentration of Fc-Th(solid line).

Supporting electrolyte, 10 mM Tris pH 7. Working electrode, gold disc (area, 0.0785 cm^2). Scan rate, 150 mVs^{-1}.

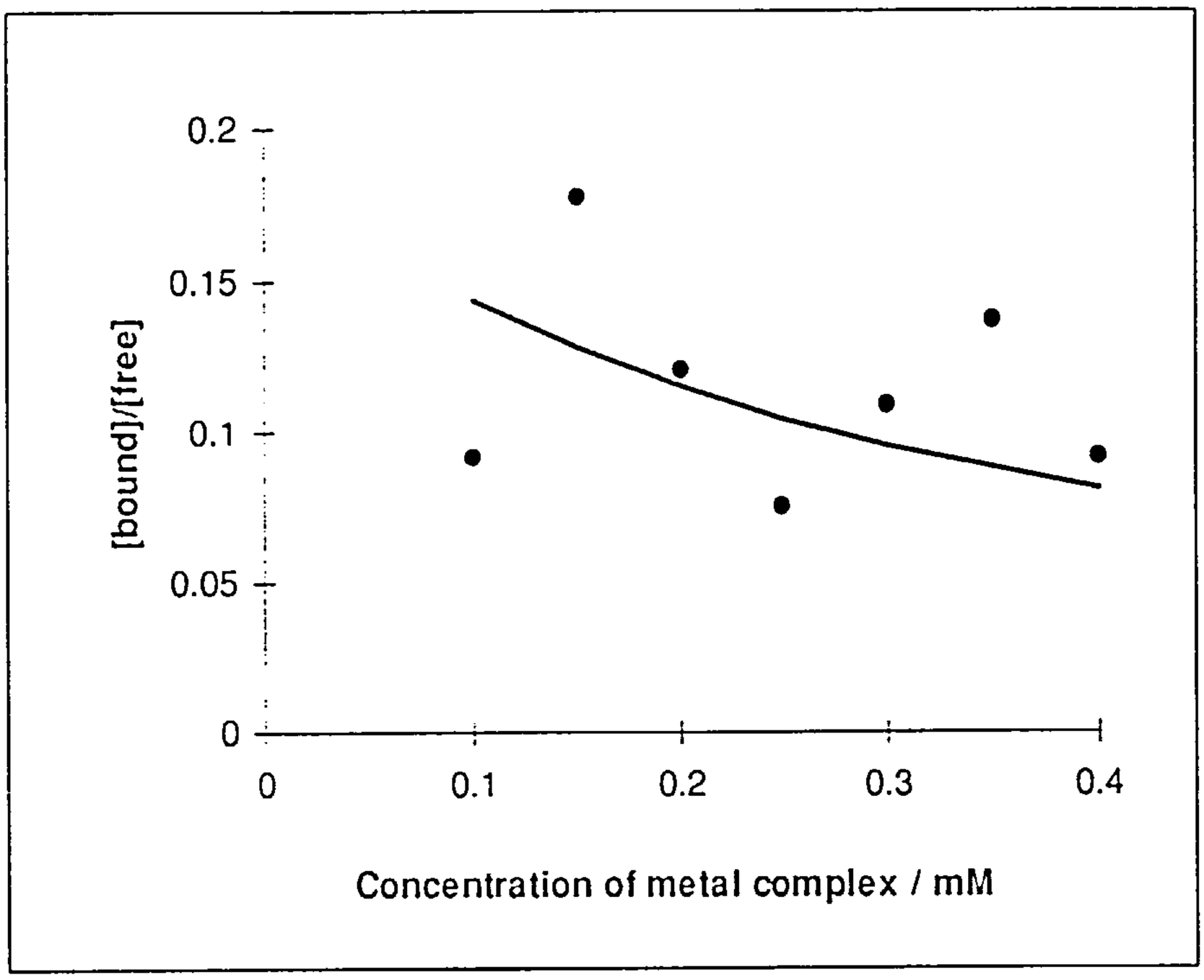

Figure 4.22.

Plot of the ratio of [bound]/[free] against the total concentration of Fc-Th calculated from the CV titration of 2.7 mM DNA with Fc-Th.

The solid line is a least-squares fit with a binding constant, [$K = (3.5 \pm 2.4) \times 10^3$ dm^3 mol^{-1}, $s = (26 \pm 12.4)$].

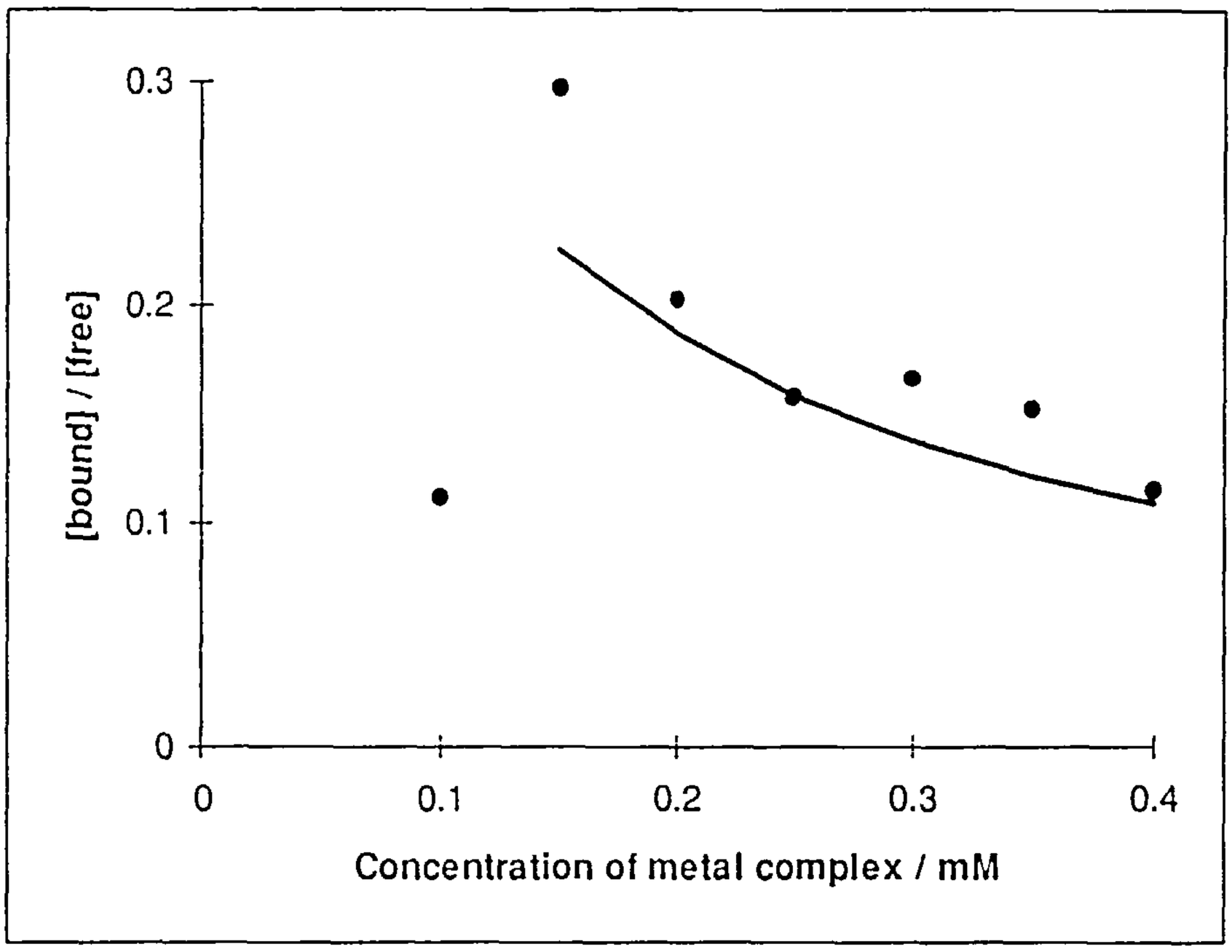

Figure 4.23.

Plot of the ratio of [bound]/[free] against the total concentration of Fc-Th calculated from the CV titration of 2.7 mM RNA with Fc-Th.

The solid line is a least-squares fit with a binding constant, [$K = (7.1 \pm 4.7) \times 10^3$ dm^3 mol^{-1}, $s = (28 \pm 10)$].

Microelectrode voltammetry was also applied to the interaction of Fc-Th with nucleic acids. Microelectrodes were also applied to this interaction to compare UME and CV and to detect the difference between Fc-Th and Fc-NMe_3 binding to DNA. The differences in the binding can be attributed to the thymine base.

Microelectrode voltammetric behavior of Fc-Th in the absence and presence of 3.5 mM DNA and 10 mM Tris buffer, pH 7.0 at a 25 μm platinum microdisc electrode is given in figure 4.24.

Titration was carried out to obtain the binding constant and the binding site sizes for the interaction of Fc-Th with DNA using steady-state voltammetry. The limiting current response for the oxidation of Fc-Th in the absence and presence of 3.5 mM DNA against the total concentration of Fc-Th in 10 mM Tris buffer, pH 7, at a 25 μm platinum disc microelectrode is plotted in figure 4.26. At higher concentration of metal complex, the slopes ofr the plots are about same and the effect of viscosity on the diffusion rates is small. The ratio of [bound]/[free] against the total concentration of Fc-Th calculated from the decrease in the limiting current is plotted in figure 4.28. The magnitude of the binding constant of Fc-Th to DNA determined using titration results is [$K = (6.4 \pm 0.4) \times 10^3$ dm^3 mol^{-1} , $s = (25 \pm 1)$]. The standard deviations of the magnitude of the binding constant for interaction of Fc-Th with DNA as seen is smaller in the case of microelectrode voltammerty. Since the limiting current at a microelectrode is directly proportional the diffusion coefficient of the metal complex, the contribution of the bound metal complex to the limiting current is small as we observed in the binding of $Ru(NH_3)_6^{3+}$ to DNA at UME (figure 4.6). Therefore. the limiting current at a microdisc is directly proportional to the free metal concentration. As in CV experiments, bound metal contributes to the diffusion

current, the decrease in the current is less. This explains the smaller apparent binding constant measured by cyclic voltammetry ($K_{UME} > K_{CV}$). The magnitude of the binding constant of Fc-Th to DNA is larger than the binding constant of Fc-NMe_3 to DNA. This confirms that thymine has a significant role on the binding as well as electrostatic forces due to the single positive charge. Fc-NMe_3 has no hydrogen bonding groups and its interaction with DNA is therefore essentially due to the single positive charge on the nitrogen atom.

Voltammetric behavior of Fc-Th, at a 25 μm platinum microdisc electrode, in the absence and presence of 3.5 mM RNA and 10 mM Tris buffer, pH 7.0 is given in figure 4.25.

Titration of Fc-Th against RNA was carried out to determine the binding constant of Fc-Th to RNA using the microelectrode technique. Steady-state limiting current against the total concentration of Fc-Th in the absence and presence of 3.5 mM RNA is plotted in figure 4.27. At small concentrations of metal complex, the slopes are different. But at higher concentrations of metal complex, the slopes are almost same and viscosity effect is very small. Also, to see change in the binding with concentration a plot of the ratio of [bound]/[free] against the total concentration of Fc-Th which was calculated from the reduction in the diffusion limiting current is given in figure 4.29. The magnitude of the binding constant of Fc-Th to RNA calculated from the titration is [$K = (1.2 \pm 0.15) \times 10^4$ dm^3 mol^{-1} , $s = (26 \pm 1.6)$]. In the case of steady-state voltammetry, less scatter was observed. The deviations of the binding constant and the binding site sizes is much smaller. This confirms that the binding constant determined at UME is more reliable. The magnitude of the binding constant of Fc-Th to RNA [$K = (1.2 \pm 0.15) \times 10^4$ dm^3 mol^{-1} , s

= (26 ± 1.6)] is about twice that for DNA [$K = (6.4 \pm 0.4) \times 10^3$ dm^3 mol^{-1} , $s = (25 \pm 1)$]. This is may be because RNA is partially single stranded and the thymine has more oppurtunities for hydrogen bonding to the bases than in the case of DNA.

The effect of ionic strength on the interaction of Fc-Th with DNA and RNA was also investigated. The binding constant was decreased by the addition of potassium chloride. A significant contribution to the binding is an electrostatic interaction. Since the major difference between Fc-Th and Fc-NMe_3 is only thymine and the binding of Fc-Th to DNA is larger than the binding of Fc-NMe_3 to DNA, thymine has a role in the binding of Fc-Th to DNA. A plot of current against the concentration of potassium chloride both in the case of DNA and RNA is given in figures 4.30. Significant binding of Fc-Th to RNA is observed even in 20 mM KCl which suggests hydrogen-bonding interactions may be important.

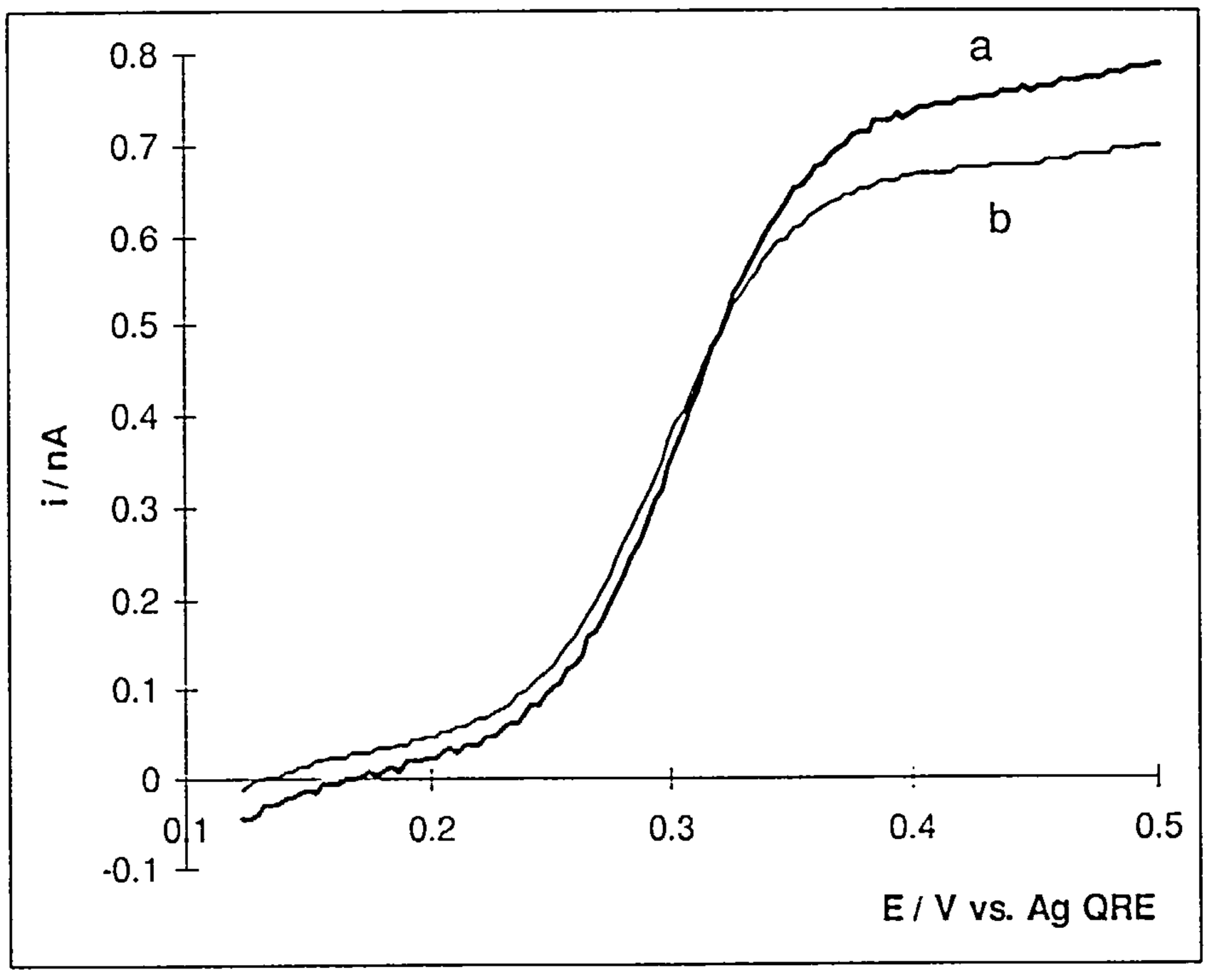

Figure 4.24.

Microelectrode voltammograms of 0.5 mM Fc-Th (a) in the absence and (b) presence of 3.5 mM DNA.

Supporting electrolyte. 10 mM Tris pH 7. Working electrode. platinum disc (diameter, 25 μm).

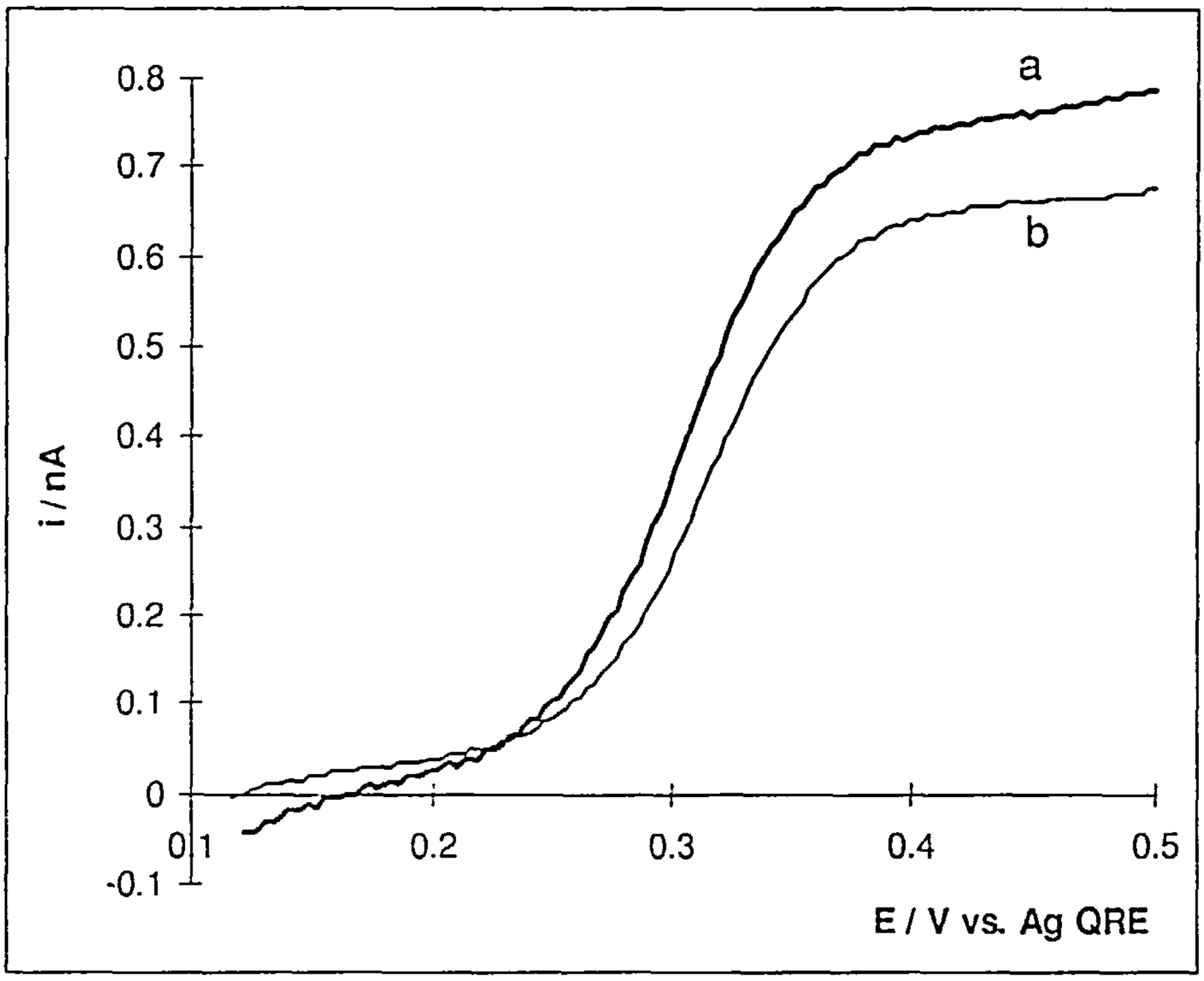

Figure 4.25.

Microelectrode voltammograms of 0.5 mM Fc-Th (a) in the absence and (b) presence of 3.5 mM RNA.

Supporting electrolyte, 10 mM Tris pH 7. Working electrode, platinum disc (diameter, 25 μm).

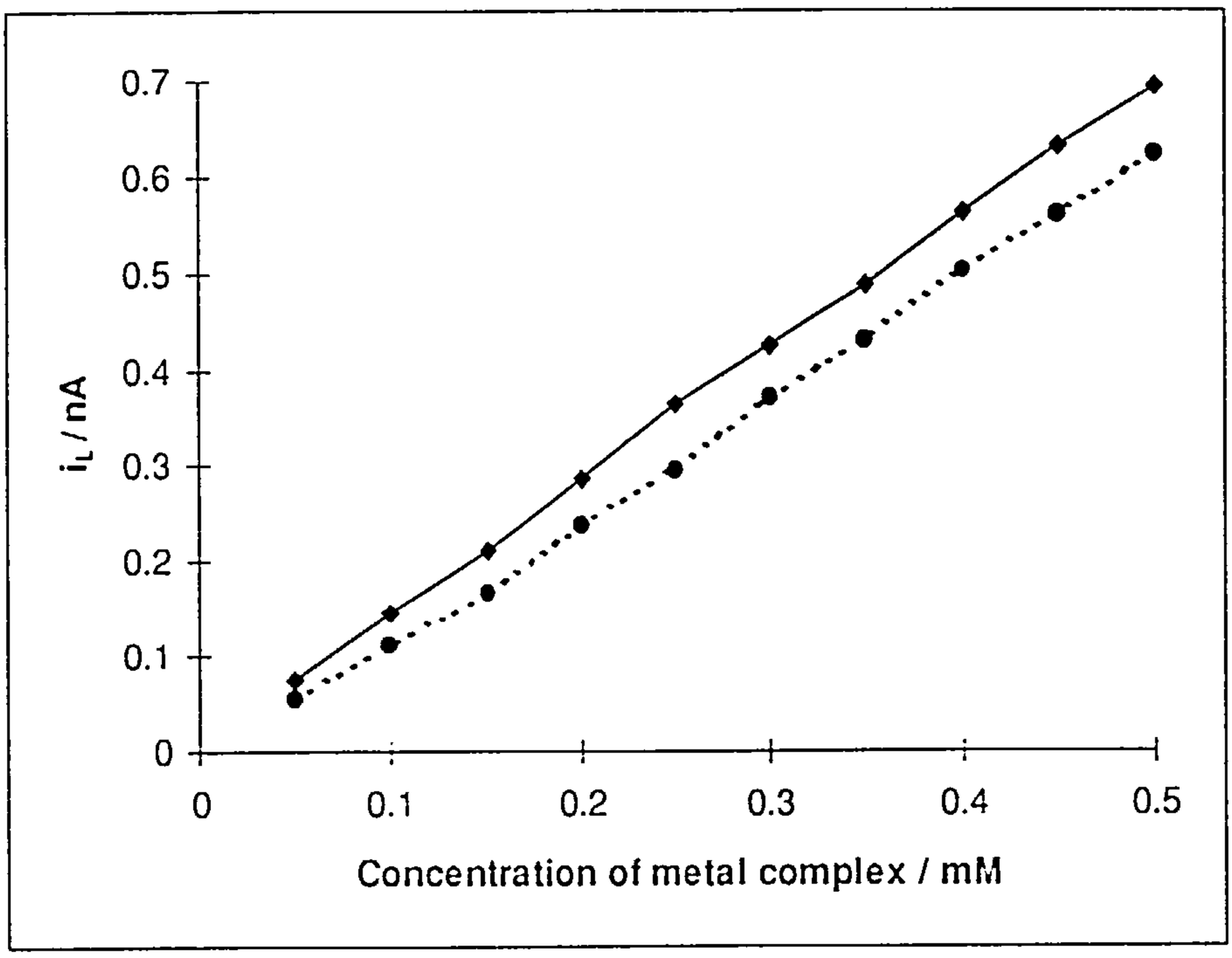

Figure 4.26.

The UME titration of 3.5 mM DNA with Fc-Th (dashed line).

A plot of current against the total concentration of Fc-Th (solid line).

Supporting electrolyte, 10 mM Tris pH 7. Working electrode, platinum disc (diameter, 25 μm).

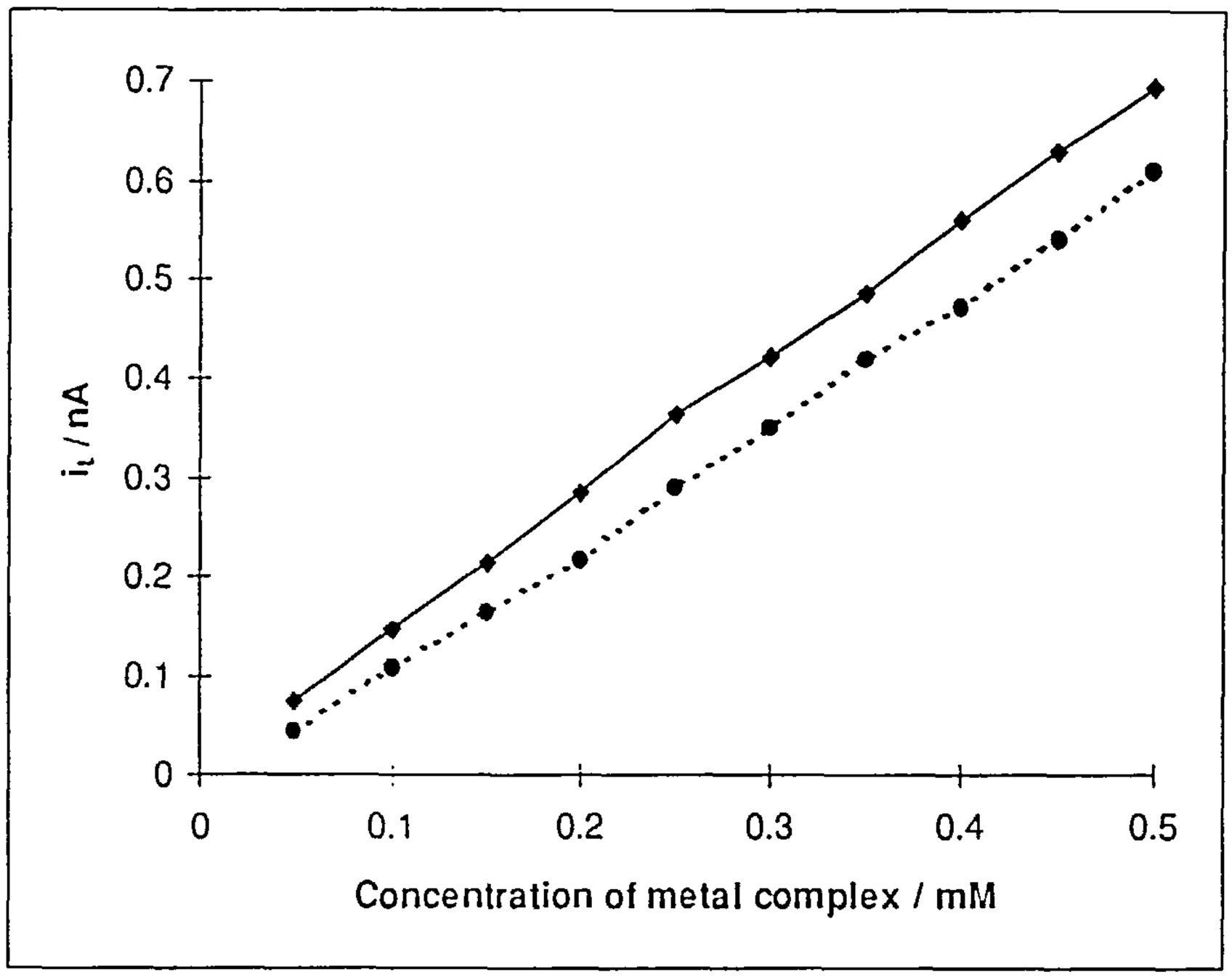

Figure 4.27.

The UME titration of 3.5 mM RNA with Fc-Th (dashed line).

A plot of current against the total concentration of Fc-Th (solid line).

Supporting electrolyte, 10 mM Tris pH 7. Working electrode, platinum disc (diameter, 25 μm).

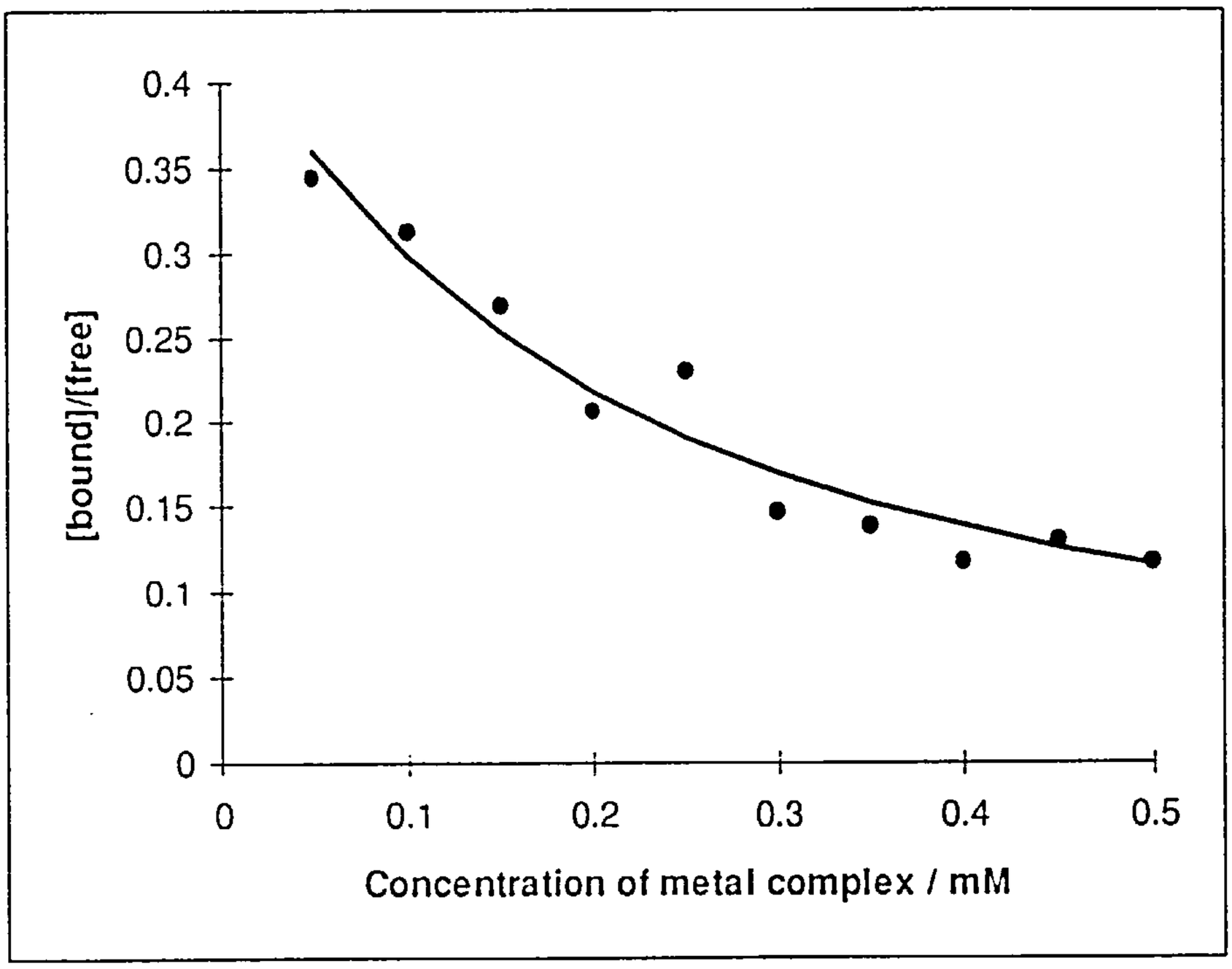

Figure 4.28.

Plot of the ratio of [bound]/[free] against the total concentration of Fc-Th calculated from the UME titration of 3.5 mM DNA with Fc-Th.

The solid line is a least-squares fit with a binding constant, [$K = (6.4 \pm 0.4) \times 10^3$ dm^3mol^{-1}, $s = (25 \pm 1)$].

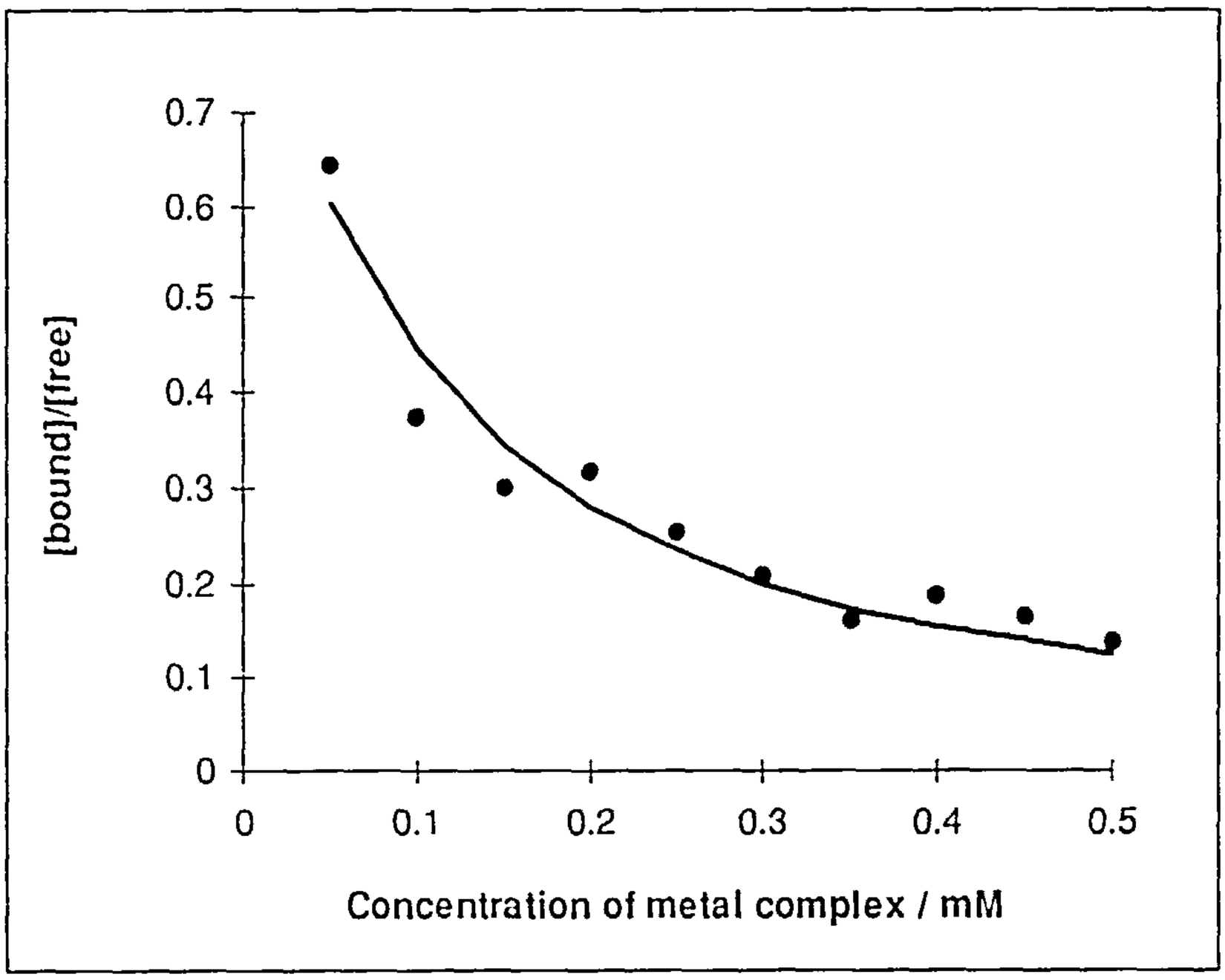

Figure 4.29.

Plot of the ratio of [bound]/[free] against the total concentration of Fc-Th calculated from the UME titration of 3.5 mM RNA with Fc-Th.

The solid line is a least-squares fit with a binding constant, [$K = (1.2 \pm 0.15) \times 10^4$ dm^3 mol^{-1} , $s = (26 \pm 1.6)$].

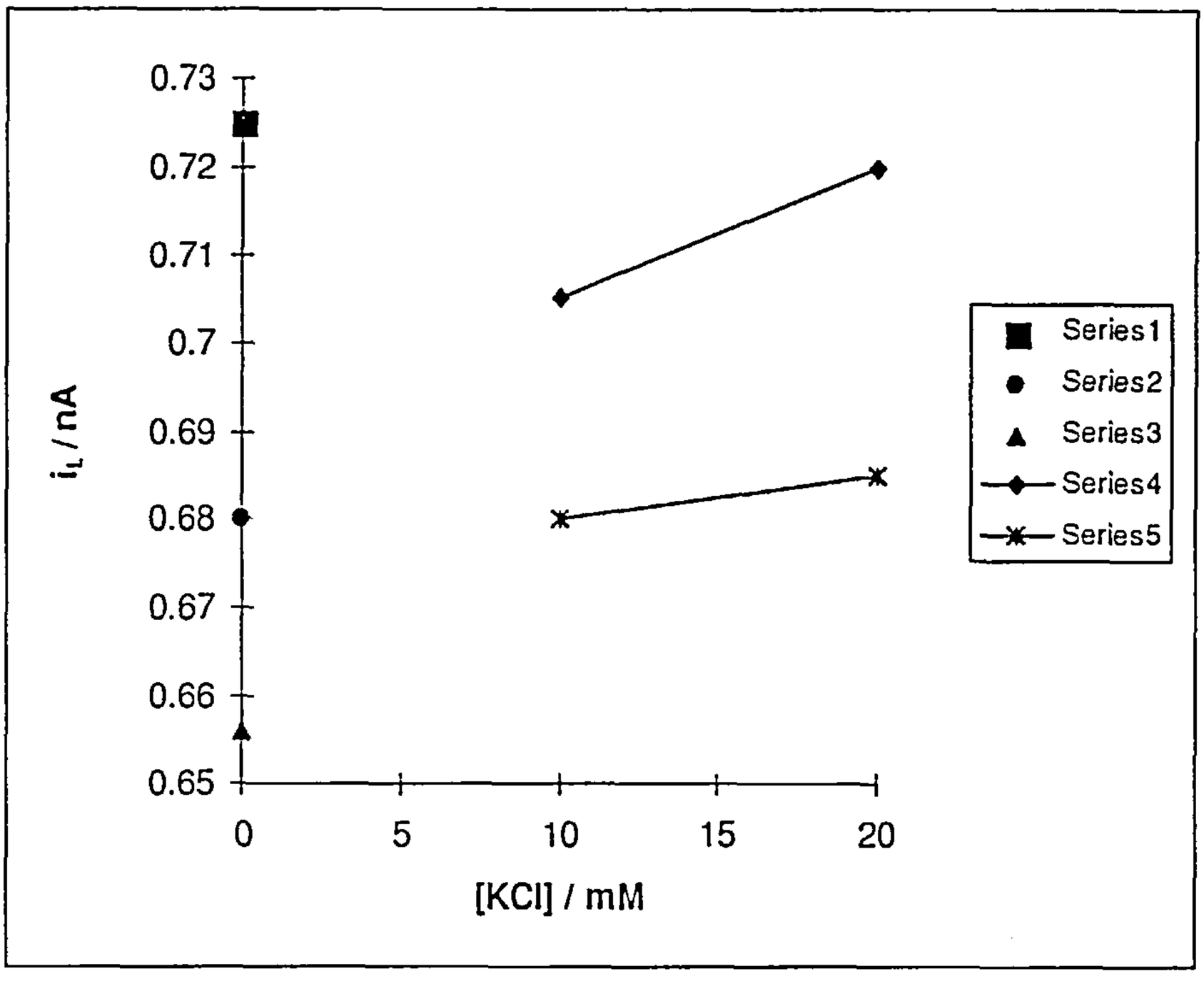

Figure 4.30.

The dependence of ionic strength on the binding. Plots of current against the concentration of potassium chloride in the experiment of the binding of Fc-Th to DNA and RNA.

Series 1. The limiting current for a solution containing only Fc-Th in 10 mM Tris buffer.

Series 2. The limiting current for a solution containing Fc-Th and DNA in 10 mM Tris buffer.

Series 3. The limiting current for a solution containing Fc-Th and RNA in 10 mM Tris buffer.

Series 4. The limiting current for a solution containing Fc-Th, DNA and potassium chloride in 10 mM Tris buffer Series

5. The limiting current for a solution containing Fc-Th, RNA and potassium chloride in 10 mM Tris buffer.

4.2.3. BIS(HEXAMETHYLBENZENE)IRON(II) CLORIDE

Cyclic voltammetry was applied to the interaction of the binding of $Fe(bz)_2^{2+}$ to DNA in solution phase. CV behavior of $Fe(bz)_2^{2+}$ in 50 mM Tris buffer, pH 7.0, in the absence and presence of DNA is given in figure 4.31. $Fe(bz)_2^{2+}$ has been reported to show antitumor activity and its interaction with nucleic acid is therefore of interest.

Cyclic voltammetric titration of DNA against $Fe(bz)_2^{2+}$ was carried out to determine the binding constant and the binding site sizes. Results for the titration of 2.7 mM DNA with $Fe(bz)_2^{2+}$ in 50 mM Tris buffer, pH 7.0 at a gold disc electrode are given in figure 4.32. A plot of the ratio of [bound]/[free] against the total concentration of $Fe(bz)_2^{2+}$ is given in figure 4.33. The magnitude of the binding constant of $Fe(bz)_2^{2+}$ to DNA in 50 mM Tris buffer gave a value of [$K = (1.7 \pm 0.2) \times 10^3$ dm^3 mol^{-1} , $s = (3.9 \pm 0.2)$]. As we mentioned before, in CV experiments the contribution of bound metal to the diffusion current is not as small as in UME, the analysis using $\frac{i_{noDna} - i_{dna}}{i_{dna}} = \frac{bound}{free}$ may not be certain in the determination of the binding constant. Therefore, the binding constant of $Fe(bz)_2^{2+}$ to DNA is only an approximate determination. As the ionic strength increased by adding potassium chloride to a solution of $Fe(bz)_2^{2+}$-DNA the binding constant decreased. At higher concentration of potassium chloride the peak current increased further. The peak current for reduction of $Fe(bz)_2^{2+}$ in the prensence of 2.7 mM DNA is plotted against the concentration of potassium chloride in figure 4.34.This is also a typical behavior of the electrostatic binders. As previously reported [24], binding of $Fe(bipy)_3^{2+}$ is electrostatic. The magnitude of the binding of $Fe(bz)_2^{2+}$ to DNA is almost equal to the binding of Fe(bipy) to DNA.

Epa = -0.572 V	Epc = -0.670 V	ΔEp = 98 mV	$E^{o'}$ = 0.621 V

Table 4.4. Parameters of $Fe(bz)_2^{2+}$ CV determined in this work.

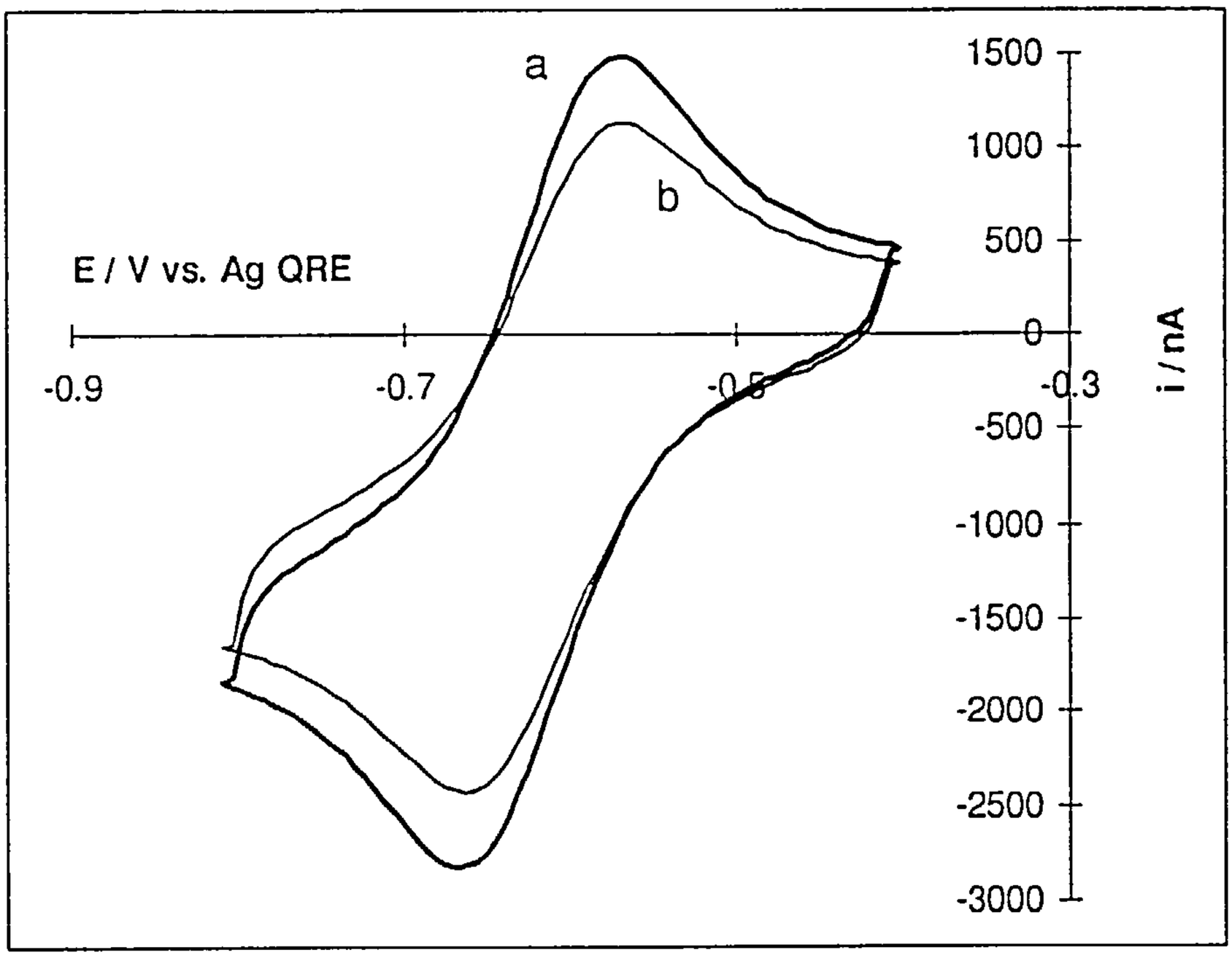

Figure 4.31.

Cyclic voltammograms of 0.35 mM $Fe(bz)_2^{2+}$ in the (a) absence and (b) presence of 2.7 mM DNA.

Supporting electrolyte, 50 mM Tris pH 7. Working electrode, gold disc (area, 0.0785 cm^2). Scan rate, 500 mV s^{-1}.

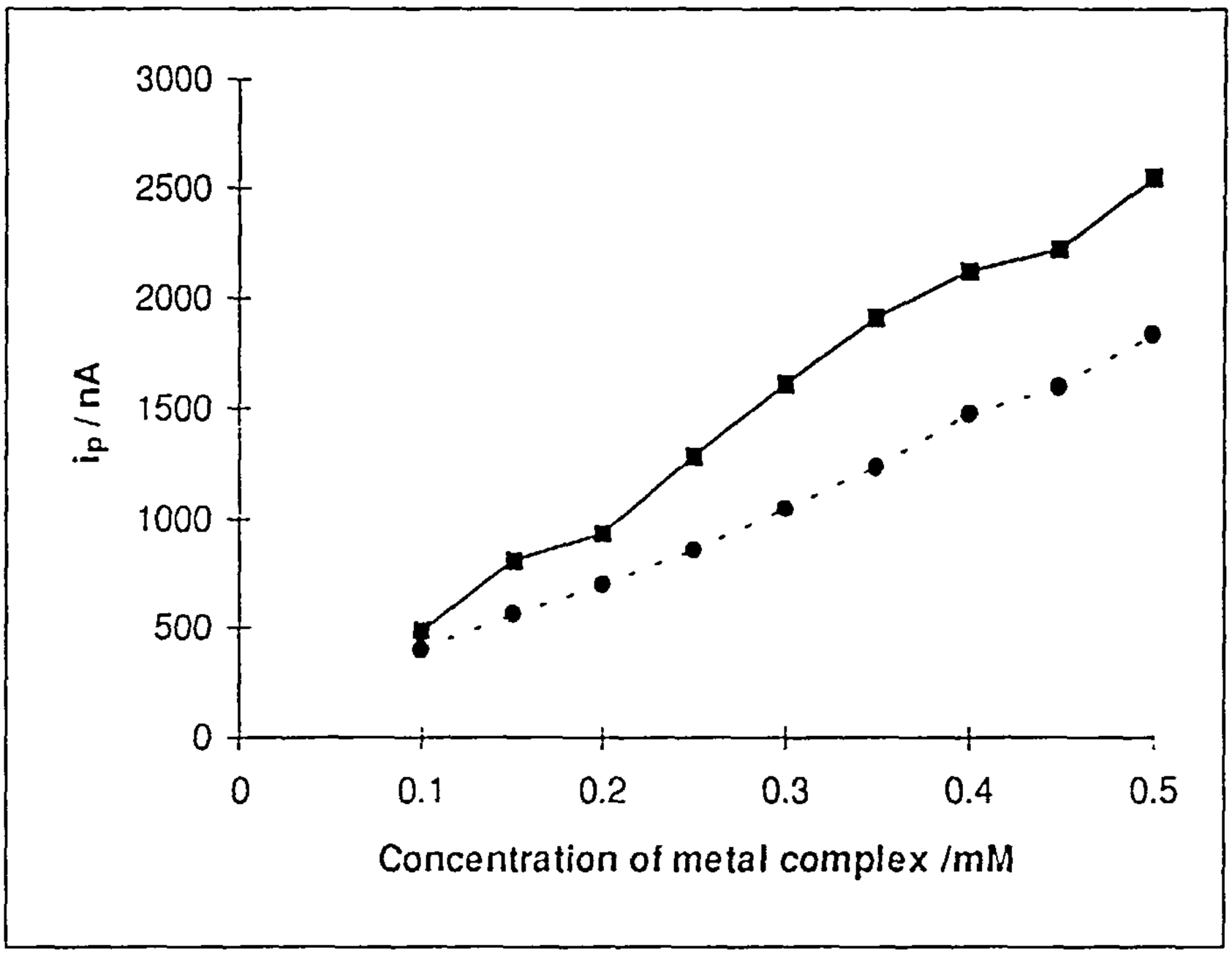

Figure 4.32.

The CV titration of 2.7 mM DNA with $Fe(bz)_2^{2+}$ (dashed line).

A plot of current against the total concentration of $Fe(bz)_2^{2+}$ (solid line).

Supporting electrolyte, 50 mM Tris pH 7. Working electrode, gold disc (area; 0.0785 cm^2). Scan rate, 500 mVs^{-1}.

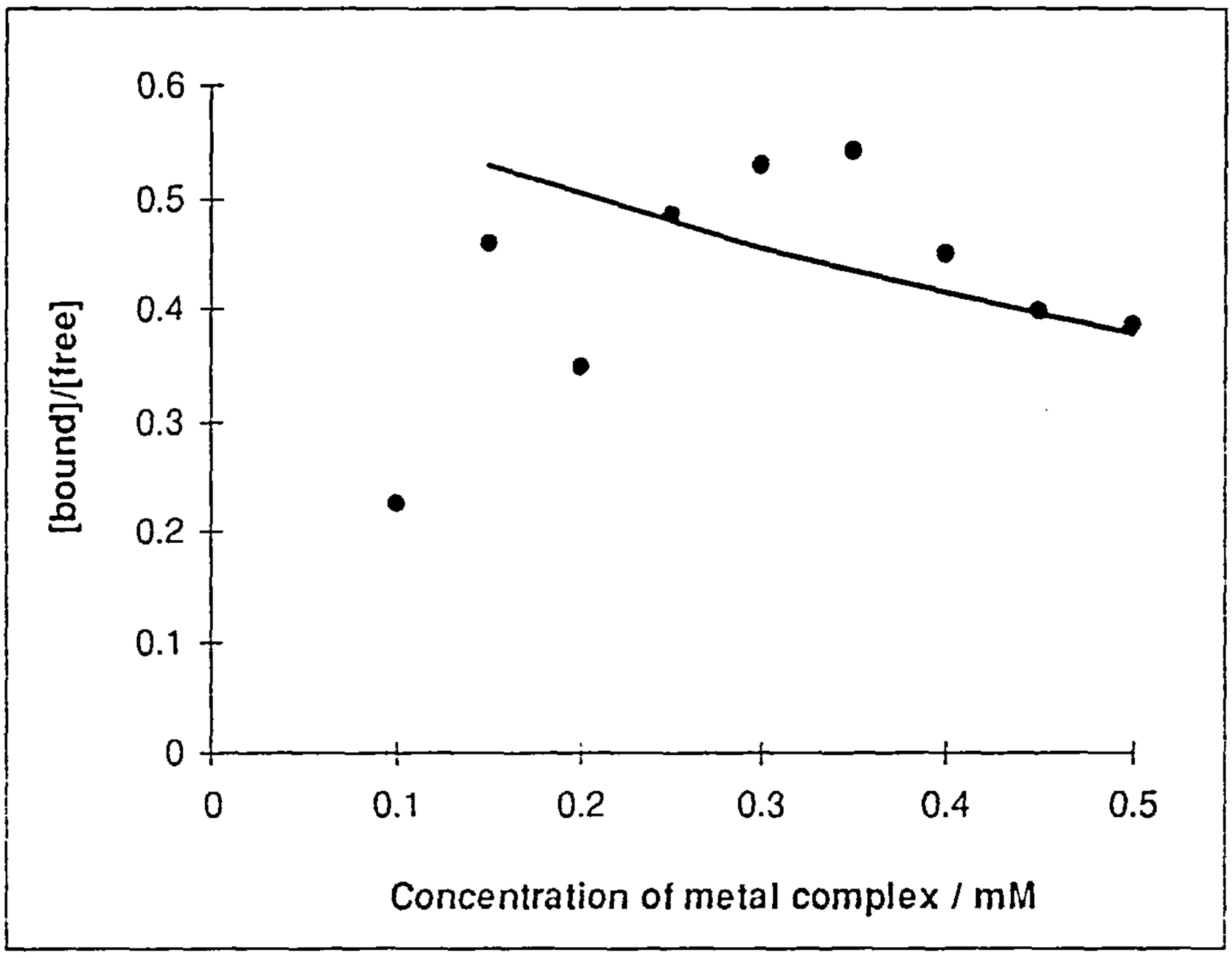

Figure 4.33.

Plot of the ratio of [bound]/[free] against the total concentration of $Fe(bz)_2^{2+}$ calculated from the CV titration of 2.7 mM DNA with $Fe(bz)_2^{2+}$.

The solid line is a least-squares fit with a binding constant, [$K = (1.7 \pm 0.2) \times 10^3$ dm^3 mol^{-1}, $s = (3.9 \pm 0.2)$].

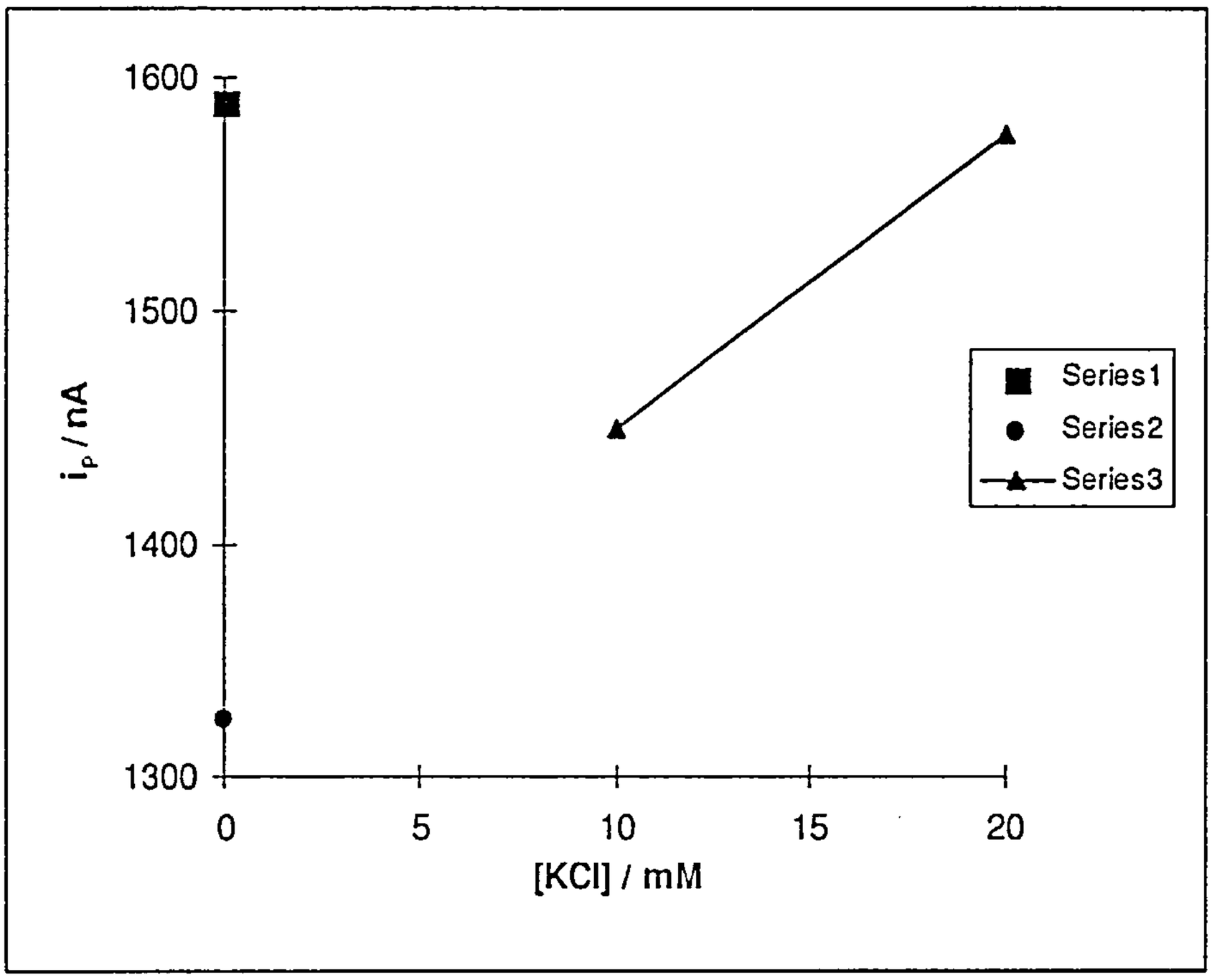

Figure 4.34.

The dependence of ionic strength on the binding. Plot of current against the concentration of potassium chloride in the experiment of the binding of $Fe(bz)_2^{2+}$.

Series 1. The peak current for a solution containing only $Fe(bz)_2^{2+}$ in 50 mM Tris buffer.

Series 2. The peak current for a solution containing $Fe(bz)_2^{2+}$ and DNA in 50 mM Tris buffer.

Series 3. The peak current for a solution containing $Fe(bz)_2^{2+}$, DNA and potassium chloride in 50 mM Tris buffer.

4.2.4. TRIS(1,10-PHENANTHROLINE)IRON(II) PERCHLORATE

The interaction of $Fe(phen)_3^{2+}$ with DNA was carried out using cyclic voltammetry. CV behavior of $Fe(phen)_3^{2+}$ in 50 mM NaCl 5 mM Tris buffer, pH 7.0, in the absence and presence of DNA is given in figure 4.35.

Titration of $Fe(phen)_3^{2+}$ with DNA was carried out to determine the binding constant and the binding site sizes. Titration results were calculated from the peak current for oxidation of $Fe(phen)_3^{2+}$ in the absence and presence of 2.7 mM DNA in 50 mM NaCl, 5 mM Tris buffer, pH 7.0 are given in figure 4.36. A plot of the ratio of [bound]/[free] against the total concentration of $Fe(phen)_3^{2+}$ is given in figure 4.37. The magnitude of the binding constant of $Fe(phen)_3^{2+}$ to DNA was [$K = (1.44 \pm 0.10) \times 10^3$ dm^3 mol^{-1} , $s = (4.0 \pm 0.13)$].

Epa = 0.874 V	Epc = 0.782 V	ΔEp = 92 mV	$E^{o'}$ = 0.823 V

Table 4.5. Parameters of $Fe(phen)_3^{2+}$ CV determined in this work.

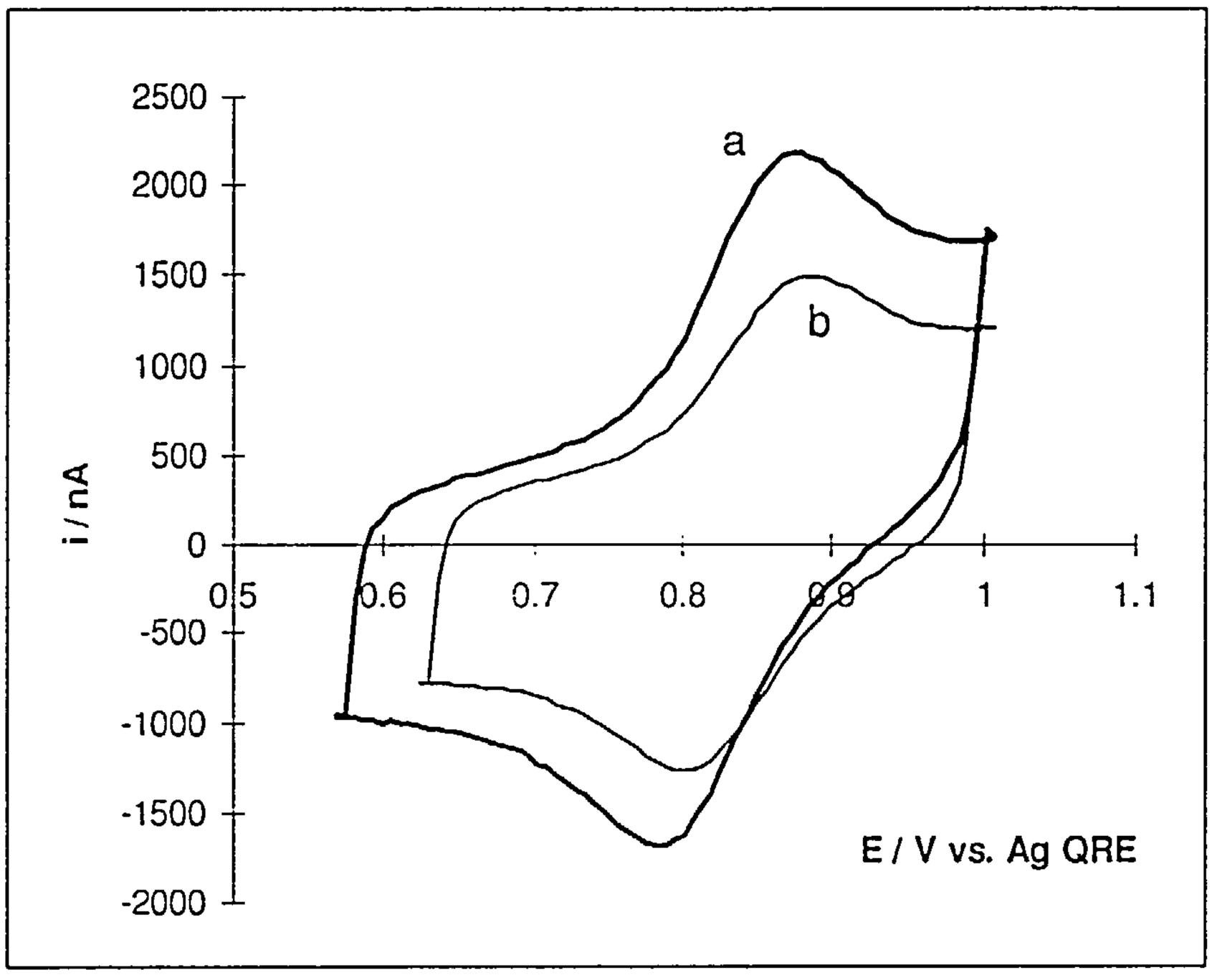

Figure 4.35.

Cyclic voltammograms of 0.3 mM $Fe(phen)_3^{2+}$ in the (a) absence and (b) presence of 2.7 mM DNA.

Supporting electrolyte, 50 mM NaCl. 5 mM Tris pH 7. Working electrode, platinum disc (area, 0.0785 cm^2). Scan rate, 500 mV s^{-1}.

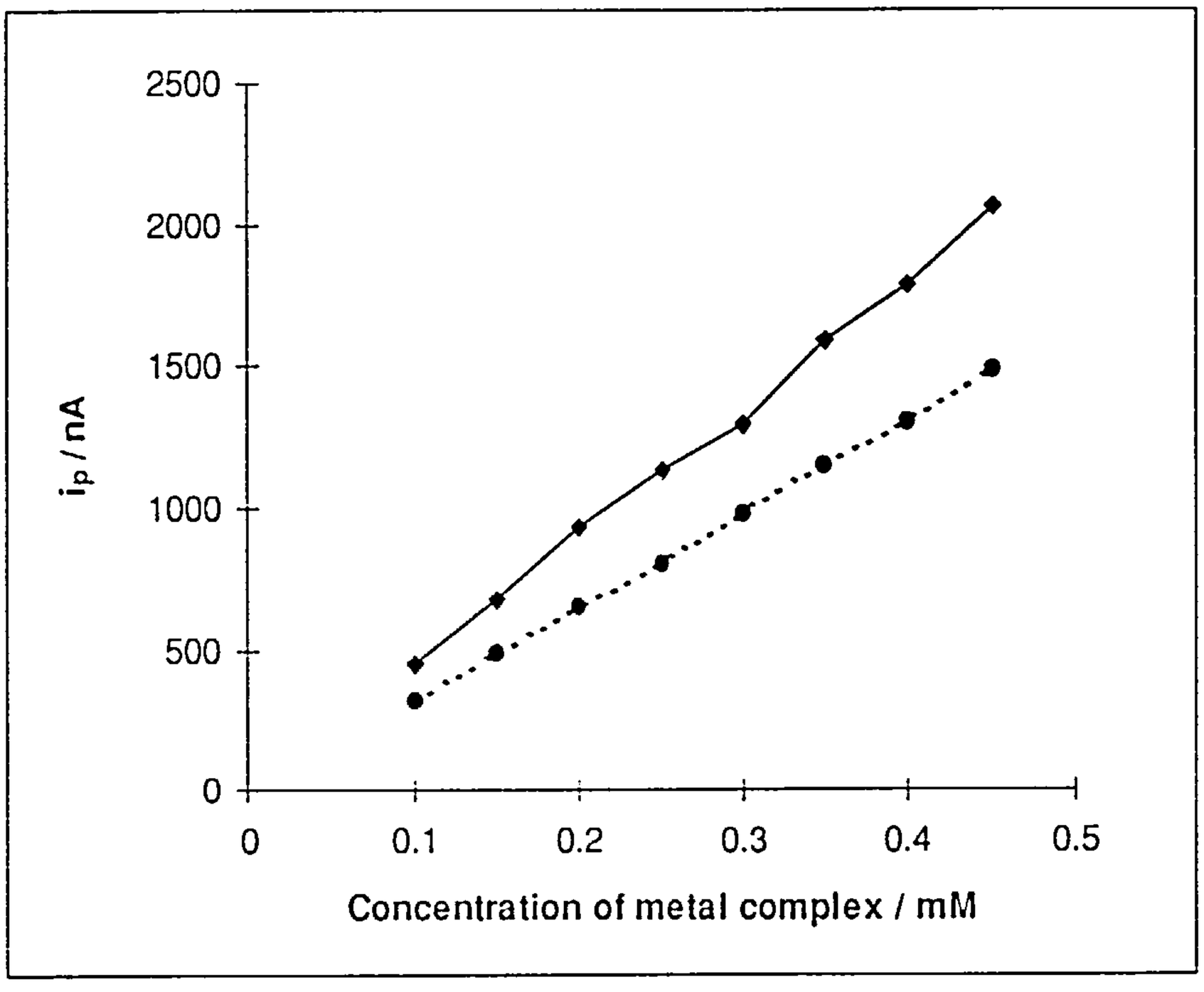

Figure 4.36.

The CV titration of 2.7 mM DNA with $Fe(phen)_3^{2+}$ (dashed line).

A plot of current against the total concentration of $Fe(phen)_3^{2+}$ (solid line).

Supporting electrolyte, 50 mM NaCl, 5 mM Tris buffer, pH 7. Working electrode, platinum disc (area; 0.0785 cm^2). Scan rate, 500 mVs^{-1}.

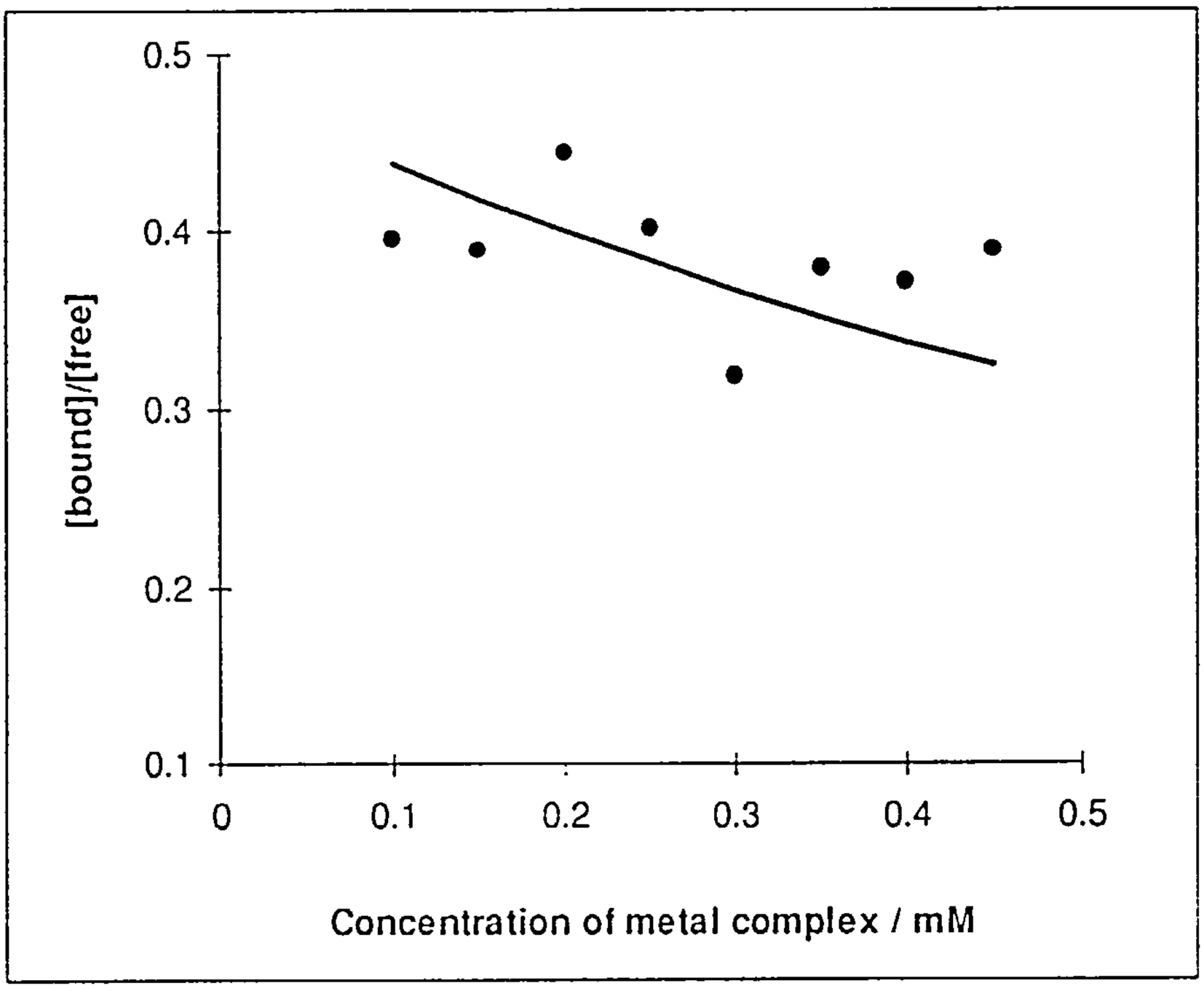

Figure 4.37.

Plot of the ratio of [bound]/[free] against the total concentration of $Fe(phen)_3^{2+}$ calculated from the CV titration of 2.7 mM DNA with $Fe(phen)_3^{2+}$.

The solid line is a least-squares fit with a binding constant, [$K = (1.44 \pm 0.10) \times 10^3$ dm^3 mol^{-1} , $s = (4.0 \pm 0.13)$].

Binding of $Fe(phen)_3^{2+}$ to DNA was also carried out using a microelectrode. Figure 4.38 shows the voltammetric behavior of $Fe(phen)_3^{2+}$; in 50 mM NaCl 5 mM Tris, pH 7.0, in the absence and presence of DNA using a 50 μm platinum microdisc electrode.

Microelectrode voltammetry was also applied to the titration of $Fe(phen)_3^{2+}$ against DNA to determine the binding constant of $Fe(phen)_3^{2+}$ to DNA. Results for the titration of $Fe(phen)_3^{2+}$ with 2.7 mM DNA in 50 mM NaCl 5 mM Tris, pH 7.0 at a platinum microdisc are given in figure 4.39. A plot of the ratio of [bound]/[free] against the total concentration of $Fe(phen)_3^{2+}$ is given in figure 4.40. The magnitude of the binding constant of $Fe(phen)_3^{2+}$ to DNA was [$K = (1.3 \pm 0.6) \times 10^4$ dm^3 mol^{-1}, $s = (3.8 \pm 0.9)$]. Figure 4.41 shows the dependence of the current against the concentration of potassium chloride in the interaction of $Fe(phen)_3^{2+}$ with DNA. The binding constant decreased with the addition of potassium chloride to a solution of $Fe(phen)_3^{2+}$-DNA. But the binding constant did not decrease further with increasing ionic strength. As seen in plot of *i vs.* [KCl] for $Fe(bz)_2^{2+}$, the current increases further showing a typical electrostatic behaviour. Phenanthroline (phen) is an aromatic planar molecule. The binding of $Fe(phen)_3^{2+}$ to DNA is due to the partial insertion of the phenanthroline ligand between the base pairs (known as intercalation) [24]. $Fe(phen)_3^{2+}$ can also interact with sugar-phosphate backbone electrostatically, and through hydrophobic interactions. Therefore, the decrease in the binding constant of $Fe(phen)_3^{2+}$ to DNA at some higher ionic strength is most probably due to some electrostatic interactions between the cationic complex and the sugar-phosphate backbone.

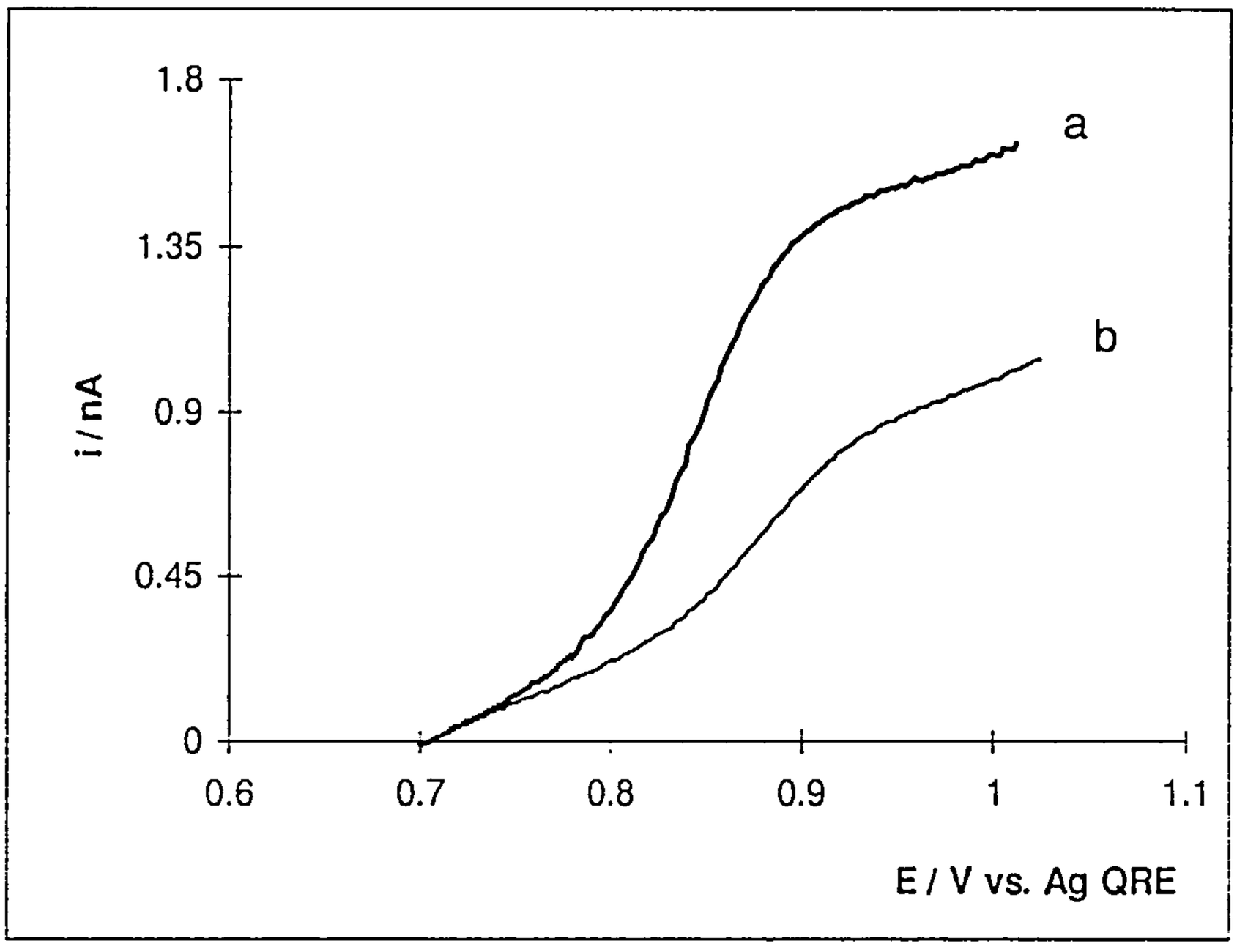

Figure 4.38.

Microelectrode voltammograms of 0.5 mM $Fe(phen)_3^{2+}$ in the (a) absence and (b) presence of 2.7 mM DNA.

Supporting electrolyte, 50 mM NaCl, 5 mM Tris pH 7. Working electrode, platinum disc (diameter, 50 μm).

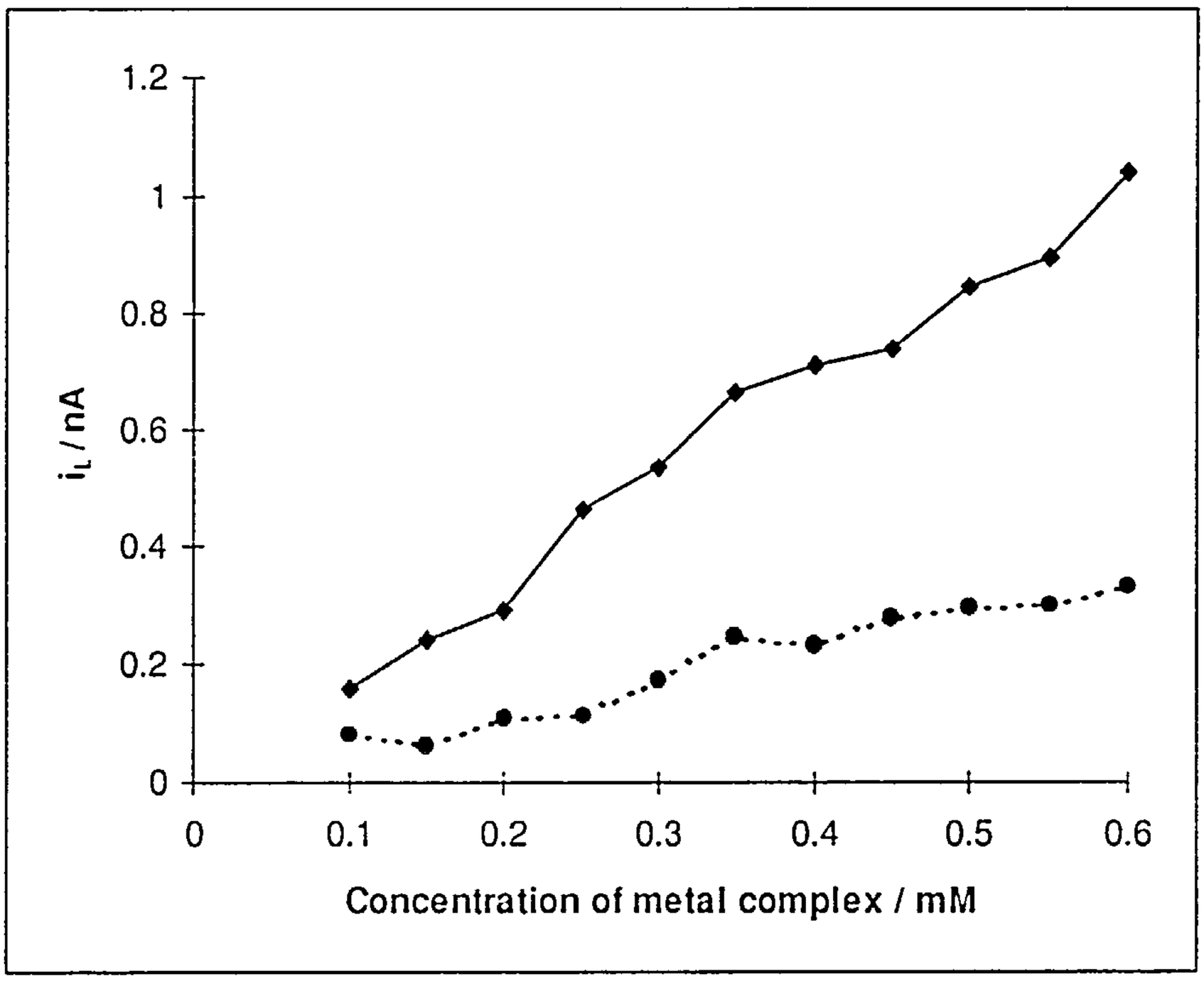

Figure 4.39.

The UME titration of 2.7 mM DNA with $Fe(phen)_3^{2+}$ (dashed line).

Plot of current against the concentration of $Fe(phen)_3^{2+}$ (solid line).

Supporting electrolyte, 50 mM NaCl, 5 mM Tris pH 7. Working electrode, platinum disc (diameter, 50 μm).

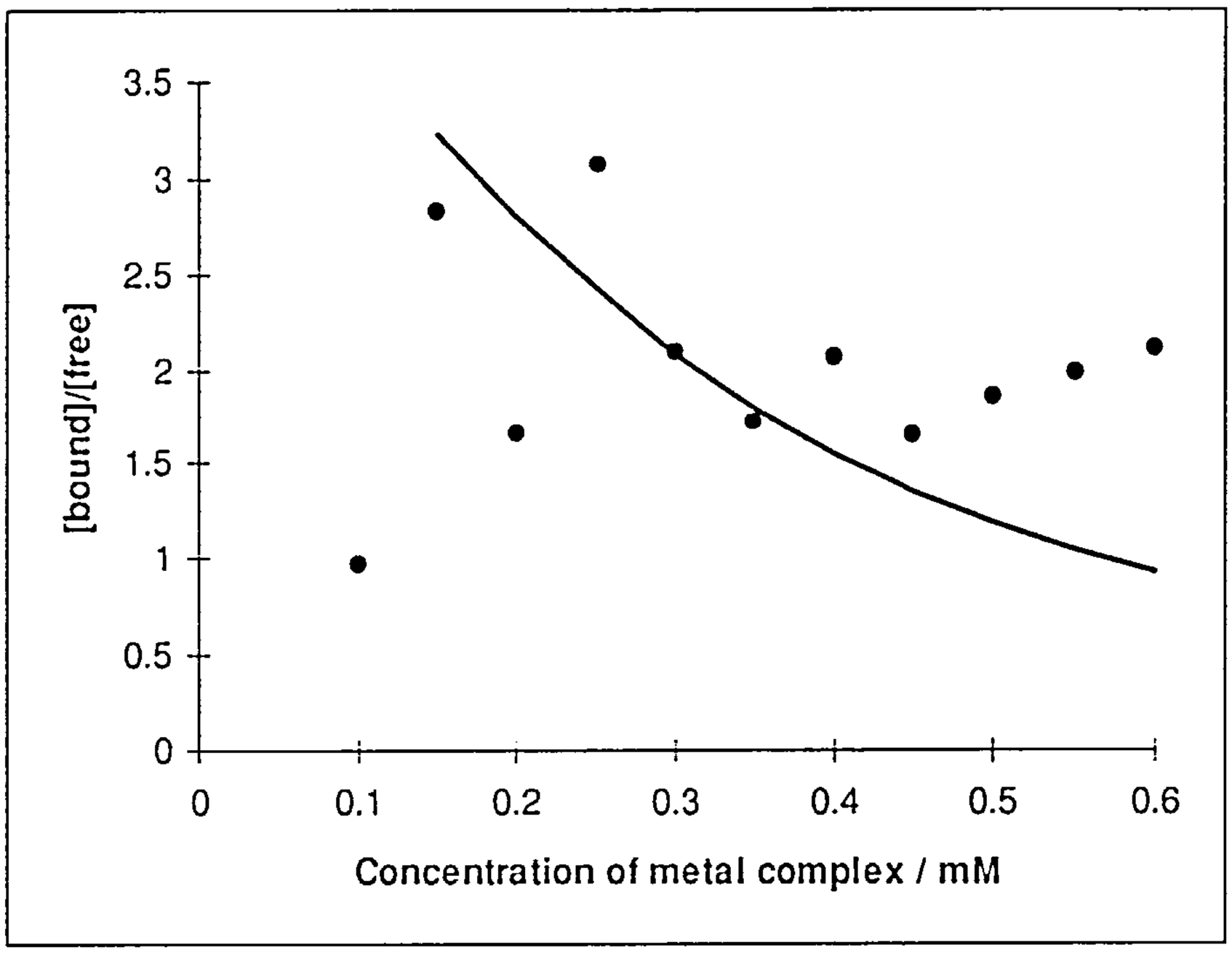

Figure 4.40.

Plot of the ratio of [bound]/[free] against the total concentration of $Fe(phen)_3^{2+}$ calculated from the UME titration of 2.7 mM DNA with $Fe(phen)_3^{2+}$.

The solid line is a least-squares fit with a binding constant, [$K = (1.3 \pm 0.6)\times10^4$ dm^3 mol^{-1}, $s = (3.8 \pm 0.9)$].

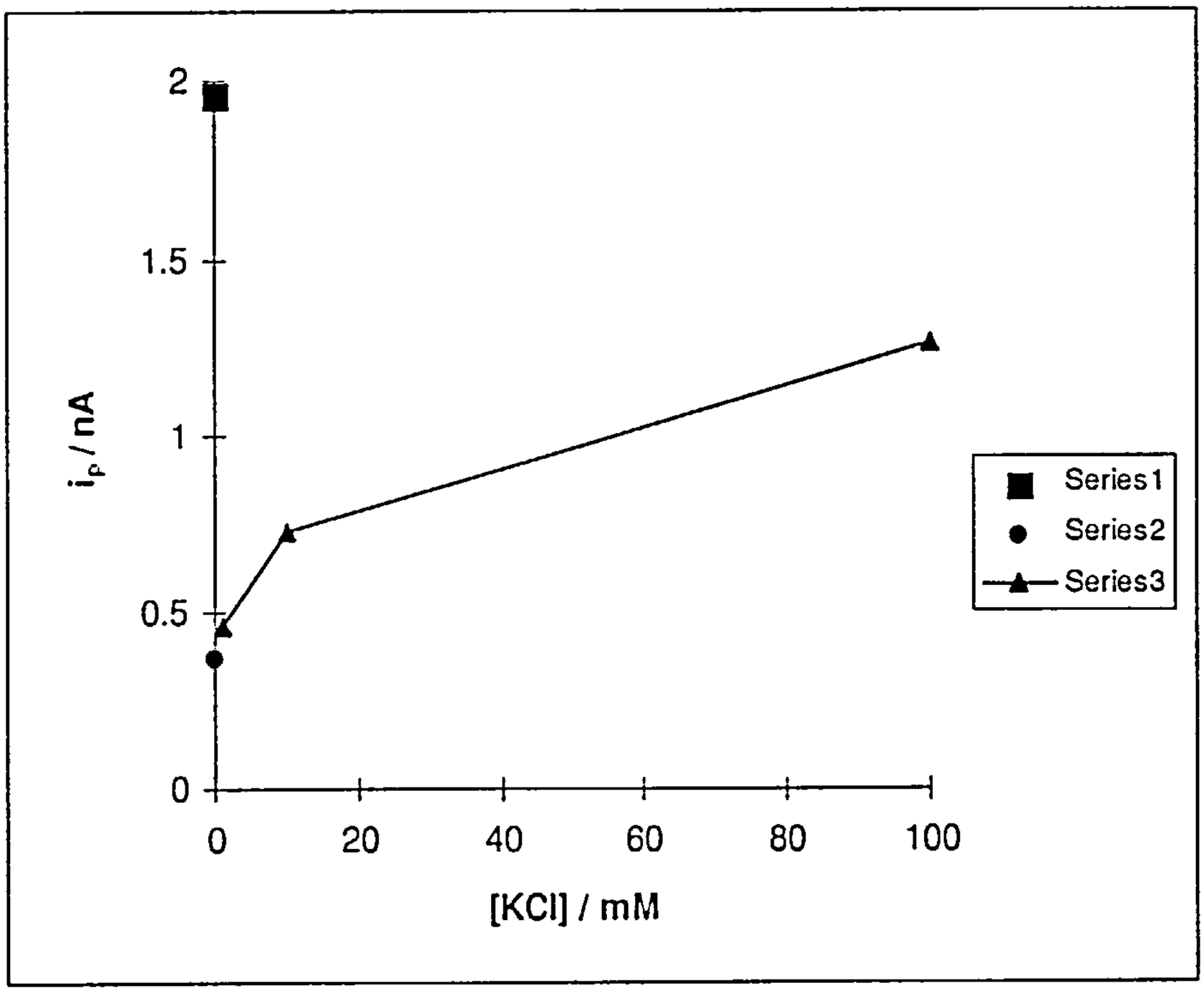

Figure 4.41.

The effect of ionic strength on the binding. Plot of current against the concentration of potassium chloride in the experiment of the binding of $Fe(phen)_3^{2+}$ with DNA.

Series 1. The peak current for a solution containing only $Fe(phen)_3^{2+}$ in 50 mM NaCl, 5 mM Tris buffer.

Series 2. The peak current for a solution containing $Fe(phen)_3^{2+}$ and DNA in 50 mM NaCl, 5 mM Tris buffer.

Series 3. The peak current for a solution containing $Fe(phen)_3^{2+}$, DNA and potassium chloride in 50 mM NaCl, 5 mM Tris buffer.

4.2.5. TRIS(2,2'-BIPYRIDYL)IRON(II) CLORIDE

The interaction of $Fe(bpy)_3^{2+}$ with DNA was investigated using cyclic voltammetry. Cyclic voltammetric behavior of $Fe(bpy)_3^{2+}$ in 10 mM NaCl, 10 mM Tris buffer, pH 7.0, in the absence and presence of DNA is given in figure 4.42.

To obtain the binding constant of $Fe(bpy)_3^{2+}$ to DNA, a titration experiment was carried out. Cyclic voltammetric titration of $Fe(bpy)_3^{2+}$ with DNA in 10 mM Tris 10 mM NaCl, pH 7.0 at a platinum disc electrode is given in figure 4.43. The peak current response for the oxidation of $Fe(bpy)_3^{2+}$ in the absence and presence of DNA is plotted. The amount of bound complex, [$Fe(bpy)_3^{2+}$-DNA], was determined using the reduction in the anodic peak current in the presence of DNA. A plot of the ratio of [bound]/[free] against the total concentration of $Fe(bpy)_3^{2+}$ is given in figure 4.44. The magnitude of the binding constant of $Fe(bpy)_3^{2+}$ to DNA was [$K = (1.0 \pm 0.07) \times 10^3$ dm^3 mol^{-1} , $s = (4.1 \pm 0.1)$].

Epa = 0.847 V	Epc = 0.732 V	ΔEp = 115 mV	$E^{o'}$ = 0.785 V

Table 4.6. Parameters of $Fe(bpy)_3^{2+}$ CV determined in this work.

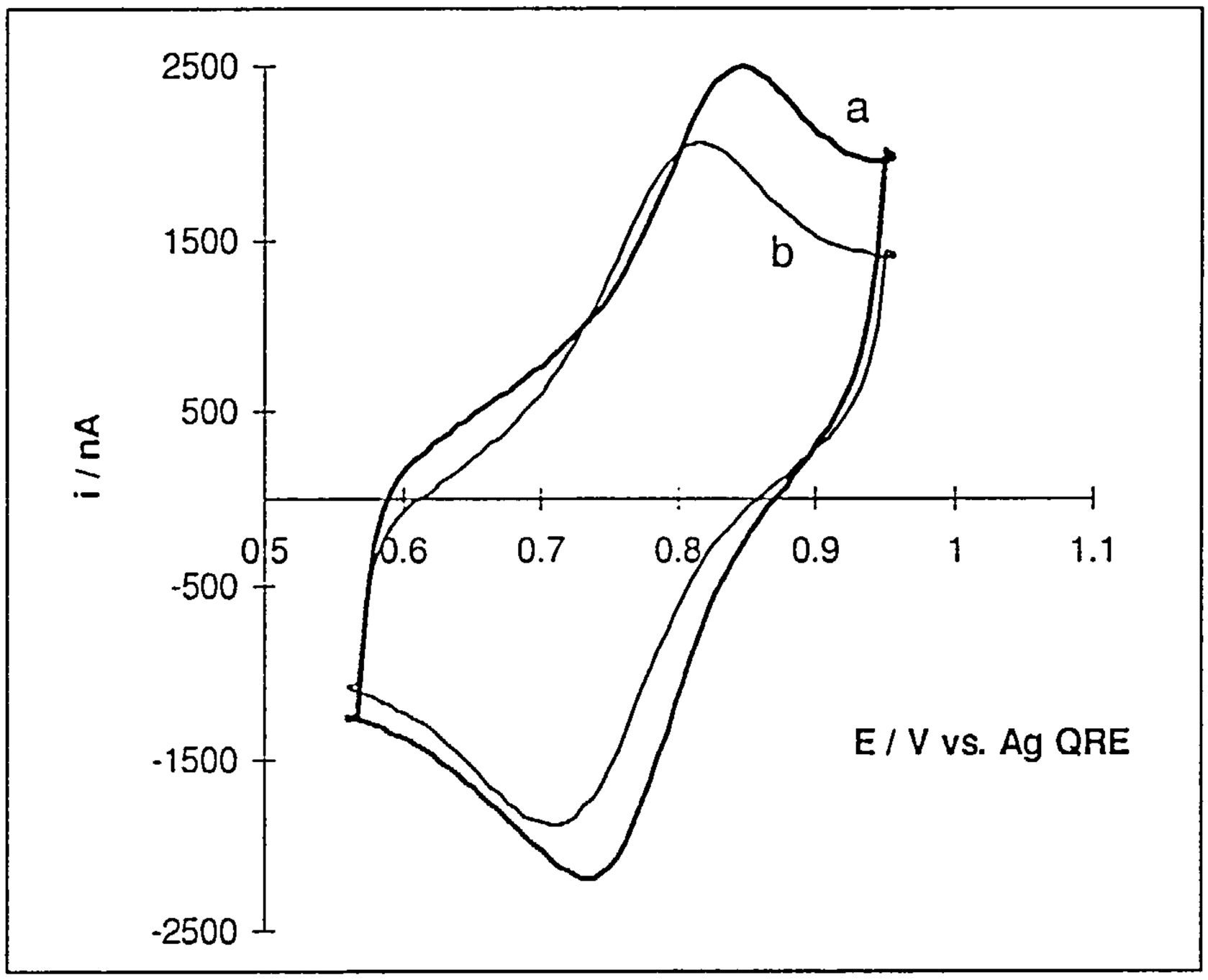

Figure 4.42.

Cyclic voltammograms of 0.35 mM $Fe(bpy)_3^{2+}$ in the (a) absence and (b) presence of 2.7 mM DNA.

Supporting electrolyte, 10 mM NaCl, 10 mM Tris pH 7. Working electrode, platinum disc (area, 0.0785 cm^2). Scan rate, 500 mV s^{-1}.

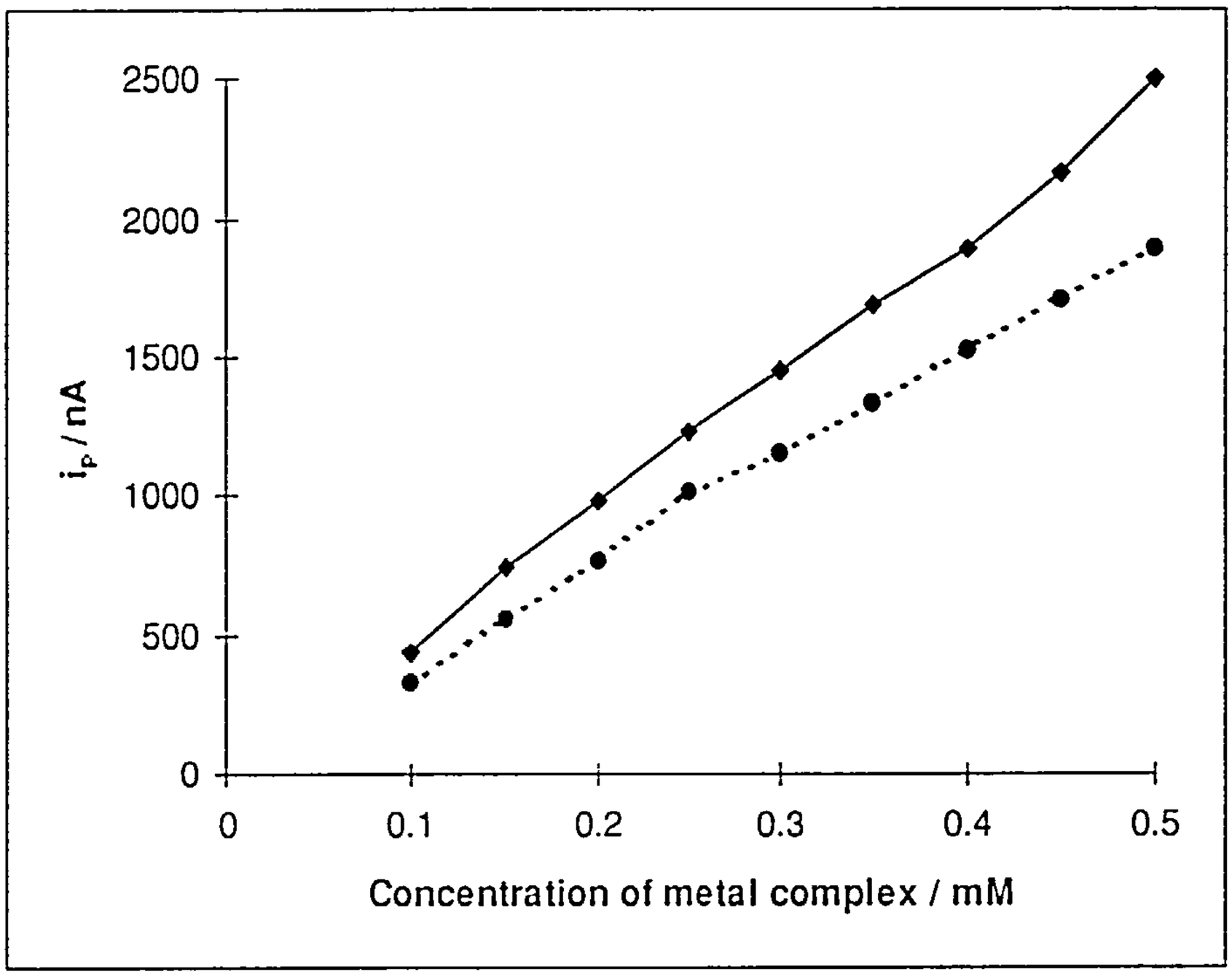

Figure 4.43.

The CV titration of 2.7 mM DNA with $Fe(bpy)_3^{2+}$ (dashed line).

Plot of current against the total concentration of $Fe(bpy)_3^{2+}$ (solid line).

Supporting electrolyte, 10 mM NaCl, 10 mM Tris buffer pH 7. Working electrode, platinum disc (area ; 0.0785 cm^2). Scan rate, 500 mVs^{-1}.

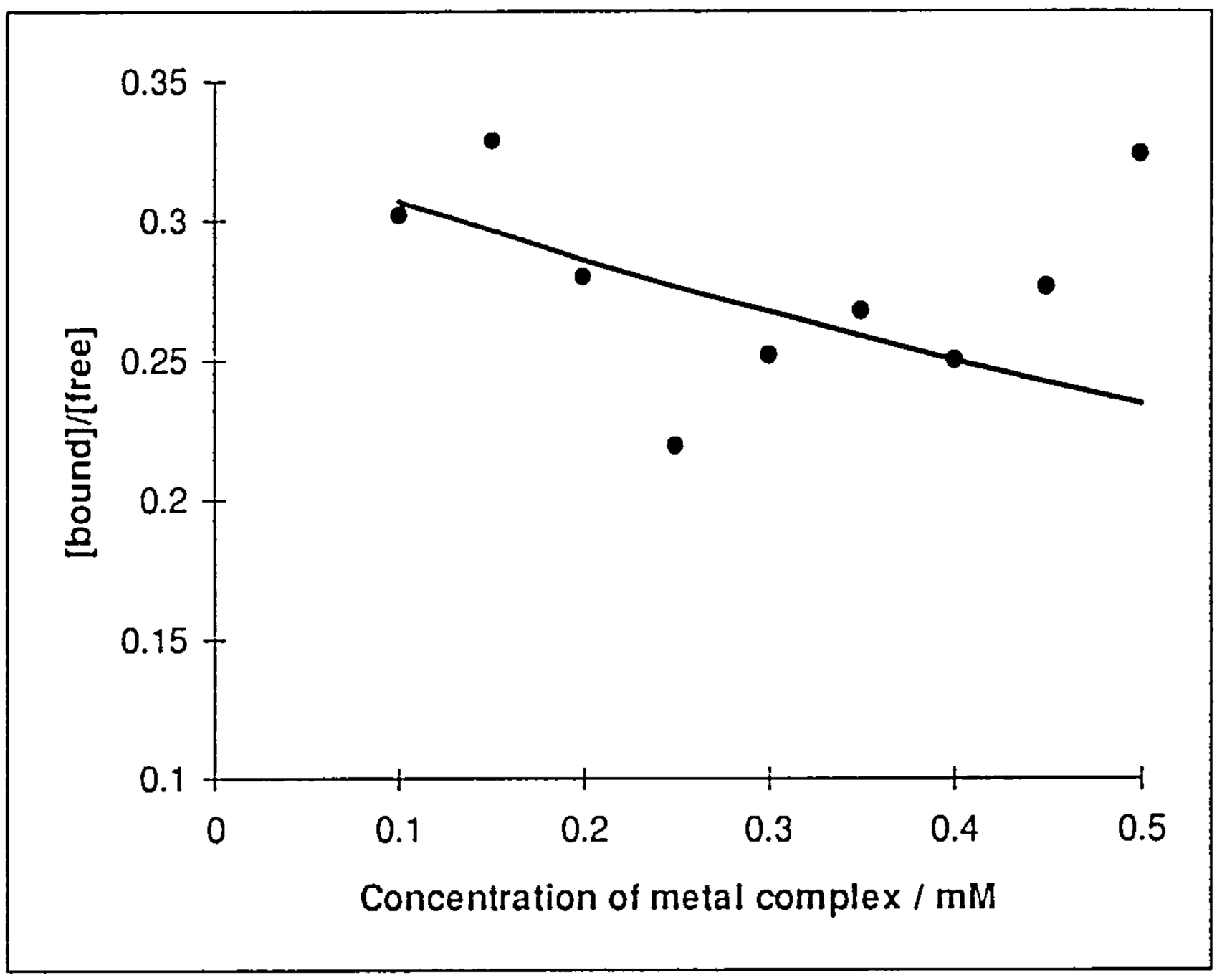

Figure 4.44.

Plot of the ratio of [bound]/[free] against the total concentration of $Fe(bpy)_3^{2+}$ calculated from the CV titration of 2.7 mM DNA with $Fe(bpy)_3^{2+}$.

The solid line is a least-squares fit with a binding constant, [$K = (1.0 \pm 0.07) \times 10^3$ dm^3 mol^{-1} , $s = (4.1 \pm 0.1)$].

Microelectrode voltammetry was also applied to the study of the interaction of $Fe(bpy)_3^{2+}$ with DNA. Microelectrode voltammograms of $Fe(bpy)_3^{2+}$, in 10 mM Tris 10 mM NaCl, pH 7.0, in the absence and presence of DNA are given in figure 4.45.

To measure the binding constant of $Fe(bpy)_3^{2+}$ to DNA by the microelectrode technique, the titration was carried out in 10 mM NaCl and 10 mM Tris buffer using a platinum microelectrode. Figure 4.46 shows the limiting currents of $Fe(bpy)_3^{2+}$ with and without DNA against the total concentration. The decrease in the limiting current of $Fe(bpy)_3^{2+}$ in the absence and presence of mM DNA used to calculate the amount of bound metal complex. A plot of the ratio of [bound]/[free] versus the total concentration of $Fe(bpy)_3^{2+}$ is given in figure 4.47. The magnitude of the binding constant of $Fe(bpy)_3^{2+}$ to DNA calculated from the titration results is [$K = (1.48 \pm 0.23) \times 10^3$ dm^3 mol^{-1} , $s = (4.1 \pm 0.3)$]. The binding constant of $Fe(bpy)_3^{2+}$ to DNA obtained from the titration experiment at platinum microelectrode is a little bit larger than the binding constant determined from the titration experiment carried out by cyclic voltammetry. As we mentioned above, this is probably due to the absence of the contribution of the bound complex to the current. It is known that tris(bipyridine) metal complexes bind to DNA predominantly by electrostatic interaction with the anionic sugar-phosphate backbone of the double helix [17,19]. It is also reported that bipyridine ligand is not favored to intercalate into double helix because it possesses a smaller aromatic surface area and slight non-planarity compared to the phenanthroline ligand [19].

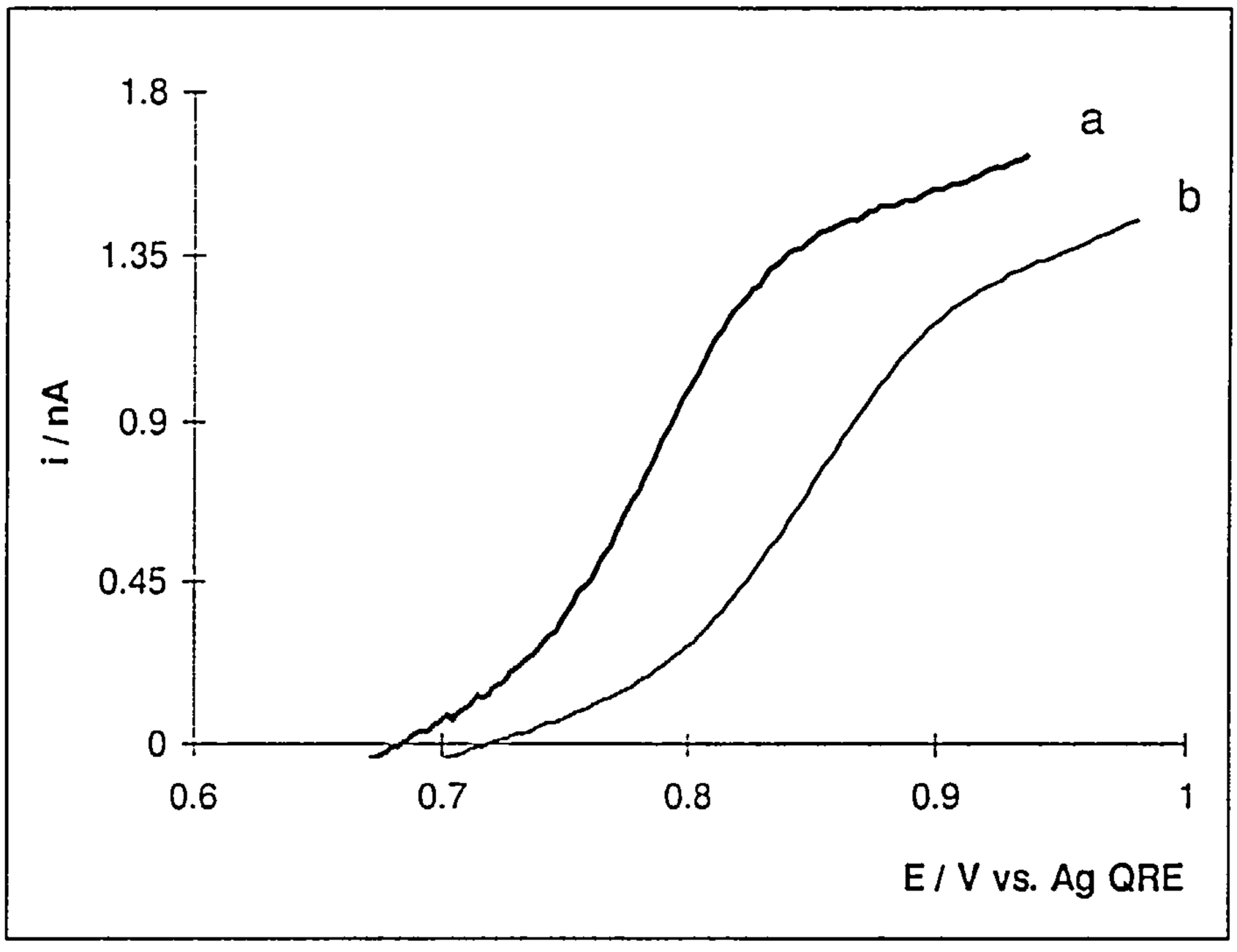

Figure 4.45.

Microelectrode voltammograms of 0.45 mM $Fe(bpy)_3^{2+}$ in the (a) absence and (b) presence of 2.7 mM DNA.

Supporting electrolyte, 10 mM NaCl, 10 mM Tris pH 7. Working electrode, platinum disc (diameter, 50 μm).

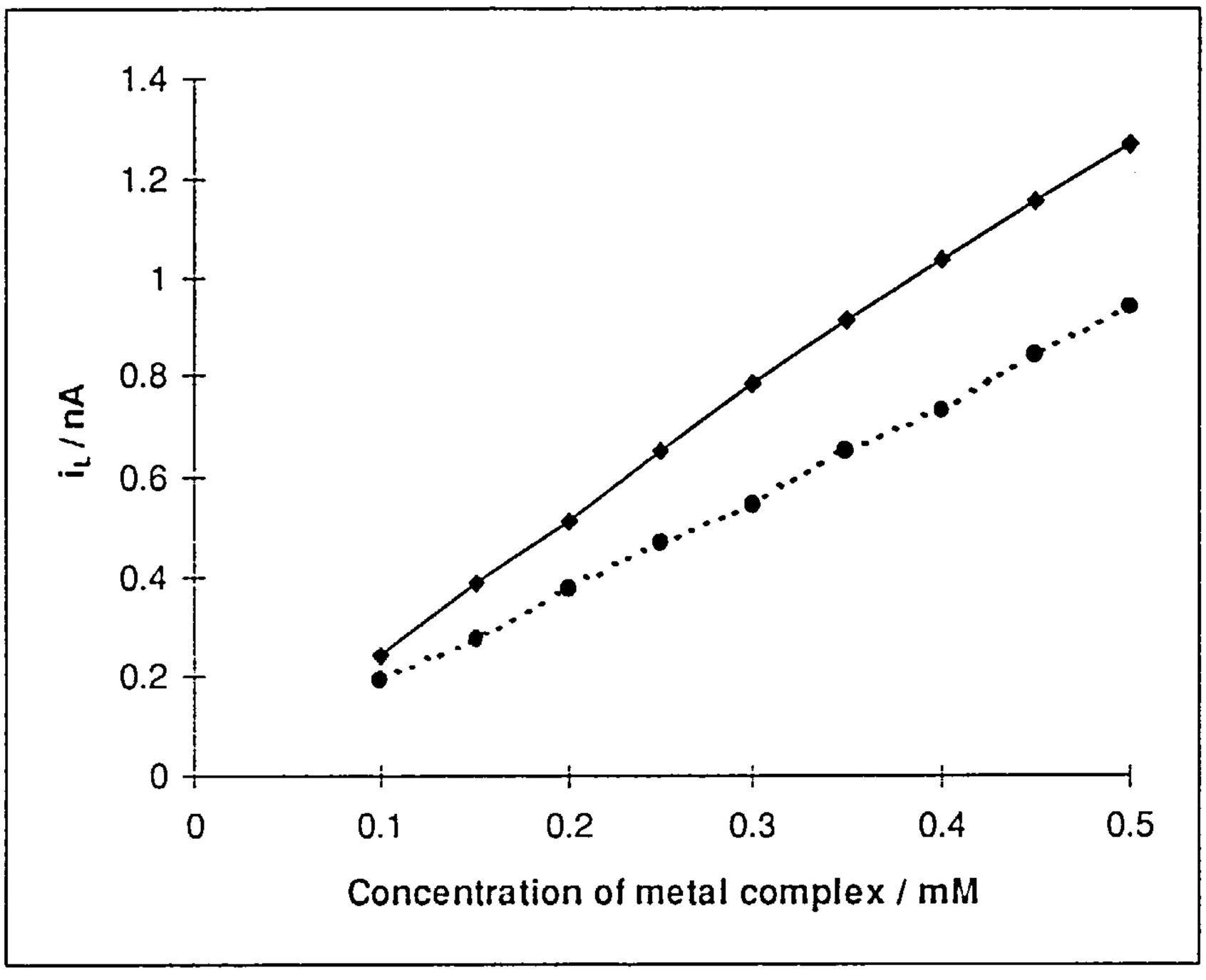

Figure 4.46.

The UME titration of 2.7 mM DNA with $Fe(bpy)_3^{2+}$ (dashed line).

Plot of current against the total concentration of $Fe(bpy)_3^{2+}$ (solid line).

Supporting electrolyte, 10 mM NaCl, 10 mM Tris buffer pH 7. Working electrode, platinum disc (diameter, 50 μm).

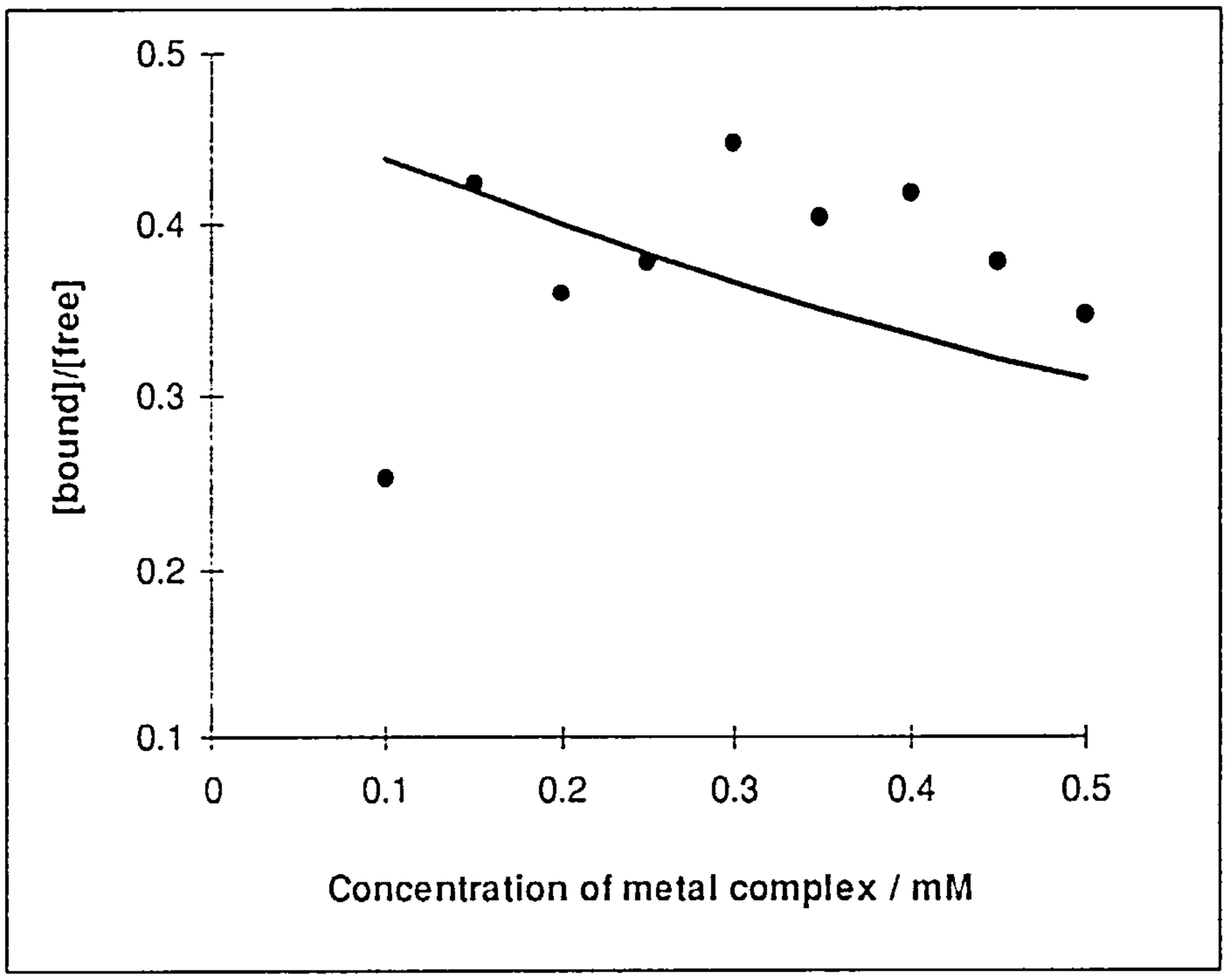

Figure 4.47.

Plot of the ratio of [bound]/[free] against the total concentration of $Fe(bpy)_3^{2+}$ calculated from the UME titration of 2.7 mM DNA with $Fe(bpy)_3^{2+}$.

The solid line is a least-squares fit with a binding constant, [$K = (1.48 \pm 0.23) \times 10^3$ dm^3 mol^{-1} , $s = (4.1 \pm 0.3)$].

4.3. DISCUSSION & COMPARISON WITH OTHER STUDIES

The binding constant of $Fe(phen)_3^{2+}$ which binds to DNA mainly by intercalation obtained here by microelectrode voltammetry [$K = 1.3 \times 10^4$ dm^3 mol^{-1} , $s = 3.8$]in 50 mM NaCl, 5 mM Tris buffer agrees very well with the reported binding constant of $Fe(phen)_3^{2+}$ [$K = 1.4 \times 10^4$ dm^3 mol^{-1} ($s = 4$)] [24]. Also, the binding constant of $Ru(phen)_3^{2+}$ in 50 mM NaCl [15] obtained by equilibrium dialysis is [$K = 6.2 \times 10^3$ dm^3 mol^{-1}] and in 100 mM NaCl [21] is [$K = 2.13 \times 10^4$ dm^3 mol^{-1}]. This results show that $Fe(phen)_3^{2+}$ binds to DNA more strongly than $Ru(phen)_3^{2+}$ (under similiar conditions). It is also reported that the magnitude of the binding constant $Co(phen)_3^{3+}$ to DNA in 50 mM NaCl, 5 mM Tris measured is [$K = 2.6 \times 10^4$ dm^3 mol^{-1}, $s = 5$].

The binding constant of $Fe(bpy)_3^{2+}$ to DNA found here is [$K = 1.48 \times 10^3$ dm^3 mol^{-1} , $s = 4.15$] using titration experiment carried out by microelectrode voltammetry and [$K = 1.01 \times 10^3$ dm^{3}mol^{-1} , $s = 4.13$] by cyclic voltammtery also agrees with that measured by previous workers [24] [$K = 1.1 \times 10^3$ dm^{3}mol^{-1}, $s = 4$]. The larger binding constant of $Fe(phen)_3^{2+}$ to DNA even at higher ionic concentration electrolyte shows that the interaction involving intercalation is much stronger than the electrostatic interaction. The binding constant of $Co(bpy)_3^{3+}$ which bind to DNA by electrostatic interaction has also been studied in 50 mM NaCl solution. The observed binding constant is [$K = 1.4 \times 10^4$ dm^{3}mol^{-1}, $s = 3$] [24].

	K + s (determined by CV)	K + s (determined by UME)	K + s (published)
$Ru(NH_3)_6^{3+}$ with DNA in 10 mM Tris buffer	$K=(1.0\pm0.18)\times10^4$ dm^3 mol^{-1}, $s=(1.8\pm0.03)$	$K=(1.47\pm0.04)\times10^5$ dm^3 mol^{-1}, $s=(1.6\pm0.01)$	
Fc-Th with DNA in 10 mM Tris buffer	$K=(3.5\pm2.4)\times10^3$ dm^3 mol^{-1}, $s=(26\pm12.4)$	$K=(6.4\pm0.4)\times10^3$ dm^3 mol^{-1}, $s=(25\pm1)$	
Fc-Th with RNA in 10 mM Tris buffer	$K=(7.1\pm4.7)\times10^3$ dm^3 mol^{-1}, $s=(28\pm10)$	$K=(1.2\pm0.15)\times10^4$ dm^3 mol^{-1}, $s=(26\pm1.6)$	
Fc-Th with RNA in 50 mM Tris buffer	$K=(2.3\pm2.1)\times10^3$ dm^3 mol^{-1}, $s=(23.3\pm13.5)$		
$Fc\text{-}NMe_3$ with DNA in 10 mM Tris buffer	$K=(2.1\pm1.3)\times10^3$ dm^3 mol^{-1}, $s=(18.6\pm9.2)$	$K=(1.4\pm0.2)\times10^3$ dm^3 mol^{-1}, $s=(19\pm1.2)$	
$Fe(bz)_2^{2+}$ with DNA in 50 mM Tris buffer	$K=(1.7\pm0.2)\times10^3$ dm^3 mol^{-1}, $s=(3.9\pm0.2)$		
$Fe(phen)_3^{2+}$ with DNA in 50 mM NaCl, 5 mM Tris buffer	$K=(1.44\pm0.1)\times10^3$ dm^3 mol^{-1}, $s=(4\pm0.13)$	$K=(1.3\pm0.6)\times10^4$ dm^3 mol^{-1}, $s=(3.8\pm0.9)$	$K=1.4\times10^4$ dm^3 mol^{-1} $s=4$
$Fe(bipy)_3^{2+}$ with DNA in 10 mM NaCl, 10 mM Tris buffer	$K=(1.0\pm0.07)\times10^3$ dm^3 mol^{-1}, $s=(4.1\pm0.1)$	$K=(1.48\pm0.23)\times10^3$ dm^3 mol^{-1}, $s=(4.1\pm0.3)$	$K=1.1\times10^3$ dm^3 mol^{-1} $s=4$
$Ru(phen)_3^{2+}$ with DNA			$K=6.2\times10^3$ dm^3 mol^{-1} (in 50 mM NaCl) $K=2.13\times10^4$ dm^3 mol^{-1} (in 100 mM NaCl)
$Ru(phen)_3^{2+}$ with DNA			$K=2.6\times10^4$ dm^3 mol^{-1} (in 50 mM NaCl, 5 mM Tris)
$Co(bipy)_3^{3+}$ with DNA			$K=1.4\times10^4$ dm^3 mol^{-1} (in 50 mM NaCl)

Table 4.7. Table of binding constants and binding site sizes of metal complexes to nucleic acids.

4.4. CONCLUSIONS

Voltammetric methods have been used here to investigate the interaction of several metal complexes with nucleic acids. Both cyclic voltammetry and steady-state voltammetry have been found to be useful in the studies of the interaction of metal complexes with nucleic acids. Since the bound metal does not contribute significantly to the diffusion current at microelectrodes, the current is directly proportional to the diffusion coefficient of free metal complex. Therefore, the anaysis of the data is simplier and more reliable.

Microelectrode results show that $Ru(NH_3)_6^{3+}$ binds to DNA very strongly even at a small concentration of DNA. At higher metal concentration, since slopes of the current *vs.* metal concentration curves are roughly same, the solution viscosity has no effect on the binding. Microelectrode voltammetry indicated that the binding of ferrocenyl derivatives to DNA and RNA in solution phase involves mainly electrostatic interaction plus some contributions of non-electrostatic binding between thymine and the bases of DNA. Voltammetric experiments show that the binding of Fc-Th to DNA is stronger than the binding of $Fc\text{-}NMe_3$ to DNA under same conditions. This also is an evidence of some non-electrostatic interaction available between Fc-Th and DNA. Also, the magnitude of the binding constant of Fc-Th to RNA [$K = (1.2 \pm 0.15) \times 10^3$ dm^3 mol^{-1} , $s = (26 \pm 1.6)$] is about twice that for DNA [$K = (6.4 \pm 0.4) \times 10^3$ dm^3 mol^{-1}, $s = (25 \pm 1)$]. Since RNA is partially single stranded, the possibility of hydrogen bonding between Fc-Th and the bases is higher than with DNA. $Fe(phen)_3^{2+}$ binds to DNA by intercalation as reported. The binding of $Fe(bipy)_3^{2+}$ is mainly electrostatic and weaker than $Fe(phen)_3^{2+}$. The binding of $Fe(bz)_2^{2+}$ also displays an ionic strength dependence characteristic of electrostatic interation. The magnitude of the binding constant of $Fe(bz)_2^{2+}$ to DNA is approximately

the same as the binding constant of $Fe(bipy)_3^{2+}$ to DNA. Also, the binding constant of $Fe(bz)_2^{2+}$ to DNA decreases at higher ionic strength, the binding constant of $Fe(phen)_3^{2+}$ to DNA does not decrease further. In this way the effect of ionic strength can differentiate electrostatic and non-electrostatic interactions.

4.5. REFERENCES

1. S. J. Lippard, *Acc. Chem. Res.* **1978**, 11, 211.

2. J. J. Roberts and A. J. Thomson, *Prog. Nucl. Acids Res. Mol. Biol.* **1979**, 22, 71.

3. J. C. Dabrowiak, in *Advances in Inorganic Biochemistry*; G. L. Eichhorn, and L. G. Marzilli, Eds., Elsevier Biomedical: New York, **1982**, Vol.4, pp 69-113.

4. S. M. Hecht, *Acc. Chem. Res.*, **1986**, 19, 383.

5. J. Reedijk, *Pure Appl. Chem.*. **1987**, 59, 181.

6. L. A. Basile and J. K. Barton in *Metal ions in Biological Systems*; H. Sigel, Ed., Marcel Dekker: New York, **1989**; Vol. 25, pp 31-103.

7. P. B. Dervan, *Science*, **1986**. 232, 464.

8. D. S. Sigman, *Acc. Chem. Res.*, **1986**, 19, 180.

9. P. G. Schultz and P. B. Dervan, *J. Biomol. Struct. Dyn.*, **1984**, 1. 1133.

10. J. K. Barton, *Science*, **1986**. 233, 727.

11. J. K. Barton, *Comm. Inorg. Chem.*, **1985**, 3, 321.

12. G. Dougherty and J. R. Pilbrow, *Int. J. Biochem.*, **1984**, 16, 1179.

13. S. Neidle and Z. Abraham. *CRC Crit. Rev. Biochem.*, **1984**, 17. 73.

14. J. K. Barton, *J. Biomol. Struct. Dyn.*, **1983**, 1, 621.

15. J. K. Barton, A. T. Danishefsky and J. M. Goldberg, *J. Am. Chem. Soc.*, **1984**, 106, 2172.

16. J. K. Barton, L. A. Basile, A. T. Danishefsky and A. Alexandrescu, *Proc. Natl. Sci.* USA, **1984**, 81, 1961.

17. J. M. Kelley, A. B. Tossi. D. J. McConnell and C. OhUigin. *Nucl. Acids Res.*, **1985**, 13, 6017.

18. J. K. Barton and E. Lolis, *J. Am. Chem. Soc.*, **1985**, 107, 708.

19. C. V. Kumar, J. K. Barton and N. J. Turro, *J. Am. Chem. Soc.*, **1985**, 107, 5518.

20. H. Y. Mei and J. K. Barton, *J. Am. Chem. Soc.*, **1986**, 108, 7414.

21. J. K. Barton, B. M. Goldberg, C. V. Kumar and N. J. Turro, J. Am. Chem. Soc., **1986**, 108, 2081.

22. B. M. Goldstein, J. K. Barton and H. M. Berman, *Inorg. Chem.*, **1986**, 25, 842.

23. C. Stradowski, H. Gorner. L. J. Currel and D. Schulte-Frohlinde, *Biopolmers*, **1987**, 26, 189.

24. M. T. Carter, M. Rodriquez and A. J. Bard, *J. Am. Chem. Soc.*, **1989**, 111, 8901.

25. H. Berg, U. Fiedler, J. Lemming and G. Horn, *Bioelectrochem. Bioenerg.*, **1985**, 14, 417.

26. E. Palecek, F. Jelen and L. Trnkova, *Gen, Physiol. Biophys.*, **1986**, 5, 315.

27. P. J. Declerck and C. De Ranter, *J. Chem. Soc. Farad. Trans.* 1., **1987**, 83, 257.

28. E. Palecek, *Bioelectochem. Bioenerg.*, **1986**, 15, 275.

29. E. Palecek, E. Lukasova. F. Jelen and M. Vojtiskova, *Bioelectrochem. Bioenerg.*, **1981**, 8, 497.

30. J.-M. Sequaris and P. Valenta. *J. Electroanal. Chem.*, **1987**, 227, 11.

31. M. T. Carter and A. J. Bard. *J. Am. Chem. Soc.*, **1987**, 109. 7528.

CHAPTER FIVE

SURFACE ELECTROCHEMISTRY OF THE INTERACTION OF METAL COMPLEXES WITH NUCLEIC ACIDS

5.1. INTRODUCTION

This chapter describes electrochemical studies of the interaction of transition metal complexes with nucleic acid immobilised on a chemically modified gold electrode surface. The procedure for the preparation of self-assembled monolayers is given in chapter three. Binding of metal complexes to DNA was carried out by the application of adsorptive-cyclic voltammetry to determine their accumulation on the electrode surface. The reversible electrochemical behavior of many metal complexes allows us to study the interaction of metal complexes with DNA and RNA using electroanalytical techniques.

Adsorption of DNA and RNA on the mercury and carbon electrode surface has been extensively studied [1-10]. Another method for holding DNA to a surface is thiol-modified DNA. A good example for this is that 6-mercapto hexyl-oligonucleotides bind to gold surface [11]. It has also been demonstrated that redox-active 5'-ferrocenyl-3 thiol modified oligonucleotides which immobilize on gold surfaces via sulfur bonds exhibit reversible electrochemistry [12].

It is reported that the self-assembly process is one of the most effective methods for producing monolayers [13]. In this method, a reactive group at one end of the molecule, for example thiol, binds covalently to the surface. The discovery of self-assembly

of thiol-terminated molecules on the gold surface has an important role in the chemistry of interfaces and opened a new area in the development of chemical sensors and biosensors.

In this chapter we studied the interaction of ferrocenyl-derivatives, $Ru(NH_3)_6^{+3}$ and $Fe(phen)_3^{+2}$ with nucleic acids on a gold electrode surface using cyclic voltammetry. Chemically modified surfaces were designed to immobilise nucleic acids using electrostatic interactions with the phosphate backbone and enabled us to exploit the sensitivity of adsorptive-transfer voltammetry.

5.2. RESULTS & DISCUSSION

5.2.1. INTERACTION OF Fc-Th AND Fc-NMe_3 WITH NUCLEIC ACID IMMOBILISED ON A GOLD ELECTRODE SURFACE

Cyclic voltammetry was utilized to investigate the interaction of Fc-Th with DNA and RNA immobilised on gold electrode surfaces.

Gold electrodes were modified here by adsorption of 4-mercaptopyridine with subsequent methylation of pyridine nitrogen to produce a positively charged cationic monolayer. Following adsorption of DNA onto gold surfaces, electrodes were dipped into solutions of Fc-Th. Then electrodes were transfered to a fresh solution of Tris buffer in the electrochemical cell (further information for the preparation of surfaces is given in chapter three). Figure 5.1 shows schematic of the interaction of fereocene derivatives with nucleic acids.

Cyclic voltammetry was applied to detect the binding of Fc-Th to DNA immobilised on a gold electrode surface. Figure 5.2 shows the cyclic voltammogram of a 1 mm diameter gold electrode after adsorption of DNA and Fc-Th followed by transfer to fresh 10 mmol dm^{-3} Tris buffer, pH 7. Surface waves at about +0.4 V were observed for Fc-Th. Also the peak current is proportional to the scan rate as given in figure 5.3. The charge passed on the electrode surface was used to calculate the mass associated with Fc-Th on the gold surface. The dependency of the surface coverage (see equation 2.7) on the concentration of Fc-Th was also investigated. An estimation of surface coverage calculated from the charge passed on the gold electrode surface at each concentration of Fc-Th is plotted in figure 5.4. The line represents a theoretical Langmuir isotherm in which the surface coverage is approximately 0.22 nmol cm^{-2} due to Fc-Th.

Surface electrochemistry was also applied to investigate the binding interaction of Fc-Th with RNA immobilised on a gold electrode surface. Following adsorption of RNA onto modified gold electrodes, and rinsing with 10 mM Tris buffer, the electrodes were dipped into a solution of Fc-Th. After transfer to a fresh 10 mM Tris buffer solution, cyclic voltammetry was applied to detect the binding of Fc-Th to RNA on the surface. Figure 5.5 shows the cyclic voltammogram of 1 mm diameter gold electrode after adsorption of RNA and Fc-Th followed by transfer to fresh 10 mM Tris buffer. The surface coverage determined from the charge on the surface due to Fc-Th on RNA modified gold surface was about 0.2 nmol cm^{-2}.

The interaction of Fc-NMe_3 with DNA or RNA immobilised on gold electrode surfaces was carried out using adsorptive-transfer voltammetry. After producing a cationic monolayer on the surface, the electrode was dipped into a solution of DNA or RNA to

adsorb nucleic acid. Then the electrode was dipped into a solution of Fc-NMe_3. After transfer to fresh 10 mM Tris buffer solution, cyclic voltammetry was run to determine the binding of Fc-NMe_3 to DNA and RNA. Figures 5.6 and 5.7 show the cyclic voltammograms of the interaction of Fc-NMe_3 with DNA and RNA immobilised on 1 mm diameter gold disc electrode surfaces respectively. No measureable surface waves were observed due to Fc-NMe_3. A small peak at +0.6 V was observed, possibly due to adsorption of iodide.

Fc-NMe_3 is a positively charged metal complex. In solution, cyclic voltammetry and steady-state microelectrode voltammetry showed that the binding of Fc-NMe_3 to DNA is a purely electrostatic interaction between the cationic ferrocenyl derivative and the anionic phosphate groups of DNA. The absence of detectable binding of Fc-NMe_3 to DNA or RNA immobilised on modified gold surface may be due to the electrostatic repulsion by the cationic pyridinum nitrogens. These adsorptive-transfer voltammetry experiments provide evidence for a non-electrostatic binding between Fc-Th and DNA and RNA.

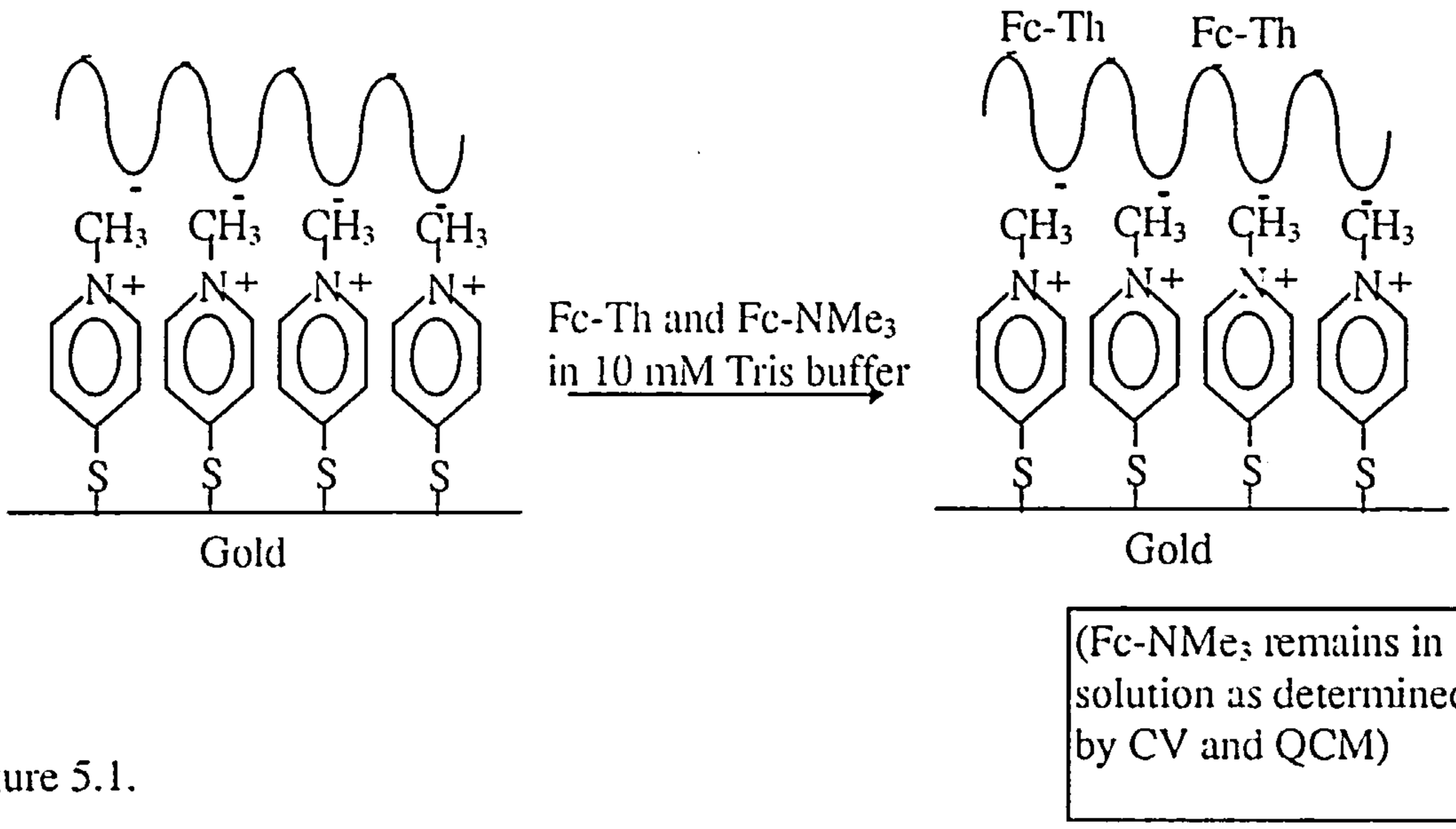

Figure 5.1.

Schematic illustration of the interaction of ferrocene derivatives with nucleic acid adsorbed surfaces.

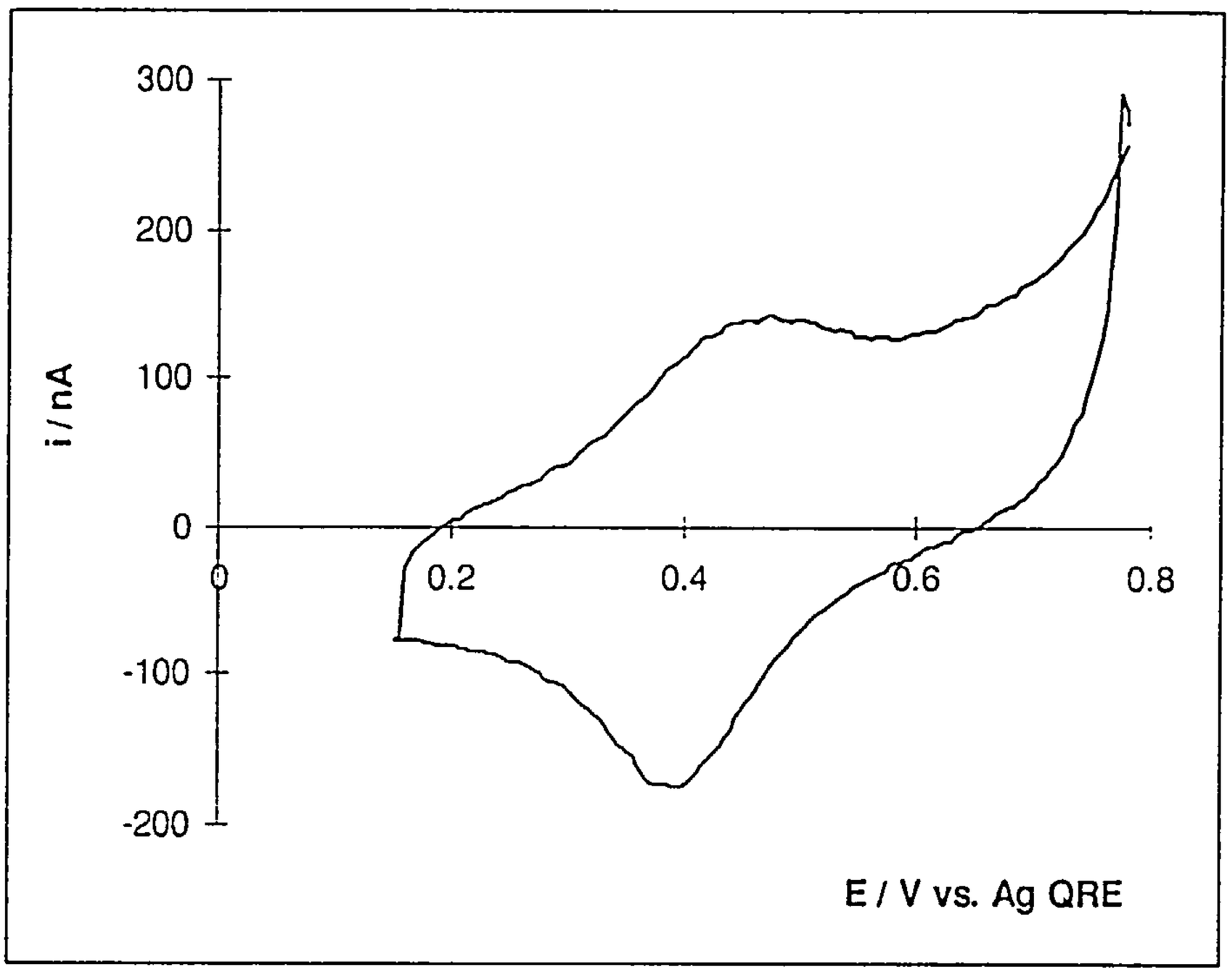

Figure 5.2.

Cyclic voltammogram of a 1 mm diameter gold electrode after adsorption of DNA and Fc-Th followed by transfer to fresh 10 mM Tris buffer. Scan rate 100 mV s^{-1}.

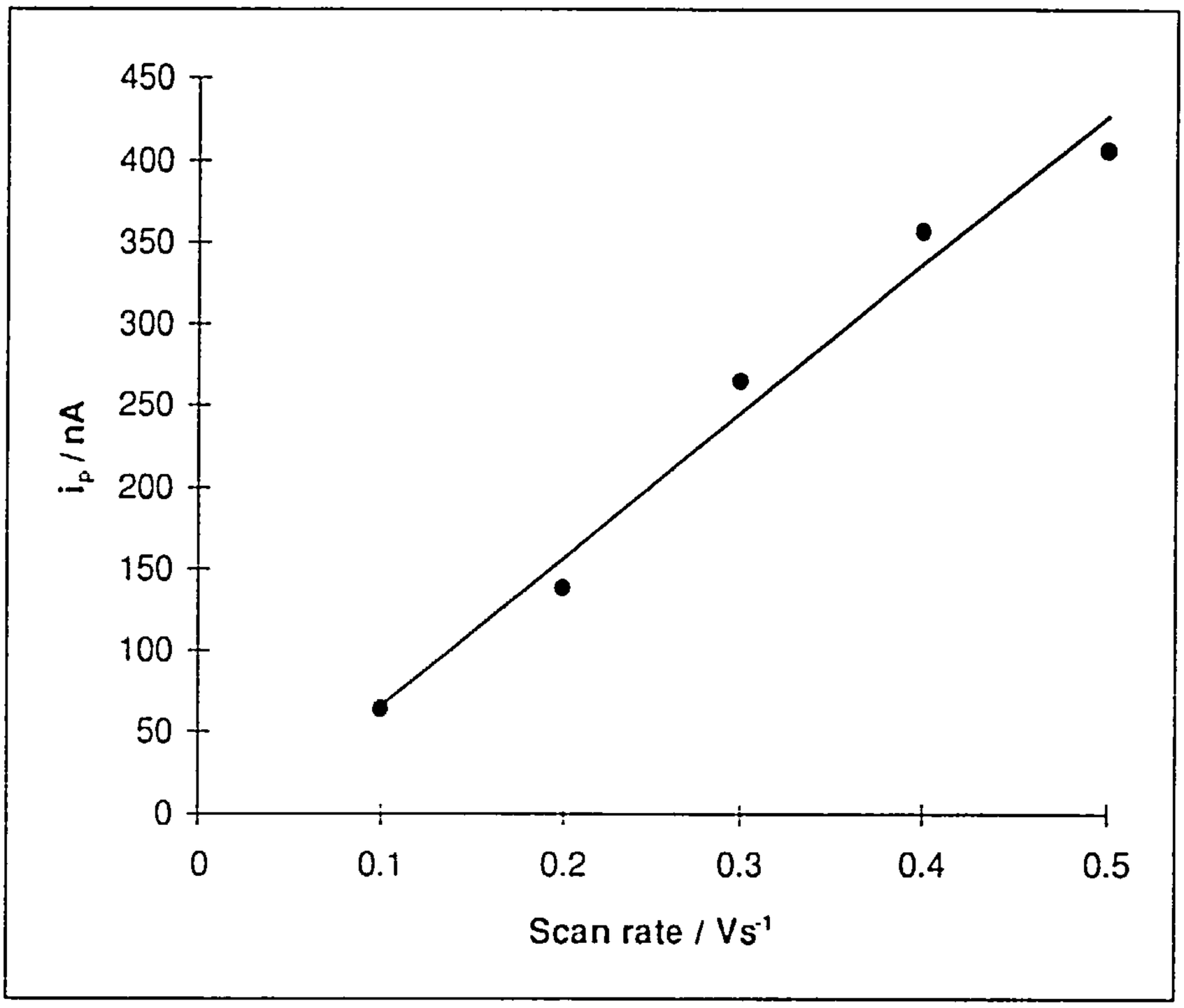

Figure 5.3.

A plot of peak current against the scan rate observed in binding of Fc-Th to DNA adsorbed on the pyridinium-modified gold surface.

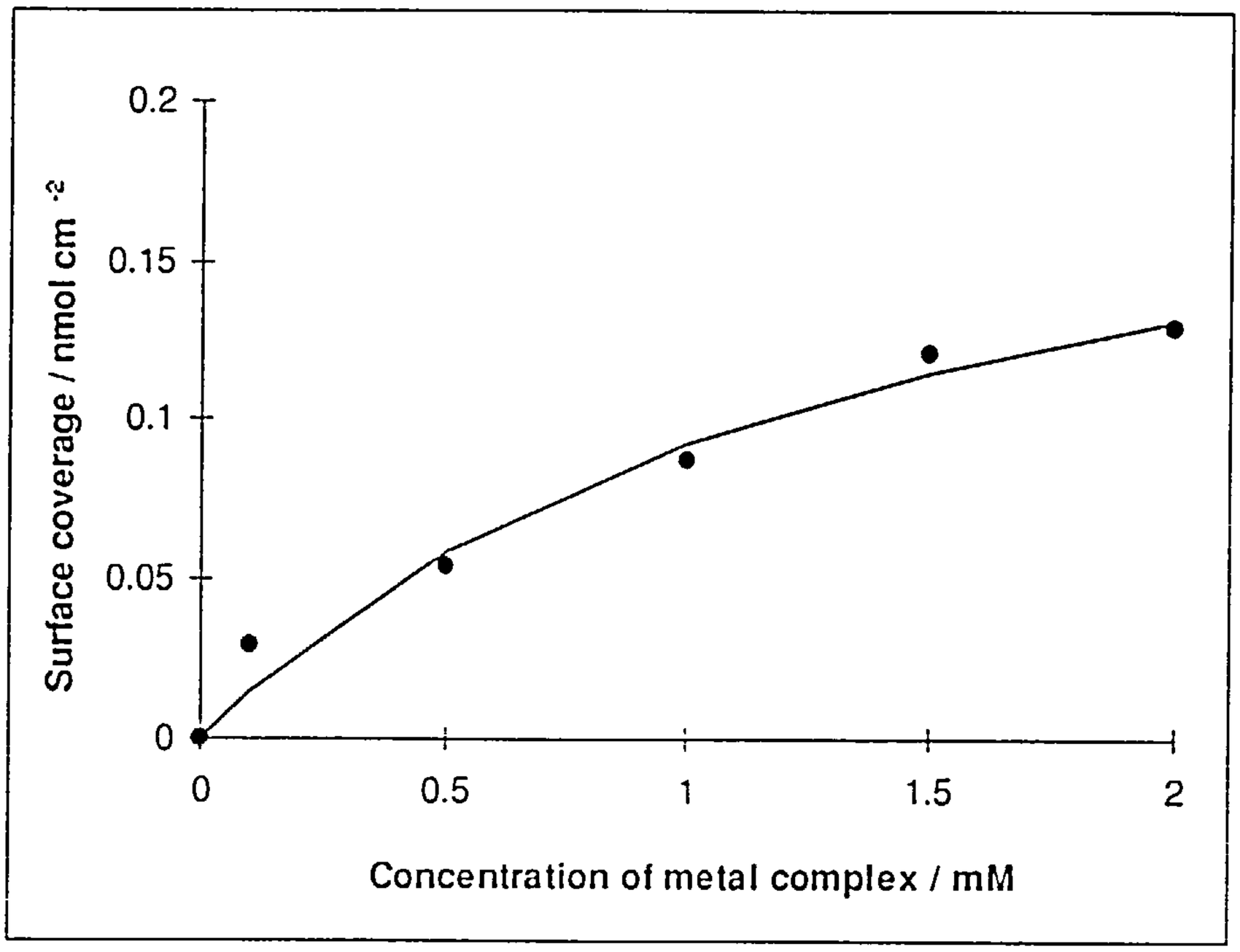

Figure 5.4.

Plot of surface coverage of Fc-Th against the concentration determined from its interaction with DNA adsorbed gold surface. The solid line represents a theoretical Langmiur isotherm in which the maxium surface coverage is 0.22 nmol cm^{-2}.

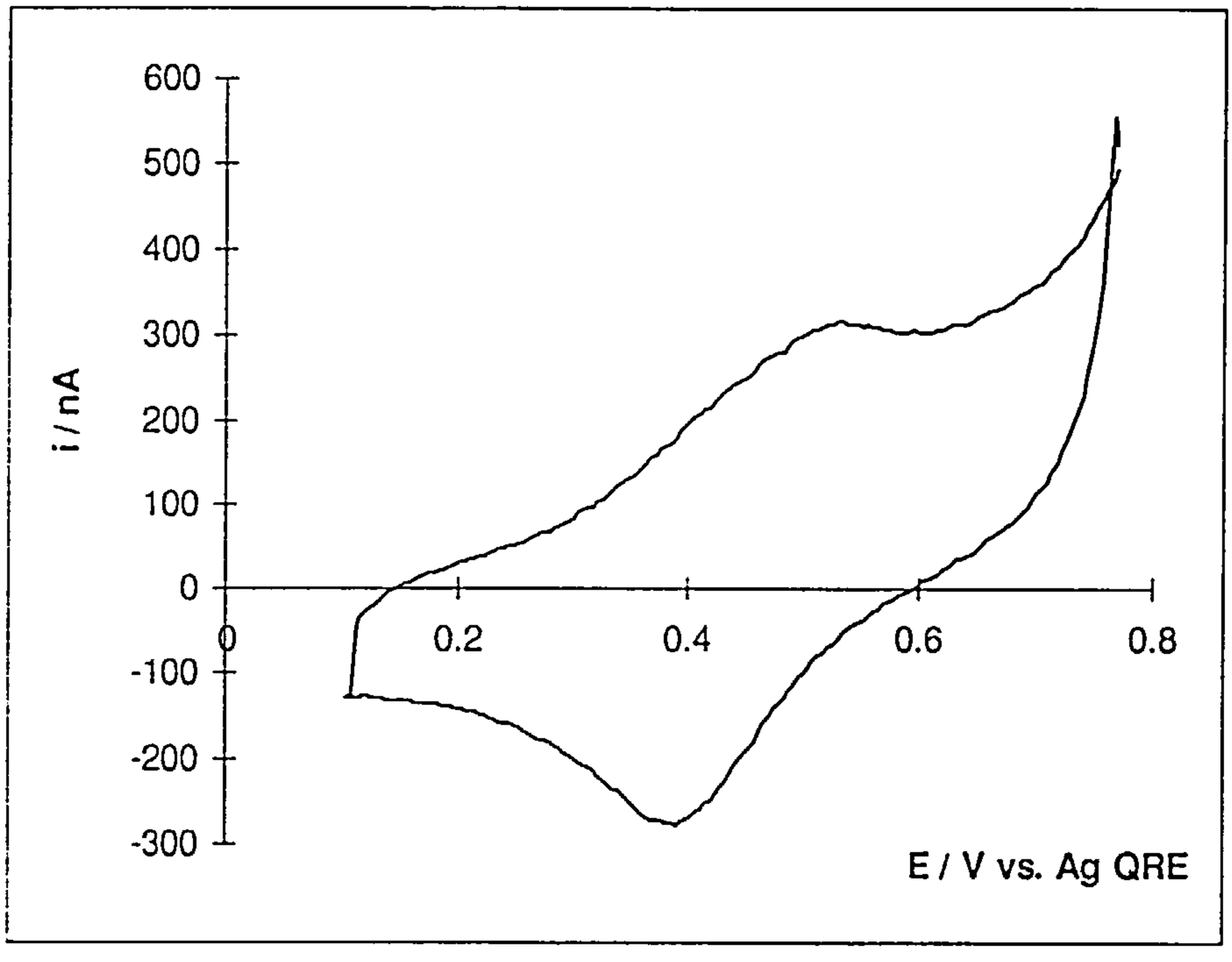

Figure 5.5.

Cyclic voltammogram of 1 mm diameter gold electrode after adsorption of RNA and Fc-Th followed by transfer to fresh 10 mM Tris buffer. Sweep rate 100 mVs^{-1}.

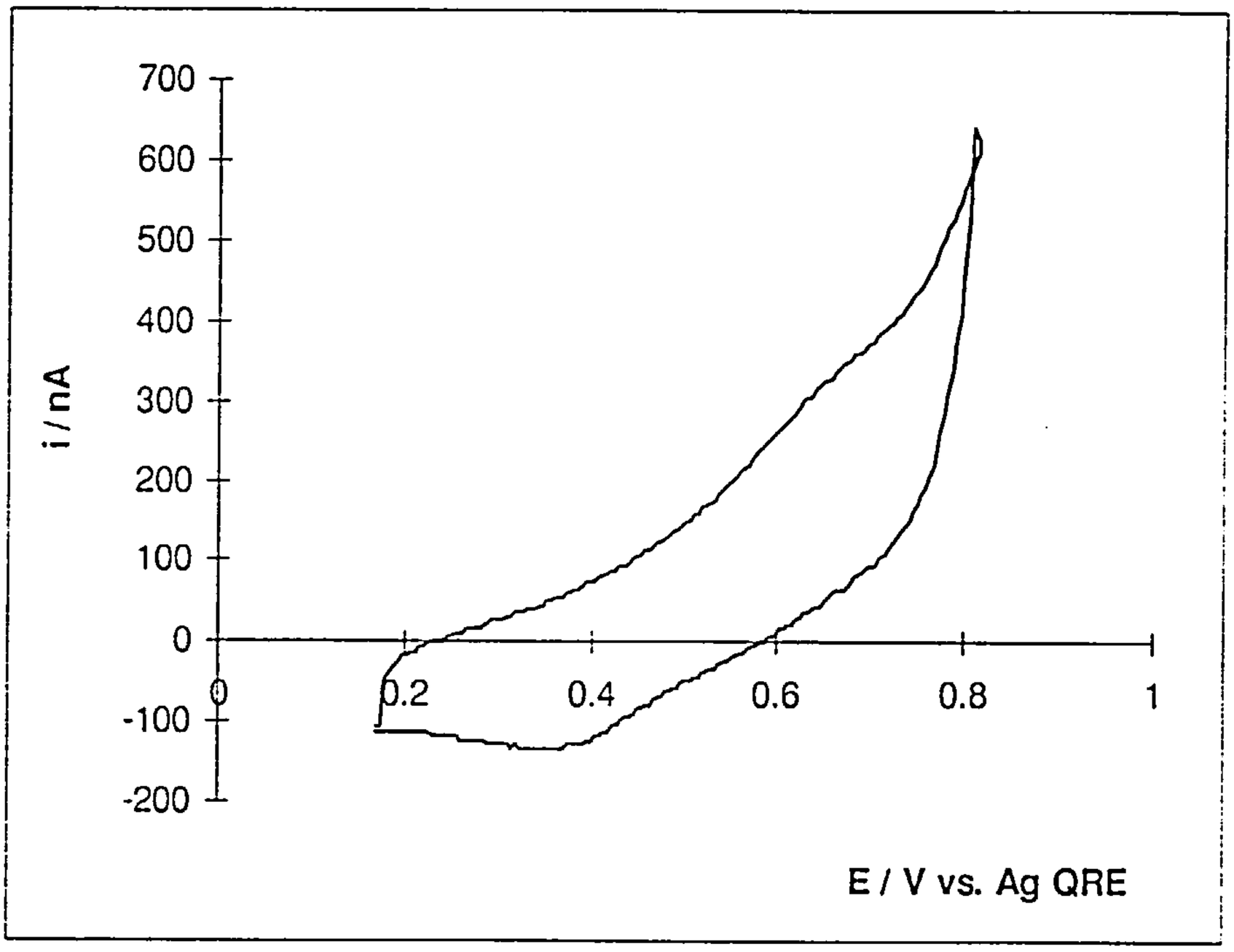

Figure 5.6.

Cyclic voltammogram of a 1 mm diameter gold electrode after adsorption DNA and Fc-NMe_3 followed by transfer to fresh 10 mM Tris buffer. Sweep rate 100 mVs^{-1}.

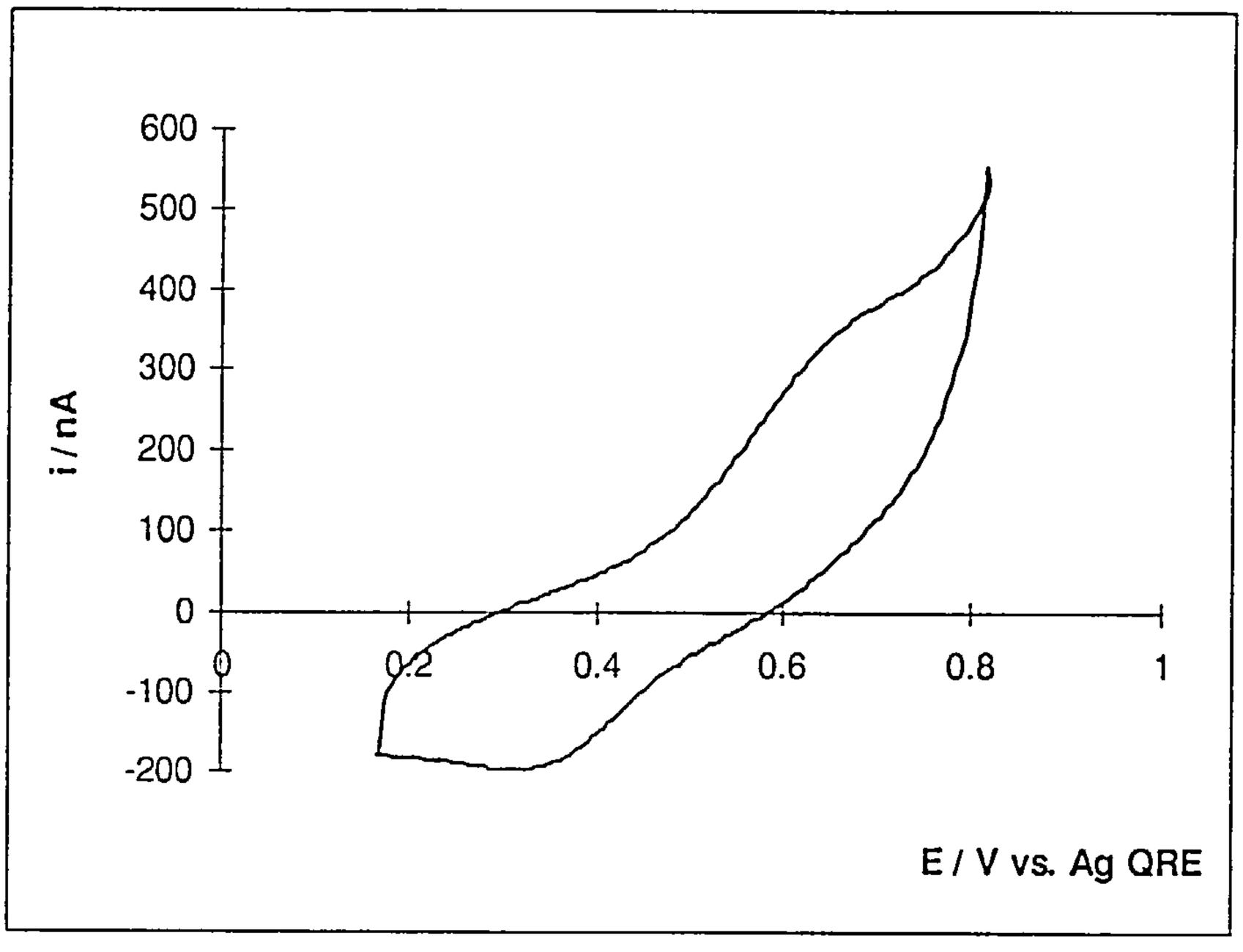

Figure 5.7.

Cyclic voltammogram of 1 mm gold electrode after adsorption of RNA and Fc-NMe_3 followed by transfer to a fresh 10 mM Tris buffer. Sweep rate, 100 mVs^{-1}.

5.2.3. INTERACTION OF HEXAMMINERUTHENIUM (III) CHLORIDE WITH DNA

Interaction of $Ru(NH_3)_6^{+3}$ with DNA immobilised on a pyridinium-modified gold electrode surface was carried out using cyclic voltammetry to make an estimation of the surface coverage of $Ru(NH_3)_6^{+3}$ on the surface. Following adsorption of DNA, gold electrodes were dipped into solutions of $Ru(NH_3)_6^{+3}$. After transfer to a fresh 10 mM Tris buffer solution in the electrochemical cell, cyclic voltammetry was applied to investigate the binding interaction of $Ru(NH_3)_6^{+3}$ with DNA on the electrode surface. Figure 5.8 shows the schematic of the interaction of $Ru(NH_3)_6^{+3}$ with DNA adsorbed surface. Figure 5.9 shows a cyclic voltammogram of a 1 mm diameter gold electrode after adsorption of DNA and $Ru(NH_3)_6^{+3}$ followed by transfer to fresh 10 mM Tris buffer We also made a futher experiment to see if $Ru(NH_3)_6^{+3}$ binds to the surface in the absence of methyl iodide. In the absence of methyl iodide no surface wave for $Ru(NH_3)_6^{+3}$ was observed as seen in figure 5.13. The absence of observation of surface wave in the absence of methyl iodide for $Ru(NH_3)_6^{+3}$ is also the experimental evidence of the surface modification and indicates that quaternisation of the pyridine nitrogen is essential for the immobilisation of DNA. Figure 5.10 shows the dependency of peak current on the scan rate. Peak current increases with scan rate as expected for a surface process.

The dependency of the mass adsorbed of $Ru(NH_3)_6^{+3}$ on its concentration was examined to calculate the surface coverage and to determine the mass adsorbed collected at each concentration. A plot of mass adsorbed against concentration of $Ru(NH_3)_6^{+3}$ is given in figure 5.11. An estimation of surface coverage determined is approximately 0.32 nmol cm^{-2}. The surface coverage of $Ru(NH_3)_6^{+3}$ determined here is larger than the surface coverage observed for Fc-Th. Since $Ru(NH_3)_6^{+3}$ is a highly positively charged metal

complex and also having possibilities of hydrogen bonding via NH_3 groups and phosphate groups of DNA, the interaction between $Ru(NH_3)_6^{+3}$ and DNA is much stronger than between Fc-Th and DNA.

We also examined the dependence of the mass adsorbed of DNA on its concentration to estimate roughly the amount of immobilised DNA on the electrode surface. For this purpose we kept the concentration of $Ru(NH_3)_6^{+3}$ constant. A plot of mass adsorbed against the concentration of DNA in 10 mM Tris buffer solution is given in figure 5.12. The line represent a langmiur isotherm in which the surface coverage of DNA is approximately 0.36 nmol cm^{-2}. In our solution experiment section 4.2.1 of chapter 4 we found that DNA (0.4 mM used in titration experiment) is saturated at 0.1 mM $Ru(NH_3)_6^{+3}$. We can convert roughly between the amounts of adsorbed $Ru(NH_3)_6^{+3}$ and DNA by multiplying by a factor of 4 (0.4/0.1). We further multiply the amount of DNA determined on the surface by 2, because we assume that 1/2 phosphate binds to pyridinium nitrogens and 1/2 phosphate binds to $Ru(NH_3)_6^{+3}$.

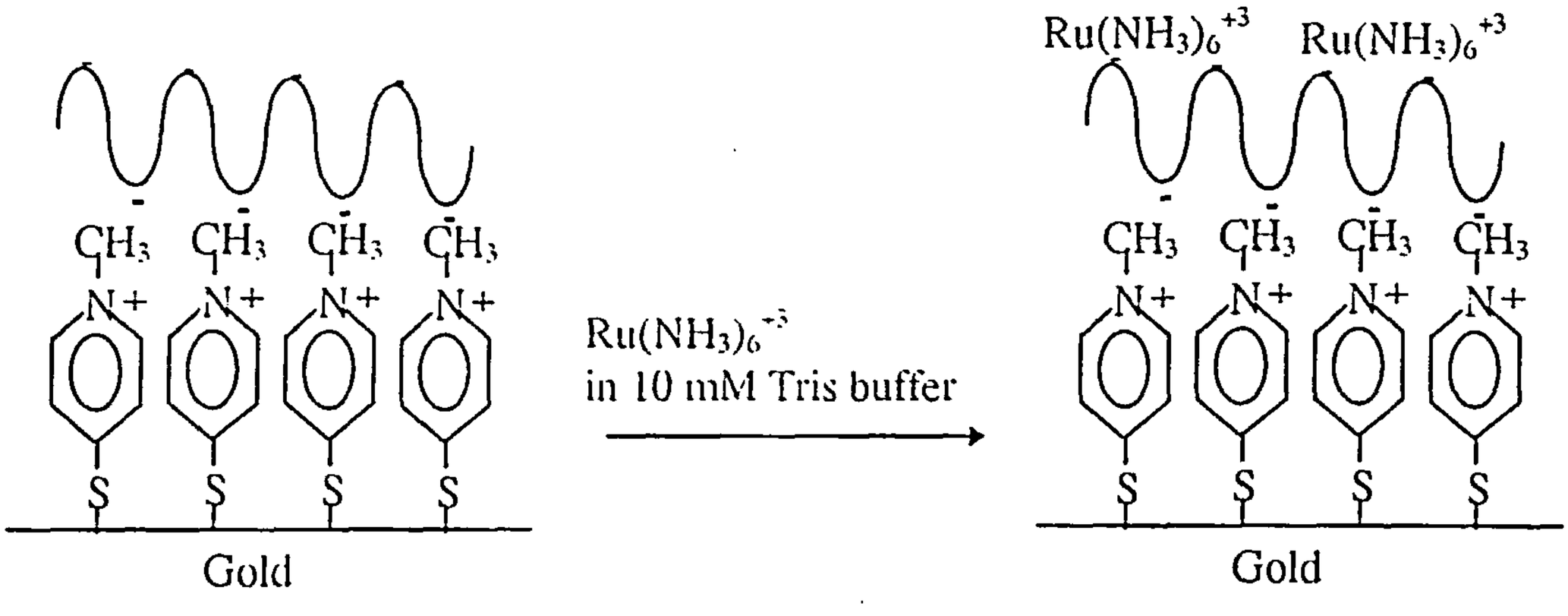

Figure 5.8.

Schematic illustration of binding of $Ru(NH_3)_6^{+3}$ with DNA immobilised surface.

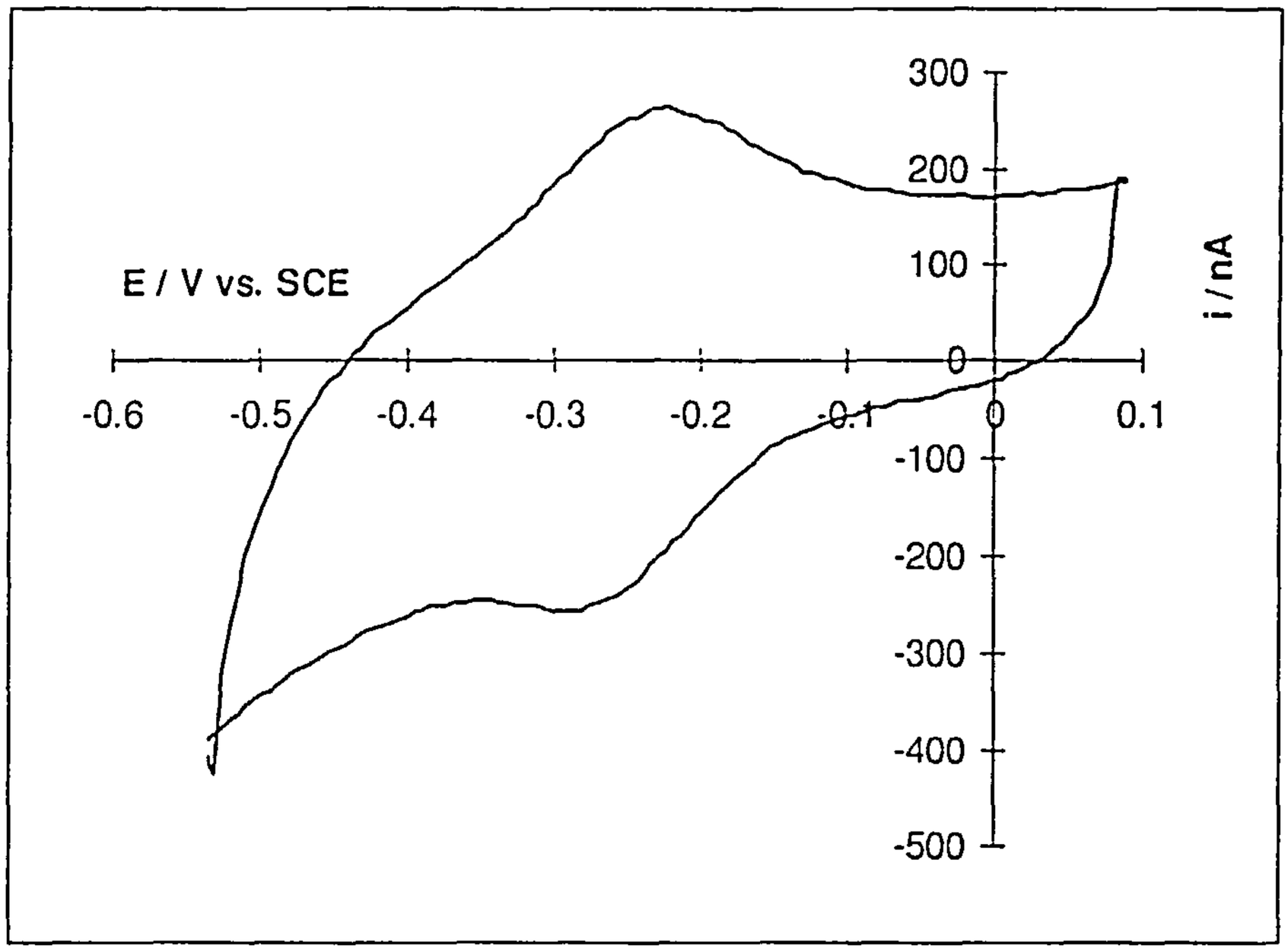

Figure 5.9.

Cyclic voltammogram of 1 mm diameter gold electrode after adsorption of DNA and $Ru(NH_3)_6^{+3}$ followed by transfer to a fresh 10 mM Tris buffer. Scan rate 100 mVs^{-1}.

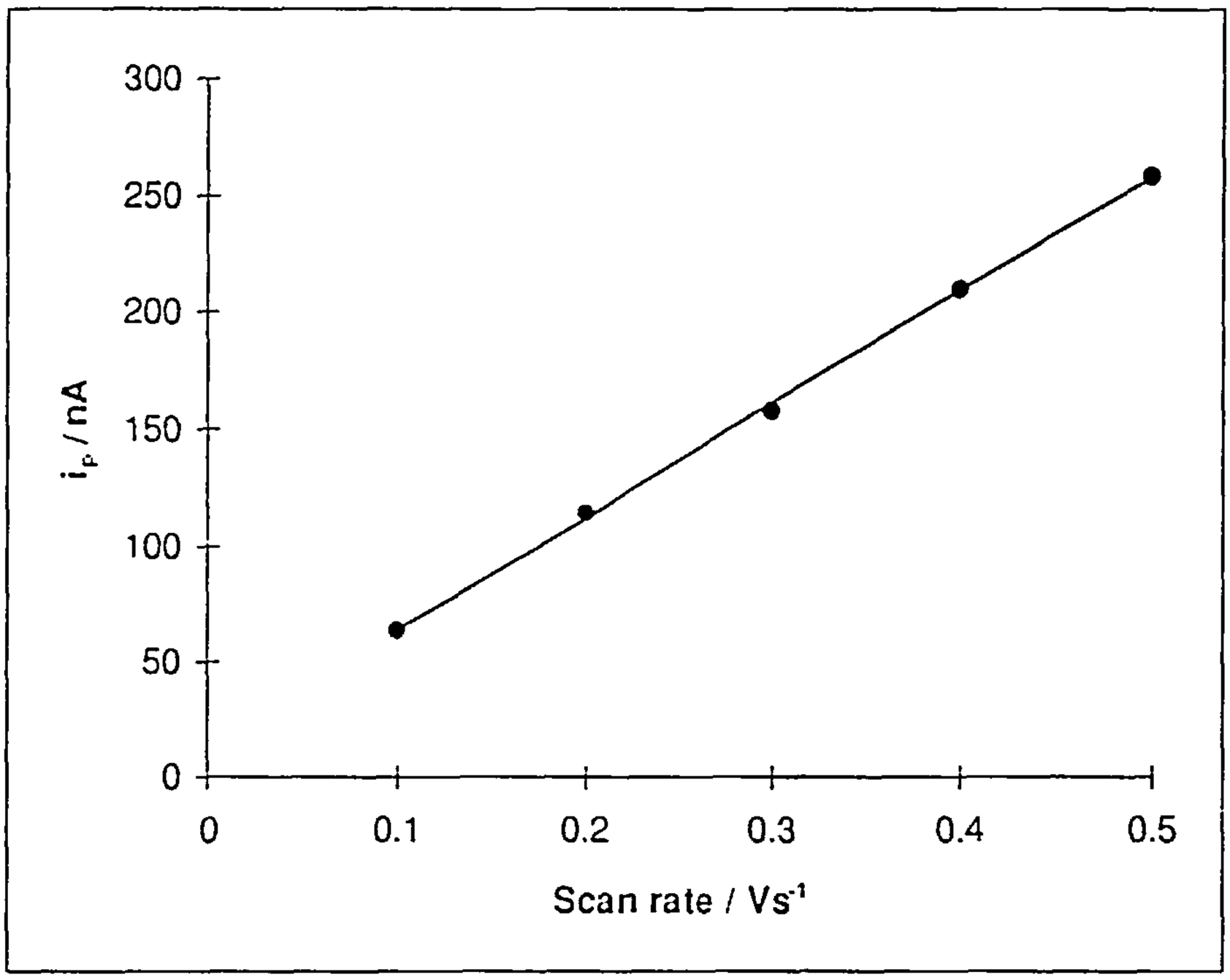

Figure 5.10.

A plot of peak current against scan rate determined from the interaction of $Ru(NH_3)_6^{+3}$ with DNA adsorbed on a 1 mm diameter gold electrode.

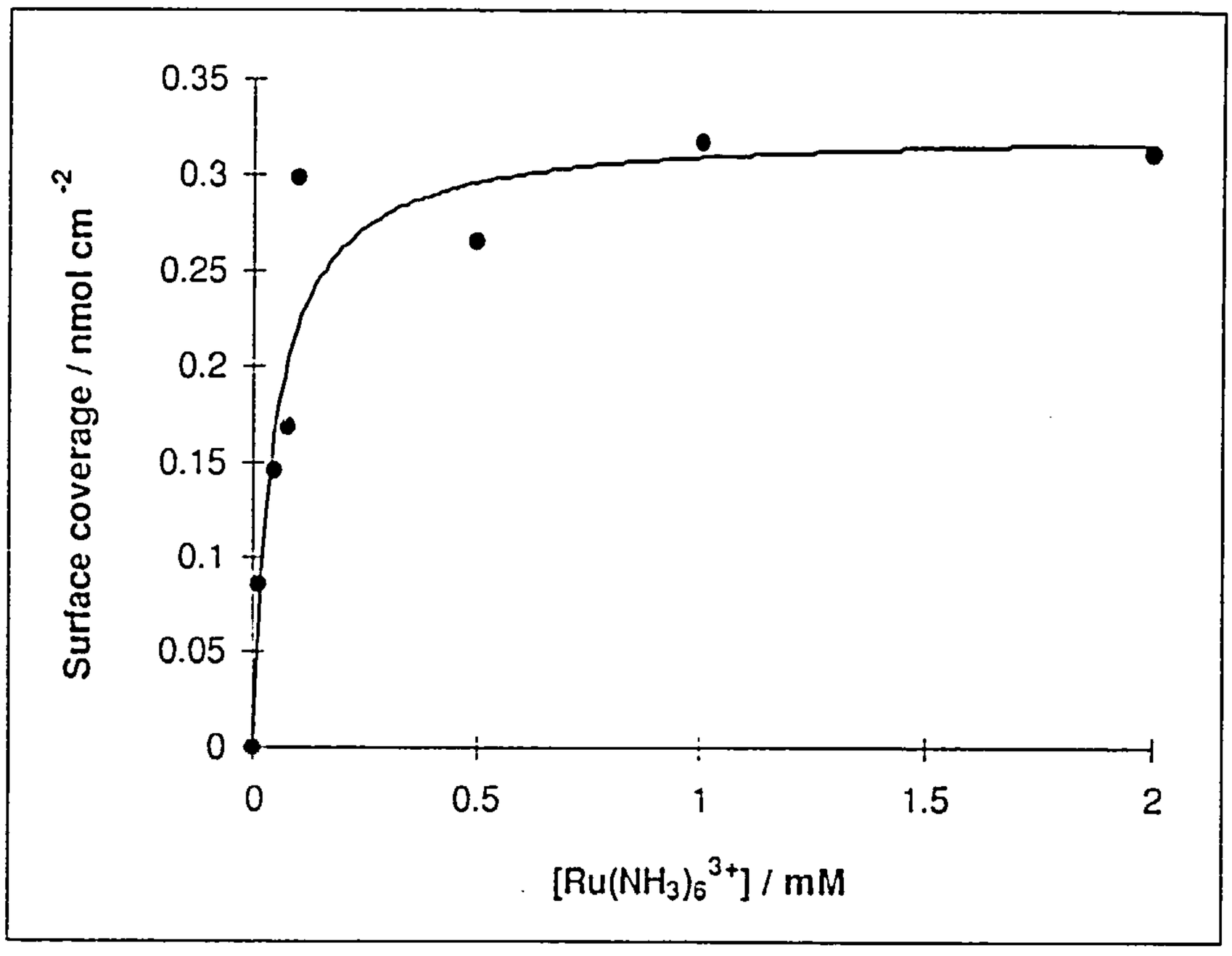

Figure 5.11.

A plot of surface coverage of $Ru(NH_3)_6^{+3}$ determined from its interaction with DNA adsorbed gold electrode surface. The solid line represent a theoretical Langmiur isotherm in which maxium surface coverage is 0.32 nmol cm^{-2}.

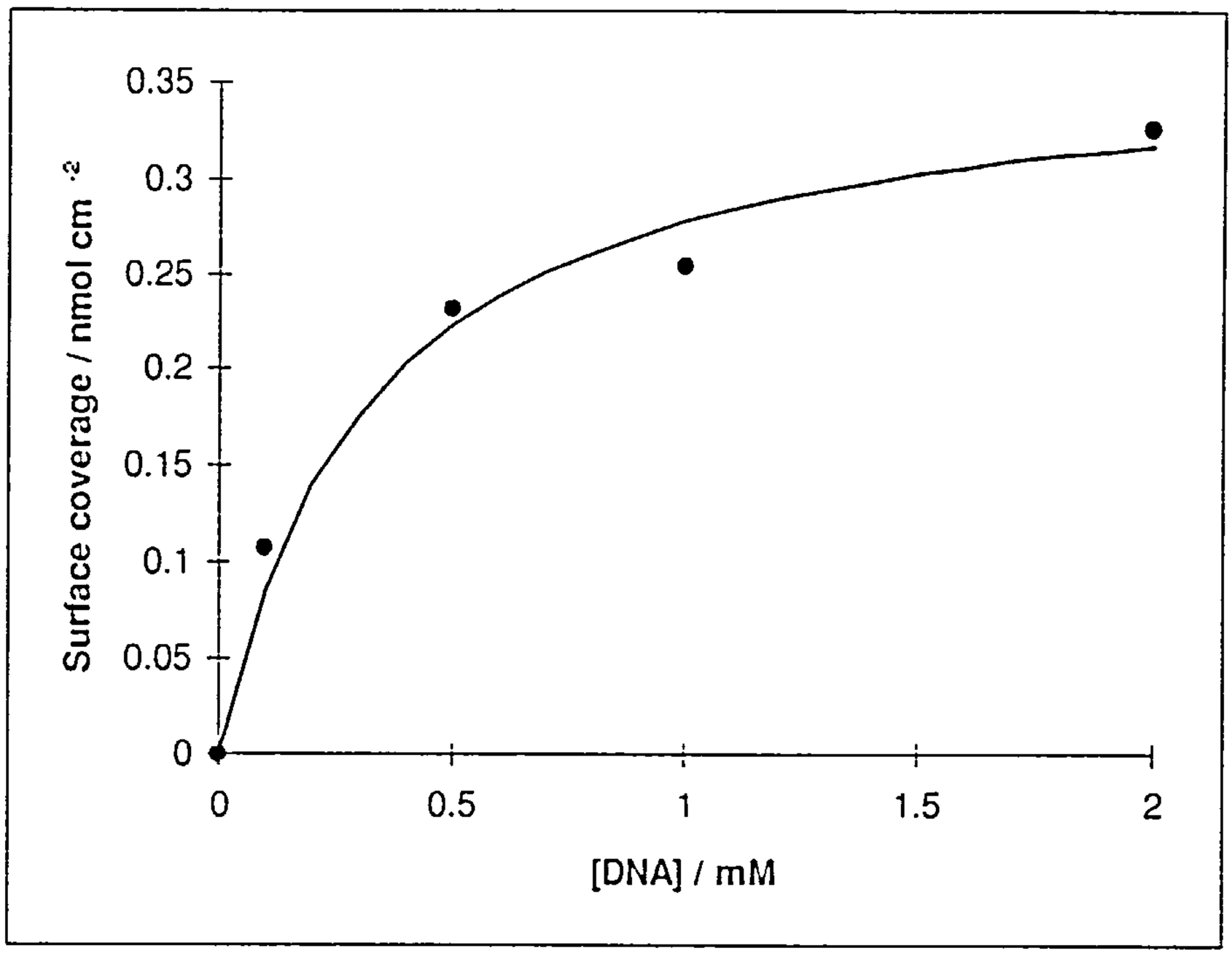

Figure 5.12.

A plot of the surface coverage of DNA against its concentration estimated from the interaction of $Ru(NH_3)_6^{+3}$ with DNA adsorbed gold surface. The solid line represents a theoretical Langmiur isotherm in which maxium surface coverage is 0.36 nmol cm^{-2}.

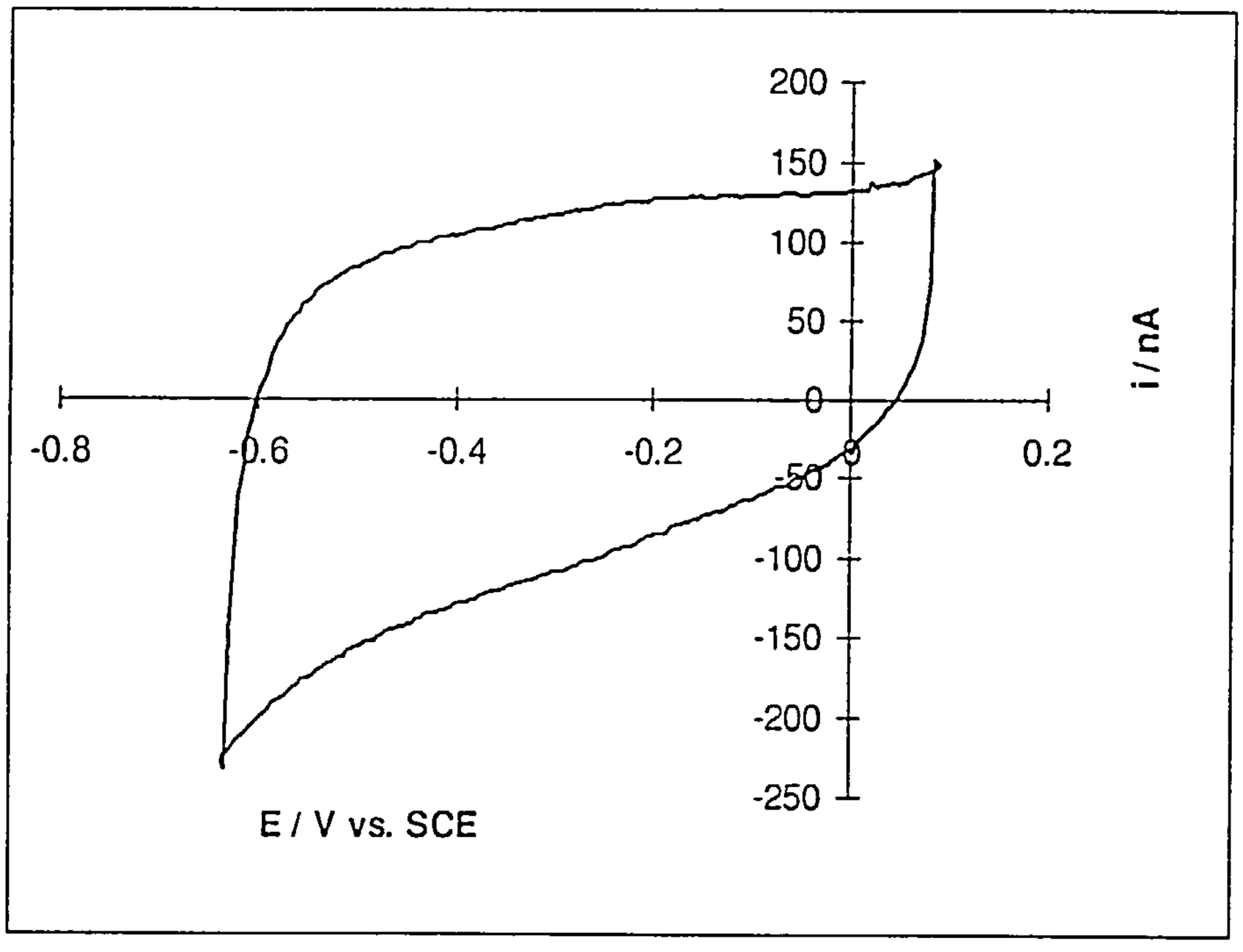

Figure 5.13.

Cyclic voltammogram of 1 mm diameter gold electrode after adsorption of 4-mercaptopyridine only and dipped into solutions of DNA and $Ru(NH_3)_6^{+3}$ followed by transfer to fresh 10 mM Tris buffer. Scan rate, 100 mVs^{-1}.

5.2.4. INTERACTION OF TRIS(1,10-PHENANTHROLINE)IRON(III) PERCLORATE WITH DNA

Cyclic voltammetry was applied to study the binding interaction of $Fe(phen)_3^{+2}$ with DNA immobilised on a gold electrode surface. Following adsorption of DNA onto the gold electrode surface, the electrode was dipped into a solution of $Fe(phen)_3^{+2}$. After transfer to a fresh solution of 10 mM Tris buffer in electrochemical cell, cyclic voltammetry was applied to investigate the binding of $Fe(phen)_3^{+2}$ to DNA immobilised on a gold electrode surface as illustrated in figure 5.14. Figure 5.15 shows cyclic voltammogram of a 1 mm diameter gold electrode after adsorption of DNA and $Fe(phen)_3^{+2}$ followed by transfer to fresh 10 mM Tris buffer. Unfortunately, we were not be able to observe a surface wave for the interaction of $Fe(phen)_3^{+2}$ with DNA. This may be due to the oxidation of H_2O at potential where $Fe(phen)_3^{+2}$ appears. It could also be due to 4-mercaptopyridine being oxidised and removed from the surface.

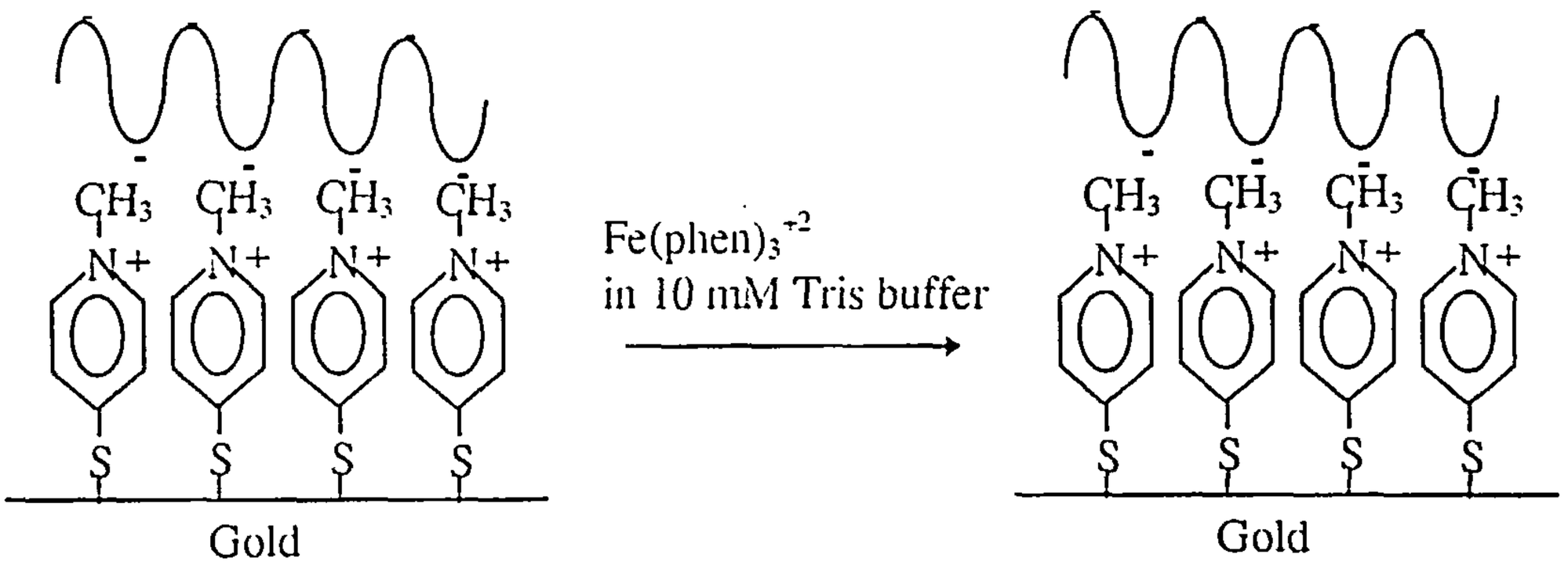

Figure 5.14.

Schematic illustration of the interaction of $Fe(phen)_3^{+2}$ with DNA adsorbed gold electrode surface.

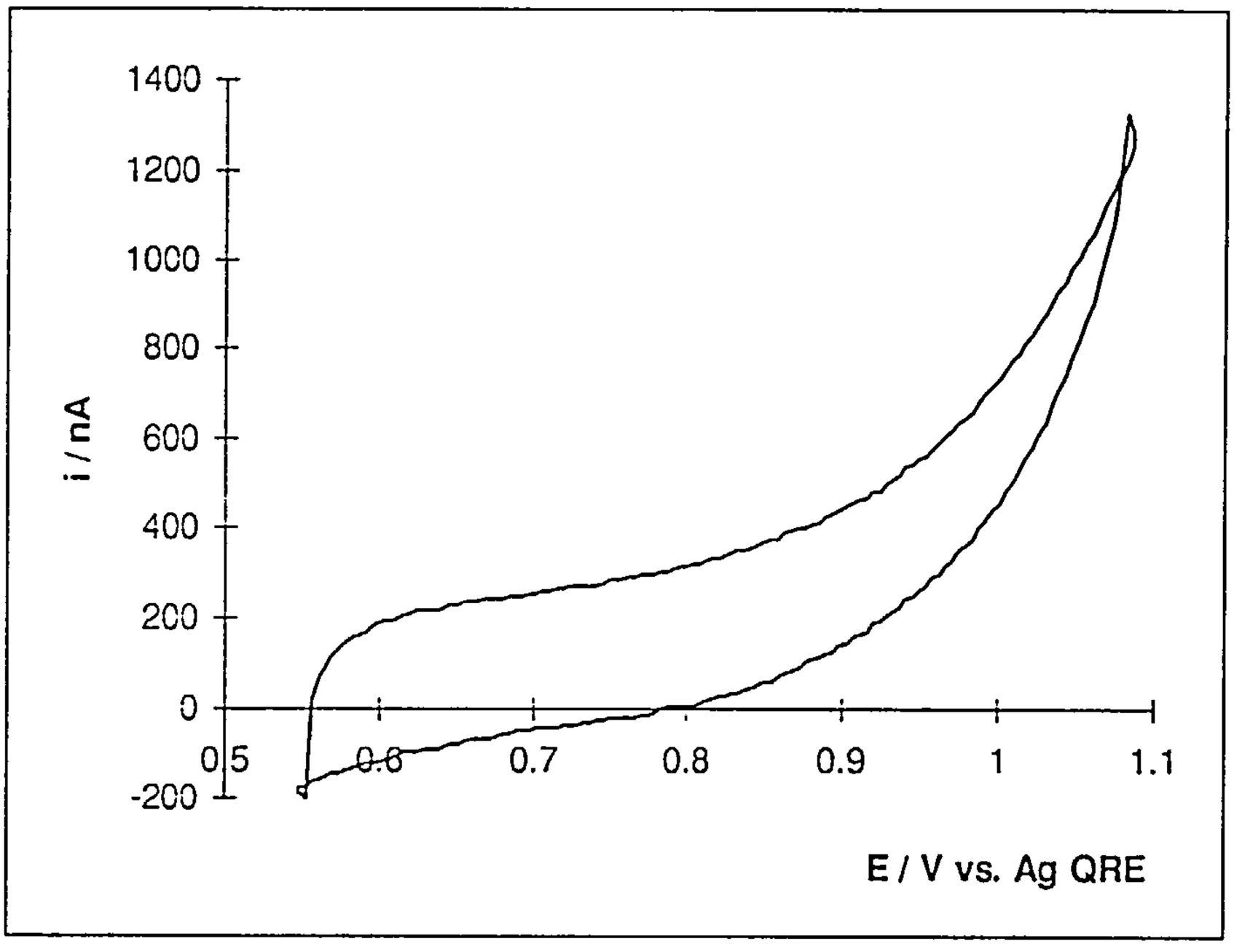

Figure 5.15.

Cyclic voltammogram of a 1 mm diameter gold electrode after adsorption of DNA and $Fe(phen)_3^{+2}$ followed by transfer to fresh 10 mM Tris buffer . Scan rate, 100 mVs^{-1}.

5.3. CONCLUSIONS

Binding of Fc-Th to nucleic acids adsorbed on a modified gold electrode surface but not Fc-NMe_3 shows that a single nucleobase produces a significant change in the mode of binding to nucleic acids. The estimated maxium surface coverage is about 0.22 nmol cm^{-2}. No detectable binding of Fc-NMe_3 was observed on the surface. Fc-NMe_3 has an only one positive charge on the nitrogen. Therefore, Fc-NMe_3 has only electrostatic possibilities for binding. The absence of detectable binding of Fc-NMe_3 can be rationalised as a consequence of the proximity of the cationic pyridinium nitrogens in the monolayer. Adsorptive-transfer voltammetry therefore provides evidence of non-electrostatic interaction between Fc-Th and DNA immobilised electrode surface.

$Ru(NH_3)_6^{+3}$ also binds to DNA on the surface. $Ru(NH_3)_6^{+3}$ is highly positively charged molecule and can bind to DNA by electrostatic attraction. The NH_3 groups may also influence the binding via hydrogen bonding interactions with oxygen atoms of phosphate groups. The maximum surface coverage determined was about 0.32 nmol cm^{-2}. The observed surface coverage of $Ru(NH_3)_6^{+3}$ is larger than the surface coverage of Fc-Th. This is probably due to $Ru(NH_3)_6^{+3}$ having a stronger binding to DNA as detected in solution experiments (chapter 4). We also used our successful titration experiment carried out using microelectrode voltammetry in solution to make a crude estimate of the amount of DNA on the surface. The estimated surface coverage of DNA was about 0.36 nmolcm^{-2}. Methylation of 4-mercaptopyridine to produce cationic pyridinium was essential to immobilise DNA on the surface. The experimental adsorption isotherms roughly follow the Langmiur theory.

No surface wave was observed in the experiment with $Fe(phen)_3^{+2}$. A possible explanation is that thiols could be removed at high positive potential where the oxidation of $Fe(phen)_3^{+2}$ occurs.

5.4. REFERENCES

1. D-W. Pang, M. Zhang, Z-L. Wang, Y-P. Qi, J-K. Cheng and Z-Y. Liu, J. *Electroanal. Chem.*, **1996**, 403, 183.

2. A. M. O. Brett and S. H. P. Serrano, *J. Braz. Chem. Soc.*, **1995**, Vol. 6, No. 1, 97.

3. C. Teijerio, P. Perez, D. Marin and E. Palecek, *Biolectrochem. Bioenerg.*, **1995**, 38, 77.

4. D-W. Pang, Y-P. Qi, Z-L. Wang, J-K. Cheng and J-W. Wang, *Electroanalysis*, **1995**, 7, 774.

5. J. Swiatek, *J. Coord. Chem.*, **1994**, 33, 191.

6. C. M. A. Brett, A. M. O. Brett and S. H. P. Serrano, *J. Electranal. Chem.*, **1994**, 366, 225.

7. J. Wang, X. Cai, J. Wang, C. Jonsson and E. Palecek, *Anal. Chem.*, **1995**, 67, 4065.

8. E. Palecek, *Anal. Biochem.*, **1988**, 170, 421.

9. C. G. Siontorou, A. M. O. Brett and D. P. Nikolelis, *Talanta*, **1996**, 43, 1137.

10. M. Fojta, C. Teijeiro and E. Palecek, *Bioelectrochem. Bioeneg.*, **1994**, 34, 69.

11. D. Rekesh, Y. Lyubchenko, L. S. Shlyakhtenko and S. M. Lindsay, *Biophys. J.*, **1996**, 71, 1079.

12. R. C. Mucic, M. K. Herrlein, C. A. Mirkin and R. L. Letsinger, *Chem. Commun.*, **1996**, 555.

13. H. C. Yang, K. Aoki, H. G. Hong, D. D. Sackett, M. F. Arendt, S. L. Yau, C. M. Bell and T. E. Mallouk, *J. Am. Chem. Soc.*, **1993**, 115, 11855.

CHAPTER SIX

MEASUREMENTS OF DNA-METAL COMPLEX BINDING BY THE APPLICATION OF THE QUARTZ CRYSTAL MICROBALANCE

6.1. INTRODUCTION

This chapter describes the quantitative application of the quartz crystal microbalance (QCM) to the study of determination of the mass changes associated with metal complex-DNA interactions on modified surfaces. The QCM is employed here to make an estimation of surface coverage associated with the binding interaction of thiols, metal complexes and nucleic acids on platinum and gold electrodes.

Adsorption of thiols on gold and platinum surfaces has been used in several studies [1-4]. Quartz crystal microgravimetry has been applied to calculate the surface coverage of self-assembled monolayers of thiols [4]. Adsorption of DNA onto surface modified gold has also been monitored by quartz crystal microbalance [5-6]. Quantitative analysis of a DNA probe having a thiol group immobilised on a gold surface has been studied using quartz crystal microgravimetry [7].

In this chapter we use the quartz crystal microgravimetry to determine the mass change due to adsorption of 4-mercaptopyridine and nucleic acids onto gold and platinum surfaces. The quantitative analysis of the interaction of ferrocene derivatives, ruthenium and iron complexes with nucleic acid immobilised on surfaces is also reported.

6.2. RESULTS & DISCUSSION

6.2.1. MEASUREMENT OF ADSORPTION OF 4-MERCAPTOPYRIDINE

Quartz crystal microgravimetry was applied to estimate the surface coverage on adsorption of 4-mercaptopyridine onto gold-coated quartz crystals. For this purpose clean and dry quartz crystals were prepared as described in chapter three. Experiments were carried out in solution. Before the addition of 4-mercaptopyridine solution , ethanol was placed in the cell containing a gold or platinum coated crystal. The schematic of adsorption of 4-mercatopyridine on surfaces is given in figure 6.1. We used different concentrations of 4-mercaptopyridine prepared in ethanol. The dependency of frequency change against the concentration of 4-mercaptopyridine was investigated. Frequency decreased with increasing concentration of 4-mercaptopyridine. A decrease in frequency indicates an increase in adsorbed mass of 4-mercaptopyridine. Mass increases as frequency decreases according to the Sauerbrey equation. Figure 6.2 shows the mass adsorbed of 4-mercaptopyridine on a gold-coated quartz crystal against the concentration. The estimation of mass on the gold surface calculated from this line representing a theoretical Langmiur isotherm is approximately 9 nmol cm^{-2} It has been found that density or viscosity of the adjacent solution also has a contribution to the frequency change [4]. Therefore, a change in frequency may be observed on changing the bulk properties of the solution.

Pt-coated quartz crystals were also applied to investigate the adsoprtion of 4-mercaptopyridine onto platinum surface. The decrease in frequency with adsorption of 4-mercaptopryridine observed is 35 Hz. This decrease corresponds to 1.7 nmol cm^{-2}

adsorbed on the platinum-coated surface. Figure 6.3 shows that the adsorption of 4-mercaptopyridine is complete in about 10 minutes.

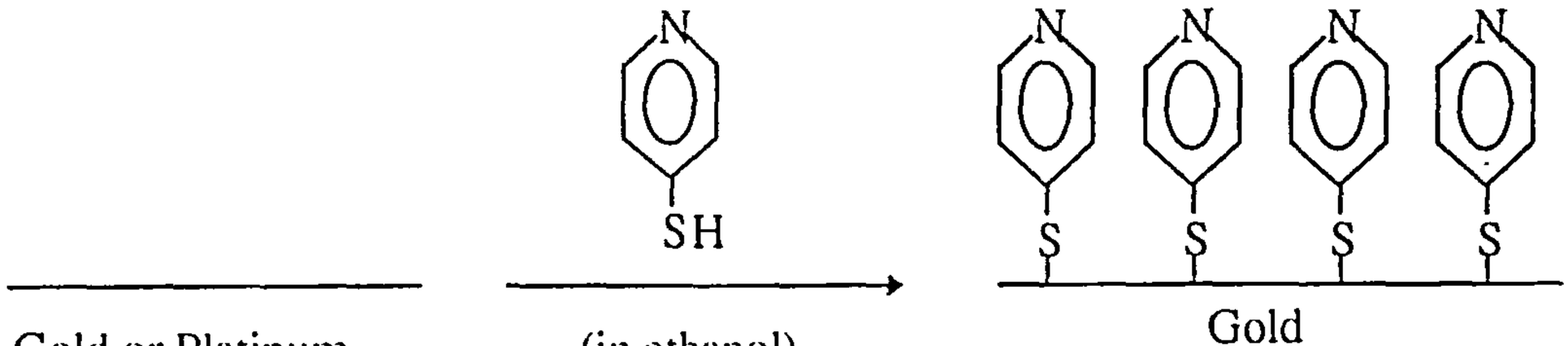

Figure 6.1.

Schematic illustration of adsorption of 4-mercaptopyridine on surfaces.

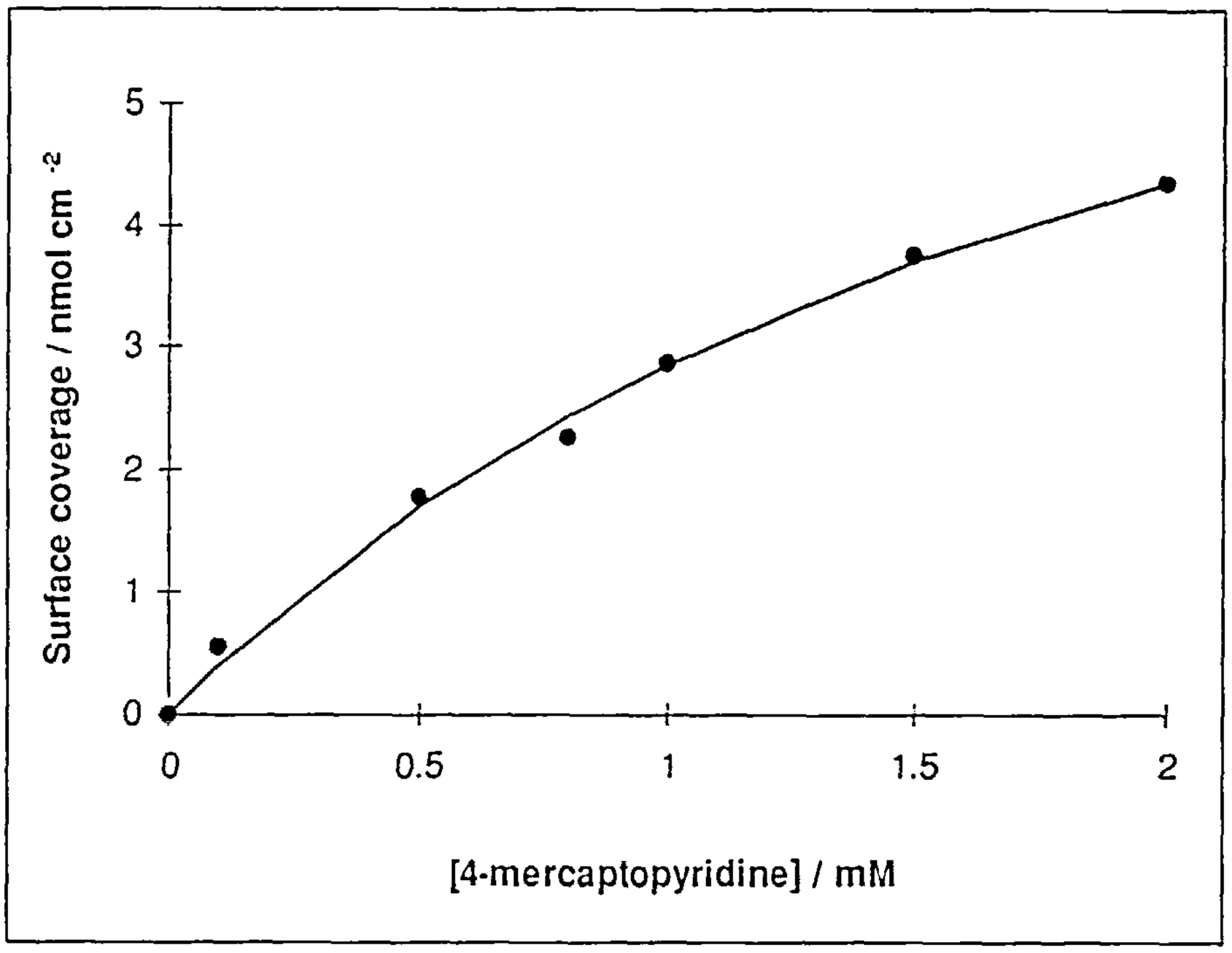

Figure 6.2.

The surface coverage of 4-mercaptopyridine on a gold-coated crystal calculated from Sauerbrey equation. The solid line represent a theoretical Langmiur isotherm in which the surface coverage is 9 nmol cm^{-2}.

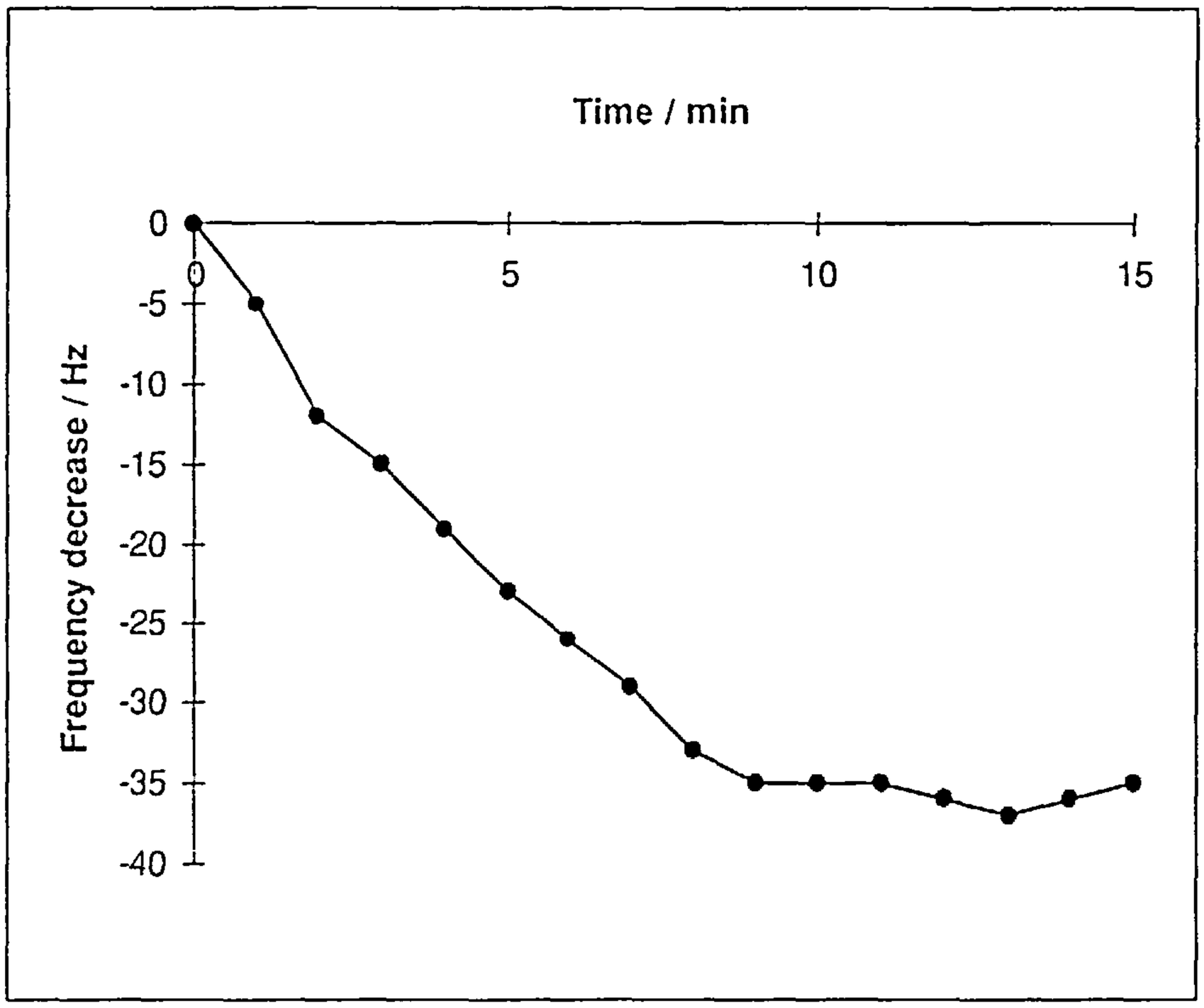

Figure 6.3.

A plot of frequency change of surface coverage of adsorption of 4-mercaptopyridine on a platinum surface against time.

6.2.2. METHYLATION OF 4-MERCAPTOPYRIDINE

The frequency change for the experiment of the methylation of 4-mercaptopyridine to produce a cationic surface was not carried out in-situ because methyl iodide is an extremely toxic compound and carcinogenic. The schematic of the preparation of cationic pyridinum surfaces is given in figure 6.4.

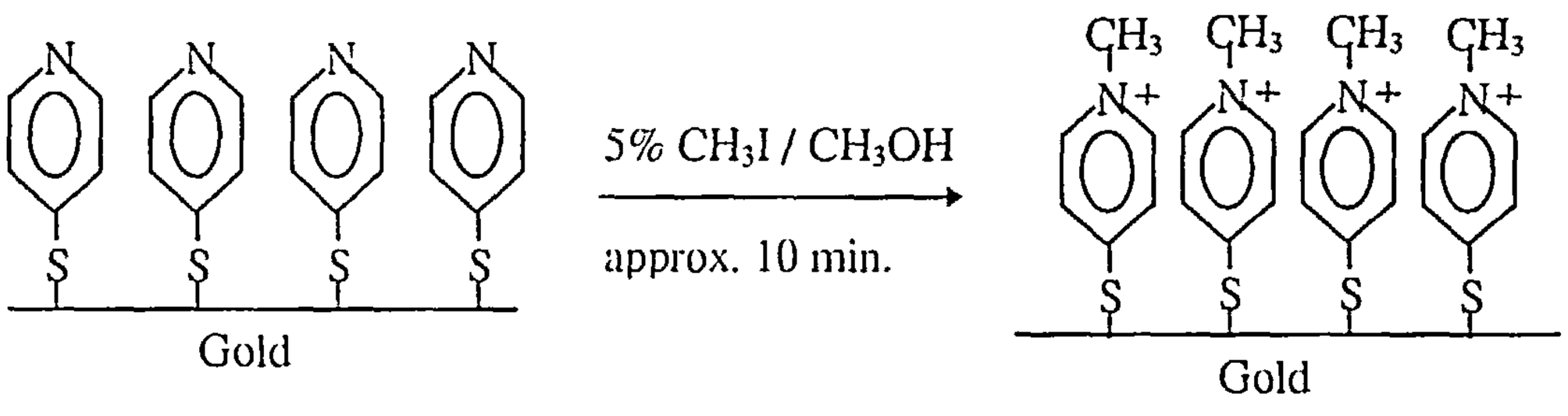

Figure. 6.4.

Schematic illustration of the preparation of the cationic surfaces.

6.2.3. MEASUREMENT OF THE INTERACTION OF DNA WITH CATIONIC SURFACE

Pt and Au-coated quartz crystal oscillators modified with 4-mercaptopyridine and methyl iodide were used to investigate the interaction of DNA with cationic surfaces and to estimate the amount of adsorbed DNA. After producing a positively charged cationic surface on which DNA can adsorb, measurement of frequency change for the

immobilisation of DNA was carried out using the quartz crystal microbalance. Figure 6.5 shows the schematic of adsorption of DNA.

Addition of DNA in 10 mM Tris buffer, pH 7 to a cell containing only 10 mM Tris buffer in contact with the modified cationic platinum surface gave a frequency decrease of 36 Hz. The frequency decrease indicates a 0.67 nmol cm^{-2} mass due to adsorption of DNA. But sometimes especially, at higher concentration of DNA we observed an unusual behavior which is not usually seen on gold surface as plotted in figure 6.6. Frequency first decreases with addition of DNA to the cell, then later increases again. This is may be because the thiol modification of the platinum surface is not as stable as on gold.

To estimate the amount of DNA on the surface using Au-coated crystals, a fresh solution of DNA was placed in the cell containing a 10 mM Tris buffer. Figure 6.7 shows the dependence of the mass increase for the immobilisation of DNA on a cationic gold-coated quartz crystal against the concentration of DNA. The line represents a theoretical Langmiur isotherm in which the surface coverage equals 1.2 nmol cm^{-2}. An estimation of the approximate number of monolayers due to immobilisation of DNA on Au surface observed here is 0.5. The higher mass of DNA on the surface is found by quartz crystal microgravimetry than electrochemical study. This may be because the viscosity of DNA in solution may have a contribution to the total frequency decrease. Also, the adsorbed DNA may have some water molecules attached increasing the mass observed in the QCM experiment. The determination of adsorbed DNA by CV in chapter 5 may also be an underestimate due to reversible binding of $Ru(NH_3)_6^{3+}$ and its loss during the transfer step.

Figure 6.8 shows admittance against time determined in the adsorption of DNA. It is reported [8] that a significant change was observed in the experiment of adsorption of DNA. In our experiment the admittance change is approximately 2.5 %. This is not a very significant change and the immobilised DNA in our experiments behaves as a rigid layer and the Sauerbrey approximation is reasonable.

We also examined if DNA binds to 4-mercaptopyridine or not. The decrease in frequency observed was about 8 Hz. The frequency decrease may be due to the viscosity and density of DNA solutions and is anyway not a very significant decrease.

The observed adsorption is owing to the electrostatic interaction between the negatively charged phosphate groups of DNA molecule and the positively charged modified surface.

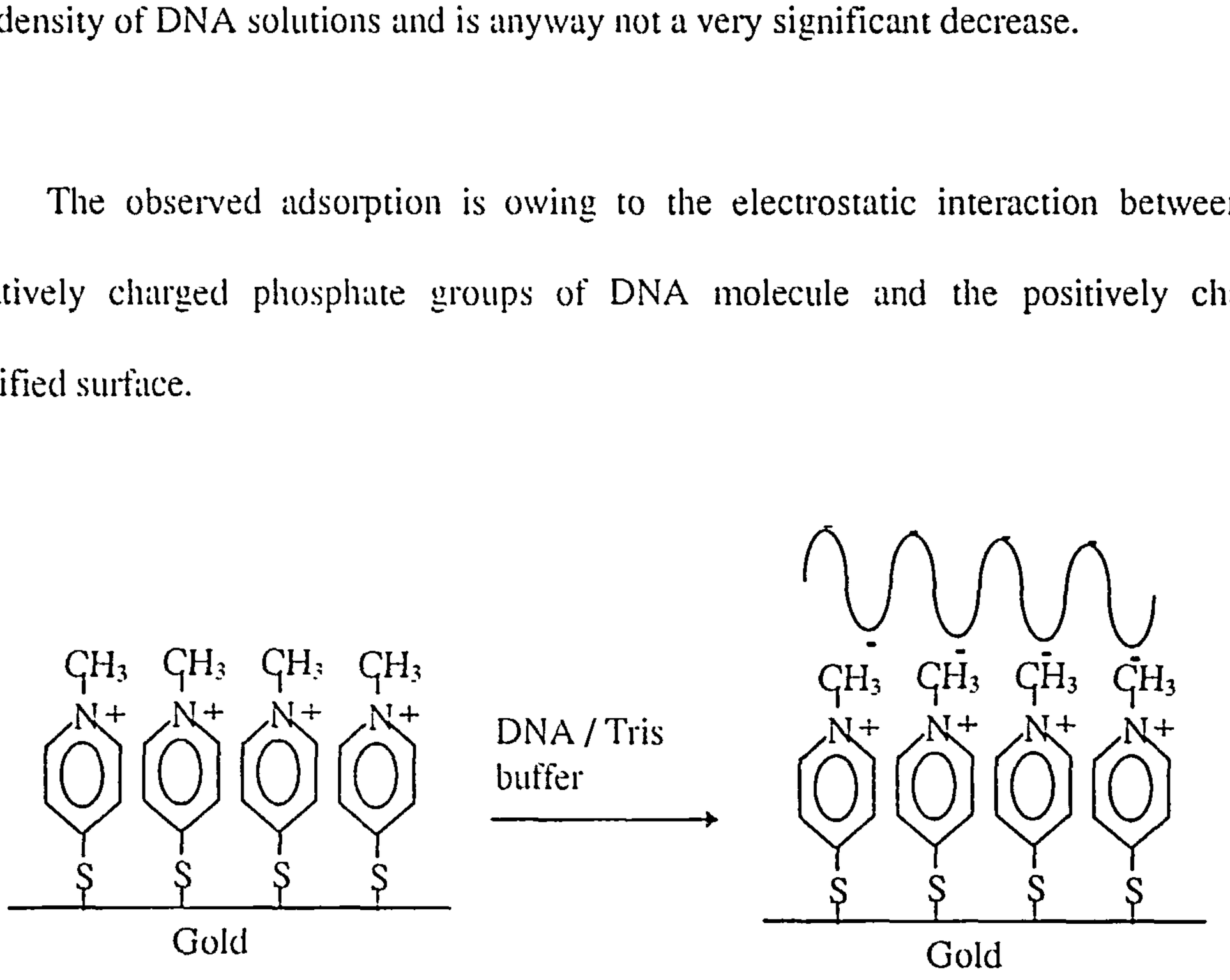

Figure 6.5.

Schematic illustration of adsorption of DNA on surfaces.

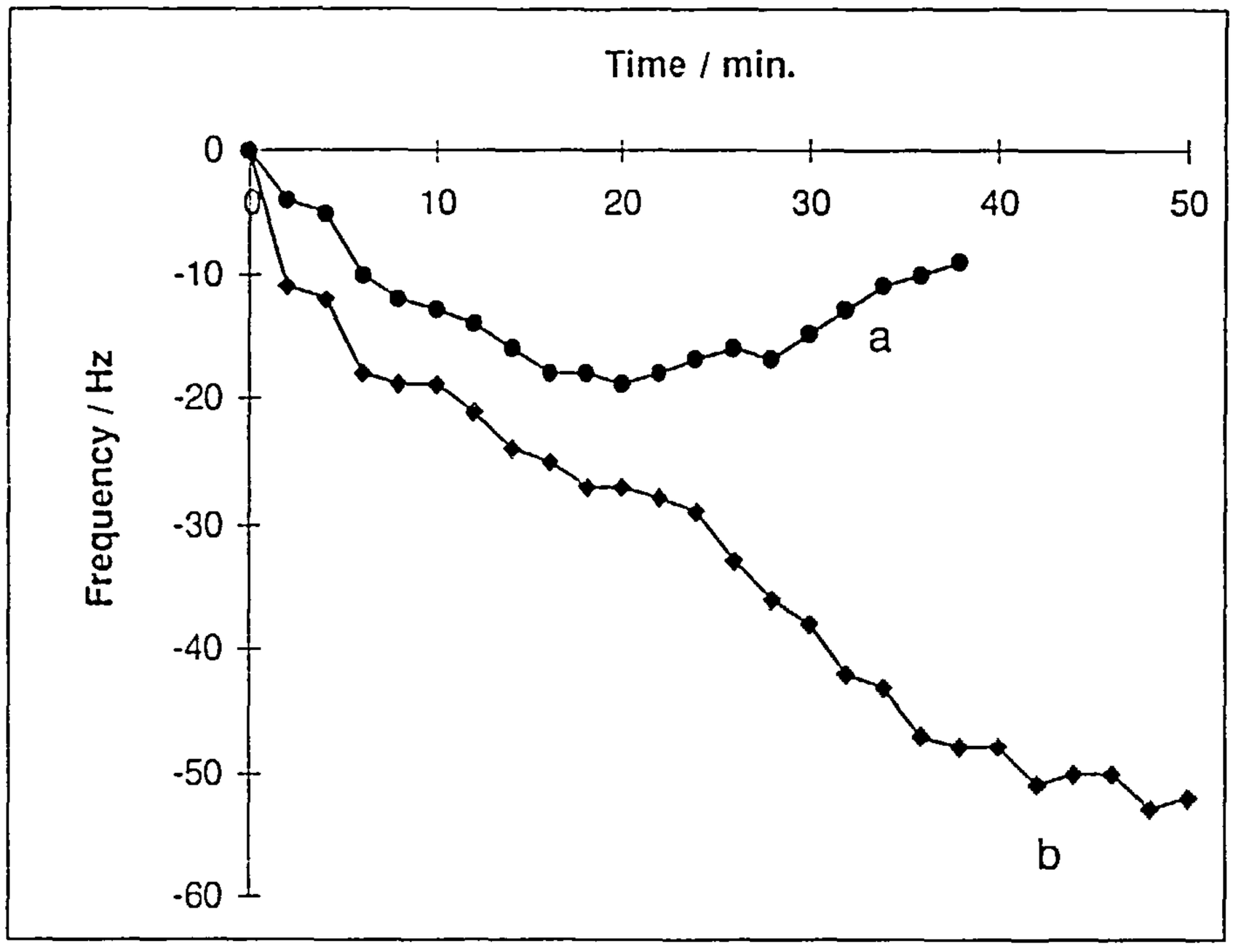

Figure 6.6.

A plot of frequency change of DNA to platinum (a) and gold (b) surface against time.

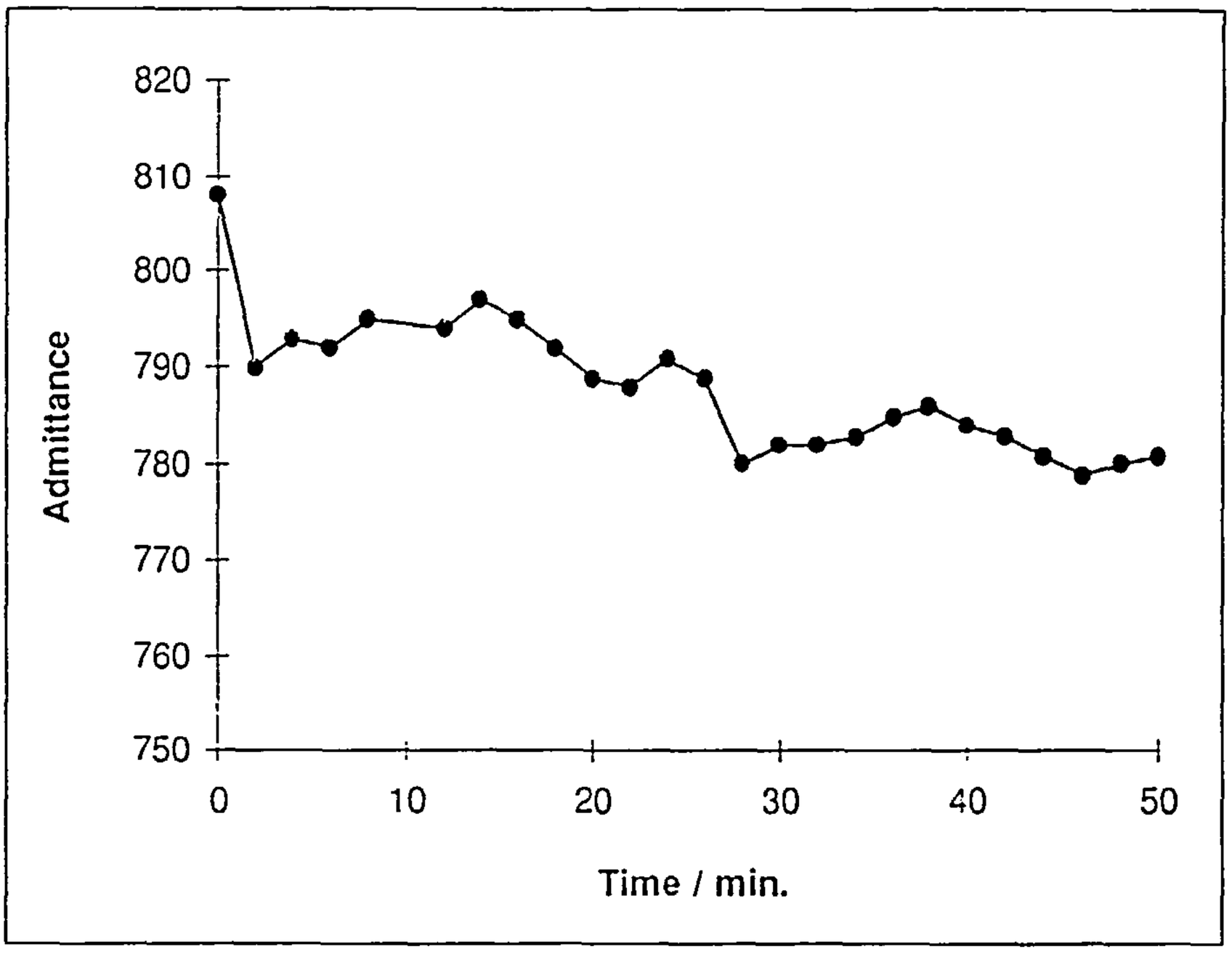

Figure 6.8.

A plot of the dependency of admittance on time with the binding of DNA to the cationic surface.

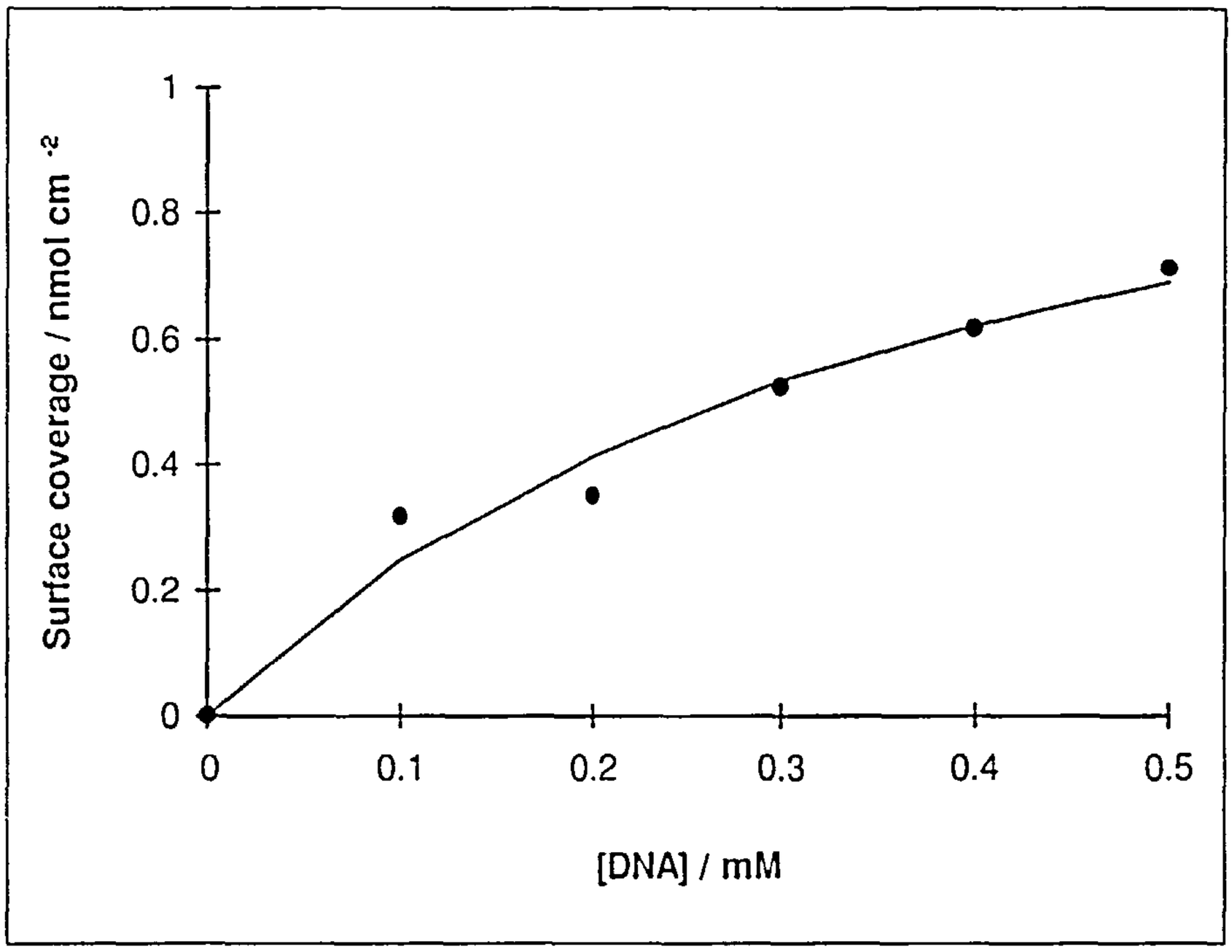

Figure 6.8.

Plot of surface coverage of DNA on a gold-coated crystal calculated from Sauerbrey equation. The solid line represents a theoretical Langmiur isotherm in which the maximum surface coverage is 1.2 nmol cm^{-2}.

6.2.4. MEASUREMENTS OF THE INTERACTION OF Fc-Th AND Fc-NMe_3 WITH IMMOBILISED DNA

Quartz crystal microbalance was applied to investigate the binding of Fc-Th to DNA immobilised on a Pt-coated quartz crystal. Gravimetric measurements indicated a measureable frequency decrease on addition of a solution of Fc-Th in 10 mM Tris buffer to a cell containing only buffer in contact with DNA immobilised on a Pt-coated quartz crystal. Figure 6.9 shows schematic of the interaction Fc-Th and Fc-NMe_3 with DNA immobilised on the surface. The frequency change after addition of Fc-Th observed was 59 Hz. The calculated surface coverage of Fc-Th is 0.67 nmol cm^{-2}. The smaller coverage in the electrochemical experiment is probably due to desorption of Fc-Th following transfer.

Au and Pt-coated quartz crystal oscillators were used to investigate the binding of Fc-NMe_3 to DNA-derivitised gold and platinum surfaces. No significant frequency change was observed with addition of Fc-NMe_3 into the cell containing modified crystal and 10 mM Tris buffer solution.

Both adsorptive-transfer voltammetry and quartz crystal microgravimetry did not provide evidence for the binding of Fc-NMe_3 to nucleic acid adsorbed surfaces. However, voltammetric experiments in solution show that the binding of Fc-NMe_3 to DNA is purely electrostatic. The binding of Fc-Th to nucleic acid modified surface was detected in QCM experiment. The amount of Fc-Th on the surface estimated in QCM experiment is larger than that in CV experiment. The reason for this may be due to a possible desorption of Fc-Th after transfering to the buffer solutions. Quartz crystal microbalance indicates that the

binding of Fc-Th to surface-immobilised DNA can be attributed to a non-electrostatic interaction.

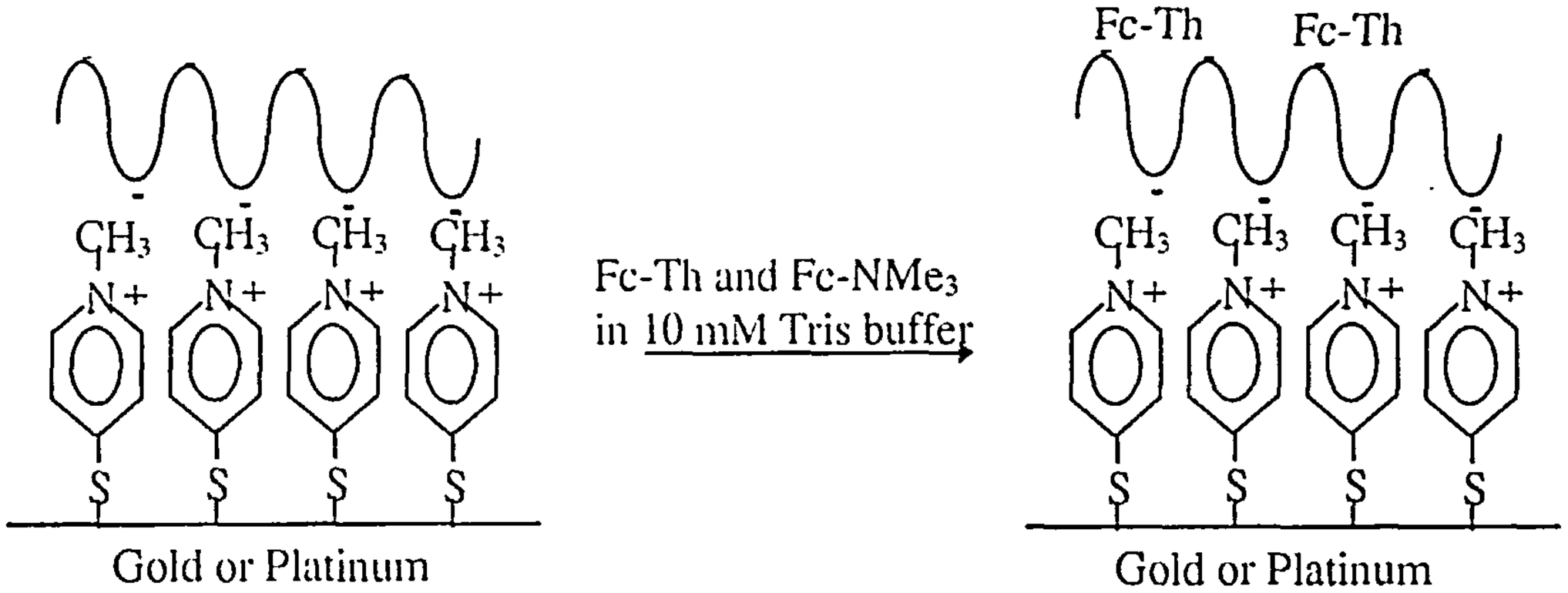

Figure 6.9.

Schematic illustration of the interaction of ferrocene derivatives with DNA adsorbed on modified surfaces.

6.2.5. MEASUREMENT OF THE INTERACTION OF HEXAMMINERUTHENIUM(III) CHLORIDE WITH DNA

The quartz crystal microbalance was applied to the study of the binding interaction of $Ru(NH_3)_6^{+3}$ with DNA on modified gold and platinum surfaces. Gravimetric measurement of $Ru(NH_3)_6^{+3}$-DNA interaction on a platinum surface shows a measureable frequency decrease with addition of $Ru(NH_3)_6^{+3}$ in 10 mM Tris buffer solution. A

schematic of the interaction of $Ru(NH_3)_6^{+3}$ with DNA adsorbed on the modified surface is given in figure 6.10. The frequency decrease in this interaction was about 91 Hz. The estimation of surface coverage on the platinum surface was about 1.6 nmol cm^{-2}.

Binding of $Ru(NH_3)_6^{+3}$ to DNA on a gold crystal surface was carried out by addition of varying concentrations of $Ru(NH_3)_6^{+3}$ to the cell containing only 10 mM Tris buffer. The dependence of the frequency change on concentration was examined to estimate the mass on the surface. A plot of surface coverage against the concentration of $Ru(NH_3)_6^{+3}$ is given in figure 6.11. The estimate of surface coverageof $Ru(NH_3)_6^{+3}$ on the gold surface calculated from the line representing a theoretical Langmiur isotherm is 3.5 nmol cm^{-2}. The maxium frequency decrease observed after addition of 1 mM $Ru(NH_3)_6^{+3}$ is 98 Hz. The approximate number of monolayers due to the binding of $Ru(NH_3)_6^{+3}$ to the DNA modified gold is 1. We detected 0.32 nmol cm^{-2} as the surface coverage for $Ru(NH_3)_6^{+3}$ using adsorptive-transfer voltammetry. The observation of the larger amount of mass adsorbed for $Ru(NH_3)_6^{+3}$ in QCM experiment can be due to the contribution of H_2O molecules associated with $Ru(NH_3)_6^{+3}$. The CV experiment is not sensitive to water molecules solvating $Ru(NH_3)_6^{+3}$ and may also underestimate the surface coverage due to desorption of $Ru(NH_3)_6^{+3}$.

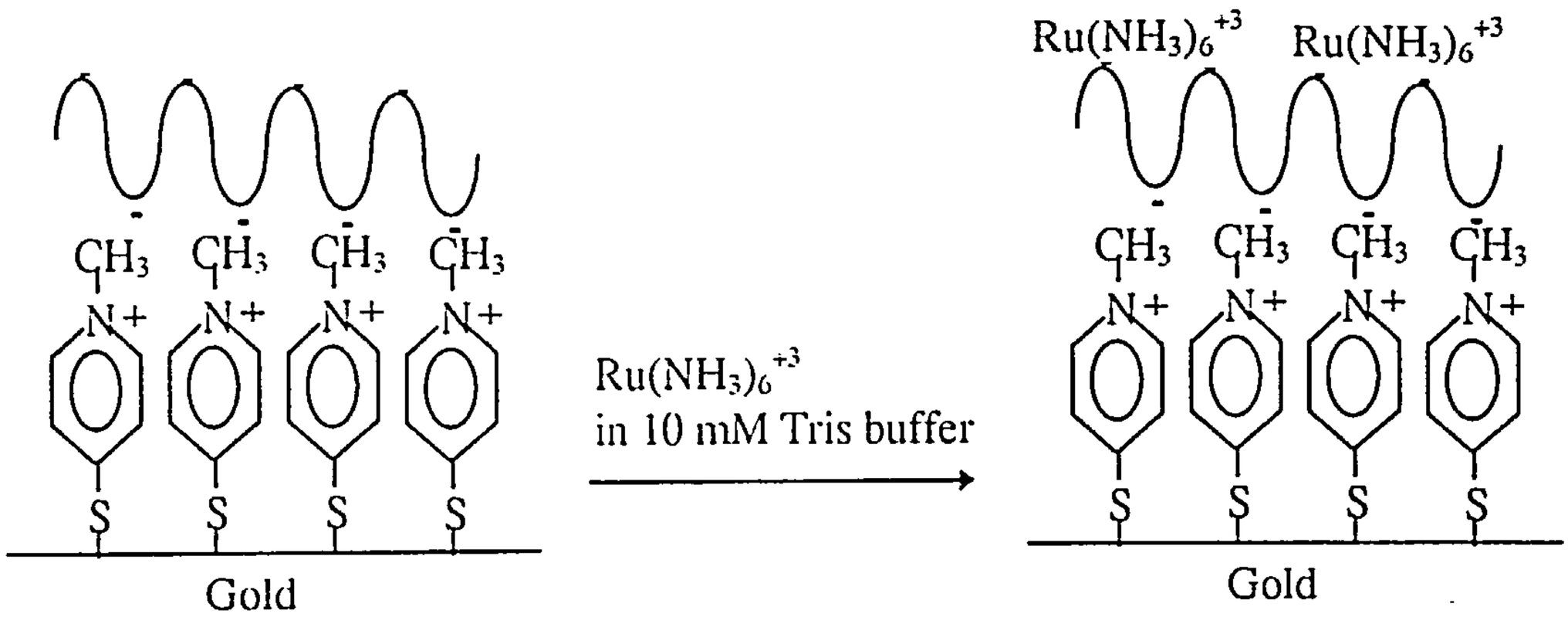

Figure 6.10.

Schematic illustration of the interaction of $Ru(NH_3)_6^{+3}$ with adsorbed DNA.

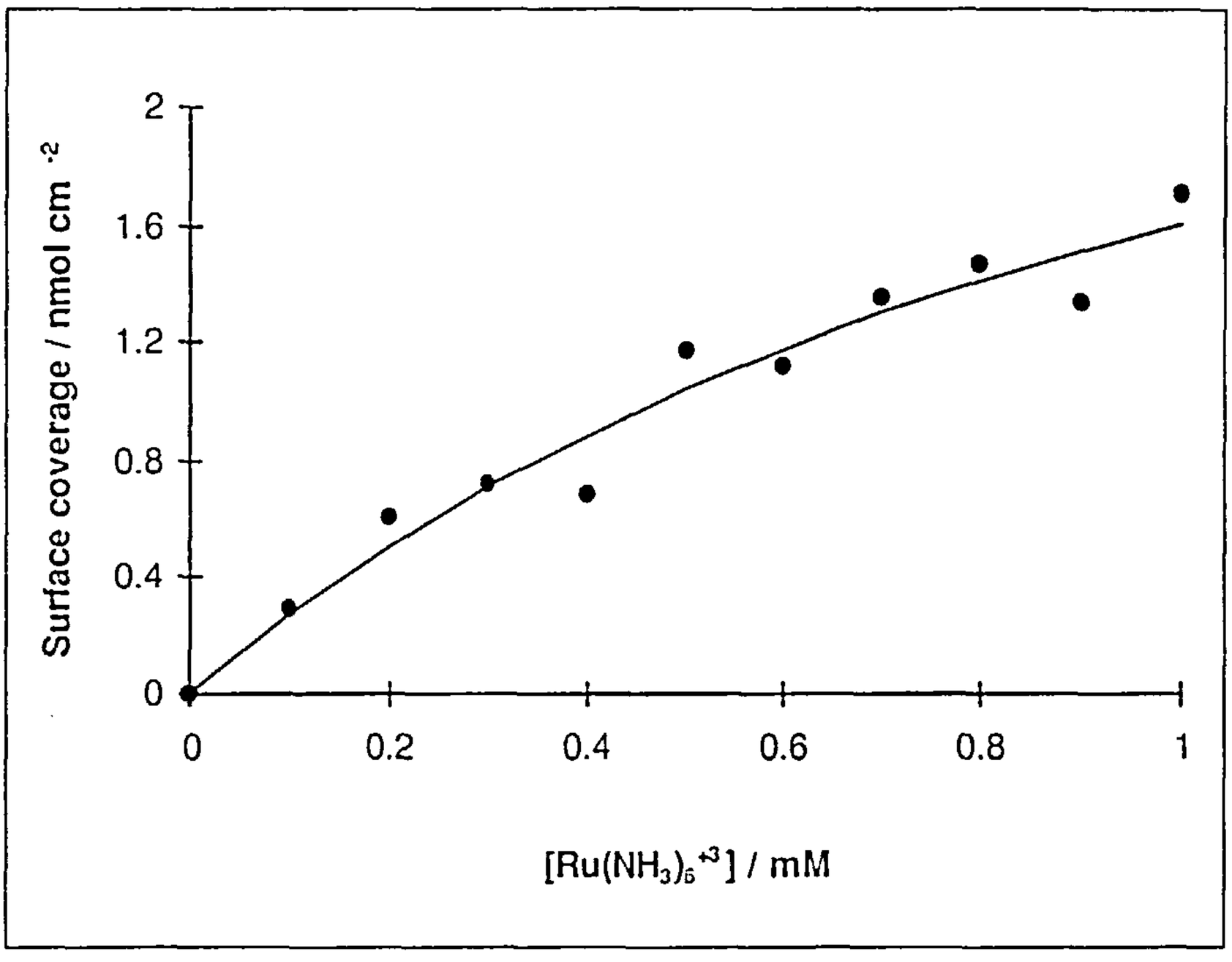

Figure 6.11.

Plot of surface coverage of $Ru(NH_3)_6^{+3}$ on a DNA immobilised gold-coated crystal calculated from Sauerbrey equation. The solid line represent a theoretical Langmiur isotherm in which surface coverage is 3.5 nmol cm^{-2}.

6.2.6. MEASUREMENT OF THE INTERACTION OF TRIS(1.10-PHENANTHROLINE)-IRON(II) PERCHLORATE

Studies of the binding interaction of $Fe(phen)_3^{+2}$ with DNA immobilised surfaces using quartz crystal microgravimetry were carried out both on gold and platinum coated crystals.

Addition of 2.0 mM $Fe(phen)_3^{+2}$ solution in the cell containing 10 mM Tris buffer and DNA immobilised platinum crystal caused a frequency decrease of about 70 Hz. An estimate of surface coverage on the platinum surface is about 0.5 nmol cm^{-2}. Figure 6.12 a shows schematic of the interaction of $Fe(phen)_3^{+2}$ with DNA adsorbed surface.

Next the dependency of the frequency change on the concentration of $Fe(phen)_3^{+2}$ was examined. Initially the surface with DNA modified Au-coated quartz crystal oscillator was in contact with 10 mM Tris buffer solution alone, and then a varying amount of $Fe(phen)_3^{+2}$ in 10 mM Tris buffer solution was added. A plot of mass change against the concentration of $Fe(phen)_3^{+2}$ is given in figure 6.13. The line represents a theoretical Langmiur isotherm in which Γ equals 1.4 nmol cm^{-2}. As a results of the binding of $Fe(phen)_3^{+2}$ to the DNA modified surface the maximum frequency decrease observed was 77 Hz.

Since there is no possiblities of the oxidation of 4-meracaptopyridine in QCM experiment the binding of $Fe(phen)_3^{+2}$ was detected and surface coverage was estimated. The calculated amount of $Fe(phen)_3^{+2}$ on the surface is larger than the amount of Fc-Th. This is probably due to a stronger interaction of $Fe(phen)_3^{+2}$ with DNA.

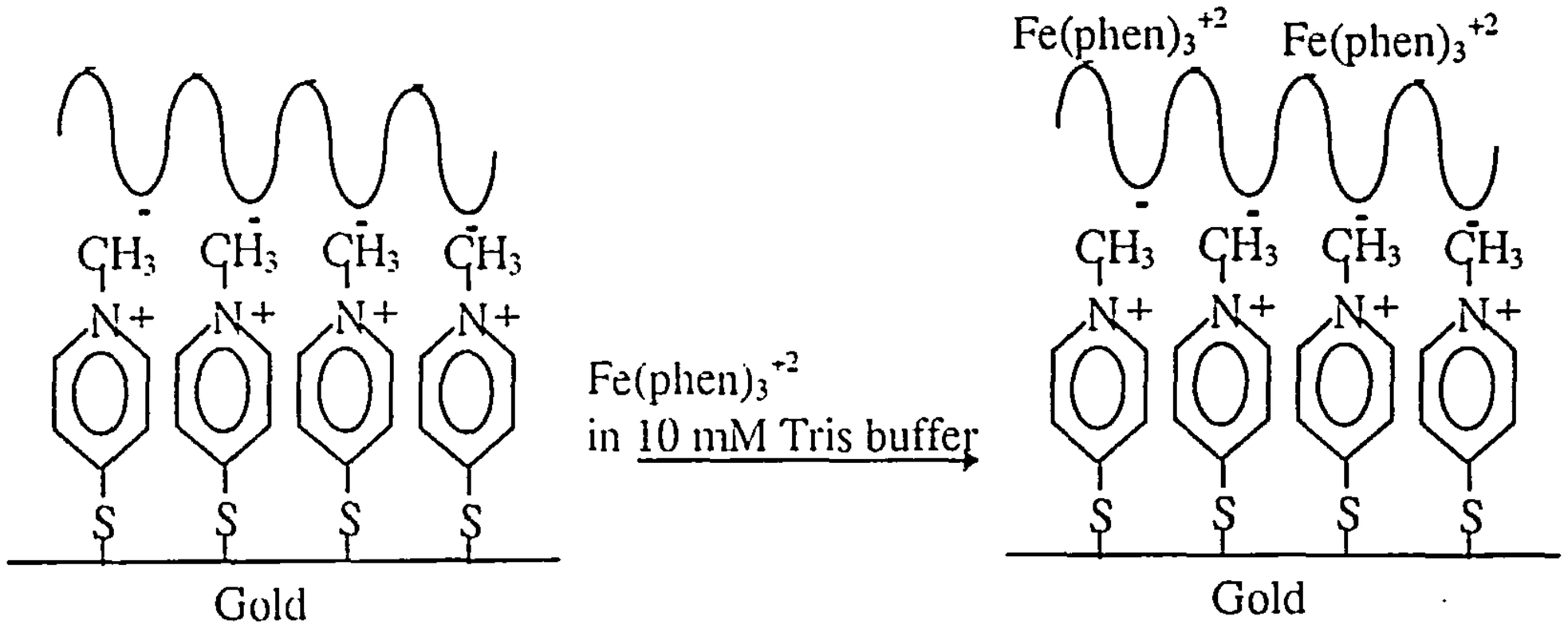

Figure 6.12.

Schematic illustration of the binding of $Fe(phen)_3^{+2}$ to DNA adsorbed surface.

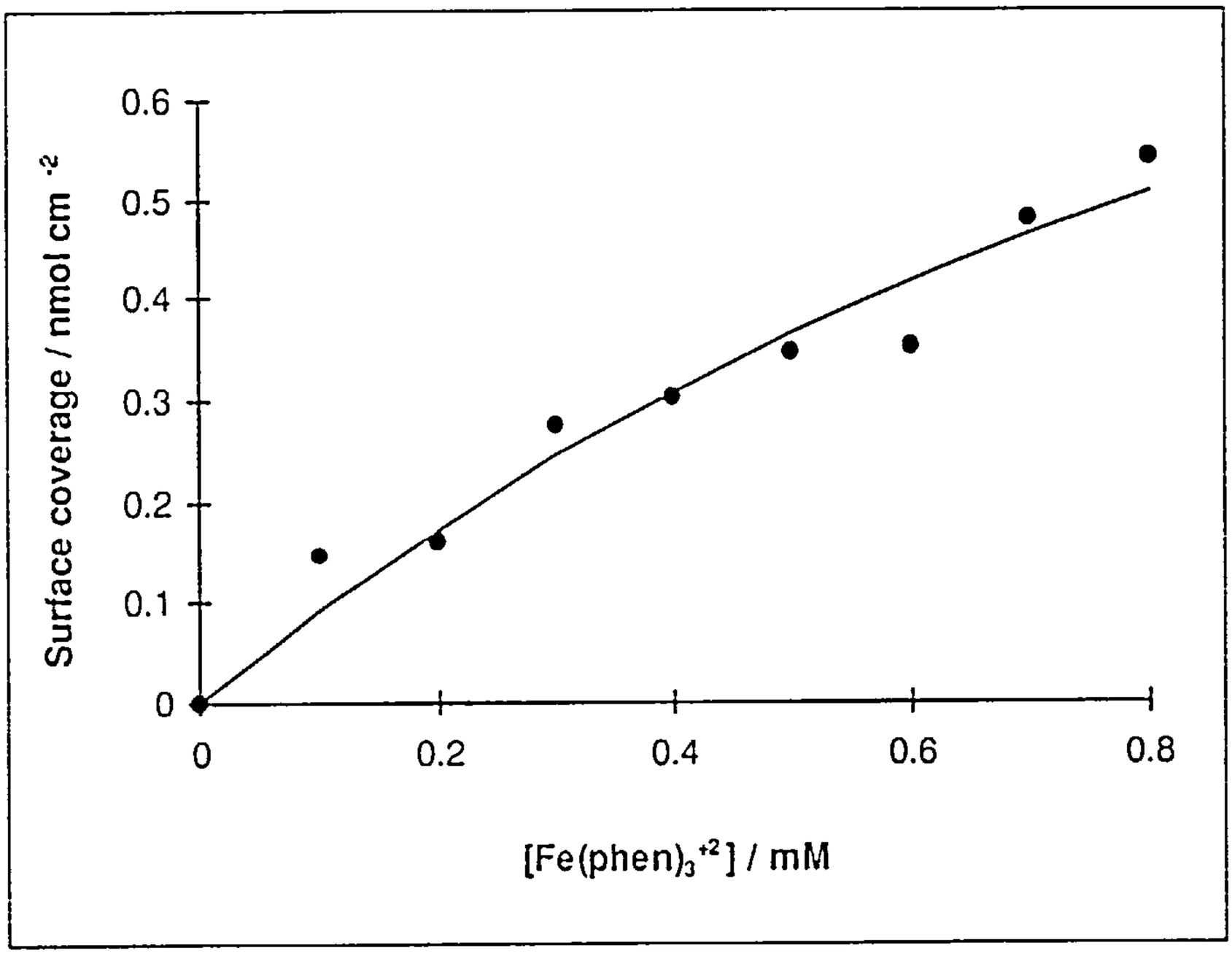

Figure 6.13.

Plot of surface coverage of $Fe(phen)_3^{+2}$ on a DNA immobilised gold-coated crystal calculated from Sauerbrey equation. The solid line represent a theoretical Langmiur isotherm in which surface coverage is 1.4 nmol cm^{-2}.

6.3. CONCLUSIONS

It has been found that the quartz crystal microgravimetry can be used to detect the mass change due to adsorption of 4-mercaptopyridine on platinum and gold surfaces. The large apparent surface coverage of 4-mercaptopyridine was caused by density effects.

Immobilisation of DNA can also be studied on surfaces. Modification of gold surfaces were usually more stable than platinum surfaces. The surface coverage of DNA observed in the QCM experiment is 1.2 nmol cm^{-2} which is larger than that estimated in the CV experiment. Several explanations for this are possible. Density and viscosity of DNA can contribute to the apparent mass in QCM experiments. Also, QCM measures water of solvation associated with DNA. The absence of significant change in admittance however showed that the immobilised layer of DNA is rigid and the Sauerbrey equation is a reasonable approximation.

The binding of Fc-Th to DNA immobilised on surfaces was detected using quartz crystal microgravimetry. The QCM experiment shows a larger amount of Fc-Th on the surface than the CV experiment. Desorption of Fc-Th might cause a smaller coverage in the CV experiment. The absence of significant frequency decrease in the presence of Fc-NMe_3 agrees with the CV experiment.

The surface coverage of $Ru(NH_3)_6^{+3}$ determined by QCM is about 3.5 nmol cm^{-2}. Since solvated H_2O molecules can contribute to the frequency change and some desorption might occur in the CV experiment, the QCM experiment may overestimate and CV underestimate the surface coverage.

Since gravimetric measurements do not involve scanning high positive potentials, the QCM experiments show binding of $Fe(phen)_3^{+2}$ to the modified surface. This results does not agree with CV experiments. As we emphasised in chapter five, thiol could be removed from the surface at high positive potential in CV experiments.

We found that the change in room temperature has no significant effect on frequency change as indicated by the results in chapter three.

6.4. REFERENCES

1. C. N. Sayre and D. M. Collard, *Langmiur*, **1995**, 11, 302.

2. J. Clavilier, V. Svetlicic and V. Zutic, *J. Electroanal. Chem.*, **1996**, 402, 129.

3. C. D. L. Hugh, J. J. Donohue and D. A. Buttry, Langmuir, **1991**, 7, 2196.

4. J. A. Roush, D. L. Thacker and M. R. Anderson, *Langmiur*, **1994**, 10, 1642.

5. S. Yamaguchi, T. Shimomura, T. Tatsuma and N. Oyama, *Anal. Chem.*, **1993**, 65, 1925.

6. X-H. Xu, H. C. Yang, T. E. Mallouk and A. J. Bard, *J. Am. Chem. Soc.*, **1994**, 116, 8386.

7. K. Ito, K. Hashimoto and Y. Ishimori, *Anal. Chim. Acta*, **1996**, 327, 29.

8. H. Su, P. Williams and M. Thompson, *Anal. Chem.*, **1995**, 67, 1010.

GENERAL DISCUSSION & CONCLUSIONS

Both cyclic voltammetry and steady-state voltammetry at microelectrodes are useful techniques in the studies of the interaction of metal complexes with nucleic acids. Since the contribution of bound metal is small at microelectrodes, the results obtained at microelectrodes are more reliable and the analysis is easier. The interaction of a number of metal complexes with nucleic acids was carried out using voltammetric techniques. At smaller concentration of titration of $Ru(NH_3)_6^{+3}$ in the titration with DNA the currents were very small showing that the contribution of bound metal is also small. Since at small concentrations of metal complex the diffusion of bound metal is very small and may be negligible, the bound/free ratio is given simply by $\frac{i_{nodna} - i_{dna}}{i_{dna}}$. The effect of viscosity on the measurement is small because the points of current vs. the concentration of $Ru(NH_3)_6^{+3}$ in the absence and presence of DNA ran parallel at high metal complex concentrations. Also, generally the larger observation of binding constant for a metal complex in microelectrode voltammetry than in cyclic voltammetry indicates the bound metal may contribute to the diffusion current in cyclic voltammetry. Steady-state voltammetry at microelectrodes indicates that the binding of Fe-NMe_3 is purely electrostatic. However, the binding of Fe-Th to DNA or RNA is mainly electrostatic with a minor but important component of non-electrostatic contributions. The effect of ionic strength is shown in experiments with $Fe(bz)_2^{+2}$-DNA and $Fe(phen)_3^{+2}$-DNA in which the binding of $Fe(bz)_2^{+2}$ to DNA is purely electrostatic and the binding of $Fe(phen)_3^{+2}$ to DNA is mainly non-electrostatic. This also indicates that the ionic strength effect could give very important information about the binding mode.

Adsorptive-transfer voltammetry and quartz crystal microgravimetry are also both useful techniques in the surface studies of the measurement of metal complex-nucleic acid interactions. They also show the effect of a single nucleobase in Fc-Th comparable to Fc-NMe_3 produces a significant change in the mode of binding to nucleic acids.

Since Au-S bonds may be removed from the surface at high positive potential where cyclic voltammograms of $Fe(phen)_3^{+2}$ are run, adsorptive-transfer voltammetry did not provide the evidence of binding: however the QCM shows the binding of $Fe(phen)_3^{+2}$ to DNA adsorbed surface. Since viscosity, density and solvated water molecules can contribute to the frequency change in QCM experiments, the apparent amount of adsorbed species may be larger than in CV experiments where metal complex can be lost by desorption into solution.